Peristaltic Transport of Real Fluids: A Study of Bifurcations of Streamlines and Heat/Mass Transfer Analysis

By

ZaheerAsghar

Department of Mathematics and Statistics

Faculty of Basic and Applied Sciences

International Islamic University, Islamabad, Pakistan

2016

Peristaltic Transport of Real Fluids: A Study of Bifurcations of Streamlines and Heat/Mass Transfer Analysis

By

ZaheerAsghar

Supervised by

Dr. Nasir Ali

Department of Mathematics and Statistics

Faculty of Basic and Applied Sciences

International Islamic University, Islamabad, Pakistan

2016

Peristaltic Transport of Real Fluids: A Study of Bifurcations of Streamlines and Heat/Mass Transfer Analysis

By

ZaheerAsghar

A Thesis
Submitted in the Partial Fulfillment of the
Requirements for the degree of

DOCTOR OF PHILOSOPHY

IN

MATHEMATICS

Supervised by

Dr. Nasir Ali

Department of Mathematics and Statistics

Faculty of Basic and Applied Sciences
International Islamic University, Islamabad, Pakistan

2016

Declaration

I, hereby declare and affirm that this research work neither as a whole nor as a part has been copied out from any source. It is further declared that I have prepared this dissertation entirely on the basis of my personal efforts made under the sincere guidance of my worthy supervisor. If any part of this thesis is proven to be copied out or found to be a reproduction of some other, I shall stand by the consequences.

Moreover, no portion of the work presented in this thesis has been submitted in support of an application for other degree or qualification in this or any other university or institute of learning.

Name and Signature of Student:_____

Zaheer Asghar

PhD (Mathematics)

Acknowledgements

First of all, I pay special thanks to Almighty Allah, Who assisted me in all walks of life and also assisted and guided me throughout my PhD work and in the accomplishment of this thesis too. Many Salat-o-Salam on our Holy Prophet Hazrat Muhammad (PBUH) Who is a source of knowledge and blessings for the entire creations.

I would like to express my very profound gratitude to my parents , parents in laws and other family members like my sister Munazza Asghar, my wife Aqsa Nasrullah, my brothers Muyassar Hussain & Muhammad Talha, my sisters Asma Kauser, Hira Mubassam, Habibah Nasrullah for their prayers and providing me with unfailing support and continuous encouragement throughout my years of study and through the process of researching and writing this thesis. This accomplishment would not have been possible without their moral support. My family is very loving and supportive that's why I accomplish each task very easily.

I would like to thank my respectable, honorable, very sincere and dedicated supervisor Dr. Nasir Ali for providing me the opportunity of taking part in PhD Mathematics program. I am so deeply grateful for his help, professionalism, valuable guidance throughout this thesis and through my entire program of study that I do not have enough words to express my deep and sincere appreciation. It is the guidance provided by my worthy supervisor that this thesis received lots of appreciation of foreign and local experts. I am also grateful to my all teachers on directing me to the right path and teaching fruitful courses with their full dedication. Special thanks to Dr. Ahmed Zeeshan on helping and guiding me in my PhD. I am also grateful to Dr. Sajid Ali and Dr. Tariq Javed for their moral support.

I am thankful to my all friends and would like to mention the names of some friends, Rai Sajjad, Abu Zar, Asif Javed, Muhammad Sami, Khurram Javed, Muhammad Irfan, Akbar Zaman, Muhammad Raheel, Muhammad Saleem, Zeeshan Asghar, Arshad Siddiqui, Mubasshir Nazir, Hafiz Atif, Muhammad Abid for their moral support. They always remain ready to assist me when I was needed.

Zaheer Asghar

Preface

Peristaltic transport of real fluids has attracted the attention of researchers because of its applications in medical science and industry. This mechanism is a fundamental and vital feature of many smooth muscle organs which transport bio-fluids. Typical examples of bio-fluids which are transported through peristaltic activity are urine, chyme, blood, spermatic fluid, bile etc. Industrial applications of peristalsis can found in the design of finger and roller pumps. In medical engineering, peristaltic systems are utilized in diabetes pumps, heart-lung machine and pharmacological delivery systems. In botanical hydrodynamics, peristalsis arises in loam dynamics in trees and plants. The literature on the peristaltic transport is quite extensive. Much of the work is based on the constitutive equations of generalized Newtonian fluid models, retarded motion expansion and polar fluids. However, despite the importance of FENE-P and visco-elasto-plastic fluid models not a single attempt is available in the literature which deals with peristaltic transport of such fluids. Moreover, the study of streamlines patterns of two-dimensional peristaltic flow and bifurcations of their critical points is relatively a new area and literature is scarce on this topic. Similarly, studies pertaining to simultaneous effects of mixed convection and viscous dissipation on peristaltic flows and heat transfer is also limited. Motivated by the above facts, the aim of this thesis is to explore the peristaltic motion with particular focus on non-Newtonian effects, streamlines topologies and their bifurcations and heat/mass transfers analysis. The thesis is composed of seven chapters. A brief description of each chapter is given below.

Chapter 1 consists of fundamentals of peristaltic flows, heat/mass transfer and bifurcation theory. A detailed literature review on peristaltic flow of real fluids is also presented.

Chapter 2numerically investigates peristaltic transport of incompressible visco-elasto-plastic fluids in a two-dimensional symmetric channel. The constitutive equation used for extra stress tensor is quite general and includes models like Maxwell A, Maxwell B, Johnson-Segalman, Oldroyd-B and Bingham model as its special case. The continuity and momentum equations under the assumptions of long wavelength and low Reynolds numbergive rise a nonlinear ordinary differential equation which is solved using shooting method and Matlab built-in routine bvp4c. Excellent correlation is observed between the results obtained by two methods. The solution obtained by bvp4c is used for further analysis of velocity profile, pressure rise per

wavelength, frictional forces and trapping phenomenon. The contents of this chapter are published in **Zeitschrift Fur NaturforschungA 70 (8) (2015) 593-603.**

Chapter 3presents the mathematical modeling and analysis of the peristaltic flow of Finitely Extendable Nonlinear Elastic-Peterlin (FENE-P) fluid both in planar channel and axisymmetric tube. An exact solution is obtained for the stream function and longitudinal pressure gradient subject to no-slip condition under the same approximations considered in chapter 1. The effects of model parameters, Deborah number and extensibility parameter, on velocity profile, trapping phenomenon and normal stress are analyzed. An enhancement in normal stress is observed with increasingDeborah number and extensibility parameter. Further, flow acceleration is observed near the channel/tube center for larger values of Deborah number while a converse trend is noted with increasing extensibility parameter. Thesize of trapped bolus decreases (increases) by increasing Deborah number (extensibility parameter). Similar trend is noted form the plots of pressure rise and frictional forces. It is also shown thatresults of Newtonian model can be deduced as a special case of FENE-P model. The contents of this chapter are publishedin **Zeitschrift Fur NaturforschungA, 69a, 462-472 (2014)**.

Chapter 4present the analysis of streamlines patterns and their bifurcation for two-dimensional peristaltic flow of Newtonian fluid in the presence of wall slip. The flow analysis is carried out both in planar channel and axisymmetric tube. Exact solution for the stream function is obtained in the wave frame under the assumptions of long wavelength and low Reynolds number for both cases. A system of nonlinear autonomous differential equations is established and the methods of dynamical systems are used to discuss the local bifurcations and their topological changes. All types of local bifurcations and their topological changes are discussed graphically. Moreover, global bifurcation diagram is used to summarize the bifurcations. The contents of this chapter are published in **Chinese Physics B Vol. 23, No. 6 (2014) 064701**.

Chapter 5investigates streamline topologies and their bifurcations for two-dimensional peristaltic channel flow in presence of buoyancy forces and constant heat source. The well-knownBoussinesq approximation is used to formulate buoyancy force term in momentum equation. Methods of dynamical systems are employed to solve the non-linear autonomous system. The results indicate that vortices contract along the vertical direction whereas they expand along horizontal direction. A global bifurcations diagram is used to summarize the bifurcations. The trapping and backward flow regions are mainly affected by increasing Grashof

number and constant heat source parameter in such a way that trapping region increases whereas backward flow region shrinks. The contents of this chapter are published in **AIP Advances 5 (9) (2015) 097142**.

Chapter 6extends the results of chapter 3 by including the mixed convective heat/mass transfer analysis and chemical reaction effects. The Boussinesq approximation to account for the effects density variations in the flow field. Moreover, the present analysis is carried out neglecting viscous dissipation and including diffusion-thermal (Dufour) and thermal-diffusion (Soret) effects. The flow equations become highly nonlinear and coupled. An exact solution of the simplified coupled linear equations for the temperature and concentration has been obtained whereas numerical solution is obtained for dimensionless stream function and pressure gradient. Tthe effects of pertinent parameterson velocity profile, temperature and concentration fields and trapping phenomenon are highlighted. Numerical integration has been performed to analyze pressure rise per wavelength. The contents of this chapter are published in the **Journal of Mechanics (2015) 1-10**.

Chapter 7presents the analysis of mixed convective peristaltic flow of incompressible viscoplastic fluid in a two-dimensional symmetric channel. The prime objective is to see the effects of plasticity of the fluid on flow and temperature characteristics. The equations governing the velocity and temperature of the fluid are solved using regular perturbation method and Matlab built-in routine bvp4c. The comparison for two solutions reveals the superiority of the numerical solution over the perturbation solution. The bvp4c solution is further utilized to investigate various features of the problem. It is found that velocity decreases at the channel center by increasing Bingham number showing a boundary layer character for large values. However, it increases by increasing Brinkman and Grashof numbers. Moreover, pressure rise per wavelength increases with Bingham number, Brinkman number and Grashof number, in the pumping region. The trapping phenomenon is also discussed in detail for several values of involved parameters. The contents of this chapter are submitted for possible publication in **International Journal of Heat and Mass Transfer**.

Contents

Nomenclature

English symbols

a_1	Half width of channel/radius of tube
b_1	Amplitude of wave
$\overline{t}$	Time
$\overline{X}$	Horizontal coordinate of fixed frame of reference
$\overline{Y}$	Vertical coordinate of fixed frame of reference
$\overline{x}$	Horizontal coordinate of moving frame of reference
$\overline{y}$	Vertical coordinate of moving frame of reference
$\overline{U}$	Longitudinal component of velocity in fixed frame
$\overline{V}$	Transverse component of velocity in fixed frame
$\overline{u}$	Longitudinal component of velocity in wave frame
$\overline{v}$	Transverse component of velocity in wave frame
$\overline{\mathbf{f}}$	Body force vector
$\overline{P}$	Pressure in fixed frame
$\overline{p}$	Pressure in wave frame
$\overline{\mathbf{I}}$	Identity tensor
$\mathbf{D}$	Deformation tensor
$\overset{\wedge}{\mathbf{D}}$	Tensor for Bingham fluid
De	Deborah number
Bn	Bingham number
Re	Reynolds number
q	Dimensionless mean flow rate in fixed frame of reference
θ	Dimensionless mean flow rate in moving frame of reference
$\mathbf{A}$	Configuration tensor
$\mathbf{R}$	End-to-end vector that connects the dumbbell beads

$\overline{R}$	Radial component of cylindrical coordinates
$\overline{Z}$	Axial component of cylindrical coordinates
R_w	Average height of channel
$\overline{\mathbf{A}}_1$	First Rivillin-Ericksen tensor
$x_{i,j}$ $i = 1, 3, 5, 7, 9$; $j = 2, 4, 6, 8$	Abscissa for eigenvalues
$y_{i,j}$ $i = 1, 3, 5, 7, 9$; $j = 2, 4, 6, 8$	Ordinate of eigenvalues
$p_{i,j}$	Trace of Jacobian
$d_{i,j}$	Product of eigenvalues
M	Bifurcation curves
R_a	Tube radius
$\overline{T}$	Temperature
$\overline{T_0}$	Constant temperature at lower wall
Q	Constant heat generation term
Gr_t	Grashof number for temperature
Pr	Prandtl number
q_c	Critical value of flow rate in fixed frame
g	Acceleration due to gravity
C	Concentration field
T_0	Constant temperature at lower wall
C_0	Constant concentration at lower wall
D^*	Coefficient of mass diffusivity
K_T	Thermal diffusion ratio
c_s	Concentration susceptibility
K_1	Chemical reaction parameter
Gr_c	Grashof number for concentration
D_f	Dufour number
S_c	Schmidt number
S_r	Soret number
$\overline{\mathbf{S}}$	Extra stress tensor
Ec	Eckert number

R_e	Characteristic length
H_0	Gaussian stiffness in the limit of small molecular extension
R_0	Maximum allowable dumbbell length
L^2	Measure of extensibility of the dumbbells
k_1	Boltzmann constant
T	Absolute temperature
A_i with $i = 1, 2 \cdots, 6$	Constants of integration
B_r	Brinkman number
C_i with $i = 1, 2, \cdots, 11$	Constants
T_j with $j = 1, 2, \cdots, 12$	Constants
$\mathbf{A}_1, \mathbf{B}_1$	Arbitrary tensors
$\overline{\mathbf{T}}$	Cauchy Stess tensor
N	Bifurcation curve
$\mathbf{C}$	Tensor
$\mathbf{L}$	Bifurcation curve
$\mathbf{L}^*$	Bifurcation curve
E^s	Stable manifold
E^u	Unstable manifold
R^n	n-dimensional real space
E	Arbitrary Open subset
Q	Heat source or sink
$\overline{H}$	Function defining the geometry of the wall
$F^{(c)}$	Connector force
tr	Trace
$< \cdot >$	Ensamble average

Greek symbols

λ	Wave length
ρ	Fluid density
∇	Gradient
ϕ_a	Amplitude ratio in tube
$\overline{\boldsymbol{\tau}}$	Extra stress tensor
λ_1	Relaxation time
λ_2	Retardation time
η	Viscosity
ξ_1	Small scalar parameter
τ_0	Basic yield stress
δ	Wave number
ε	Small dimensionless parameter
ϕ	Amplitude ratio
ψ	Stream function
η_p	Zero shear rate polymer viscosity
∇	Upper convected derivative
ΔP_λ	Pressure rise per wave length
F_λ	Frictional force
ν	Kinematic viscosity
β	Dimensionless slip parameter
η	Dimensional slip parameter
$\lambda_{i,j}\ i = 1, 3, 5, 7, 9;\ j = 2, 4, 6, 8, 10$	Eigenvalues
λ_3	Eigenvalue
λ_4	Eigenvalue
θ^*	dimensionless temperature
$\boldsymbol{\alpha}$	Vector containing bifurcation parameters

α_1	Thermal expansion coefficient
Φ	Dimensionless heat generation
α_2	Concentration expansion coefficient
γ	Chemical reaction parameter
β_1	Dimensional slip parameter
β_2	Coefficient of volume expansion

Chapter 1

Introduction

This chapter includes fundamentals concepts about peristalsis, heat/mass transfer and bifurcation theory. The frequently appearing dimensionless numbers relevant to peristaltic flow and heat/mass transfer are also defined. A review of literature on peristalsis and its interaction with heat/mass transfer is presented. The basic equations governing the flow and heat/mass transfer are also provided.

1.1 Fundamentals of peristaltic transport

1.1.1 Peristalsis

The word peristalsis stems from a Greek word "Peristaltikos" which means clasping and compressing. Therefore, it is defined as a wave of relaxation contraction to the walls of a flexible conduit, thereby pumping the enclosed material.

1.1.2 Peristaltic transport

It is form of material transport induced by a progressive wave of area contraction or expansion along the length of a distensible tube containing some material. It is also a natural way of moving the content within hollow muscular structures by successive contraction of their muscular fibers.

1.1.3 Biological and Industrial applications of peristalsis

Peristalsis is an inherent property of many biological systems having smooth muscle tubes which transport biofluids by its propulsive movements and is found in the transport of urine from kidney to bladder, the movement of chyme in the gastro intestinal tract, vassomotion of small blood vessels, the movement of spermatozoa in the ductus effrents of the male reproductive tract, the movement of ovum in the fallopian tube, swallowing of food through esophagus, transport of bile, transport of lymph in the lymphatic vessels, blood motion in the arteries and many glandular ducts.

The mechanism of peristaltic transport has been exploited for industrial applications like sanitary fluid transport, the blood pumps in heart lung machine, transport of noxious fluid in nuclear industry and transport of corrosive fluids where the contact of fluid with machinery parts is prohibited.

1.1.4 Pumping

It is characteristic feature of peristaltic transport. The operation of a pump of moving liquids from lower pressure to higher pressure under certain conditions is called pumping. For the explanation of this characteristic let us view the following:

Positive and negative pumping

The pumping is called positive or negative depending on whether the mean flow rate is positive or negative.

Peristaltic pumping

It is the situation in which pumping is positive and pressure gradient is adverse (i.e. pressure rise per wavelength (ΔP_λ) is positive).

Augmented pumping

It occurs when pumping is positive but in this case pressure gradient is favorable (i.e. pressure rise per wavelength (ΔP_λ) is negative).

Retrograde pumping

It is the situation in which pumping is negative and the pressure gradient is adverse.

Free pumping

The situation where pumping is positive but pressure gradient is neither adverse nor favorable. In other words pressure rise per wavelength (ΔP_λ) vanishes i.e., $\Delta P_\lambda = 0$.

1.1.5 Free pumping flux

It is defined as the critical value of mean flow rate corresponding to free pumping.

1.1.6 Bolus

It is defined as a volume of fluid bounded by closed streamline in the frame moving with the wave speed.

1.1.7 Trapping

In general the shape of streamline is similar to that of the boundary wall in the wave frame. However, under certain conditions some of the streamlines split and enclose a bolus, which is pushed ahead alongwith the peristaltic wave with the wave speed. This phenomenon is known as trapping.

1.2 Basic concepts of heat and mass transfer

1.2.1 Heat

It is the form of energy that can be transferred from one system to another as a result of temperature difference.

1.2.2 Conduction

It can be defined as the transfer of energy from the more energetic particles of a substance to the adjacent less energetic ones as a result of the interaction between the particles with no

movement of material.

1.2.3 Convection

It is the mode of heat transfer between a surface and the adjacent fluid that is in motion and it involves the combined effects of conduction and fluid motion.

Natural Convection

If the fluid motion occurs as a result of the density difference produced by the temperature difference, the process is called free or natural convection. In case of free convection flow is generated by the body forces that occurs as a result of the density changes arising from the temperature changes in the whole fluid. These body forces are actually generated by pressure gradients imposed on the whole fluid. The most common source of this imposed pressure field is gravity. The body forces in this case are usually termed bouyancy forces. Without the existence os gravity and thermal expansion coefficient, natural convection would not be possible.

Forced Convection

Convection is called forced convection if the fluid is forced to flow over the surface by external means such as fan, pump or the air. The term forced convection is only applied to flows in which the effects of the buoyancy forces are negligible.

1.2.4 Radiation

It is the energy emitted by the matter in the form of electromagnetic waves (or photons). Heat transfer by radiation does not require a material in which to propagate and can travel through vacuum.

1.2.5 Specific Heat

It is defined as the amount of energy needed to increase the temperature of one kilogram by one degree Celsius

1.2.6 Thermal Conductivity

It is the measure of the ability of a material to conduct heat and is designated by k. A substance with a large value of k is a good thermal conductor, whereas a substance with a small value of k is a poor thermal conductor or a good thermal insulator.

1.2.7 Thermal Diffusivity

It is defined as the ratio of the heat conducted through the material to the heat stored per unit volume. The larger the thermal diffusivity, the faster the propagation of heat into the medium. A small value of thermal diffusivity means that heat is mostly absorbed by the material and a small amount of heat will be conducted further.

1.2.8 Boussinesq Approximation

In Boussinesq approximation, which is appropriate for an almost incompressible fluid, it assumed that the variations of density are small, so that in the inertial terms, and in the continuity equation, we may substitute $\rho \rightarrow \rho_0$, a constant. However, even weak density variations are important in buoyancy and so we retain variations in ρ in the buoyancy term in the vertical equation of motion. We define the buoyancy as

$$b = g(\rho_0 - \rho)/\rho_0$$

1.3 Dimensionless Numbers

1.3.1 Reynold's number

It is interpreted as the ratio of inertial forces to the viscous forces and is denoted by Re. It is the most important dimensionless number in fluid dynamics because it is used for determining whether a flow will be laminar or turbulent. Laminar flow occurs at low Reynolds number where viscous forces are dominant and is characterized by smooth fluid motion while turbulent flow occurs at high Reynolds number and is dominant by inertial forces, producing random eddies, vortices and other flow fluctuations.

1.3.2 Wave Number

It is interpreted as the ratio of the width of the channel to the wavelength. Usually, it is denoted by the Greek symbol δ and is

$$\delta = \frac{L}{\lambda}, \tag{1.1}$$

where L is the characteristic length and λ is the wavelength.

1.3.3 Prandtl number

The relative thickness of the velocity and thermal boundary layers is best described by the dimensionless parameter, Prandtl number, defined by

$$\mathrm{Pr} = \frac{\text{Molecular diffusivity of momentum}}{\text{molecular diffusivity of heat}} = \frac{\nu}{\alpha_1} = \frac{\eta C_p}{k} \tag{1.2}$$

where ν is the kinematic viscosity, α_1 is the thermal diffusivity, C_p is the specific heat, η is the dynamic viscosity and k is the thermal conductivity. The Prandtl number of gases is about unity, which indicates that both momentum and heat dissipate through the fluid at about the same rate.

Heat diffuses very quickly in liquid metals ($\mathrm{Pr} \ll 1$) and very slowly in oils ($\mathrm{Pr} \gg 1$) relative to momentum. Consequently the thermal boundary layer is much thicker for liquid metals and much thinner for oils relative to the velocity boundary layer.

1.3.4 Eckert number

This number expresses the relation between kinetic energy of flow and enthalpy and is designated by Ec or E. This number only enters the problem when the viscous dissipation term in the energy equation is significant.

1.3.5 Brinkman number

This is interpreted as the ratio of the viscous dissipation to the heat transfer rate. This number is important in cases where large velocity changes occur over short distances such as lubricant flow. It is denoted by Br.

1.3.6 Soret and Dufour numbers

When heat and mass transfer occur simultaneously in a moving fluid, an energy flux can be generated not only by temperature gradient but by composition gradient also. The energy flux caused by a composition gradient is termed Dufour or diffusion-thermo effect. On the other hand, mass fluxes can also be created by temperature gradients and this embodies the Soret or thermo-diffusion effect. Such effects are significant when density differences exist in the flow regime. For example, when species are introduced at a surface in a fluid domain, with a different (lower) density than the surrounding fluid, both Soret and Dufour effects can become influential. Soret and Dufour effects are important for intermediate molecular weight fluids in coupled heat and mass transfer in fluid binary systems, often encountered in biophysical processes.

1.3.7 Deborah number

Whether a viscoelastic material behaves as an elastic solid or a viscous liquid depends on the material response time and its relation to the time scale of the experiment or observation. This was first proposed by Marcus Reiner, who defined the ratio of the material response time to the experimental time scale as the Deborah number, De. That is,

$$De = \frac{material\ response\ time}{\exp erimental\ time\ scale\ (Observation\ time)} \tag{1.3}$$

A high Deborah number that is long response time relative to the observation time implies viscoelastic solid behavior, whereas a low value of Deborah number (short response time relative to the time scale of the experiment) is indicative of viscoelastic fluid behavior. From conceptual standpoint, the Deborah number is related to the time one must wait to observe the onset of flow or creep.

1.3.8 Grashof number

The Grashof number is defined as

$$Gr_t = \frac{gL^3\beta_2\Delta T\rho^2}{\eta^2} \tag{1.4}$$

is a measure of natural or free convection. The meaning of this number follows from the meaning of symbols given here: g is the acceleration due to gravity, ρ is density, β_2 is coefficient of volume expansion, ΔT is the temperature gradient in Kelvin which induces density variations. Density variations are also known as buoyancy forces, because they cause macroscopic (bulk) motion of the fluid. This motion is known as natural or free convection. Thus natural convection will be enhanced by buoyancy forces (the numerator of Gr_t ratio) and decreased by viscous forces (the denominator of Gr_t ratio). It is the ratio of natural convection buoyancy force to the viscous force. It controls the ratio of length scale to natural convection boundary layer thickness.

1.3.9 Bingham number

It is proportional to (yield stress/viscous stress) and is used in momentum transfer in general and calculations in particular. It is normally defined in the following form:

$$Bn = \frac{\tau_0 L}{\eta v} \tag{1.5}$$

where τ_0 is the yield stress, L is the characteristic length and v is the fluid velocity.

1.3.10 Schmidt number

It characterizes the relative effectiveness of momentum and mass transport by diffusion, higher value of Schmidt number lead to species diffusivity rate exceed the momentum diffusivity which diminish concentration in boundary layer. This number plays a role in mass transfer that is analogous to that played by the Prandtl number in heat transfer

1.3.11 Nusselt number

It is defined as the ratio of length scale to the thermal boundary layer thickness. It is used to calculate the heat transfer coefficient. The Nusselt number represents the enhancement of heat transfer through a fluid layer as a result of convection relative to conduction across the same fluid layer. The larger the Nusselt number, the more effective the convection. A Nusselt number of $N = 1$ for a fluid layer represents heat transfer across the layer by pure conduction.

1.3.12 Amplitude Ratio

It is defined as the ratio of amplitude of the wave to either half width of the channel or radius of the tube. It is usually denoted by ϕ.

1.3.13 Slip Parameter

The condition that the relative velocity between the fluid and that of the wall being proportional to the shearing rate at the walls is called slip condition. Mathematically,

$$U_f - U_w = \pm \frac{\beta_1}{\eta} \tau_{xy} \tag{1.6}$$

where U_f is the velocity of fluid, U_w is the velocity of wall and $\beta \geq 0$ is the dimensional slip parameter and has the dimension of length. The plus $(+)$ and minus $(-)$ signs are due to the direction of the normal on the wall.

Although no-slip condition plays a vital role in the Navier-Stokes theory but there are problems where it does not hold. For instance a large class of polymeric materials slip on the solid boundaries. It is important in the polishing of artificial heart valves, internal cavities in a variety of manufactured parts and in applications where a thin film of light oil is attracted to the moving walls.

1.4 Basics of Bifurcation theory

1.4.1 Autonomous system

A system of differential equations $\overset{\bullet}{\overline{X}} = f(\overline{X})$ for $\overline{X} \in \mathbb{R}^n$, is called an autonomous system.

1.4.2 Nonautonomous system

Any system of differential equations $\overset{\bullet}{\overline{X}} = f(\overline{X}, \bar{t})$ for $\overline{X} \in \mathbb{R}^n$, is called a nonautonomous system. Moreover, any nonautonomous system can be written as an autonomous system with $\overline{X} \in \mathbb{R}^{n+1}$ simply by letting $x_{n+1} = t$ and $\overset{\bullet}{x}_{n+1} = 1$.

1.4.3 Equilibrium point

A point $\overline{X}_0 \in \mathbb{R}^n$ is called an equilibrium point or critical point of $\overset{\bullet}{\overline{X}} = f(\overline{X})$ if $f(\overline{X}_0) = 0$.

1.4.4 Hyperbolic Equilibrium point

An equilibrium point is called hyperbolic equilibrium point of $\overset{\bullet}{\overline{X}} = f(\overline{X})$ if none of the eigenvalues of the Jacobian matrix have zero real part.

1.4.5 Classification of the equilibrium point based on eigenvalues

1. An equilibrium point is called Sink if all the eigenvalues of Jacobian have negative real part.

2. Eqilibrium point is called Source if all of the eigenvalues of Jacobian matrix have positive real part.

3. Equilibrium point is called Saddle if it is hyperbolic equilibrium point and Jacobian has atleast one eigenvalue with positive real part and atleast one eigenvalue with negative real part.

1.4.6 Linearization

The linearization of a nonlinear system

$$\overset{\bullet}{\overline{X}} = f(\overline{X}) \tag{1.7}$$

is

$$\overset{\bullet}{\overline{X}} = \mathbf{C}\overline{X} = \left(Df(\overline{X}_0)\right)\overline{X} \tag{1.8}$$

1.4.7 Topological equivalence of local behavior of linear and nonlinear systems

If $\overline{X}_0$ is a hyperbolic equilibrium point of nonlinear system (1.7) then the local behavior of the nonlinear system (1.7) is topological equivalent to the local behavior of the linear system

(1.8) that is there is a continuous one-to-one map of a neighborhood of $\overline{X}_0$ onto an open set U containing the origin.

1.4.8 Bifurcation Theory

It is the mathematical study of changes in the qualitative or topological structure of a given family, such as the integral curves of a family of vector fields, and the solutions of a family of differential equations. Most commonly applied to the mathematical study of dynamical systems, a bifurcation occurs when a small smooth change made to the parameter values (the bifurcation parameter) of a system causes a sudden qualitative or topological change in its behavior. The name "Bifurcation" was first introduced by Henri Poincare in (1885) in the first paper in mathematics showing such a behavior. He also later named various types of stationary points and classified them.

1.4.9 Types of bifurcation

Local bifurcation

A local bifurcation occurs when a parameter change causes the stability of an equilibrium point. In continuous system, this corresponds to the real part of an eigenvalue of an equilibrium point passing through zero. In this case the equilibrium point is nonhyperbolic at the bifurcation point. The topological changes in the phase portraits of the system can be confined to arbitrarily small neighborhoods of bifurcation points by moving the bifurcation parameter close to the bifurcation point. Technically, consider dynamical system described by the ordinary differential equation

$$\dot{x} = f(x, \lambda), \quad f : \mathbb{R}^n \times \mathbb{R} \to \mathbb{R}^n \tag{1.9}$$

A local bifurcation occurs at (x_0, λ_0) if the Jacobian $J|_{(x_0,\lambda_0)}$ has an eigenvalue with zero real part. If the eigenvalue is zero, the bifurcation is a steady state bifurcation, but if the eigenvalue is non-zero but purely imaginary, this is a Hopf bifurcation.

Global bifurcation

Global bifurcations occur when large invariant sets, such as periodic orbits, collide with eqilibria. This causes changes in the topology of the trajectories in the phase space which cannot be confined to a small neighborhood, as in the case with local bifurcations. In fact the changes in the topology extend out to an arbitrarily large distance (hence global).

1.4.10 Co-dimension of a bifurcation

The co-dimension of a bifurcation is the number of parameters which must be varied for the bifurcation to occur. This corresponds to the co-dimension of parameter set for which the bifurcation occurs within the full space of parameters. Saddle-node bifurcations and Hopf bifurcations are the only generic local bifurcations which are really co-dimension one. The others all having higher co-dimension. However, Transcritical and Pitchfork bifurcations are also often thought of as co-dimension one, because the normal forms can be written with only one parameter. An example of a well studied co-dimension two bifurcation is the Bogdanov-Takens bifurcation.

1.4.11 Streamline topology

The study of fluid flow patterns given in terms of streamlines is called topological fluid dynamics and this context we denote a streamline fluid flow patterns in phase space as a flow, a flow topology, a streamline topology or simply a topology.

1.4.12 Separatrix

The flow on simple closed curve determined by the union of holoclinic orbit and the equilibrium point at the origin is called a Separatrix or Separatrix cycle.

1.4.13 Homoclinic orbit

A homoclinic orbit is a trajectory of a flow of a dynamical system which joins a saddle equilibrium point with itself.

1.4.14 Heteroclinic orbit

A heteroclinic orbit or a heteroclinic connection is a path in phase space which joins two different equilibrium points.

Phase Portrait

If we know the value of x at $t = 0$, we have an initial value problem

$$\overset{\bullet}{x} = f(x), \quad x(0) = x_0$$

where x_0 is the known value. When we plot the change in x during time we have an orbit. All the orbits together with the direction of arrows gives a phase portrait.

1.4.15 Structural Stability

Let E^1 be an open subset of $\mathbb{R}^n$. A vector field $f \in C^1(E^1)$ is said to be structurally stable if there is $\epsilon > 0$ such that $\forall\ I \in C^1(E^1)$ with

$$\|f - I\|_1 < \epsilon$$

f and I are topologically equivalent on E^1; i.e., there is a homeomorphism $H_1 : E^1 \to E^1$ which maps trajectories of (1) onto trajectories of $\overset{\bullet}{\overline{X}} = g(\overline{X})$ and preserves their orientation by time. In this case we also say that the dynamical system (1) is structurally stable. If a vector field $f \in C^1(E^1)$ is not structurally stable, then f is said to be structurally unstable. And $\|\cdot\|_1$ is defined by

$$\|f\|_1 = \max_{x \in K} \left|f(\overline{X})\right| + \max_{x \in K} \left\|Df(\overline{X})\right\|$$

where K is a compact subset of E^1.

1.4.16 Bifurcation value

The qualitative behavior of the solution set of a system (3) depending on a parameter $\lambda \in \mathbb{R}$ changes as the vector field f passes through a point in the bifurcation set or as the parameter λ varies through a bifurcation value λ_0. A value λ_0 of the parameter λ in Eq. (3) for which the C^1-vector field $f(x, \lambda_0)$ is not structurally stable is called bifurcation value.

1.4.17 Some important theorems

The Stable manifold Theorem:

It is one of the most important results in the local qualitative theory of ordinary differential equations. The theorem shows that near a hyperbolic equilibrium point $\overline{X}_0$, the nonlinear system (1) has stable and unstable manifolds S and U tangent at $\overline{X}_0$ to the stable and unstable subspaces E^s and E^u of the linearized system (2). Furthermore, S and U are of the same dimensions as E^s and E^u, and if $\phi_t = e^{At}$ is the flow of nonlinear system (2), then S and U are positively and negatively invariant under ϕ_t respectively and satisfy

$$\begin{aligned} \lim_{t\to\infty} \phi_t(c) &= \overline{X}_0 \quad \forall c \in S \\ \lim_{t\to-\infty} \phi_t(c) &= \overline{X}_0 \quad \forall c \in U \end{aligned}$$

Theorem

Let E^1 be an open subset of R^n containing the origin, let $f \in C^1(E^1)$, and let ϕ_t be the flow of the nonlinear system (1). Suppose that $f(0) = 0$ and that $Df(0)$ has m eigenvalues with negative real part and $n - m$ eigenvalues with positive real part. Then there exists a k-dimensional differentiable manifold S tangent to the stable subspace E^s of linear system (2) at 0 such that for all $t \geqslant 0, \phi_t(S) \subset S$ and for all $\overline{X}_0 \in S$

$$\lim_{t\to\infty} \phi_t(\overline{X}_0) = 0;$$

and there exists an $n-m$ dimensional differentiable manifold U tangent to the unstable subspace E^u of (2) at 0 such that for all $t \leqslant 0, \phi_t(U) \subset U$ and for all $\overline{X}_0 \in U$,

$$\lim_{t\to-\infty} \phi_t(\overline{X}_0) = 0.$$

The Hartman-Grobman Theorem

It is another very important result in the local qualitative theory of ordinary differential equations. The theorem shows that near a hyperbolic equilibrium point $\overline{X}_0$, the nonlinear system (1) has the same qualitative structure as the linear system (2).

Theorem

Let E^1 be an open subset of R^n containing the origin, let $f \in C^1(E^1)$, and let ϕ_t be the flow of the nonlinear system (1). Suppose that $f(0) = 0$ and that the matrix $C = Df(0)$ has no eigenvalue with zero real part. Then there exists a homeomorphism H_1 of an open set U containing the origin onto an open set V containing the origin such that for each $\overline{X}_0 \in U$, there is an open interval $I_0 \subset \mathbb{R}$ containing zero such that $\forall \overline{X}_0 \in U$ and $t \in I_0$

$$Ho\phi_t(\overline{X}_0) = e^{At} H_1(\overline{X}_0);$$

that is H_1 maps trajectories of (1) near the origin onto trajectories of (2) near the origin and preserves the parametrization by time.

1.5 Governing equations for fluid motion

In order to describe the physical behavior of the fluid flow, one needs to have some mathematical relations. In fluid mechanics, we have three basic laws which account for the motion of the fluid and those are recognized as law of conservation of mass, momentum and energy. These laws in their mathematical form gives the relations for rate of change of mass, momentum and energy at a point and are in subsection heads as following

1.5.1 Continuity equation

A continuity equation is an equation that describes the transport of a conserved quantity. Since mass, energy, momentum, electric charge and other natural quantities are conserved under their respective appropriate conditions, a variety of physical phenomena may be described using continuity equations.

For the conservation of mass, mass of the closed system always remains constant with time, as mass of the system cannot change quantity except being added or removed. It means that the quantity of mass is conserved over time. The mathematical relation expressing law of conservation of mass is known as continuity equation. For compressible fluid, it is defined as

$$\frac{d\rho}{d\bar{t}} + \rho \boldsymbol{\nabla}.\mathbf{V} = 0, \tag{1.10}$$

here ρ is the fluid density, $d/d\bar{t}$ is the material time derivative and $\mathbf{V}$ is the velocity field. The material time derivative is defined as

$$\frac{d}{d\bar{t}} = \frac{\partial}{\partial\bar{t}} + \mathbf{V}.\boldsymbol{\nabla}. \tag{1.11}$$

In view of Eq. (1.11), Eq. (1.10) takes the following form

$$\frac{\partial\rho}{\partial\bar{t}} + \boldsymbol{\nabla}.\rho\mathbf{V} = 0. \tag{1.12}$$

For an incompressible fluid, it reduces to

$$\boldsymbol{\nabla}.\mathbf{V} = 0. \tag{1.13}$$

1.5.2 Momentum equation

The momentum balance for a differential fluid element reads

$$\rho\frac{d\mathbf{V}}{d\bar{t}} = \nabla.\overline{\mathbf{T}} + \rho\mathbf{f}, \tag{1.14}$$

where $\overline{\mathbf{T}}$ is the Cauchy stress tensor and $\mathbf{f}$ denotes the body force vector.

1.5.3 Energy equation

The energy equation for fluid is defined by

$$\rho C_p\frac{dT}{d\bar{t}} = k\nabla^2 T + \overline{\mathbf{T}}.(\nabla\mathbf{V}) + Q \tag{1.15}$$

where T is the temperature and Q is the constant heat source/sink term.

1.5.4 Concentration equation

The energy equation for fluid is defined by

$$\rho\frac{dC}{d\bar{t}} = \rho D^*\nabla^2 C + \frac{\rho D^* k_T}{\Delta T}\nabla^2 T - \rho k_1 (C - C_0) \tag{1.16}$$

where C is the concentration D^* is the coefficient of mass diffusivity, k_T is the thermal diffusion ratio and k_1 is the chemical reaction parameter.

1.6 Literature Review

The study of peristaltic motion using the principles of fluid dynamics was initiated by Latham [1]. Later several researchers investigated the peristaltic motion under various assumptions. Generally, it is assumed that the flow is laminar, incompressible and two-dimensional. The geometry of the vessel is assumed to be either an axisymmetric tube, a planar channel or a curved channel. The fluid inside the vessel is assumed to obey Newtonian or Non-Newtonian constitutive law. Further, assumptions are made regarding the magnitudes of Reynolds number and wave number, commonly known as long wavelength and low Reynolds number assumptions. The continuity and momentum equations are sufficient to model the peristaltic flow under the above mentioned assumptions. However, if it is assumed that flow is under non-isothermal condition with non-zero concentration gradients, then energy and mass concentration equation are also utilized along with continuity and momentum equations. The brief review of literature on peristaltic motion of Newtonian and non-Newtonian fluids with and without heat/mass transfer effects is presented below.

1.6.1 Peristaltic transport of Newtonian fluids

Initial theoretical studies on peristaltic transport were carried out using Newtonian fluids. Though limited in scope, such attempts were quite relevant to understand the transport of urine from kidney to the bladder. A two-dimensional model of peristaltic motion under negligible inertia and small wave number was investigated by Shapiro [2]. A closed form solution of the flow problem was developed under the specified assumptions. A correlation between the theoretical and experimental results was presented by Shapiro and Latham [3] and Weinberg [4]. Shapiro et al. [5] investigated the peristaltic motion of viscous fluid in a planar channel and cylindrical tube using wavelength and vanishing Reynolds number approximations. A perturbation solution of the peristaltic flow in a planar channel was reported by Jaffrin [6] for small wave number. The realistic mathematical model representing the peristaltic flow in ureter was suggested by

Lykoudis and Roos [7] and Weinberg et al. [8]. An unsteady analysis of peristaltic motion in fixed frame of reference for arbitrary Reynolds and wave numbers was presented by Fung and Yih [9]. The dynamics of ureteral muscle was integrated in the study of peristaltic flow by Fung [10]. A review of earlier literature on peristalsis according to the assumptions on the geometry and flow was presented by Jaffrin and Shapiro [11]. Numerical simulations of two-dimensional peristaltic channel flow using finite difference method were carried out by Browns and Hung [12] and Takabatake and Ayukawa [13]. Later Takabatake et al. [14] also provided the computational results for axisymmetric case. The finite element simulations of two-dimensional peristaltic flow in a planar channel were presented by Kumar and Naidu [15]. Srivastava and Srivastava [16] discussed peristaltic motion of Newtonian fluid with superimposed pulsatile flow in a circular cylindrical tube. The solution was constructed for small amplitude ratio. Afifi and Gad [17] extended the results of ref. [16] by including the additional forces due to magnetic field and porous medium. Recently, physiologists have noted that peristaltic mechanism is involved in the fluid flow induced by myometrial contractions. Moreover, it is also noted that the myometrial contraction may occur in both symmetric and asymmetric direction [18]. Apart from that the study carried out by Eytan et al. [19] revealed that the characterization of non-pregnant women uterine contractions is very complicated as they are composed of variable amplitudes, a range of frequencies and different wavelengths. They confirmed that the width of the sagittal cross-section of the uterine cavity increase towards the fundus and the cavity is not fully occluded during the contractions. Based on these observations Eytan and Elad [20] modeled the flow in the uterine cavity as peristaltic flow in a planar channel with wave trains of different phase propagating on the upper and lower walls. They employed lubrication approximation in finding the solution. Mishra and Rao [21] analyzed the peristaltic flow of Newtonian fluid in an asymmetric channel under long wavelength and low Reynolds number assumptions. Naby et al. [22] studied the influence of inserted endoscope and fluid with variable viscosity on the peristaltic motion under the assumption of zero Reynolds number. Hayat and Ali [23] discussed the effects of variable viscosity on the peristaltic flow of a Newtonian fluid in an asymmetric channel. Elnaby and Haroun [24] presented the two-dimensional analysis of peristaltic motion to include the compliant wall effects. A detailed discussion of peristaltic flow of viscous fluid through a porous space in an asymmetric channel was made by Elshehawey et al.

[25]. They obtained the explicit expression for stream function using Adomian decomposition method. They showed that for high permeability parameter their results are in agreement with Mishra and Rao [21]. The influence of slip condition on a hydromagnetic viscous flow in an asymmetric channel was analyzed by Ebaid [26]. Ali et al. [27] studied the effects of magnetic fluid, slip condition and variable viscosity on peristaltic motion of viscous fluid. Peristaltic flow of magnetohydrodynamic (MHD) viscous fluid in an inclined asymmetric channel was discussed by Sirinivas and Pushparaj [28]. The effects of channel curvature on peristaltic motion of Newtonian fluid are analyzed by Sato et al. [29] and Ali et al. [30]. Ramanamurthy et al. [31] presented a generalized mathematical model describing the unsteady peristaltic transport of viscous fluid in a two-dimensional curved channel. The flow is investigated in the laboratory frame of reference.

Heat transfer is an important principle in biological systems and industrial fluid transport. One of the most important functions of the cardiovascular system is to maintain the temperature of the body. Also air entering the lungs must be warmed (or cooled) to body temperature. This is accomplished through all blood vessels. There are three mechanisms of heat transfer but the convection is the most applicable heat transfer modality within the circulation of fluid in human body. Study of the combined effects of heat and mass transfer has been attracting the attention of many researchers due to its applications in engineering and sciences. Some physical examples include drying of porous solid, thermal insulation, cooling of nuclear reactors and underground energy transport, geothermal energy recovery, oil extraction and thermal energy storage. Combined heat and mass transfer with chemical reaction also plays an important role in design of chemical processing equipment, in formation and dissipation of fog, in metabolic processes, in resorting of human body to heat and mass for its temperature control due to change in weather conditions. Convective heat transfer is used by human and animal bodies to loose the heat generated by metabolic processes to the environment. Thermodynamic aspects of blood becomes important in the processes such as oxygenation and hemodialysis when blood is drawn out of the body. The industrial applications include the thermal insulation, cooling of nuclear reactors, oil extraction and thermal energy storage. The process of heat transfer and fluid flow seem to pervade all aspects of our life. Due to great importance of heat and mass transfer in different areas of engineering and sciences, especially in physiological fluid flows,

interests and contributions of researchers are growing fastly in peristaltic flows. Vajravelu et al. [32] initiated the study of heat transfer in peristalsis. Srinivas et al. [33] studied the combined effects of slip and wall properties on MHD non-isothermal peristaltic transport in a planar channel. Hayat et al. [34] developed closed form solutions for stream function and temperature field for non-isothermal hydromagnetic peristaltic flow in a fluid-saturated porous channel. They have simplified their modeled problem by using the long wavelength approximation. Perturbation method is used to find the solution of the velocity and temperature fields. A similar analysis with mixed convective heat transfer in an annulus has been given by Mekheimer and Elmaboud [35]. They considered MHD fluid and discussed the problem by ignoring the viscous dissipation effects. They got such a simplified form of their problem that all the desired expressions were obtained analytically. Nadeem and Akbar have extended the work [35] by considering the temperature dependent viscosity [36]. Hina et al. [37] considered peristaltic flows of Newtonian fluid by incorporating the natural convection, viscous dissipation and chemical reaction. Mustafa et al. [38] has thrown a light on the effects of viscous dissipation along with Soret and Dufour in mixed convective peristaltic flow of nanofluid. Hayat and Asghar [39] have extended [27] by carrying out heat transfer analysis. Slip effects with wall properties and heat transfer has also been analyzed by Sirinivas et al. [40]. The effects of variable viscosity on hydromagnetic peristaltic flow in a tube were discussed by Ebaid [41] by employing Adomian decomposition method. Comparison of the results was made with the corresponding results obtained by perturbation method. Combined effects of heat and mass transfer are reported by Srinivas and Kothandapani [42] and Srinivas and Muthuraj [43]. The effects of channel curvature on heat transfer characteristics in flow of Newtonian fluid due to peristalsis were discussed by Ali et al. [44].

1.6.2 Literature Review for Non-Newtonian Fluids

The study of non-Newtonian fluids has received special attention of researchers for last few years. This is because of the fact that most of the real fluids occuring in physiology and industry are non-Newtonian. Blood, chyme, mixed form of foodstuff, cervical mucus and bile are some examples of non-Newtonian biofluids. Other examples of non-Newtonian fluids are polymeric liquids, drilling muds, saliva, synovial fluid found in joints and slurries. Unlike the Newtonian

fluids there is no any single constitutive equation that describes the behavior of Non-Newtonian fluids. Therefore several constitutive equations have been used in the literature to capture various non-Newtonian effects. Peristaltic motion of non-Newtonian fluids was initiated by Raju and Devanathan [45]. They used the power-law model to characterize the non-Newtonian rheology. In continuation, they carried out the analysis of peristaltic motion for a simple fluid with fading memory [46]. Bohme and Friedrich [47] examined the peristaltic transport of viscoelastic fluid with integral constitutive equation. Peristaltic motion of a micropolar fluid was analyzed by Devi and Devanathan [48]. They followed the small wave amplitude assumption in their analysis. Srivastava and Srivastava [49] investigated the peristaltic flow of blood using Casson model. The study of peristaltic motion of second order fluid in planar channel and axisymmetric tube was carried out by Siddiqui et al. [50] and Siddiqui and Schwarz [51] , respectively. Siddiqui and Shwarz [52] also studied peristaltic motion for third order fluid under the approximations of long wavelength and low Reynolds number. Hayat et al. [53] extended the flow analysis presented in ref. [52] for axisymmetric case. They solved the governing equation both analytically and numerically. The viscoelastic effects in peristaltic motion using the constitutive equation of Johnson-Segalman fluid were also analyzed by Hayat et al. [54]. Srinivasacharya et al. [55] analyzed the peristalsis of a micropolar fluid is a circular tube by taking small Reynolds number and long wavelength considerations. The influence of wall properties on the peristaltic flows in channel/tube has been studied by Muthu et al. [56]. Mishra and Rao [57] studied the peristaltic motion of power law fluid in an axisymmetric porous tube under long wavelength and low Reynolds number assumptions. They discussed the trapping and reflux phenomena for various parameters of interest that governs the flow. The influence of stress relaxation and retardation on peristaltic transport was studied by Hayat et al. [58] using Oldroyd-B model. Elshahed and Haroun [59] extended the ref. [54] by including magnetohydrodynamics effects. Hakeem et al. [60] discussed the axisymmetric flow of generalized Newtonian MHD fluid by considering the power law model. They used perturbation method in terms of small Hartmann number and used numerical integration to discuss the pressure rise per wavelength and frictional forces.A closed form solution for peristaltic flow of power law fluids under the assumptions of long wavelength and low Reynolds number was presented Hayat and Ali [62] . An extension of results presented in ref. [60] for asymmetric

channel was given by Reddy et al. [63]. Perturbation solution for the peristaltic flow of Carreau fluid was obtained by Ali and Hayat [64]. Hayat et al. [65, 66] provided the solution for MHD peristaltic motion of third and fourth order fluids in planar channel. The peristaltic flow analysis of third and fourth order fluid using regular perturbation method in asymmetric channel was presented by Haroun [67, 68]. The effects of wall slip on peristaltic motion of third order fluid in an asymmetric channel were explored by Hayat et al. [69]. Hayat et al. [70] have also analyzed the Hall effects on MHD peristaltic flow of Maxwell fluid in a porous medium . Wang et al. [71] numerically simulated the peristaltic flow of Johnson-Segalman fluid in a deformable tube. Unsteady peristaltic flow analysis in an axisymmetric tubular vessel by using power law model was presented by Ikbal et al. [72]. MHD peristaltic transport of Sisko fluid in symmetric and asymmetric channels was investigated by Wang et al. [73]. Hayat et al. [74] extended their previous analysis [54] for Johnson-Segalman fluid to include the effects of asymmetry of the channel. An analysis for peristaltic flow of Jeffrey fluid in an asymmetric channel under the influence of magnetic field was carried out by Kothandapani and Srinivas [75]. Hayat et al. [76] explained the effects of wall properties on peristaltic flow of Johnson-Segalman fluid. The effects of an inserted endoscope and variable viscosity on peristaltic motion were also studied by Hayat et al. [77]. The influence of inclined magnetic field on peristaltic flow of Williamson fluid was analyzed both in symmetric and asymmetric channel by Nadeem and Akram [78] . A similar analysis for fourth grade fluid was provided by Hayat et al. [79]. Pandey and Tripathi [80] discussed the peristaltic flow of Casson fluid in a finite length channel. Tripathi et al. [81] studied the interaction of viscoelasticity with peristaltic flow by taking fractional Maxwell model. A mathematical model for intestinal peristaltic flow of power law fluids with multilayers and distinct viscosities was developed by Pandey et al.[82]. The effects of permeability of porous medium on peristaltic flow of second order fluid was discussed by Elmaboud and Mekheimer [83] . Tripathi et al. [84] studied peristaltic motion of generalized Burger's fluid as a model of intestinal fluid transport. Vajravelu et al. [85] has discussed the peristaltic transport of Williamson fluid. They have analyzed the problem in an asymmetric channel with permeable walls. An unsteady peristaltic flow of Maxwell fluid was investigated by Padey and Tripathi [86]. The flow was considered in a finite length tube. The dynamic boundary condition due to compliant wall was imposed on peristaltic flow of Maxwell fluid by Hina et al. [87]. They

have made analysis in an asymmetric channel. A numerical investigation of two-dimensional peristaltic flow of viscoelastic Oldroyd-B fluid using boundary immersed technique was carried out by Ceniceros and Fisher [88]. El-Sayed et al. [89] have disclosed the effects of plasticity on peristaltic motion by considering Bingham model. In addition they also examined the effects of slip and temperature jump condition in an eccentric annuli. An investigation of unsteady peristaltic flow in digestive system by considering couple stress bio-fluid was made by Tripathi and Beg [90]. Analytical and numerical investigation for the peristaltic flow of Johnson-Segalman fluid through an axisymmetric tube with endoscope was carried out by Akbar and Nadeem [91]. Simultaneous effects of heat transfer and wall properties on peristaltic flow of Burger's fluid was analyzed by Javed et al. [92]. A study of chyme dynamics through a diseased intestine was carried out by Tripathi and Beg [93]. The Burgers' constitutive equation was used to represent the rheology of chyme fluid through uniform porous medium. Hayat et al. [94] analyzed the problem of peristaltic transport of Johnson-Segalman fluid with nanoparticles. Abo-Dahab and Abd-Alla [95] discussed the peristaltic flow of Jeffrey fluid in an asymmetric channel. They focused on the effects of magnetic field and rotation. Tripathi et al. [96] developed a mathematical model using fractional Oldroyd-B model for bio-fluid transport due to peristalsis. The analysis was made in a two-dimensional asymmetric porous-saturated channel. Nadeem and Akbar [97, 98] investigated the effects of heat transfer in peristaltic flow of Johnson-Segalman fluid and Herschel-Bulkley fluid in a non-uniform tube. Hayat et al. [99] extended the ref. [64] by performing the heat transfer analysis. The effects of heat transfer on peristaltic transport of Jeffrey fluid through a vertical porous stratum were highlighted by Vajravelu et al. [100]. The temperature and concentration variations in peristaltic annular flow of Eyring-Powell fluid were shown graphically by Akbar and Nadeem [101] . They have also discussed the effects of thermal and velocity slip [102] on peristaltic flow of Jeffrey 6-constants fluid. Mehmood et al. [103] have extended the flow analysis in ref. [80] by including heat transfer effects. The peristaltic flow of viscoelastic Jeffrey fluid through a channel with heated wall was investigated by Tripathi et al. [104]. They showed that less pressure is needed to propel the food bolus with high magnitude of Jeffrey parameter. Vajravelu et al. [105] examined the heat transfer characteristics in peristaltic transport of Herschel–Bulkley Fluid in an elastic tube. Ali et al. [106, 107] studied the peristaltic flow of third order and micropolar fluids through curved

channel. Peristaltic transport of Eyring–Powell fluid through a curved channel is examined by Abbasi et al. [108]. Recently Hayat et al. [109] investigated the peristaltic transport of Carreau fluid through a curved channel. Further recent investigation on peristaltic flow in a curved channel are made by Hina et al. [110], Hayat et al. [111, 112], Javid et al. [113] Ali [114] . Peristaltic flows of non-Newtonain nanofluids has also received great interest of the researchers. This is because of diverse applications in engineering, medical and electrical appliances. For further details, the reader is referred to refs. [115 – 124].

Topological fluid dynamics is a mathematical discipline that studies topological features of flows with complicated trajectories and their applications to fluid motions and develops group-theoretic and geometric points of view on various problems of hydrodynamical origin. It is situated at crossroads of several disciplines, including Lie group, knot theory, integrable systems and geometric inequalities. The intrusion of topological ideas in fluid mechanics goes back to seminal work of Helmholtz [125] and Kelvin [126] who established that in inviscid flow governed by Euler equation, vortex lines more with the fluid or as we might now say are 'Frozen in Fluid'. The qualitative approach on streamline patterns using the theory of dynamical systems is not a new idea in the field of fluid mechanics because a number of contributions have been made in the far past. Particularly, the early works on separation was done by Oswatitsch, Davey and Lighthill [127 – 129]. Hunt et al. [130] discussed the flow around obstacles by applying the topology to flow visualization. Brons and Hartnack [131] analyzed the streamline topologies and their bifurcations near simple degenerate critical points for two dimensional viscous incompressible flows away from the boundaries. They have used normal forms coefficients to discuss the bifurcations. Such a study near non-simple degenerate critical point close to stationary wall was made by [132]. The analysis of topological features and bifurcations for peristaltic flow of Newtonian fluid was presented by Jimenez and Sen [133].

Chapter 2

Peristaltic transport of visco-elasto-plastic fluids in a planar channel

In this chapter, we numerically investigate peristaltic transport of incompressible visco-elasto-plastic fluids in a two-dimensional symmetric channel. The constitutive equation used for extra stress tensor includes a number of well-known models like Maxwell A, Maxwell B, Johnson-Segalman, Oldroyd-B and Bingham model as its special case. The mathematical modeling of the problem is presented employing the laws of mass and momentum conservations. It is found that the flow equations in the wave frame reduce to a single nonlinear ordinary differential equation in stream function under the widely taken assumptions of long wavelength and low Reynolds number. The solution of problem is obtained by two ways; namely, shooting method and Matlab built-in routine bvp4c. The solutions obtained via both methods are in excellent agreement. A parametric study based on bvp4c solution is performed to see the effects of different parameters on velocity profile, pressure rise per wavelength, frictional forces and trapping phenomenon. The contents of this chapter are published in Zeitschrift Fur Naturforschung A 70 (8) (2015) 593 – 603.

2.1 Problem Formulation

Consider peristaltic flow of an incompressible visco-elasto-plastic fluid in a two-dimensional channel of width $2a_1$. The flow is initiated by the sinusoidal wave trains that propagate on the walls of channel with constant speed c. The shape of the wall surface is described by

$$H(\overline{X},\bar{t}) = a_1 + b_1 \left[\cos\left(\frac{2\pi}{\lambda}\ (\overline{X} - c\ \bar{t})\right)\right], \tag{2.1}$$

in which a_1 is half width of the channel, b_1 the wave amplitude, λ the wavelength, $\bar{t}$ the time, $(\overline{X},\overline{Y})$ are the rectangular coordinates with $\overline{X} - axis$ lying along the channel and $\overline{Y} - axis$ transverse to it. A schematic diagram of flow geometry is illustrated in Fig. 2.1.

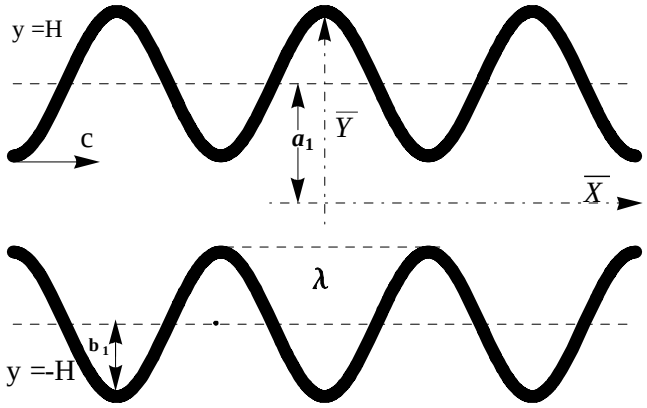

Fig. 2.1 Schematic diagram

The flow is governed by continuity and momentum equations given through Eq. (1.12) and Eq. (1.14).The peristaltic flow is inherently unsteady and two-dimensional, therefore, we define velocity field

$$\mathbf{V} = [\overline{U}\left(\overline{X},\overline{Y},\bar{t}\right), \overline{V}\left(\overline{X},\overline{Y},\bar{t}\right), 0] \tag{2.2}$$

and gradient vector

$$\nabla = \left[\frac{\partial}{\partial\overline{X}}, \frac{\partial}{\partial\overline{Y}}\right]. \tag{2.3}$$

Here $\overline{U}$ and $\overline{V}$ are the longitudinal and transverse components of velocity.

The general form of the Cauchy stress tensor ($\overline{\mathbf{T}}$) appearing in Eq. (1.14) is

$$\overline{\mathbf{T}} = -\overline{P}\,\overline{\mathbf{I}} + \overline{\boldsymbol{\tau}}. \tag{2.4}$$

Here $\overline{P}$ is pressure, $\overline{\mathbf{I}}$ the identity tensor and $\overline{\boldsymbol{\tau}}$ is extra stress tensor which for the visco-elasto-plastic fluid is defined by ([61]) as:

$$\overline{\boldsymbol{\tau}} + \lambda_1 \left((1-\xi_1)\overset{\nabla}{\overline{\boldsymbol{\tau}}} + \xi_1 \overset{\Delta}{\overline{\boldsymbol{\tau}}} \right) = 2\eta \left(\overline{\mathbf{D}} + \lambda_2 \overset{\nabla}{\overline{\mathbf{D}}} \right) + 2\tau_0 \overset{\wedge}{\overline{\mathbf{D}}}, \tag{2.5}$$

where λ_1 is relaxation time, ξ_1 $(0 \leq \xi_1 \leq 1)$ is a small scalar parameter, η is dynamic viscosity, λ_2 is retardation time and τ_0 the basic yield stress. The tensors $\overline{\mathbf{D}}$ and $\overset{\wedge}{\overline{\mathbf{D}}}$ are defined by

$$\overline{\mathbf{D}} = (1/2)\left(\overline{\mathbf{L}} + \overline{\mathbf{L}}^{*} \right), \qquad \overline{\mathbf{L}} = \nabla \mathbf{V}, \qquad \overset{\wedge}{\overline{\mathbf{D}}} = \overline{\mathbf{D}} / \sqrt{\varepsilon_1 + 2tr\overline{\mathbf{D}}^2}, \tag{2.6}$$

where * represents the transpose and ε_1 is a small positive quantity. As stated in ([61]), the presence of ε_1 is beneficial because it prevents from unboundedness when $\overline{\mathbf{D}} \to 0$. The upper and lower convected derivatives, $^{\nabla}$ and $^{\Delta}$ for an arbitrary tensor $\overline{\mathbf{A}}_1$ are defined respectively as

$$\overset{\nabla}{\overline{\mathbf{A}}}_1 = \frac{d\overline{\mathbf{A}}_1}{d\bar{t}} - \overline{\mathbf{L}}\overline{\mathbf{A}}_1 - \overline{\mathbf{A}}_1\overline{\mathbf{L}}^{*}, \qquad \overset{\Delta}{\overline{\mathbf{A}}}_1 = \frac{d\overline{\mathbf{A}}_1}{dt} + \overline{\mathbf{L}}^{*}\overline{\mathbf{A}}_1 + \overline{\mathbf{A}}_1\overline{\mathbf{L}}. \tag{2.7}$$

Now, we shall give a list of some well-known viscoelastic and plastic models that could be derived from Eq. (2.5).

1) For $\lambda_1 = \lambda_2 = \tau_0 = 0$, we have $\overline{\boldsymbol{\tau}} = 2\eta\overline{\mathbf{D}}$, which is constitutive relation for Newtonian fluid.

2) Setting $\xi_1 = \tau_0 = 0$ in Eq. (5) results in the following equation for extra stress tensor ($\overline{\boldsymbol{\tau}}$)

$$\overline{\boldsymbol{\tau}} + \lambda_1 \overset{\nabla}{\overline{\boldsymbol{\tau}}} = 2\eta \left(\overline{\mathbf{D}} + \lambda_2 \overset{\nabla}{\overline{\mathbf{D}}} \right), \tag{2.8}$$

It can easily be identified that Eq. (2.8) represents the constitutive equation of Oldroyd-B model.

3) When $\xi_1 = \tau_0 = \lambda_2 = 0$, we get the constitutive relation for UCM, i.e.,

$$\overline{\boldsymbol{\tau}} + \lambda_1 \overset{\nabla}{\overline{\boldsymbol{\tau}}} = 2\eta\overline{\mathbf{D}}, \tag{2.9}$$

4) For $\xi_1 = 1$, $\lambda_2 = \tau_0 = 0$, Eq. (2.5) reduces to LCM, represented by

$$\overline{\boldsymbol{\tau}} + \lambda_1 \overset{\Delta}{\overline{\boldsymbol{\tau}}} = 2\eta \overline{\mathbf{D}}, \tag{2.10}$$

5) Expression (2.5) reduces to Johnson-Segalman model for $\lambda_2 = 0$ and $\tau_0 = 0$, i.e.,

$$\overline{\boldsymbol{\tau}} + \lambda_1 \left((1-\xi_1) \overset{\nabla}{\overline{\boldsymbol{\tau}}} + \xi_1 \overset{\Delta}{\overline{\boldsymbol{\tau}}} \right) = 2\eta \overline{\mathbf{D}}. \tag{2.11}$$

6) The Bingham model can be recovered from Eq. (2.5) by taking $\lambda_1 = \lambda_2 = 0$. This model is capable of predicting yield stress effects and has the following form

$$\overline{\boldsymbol{\tau}} = 2\eta \overline{\mathbf{D}} + 2\tau_0 \overset{\wedge}{\overline{\mathbf{D}}}. \tag{2.12}$$

On incorporating Eq. (2.2) and Eq. (2.3), the continuity equation (1.13) gets the following form

$$\frac{\partial \overline{U}}{\partial \overline{X}} + \frac{\partial \overline{V}}{\partial \overline{Y}} = 0, \tag{2.13}$$

whereas the component form of momentum equation (1.14) in the absence of body forces, i.e., $\mathbf{f} = 0$, gives

$$\rho \left(\frac{\partial}{\partial \overline{t}} + \overline{U} \frac{\partial}{\partial \overline{X}} + \overline{V} \frac{\partial}{\partial \overline{Y}} \right) \overline{U} = -\frac{\partial \overline{P}}{\partial \overline{X}} + \frac{\partial}{\partial \overline{X}} \overline{\tau}_{\overline{XX}} + \frac{\partial}{\partial \overline{Y}} \overline{\tau}_{\overline{XY}}, \tag{2.14}$$

$$\rho \left(\frac{\partial}{\partial \overline{t}} + \overline{U} \frac{\partial}{\partial \overline{X}} + \overline{V} \frac{\partial}{\partial \overline{Y}} \right) \overline{V} = -\frac{\partial \overline{P}}{\partial \overline{Y}} + \frac{\partial}{\partial \overline{X}} \overline{\tau}_{\overline{YX}} + \frac{\partial}{\partial \overline{Y}} \overline{\tau}_{\overline{YY}}. \tag{2.15}$$

The constitutive Eq. (2.5) with the help of Eq. (2.6) and Eq. (2.7) can be written as:

$$\begin{aligned} \overline{\boldsymbol{\tau}} + \lambda_1 & \left[\begin{array}{c} (1-\xi_1) \left\{ \frac{\partial \overline{\boldsymbol{\tau}}}{\partial \overline{t}} + \overline{U} \frac{\partial \overline{\boldsymbol{\tau}}}{\partial \overline{X}} + \overline{V} \frac{\partial \overline{\boldsymbol{\tau}}}{\partial \overline{Y}} - \overline{\mathbf{L}} \overline{\boldsymbol{\tau}} - \overline{\boldsymbol{\tau}} \overline{\mathbf{L}}^* \right\} \\ + \xi_1 \left\{ \frac{\partial \overline{\boldsymbol{\tau}}}{\partial \overline{t}} + \overline{U} \frac{\partial \overline{\boldsymbol{\tau}}}{\partial \overline{X}} + \overline{V} \frac{\partial \overline{\boldsymbol{\tau}}}{\partial \overline{Y}} + \overline{\mathbf{L}} \overline{\boldsymbol{\tau}} + \overline{\boldsymbol{\tau}} \overline{\mathbf{L}}^* \right\} \end{array} \right] \\ = \; & 2\eta \left[\overline{\mathbf{D}} + \lambda_2 \left\{ \frac{\partial \overline{\mathbf{D}}}{\partial \overline{t}} + \overline{U} \frac{\partial \overline{\mathbf{D}}}{\partial \overline{X}} + \overline{V} \frac{\partial \overline{\mathbf{D}}}{\partial \overline{Y}} + \overline{\mathbf{L}} \overline{\mathbf{D}} + \overline{\mathbf{D}} \overline{\mathbf{L}}^* \right\} \right] + 2\tau_0 \overset{\wedge}{\overline{\mathbf{D}}}, \end{aligned} \tag{2.16}$$

where

$$\overline{\mathbf{L}} = \begin{pmatrix} \frac{\partial \overline{U}}{\partial \overline{X}} & \frac{\partial \overline{V}}{\partial \overline{X}} \\ \frac{\partial \overline{U}}{\partial \overline{Y}} & \frac{\partial \overline{V}}{\partial \overline{Y}} \end{pmatrix}. \tag{2.17}$$

The boundary conditions associated with the flow problem under consideration are:

$$\overline{U} = 0 \qquad \text{at } y = \pm H$$

The usual steady analysis can be performed by switching from laboratory frame $(\overline{X}, \overline{Y})$ to the wave frame $(\overline{x}, \overline{y})$. The following relationships between coordinates, velocities and pressures in the two frames hold:

$$\overline{x} = \overline{X} - c\bar{t}, \quad \overline{y} = \overline{Y}, \quad \overline{u} = \overline{U} - c, \quad \overline{v} = \overline{V}, \quad \overline{p}(\overline{x}, \overline{y}) = \overline{P}(\overline{X}, \overline{Y}, \bar{t}), \tag{2.18}$$

where $\overline{u}$, $\overline{v}$ and $\overline{p}$ are the velocity components and pressure in the wave frame, respectively. Invoking the transformations (2.18), Eq. (2.1) and Eqs. (2.13) – (2.16) take the form

$$\overline{h}(\overline{x}) = a_1 + b_1 \cos\left(\frac{2\pi\overline{x}}{\lambda}\right), \tag{2.19}$$

$$\frac{\partial \overline{u}}{\partial \overline{x}} + \frac{\partial \overline{v}}{\partial \overline{y}} = 0, \tag{2.20}$$

$$\rho\left(\overline{u}\frac{\partial}{\partial \overline{x}} + \overline{v}\frac{\partial}{\partial \overline{y}}\right)\overline{u} = -\frac{\partial \overline{p}}{\partial \overline{x}} + \frac{\partial}{\partial \overline{x}}\overline{\tau}_{\overline{x}\overline{x}} + \frac{\partial}{\partial \overline{y}}\overline{\tau}_{\overline{x}\overline{y}}, \tag{2.21}$$

$$\rho\left(\overline{u}\frac{\partial}{\partial \overline{x}} + \overline{v}\frac{\partial}{\partial \overline{y}}\right)\overline{v} = -\frac{\partial \overline{p}}{\partial \overline{y}} + \frac{\partial}{\partial \overline{x}}\overline{\tau}_{\overline{y}\overline{x}} + \frac{\partial}{\partial \overline{y}}\overline{\tau}_{\overline{y}\overline{y}}, \tag{2.22}$$

$$\begin{aligned} &\overline{\boldsymbol{\tau}} + \lambda_1 \left[\begin{array}{c} (1-\xi_1)\left\{\overline{u}\frac{\partial \overline{\boldsymbol{\tau}}}{\partial \overline{x}} + \overline{v}\frac{\partial \overline{\boldsymbol{\tau}}}{\partial \overline{y}} - \overline{\mathbf{L}}\overline{\boldsymbol{\tau}} - \overline{\boldsymbol{\tau}}\overline{\mathbf{L}}^*\right\} \\ +\xi_1\left\{\overline{u}\frac{\partial \overline{\boldsymbol{\tau}}}{\partial \overline{x}} + \overline{v}\frac{\partial \overline{\boldsymbol{\tau}}}{\partial \overline{y}} + \overline{\mathbf{L}}\overline{\boldsymbol{\tau}} + \overline{\boldsymbol{\tau}}\overline{\mathbf{L}}^*\right\} \end{array} \right] \\ = \;& 2\eta\left[\overline{\mathbf{D}} + \lambda_2\left\{\overline{u}\frac{\partial \overline{\mathbf{D}}}{\partial \overline{x}} + \overline{v}\frac{\partial \overline{\mathbf{D}}}{\partial \overline{y}} - \overline{\mathbf{L}\mathbf{D}} - \overline{\mathbf{D}\mathbf{L}}^*\right\}\right] + 2\tau_0\overset{\wedge}{\overline{\mathbf{D}}}. \end{aligned} \tag{2.23}$$

By introducing the dimensionless flow variables

$$\begin{aligned}
x &= \frac{\overline{x}}{\overline{\lambda}},\ y=\frac{\overline{y}}{a_1},\ u=\frac{\overline{u}}{c},\ v=\frac{\overline{v}}{c\delta},\ t=\frac{\pi c\overline{t}}{\delta},\ p=\frac{\delta a_1\overline{p}}{\eta c},\\
h &= \frac{\overline{h}}{a_1},\ \boldsymbol{\tau}=\frac{a_1}{c\eta}\overline{\boldsymbol{\tau}},\ h=\frac{\overline{h}}{a_1},\ \phi=\frac{b_1}{a_1}(<1),\ \mathbf{A}_1{=}\frac{a_1}{c\eta}\overline{\mathbf{A}}_1,\\
\mathbf{D} &= \frac{a_1}{c\eta}\overline{\mathbf{D}},\ \overset{\wedge}{\mathbf{D}}=\frac{a_1}{c\eta}\overset{\wedge}{\overline{\mathbf{D}}},\ \mathbf{L}=\frac{a_1}{c\eta}\overline{\mathbf{L}},\ \mathbf{L}^*=\frac{a_1}{c\eta}\overline{\mathbf{L}}^*
\end{aligned} \tag{2.24}$$

Eqs. (2.19) – (2.22) and Eq. (2.23) in components form can be put as

$$h(x)=1+\phi\cos(2\pi x), \tag{2.25}$$

$$\frac{\partial u}{\partial x}+\frac{\partial v}{\partial y}=0, \tag{2.26}$$

$$\mathrm{Re}\,\delta\left(u\frac{\partial}{\partial x}+v\frac{\partial}{\partial y}\right)u = -\frac{\partial p}{\partial x}+\delta\frac{\partial}{\partial x}\tau_{xx}+\frac{\partial}{\partial y}\tau_{xy}, \tag{2.27}$$

$$\mathrm{Re}\,\delta^3\left(u\frac{\partial}{\partial x}+v\frac{\partial}{\partial y}\right)v = -\frac{\partial p}{\partial y}+\delta^2\frac{\partial}{\partial x}\tau_{yx}+\delta\frac{\partial}{\partial y}\tau_{yy}, \tag{2.28}$$

$$\begin{aligned}
&\tau_{xx}+De_1\left[\begin{array}{c}(1-\xi)\left\{\delta\left(u\frac{\partial}{\partial x}+v\frac{\partial}{\partial y}\right)\tau_{xx}-2\delta\tau_{xx}\frac{\partial u}{\partial x}-2\tau_{xy}\frac{\partial u}{\partial y}\right\}\\ +\xi\left\{\delta\left(u\frac{\partial}{\partial x}+v\frac{\partial}{\partial y}\right)\tau_{xx}+2\delta\tau_{xx}\frac{\partial u}{\partial x}+2\delta^2\tau_{xy}\frac{\partial v}{\partial x}\right\}\end{array}\right]\\
=\ & 2\delta\frac{\partial u}{\partial x}+2De_2\left\{\delta^2\left(u\frac{\partial}{\partial x}+v\frac{\partial}{\partial y}\right)\frac{\partial u}{\partial x}-2\delta^2\left(\frac{\partial u}{\partial x}\right)^2-\left(\frac{\partial u}{\partial y}\right)^2-\delta^2\frac{\partial u}{\partial y}\frac{\partial v}{\partial x}\right\}\\
&+2\delta Bn\left(\frac{\partial u}{\partial x}\right)/\sqrt{\varepsilon+2\delta^2\left(\frac{\partial u}{\partial x}\right)^2+2\delta^2\left(\frac{\partial v}{\partial y}\right)^2+\left(\frac{\partial u}{\partial y}+\delta^2\frac{\partial v}{\partial x}\right)^2},
\end{aligned} \tag{2.29}$$

$$\begin{aligned}
&\tau_{xy}+De_1\left[\begin{array}{c}(1-\xi_1)\left\{\delta\left(u\frac{\partial}{\partial x}+v\frac{\partial}{\partial y}\right)\tau_{xy}-\delta\tau_{xy}\frac{\partial u}{\partial x}-\tau_{yy}\frac{\partial u}{\partial y}-\delta^2\tau_{xx}\frac{\partial v}{\partial x}-\delta\tau_{xy}\frac{\partial v}{\partial y}\right\}\\ +\xi_1\left\{\delta\left(u\frac{\partial}{\partial x}+v\frac{\partial}{\partial y}\right)\tau_{xy}+\delta\tau_{xy}\frac{\partial u}{\partial x}+\delta^2\tau_{yy}\frac{\partial v}{\partial x}+\tau_{xx}\frac{\partial u}{\partial y}+\delta\tau_{xy}\frac{\partial v}{\partial y}\right\}\end{array}\right]\\
=\ & \left(\frac{\partial u}{\partial y}+\delta^2\frac{\partial v}{\partial x}\right)+2De_2\left\{\frac{\delta}{2}\left(u\frac{\partial}{\partial x}+v\frac{\partial}{\partial y}\right)\left(\frac{\partial u}{\partial y}+\delta^2\frac{\partial v}{\partial x}\right)-\delta\frac{\partial u}{\partial y}\frac{\partial v}{\partial y}-\delta^3\frac{\partial u}{\partial x}\frac{\partial v}{\partial x}\right\}\\
&+Bn\left(\frac{\partial u}{\partial y}+\delta^2\frac{\partial v}{\partial x}\right)/\sqrt{\varepsilon+2\delta^2\left(\frac{\partial u}{\partial x}\right)^2+2\delta^2\left(\frac{\partial v}{\partial y}\right)^2+\left(\frac{\partial u}{\partial y}+\delta^2\frac{\partial v}{\partial x}\right)^2},
\end{aligned} \tag{2.30}$$

$$
\begin{aligned}
&\tau_{yy} + De_1 \left[\begin{array}{c} (1-\xi_1)\left\{\delta\left(u\frac{\partial}{\partial x} + v\frac{\partial}{\partial y}\right)\tau_{yy} - 2\delta^2\tau_{xy}\frac{\partial v}{\partial x} - 2\delta\tau_{yy}\frac{\partial v}{\partial y}\right\} \\ +\xi_1\left\{\delta\left(u\frac{\partial}{\partial x} + v\frac{\partial}{\partial y}\right)\tau_{yy} + 2\tau_{xy}\frac{\partial u}{\partial y} + 2\delta\tau_{yy}\frac{\partial v}{\partial y}\right\} \end{array} \right] \\
= \;& 2\delta\frac{\partial v}{\partial y} + 2De_2\left\{\delta^2\left(u\frac{\partial}{\partial x} + v\frac{\partial}{\partial y}\right)\frac{\partial v}{\partial y} - 2\delta^2\left(\frac{\partial v}{\partial y}\right)^2 - \delta^4\left(\frac{\partial v}{\partial x}\right)^2 - \delta^2\frac{\partial u}{\partial y}\frac{\partial v}{\partial x}\right\} \\
&+2\delta Bn\left(\frac{\partial v}{\partial y}\right)\Big/\sqrt{\varepsilon + 2\delta^2\left(\frac{\partial u}{\partial x}\right)^2 + 2\delta^2\left(\frac{\partial v}{\partial y}\right)^2 + \left(\frac{\partial u}{\partial y} + \delta^2\frac{\partial v}{\partial x}\right)^2}. \qquad (2.31)
\end{aligned}
$$

where the dimensionless numbers are

$$
De_1 = \frac{\lambda_1 c}{a_1}, \quad De_2 = \frac{\lambda_2 c}{a_1}, \quad Bn = \frac{a_1\tau_0}{\eta c}, \quad \delta = \frac{a_1}{\lambda}, \quad \mathrm{Re} = \frac{\rho c a_1}{\eta}, \quad \varepsilon = \frac{\varepsilon_1 a_1^2}{c^2}\,(0 < \varepsilon \ll 1) \qquad (2.32)
$$

The subsequent analysis is based on the elimination of stresses from Eqs. (2.27) − (2.28). However, it is difficult to obtain the exact expressions of stresses from Eqs. (2.29) − (3.31). Even if one is able to do that, Eqs. (2.27) − (2.28) after substitution of these expressions are not easy to handle. The simplest case for a Newtonian fluid is even treated by approximate methods or numerical technique. Not a single attempt is available in the literature where the problem of peristaltic flow of non-Newtonian fluid in a channel or tube is treated without using some assumptions. Fortunately appropriate assumptions can be made due to the relevance of peristalsis with physiology. For example, in small intestine, ureter and in many other ducts where the bio-fluid is transported by peristaltic activity, the wavelength of the wave is quite large as compared to the radius of the vessel. Further, the flow in such ducts due to peristalsis can be treated as creeping flow i.e. the Reynolds number for such flows is very small. The above two assumptions are usually referred as the long wavelength and low Reynolds number assumptions in literature. The parameter characterizing the ratio of radius of the channel to wavelength of the peristaltic wave in present study is δ. Thus for the flow under consideration we assume $\delta \approx 0$ and $\mathrm{Re} \approx 0$. A typical example where the above assumptions may be valid is the movement of chyme in small intestine where both δ and Re are very much less than unity [59]. Some relevant studies regarding the applications of long wavelength and low Reynolds number assumptions in peristaltic flows can be found in refs. [5, 32, 34, 65, 102, 103]. In view of

aforementioned assumptions, Eqs. $(2.27)-(2.31)$ reduce to

$$0 = -\frac{\partial p}{\partial x}+\frac{\partial}{\partial y}\tau_{xy}, \tag{2.33}$$

$$0 = -\frac{\partial p}{\partial y}, \tag{2.34}$$

$$\tau_{xx}-2De_1(1-\xi_1)\tau_{xy}\frac{\partial u}{\partial y}=-2De_2\left(\frac{\partial u}{\partial y}\right)^2, \tag{2.35}$$

$$\tau_{xy}+De_1\left[-(1-\xi_1)\tau_{yy}\frac{\partial u}{\partial y}+\xi_1\tau_{xx}\frac{\partial u}{\partial y}\right]=\left(\frac{\partial u}{\partial y}\right)+Bn\left(\frac{\partial u}{\partial y}\right)/\sqrt{\varepsilon+\left(\frac{\partial u}{\partial y}\right)^2}, \tag{2.36}$$

$$\tau_{yy}+2\xi_1De_1\tau_{xy}\frac{\partial u}{\partial y}=0. \tag{2.37}$$

From Eqs. $(2.35)-(2.37)$, we can easily find the expressions for components of stress tensor as

$$\tau_{xy} = \frac{1}{\left[1+4\xi_1(1-\xi_1)De_1^2\left(\frac{\partial u}{\partial y}\right)^2\right]}\left[\begin{array}{c}2De_1De_2\xi_1\left(\frac{\partial u}{\partial y}\right)^3+\left(\frac{\partial u}{\partial y}\right)\\ +Bn\left(\frac{\partial u}{\partial y}\right)/\sqrt{\varepsilon+\left(\frac{\partial u}{\partial y}\right)^2}\end{array}\right], \tag{2.38}$$

$$\tau_{xx} = 2De_1(1-\xi_1)\tau_{xy}\frac{\partial u}{\partial y}-2De_2\left(\frac{\partial u}{\partial y}\right)^2, \tag{2.39}$$

$$\tau_{yy} = -2\xi_1De_1\tau_{xy}\frac{\partial u}{\partial y}. \tag{2.40}$$

Now on defining the stream function by the relation

$$u=\frac{\partial\psi}{\partial y}, \qquad v=-\frac{\partial\psi}{\partial x}, \tag{2.41}$$

the continuity equation (2.26) is identically satisfied, while Eqs. $(2.38)-(2.40)$ take the form

$$\tau_{xy} = \frac{1}{\left[1+4\xi_1(1-\xi_1)De_1^2\left(\frac{\partial^2\psi}{\partial y^2}\right)^2\right]}\left[\begin{array}{c}2De_1De_2\xi_1\left(\frac{\partial^2\psi}{\partial y^2}\right)^3+\left(\frac{\partial^2\psi}{\partial y^2}\right)\\ +Bn\left(\frac{\partial^2\psi}{\partial y^2}\right)/\sqrt{\varepsilon+\left(\frac{\partial^2\psi}{\partial y^2}\right)^2}\end{array}\right], \tag{2.42}$$

$$\tau_{xx} = 2De_1(1-\xi_1)\tau_{xy}\frac{\partial^2\psi}{\partial y^2}-2De_2\left(\frac{\partial^2\psi}{\partial y^2}\right)^2, \tag{2.43}$$

$$\tau_{yy} = -2\xi_1De_1\tau_{xy}\frac{\partial^2\psi}{\partial y^2}. \tag{2.44}$$

Substituting the value of τ_{xy} in Eq. (2.33) and eliminating the pressure between Eqs. (2.33) and (2.34) results in the following compatibility equation

$$\frac{\partial^2}{\partial y^2}\left[\frac{2De_1De_2\xi_1\left(\frac{\partial^2\psi}{\partial y^2}\right)^3+\left(\frac{\partial^2\psi}{\partial y^2}\right)+Bn\left(\frac{\partial^2\psi}{\partial y^2}\right)/\sqrt{\varepsilon+\left(\frac{\partial^2\psi}{\partial y^2}\right)^2}}{1+4\xi_1(1-\xi_1)De_1^2\left(\frac{\partial^2\psi}{\partial y^2}\right)^2}\right]=0. \tag{2.45}$$

The boundary conditions in the wave frame for symmetric case are ([64]) as

$$\psi = -\frac{q}{2},\quad \frac{\partial\psi}{\partial y}=-1,\quad at\ y=-h, \tag{2.46}$$

$$\psi = \frac{q}{2},\quad \frac{\partial\psi}{\partial y}=-1,\quad at\ y=h, \tag{2.47}$$

$$q = \theta-2. \tag{2.48}$$

where θ and q are the dimensionless mean flow rates in the fixed and wave frames, respectively. The Dritchlet boundary conditions on ψ follows from the definition of flow rate in wave frame, i.e.,

$$q=\int_{-h}^{h}udy. \tag{2.49}$$

In view of Eq. (2.41), one can write

$$q=\int_{-h}^{h}\frac{\partial\psi}{\partial y}dy=\psi(h)-\psi(-h). \tag{2.50}$$

Eq. (2.50) is satisfied if we choose $\psi(h)=q/2$ and $\psi(-h)=-q/2$. The Neuman boundary conditions on ψ represent the well known no-slip conditions.

The pressure rise per wavelength (ΔP_λ) and frictional forces (F_λ) on the wall are defined by

$$\Delta P_\lambda = \int_0^1\left(\frac{dp}{dx}\right)dx, \tag{2.51}$$

$$F_\lambda = \int_0^1 h^2\left(-\frac{dp}{dx}\right)dx. \tag{2.52}$$

2.2 Solution Methodology

An exact solution of Eq. (2.45) subject to boundary conditions (2.46) and (2.47) is difficult to obtain due to its nonlinear nature. Therefore, we have computed numerical solutions by using shooting method and Matlab built-in routine bvp4c which is based on the collocation method. bvp4c is a finite difference code that implements the 3-stage Labatto IIIa formula. This is collocation formula and the collocation polynomial provides a C^1-continuous solution that is fourth order accurate. Mesh selection and error control are based on the residual of the continuous solution. Analytical condensation is used when the system of algebraic equations is formed. Further details can be found in [134]. Table. 2.1 and Fig. 2.2 present a comparison of both solutions. This comparison shows that both the solutions are in excellent agreement. In limiting case when De_1, De_2 and Bn approach to zero, our results reduce to those for the case of Newtonian fluid. For rest of the plots, the solution obtained by bvp4c is utilized.

2.3 Results and Discussion

In this section, we discuss the numerical results through their graphical representation. The effects of emerging parameters (De_1, De_2 and Bn) on velocity profile, pressure rise per wavelength, frictional forces, normal and shear stresses and trapping phenomenon.

The effects of model parameters on velocity profile are shown in Figs. 2.3 to 2.5. In the model parameters, $De_{1,2}$ highlight the effects of elasticity whereas Bn shows the effects of plasticity. From Fig. 2.3 we note that the magnitude of the velocity decreases at the centre of channel by increasing elasticity (De_1), which perhaps is a result of increased shear thickening of viscosity. Since De_1 and De_2 are concerned with relaxation and retardation times, so their effects on velocity profile should also be opposite. From Fig. 2.4 we note that De_2 leaves opposite effects to the effects of De_1 on velocity profile because it increases at the centre whereas it decreases near the walls. From Fig. 2.5 we observe that increasing plasticity (Bn) results in decrease of velocity at the center and for the larger values of Bn (means for higher values of yield stress), fluid behaves like a solid. For such values of Bn the velocity profile approaches to uniformity.

Figs. $2.6-2.11$, have been plotted to see the influence of model parameters on pressure rise per wavelength (ΔP_λ) and frictional forces (F_λ). These figures show that De_2 and Bn leave

similar effects on ΔP_λ and F_λ whereas the effects of De_1 on ΔP_λ and F_λ are opposite to the effects that of De_2 and Bn. Fig. 2.6 shows that ΔP_λ decreases by increasing elasticity (De_1) up to a certain critical value of flow rate (θ) in retrograde pumping region ($q < 0$ and $\Delta P_\lambda > 0$) and peristaltic pumping region ($q > 0$ and $\Delta P_\lambda > 0$) but it begins to increase after this critical value in augmented pumping region ($q > 0$ and $\Delta P_\lambda < 0$). Fig. 2.7 also shows an increase in ΔP_λ and F_λ in retrograde and peristaltic pumping regions by increasing De_2 while it predicts a decrease in ΔP_λ and F_λ in augmented pumping region. From Fig. 2.9 we note that frictional forces increase up to a certain critical value of flow rate by increasing De_1, while they decrease onward. It means that a resistance caused by frictional forces is observed for $q < -0.7$ but these forces get weaker afterwards. The effects of De_2 and Bn on frictional forces are similar but opposite to the effects of De_1.

We have prepared Figs. $2.12 - 2.14$ in order to see the behavior of stresses by increasing the value of parameters De_1, De_2 and Bn. From Figs. 2.12 and 2.13 we note that the normal stress components τ_{xx} and τ_{yy} decrease in the entire channel by increasing all the parameters De_1, De_2 and Bn. The shear stress (τ_{xy}) profile for different values of parameters is presented in Fig. 2.14. From this figure we note that τ_{xy} increases by increasing De_1 but a continuous decrease in its profile is observed by increasing De_2 and Bn.

Now we report some results about an interesting phenomenon in peristalsis, called trapping. In this phenomenon an amount of fluid called *Bolus* is trapped due to contraction of walls. To see the influence of non-Newtonian parameters De_1, De_2 and Bn on trapping, we have prepared Figs. $2.15 - 2.17$. Here we observe that these parameters affect the trapping phenomenon in a similar way as they affected the velocity profile. In fact size and circulation of bolus decrease by increasing De_1 and Bn. However, its size and circulation increases for large values of De_2.

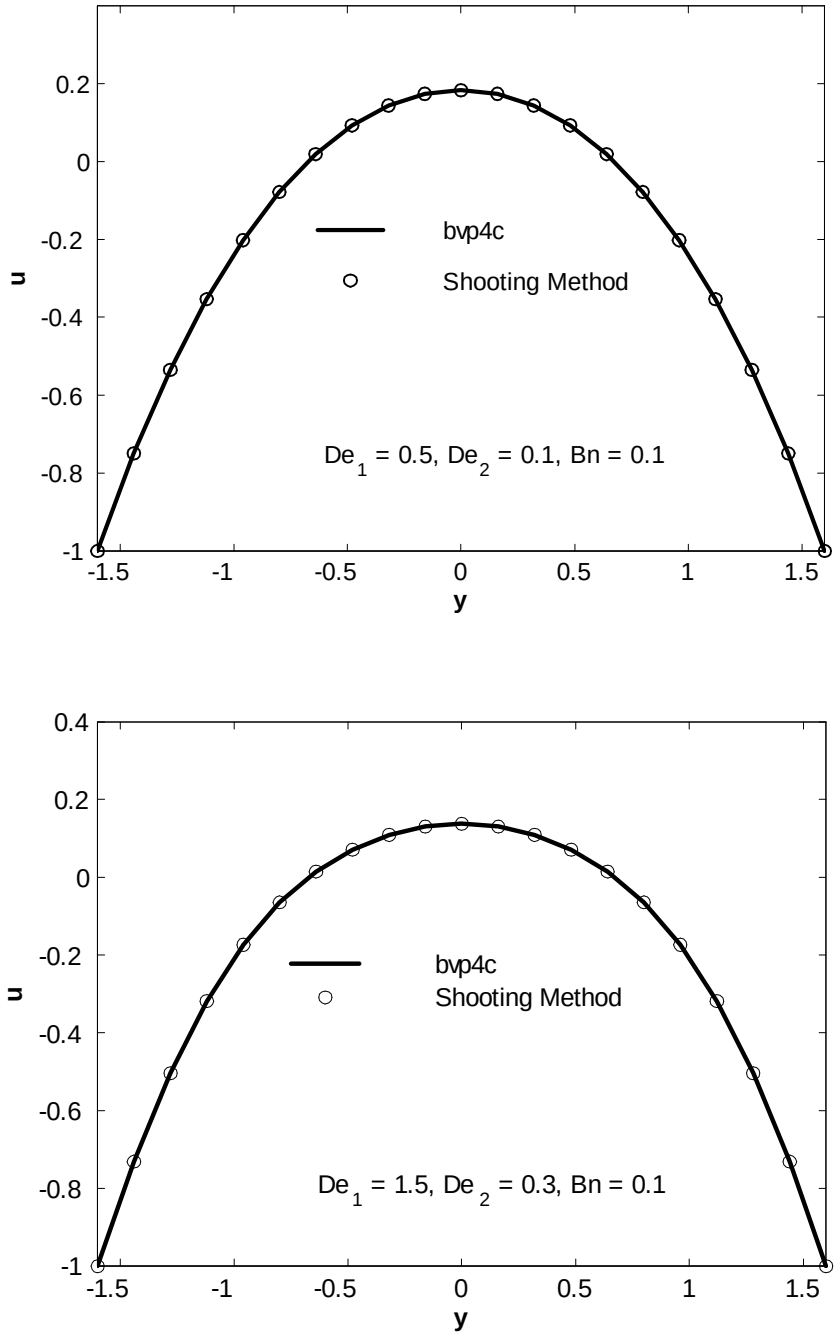

Fig. 2.2: Comparison of solution by bvp4c and shooting method

with $\theta = 1.4, \phi = 0.6$ $\xi_1 = 0.8,$ $\varepsilon = 0.2$

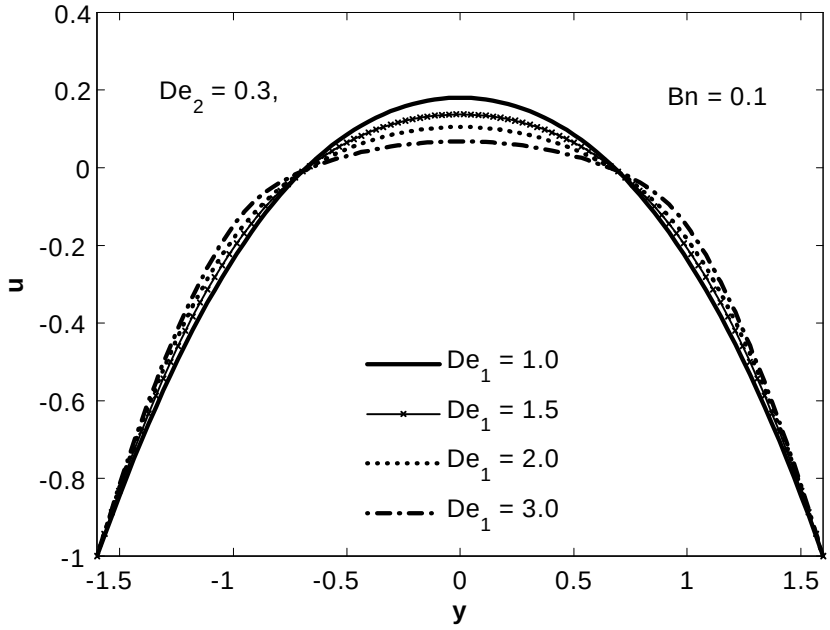

Fig. 2.3: Velocity for De_1 with $\theta = 1.4,\ \phi = 0.6,\ \xi_1 = 0.8,\ \varepsilon = 0.2$

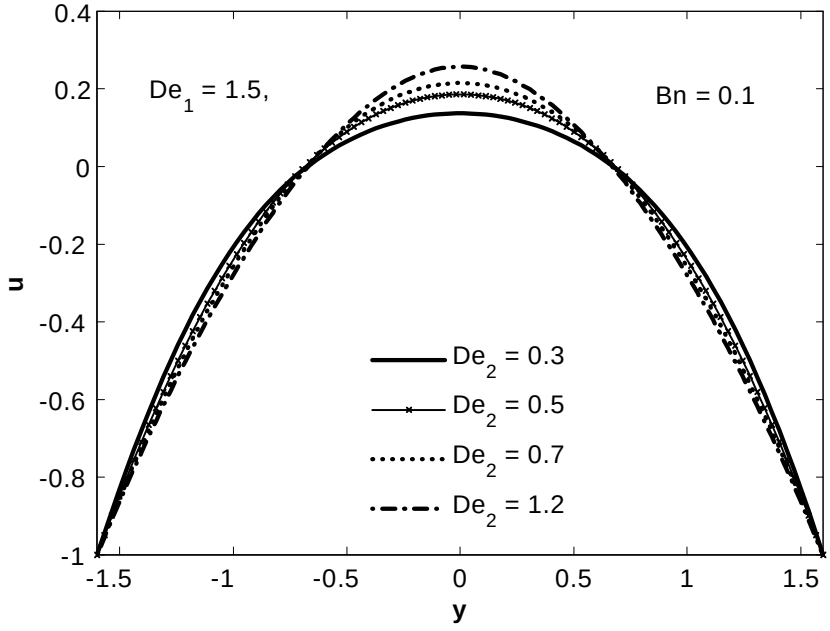

Fig. 2.4: Velocity for De_2 with $\theta = 1.4,\ \phi = 0.6,\ \xi_1 = 0.8,\ \varepsilon = 0.2$

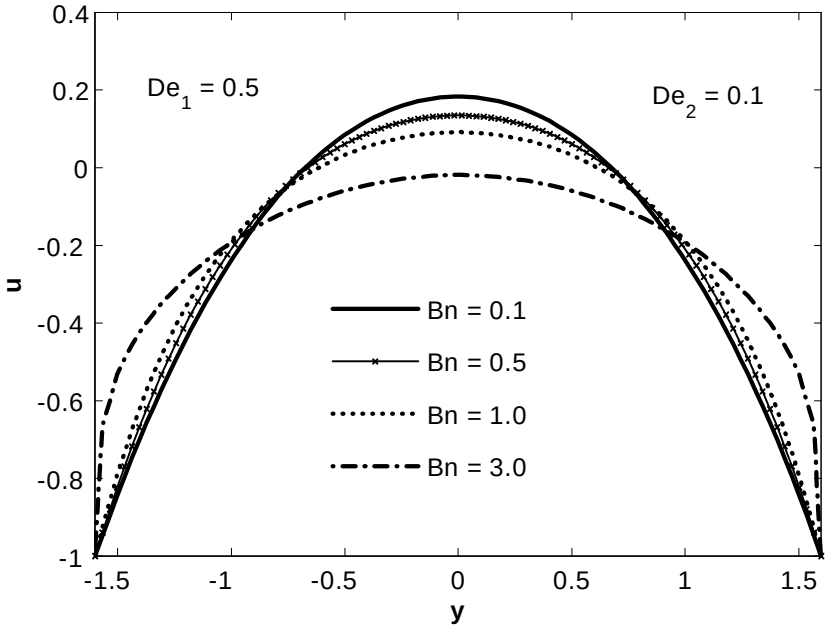

Fig. 2.5: Velocity for Bn with $\theta = 1.4,\ \phi = 0.6,\ \xi_1 = 0.8,\ \varepsilon = 0.2$

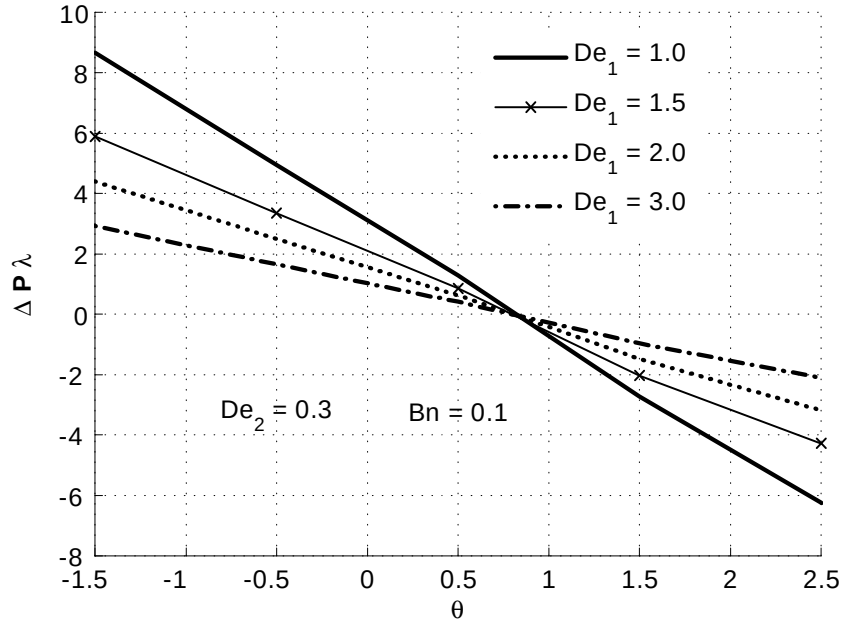

Fig. 2.6: ΔP_λ for De_1 with $\phi = 0.6,\ \xi_1 = 0.8,\ \varepsilon = 0.2$

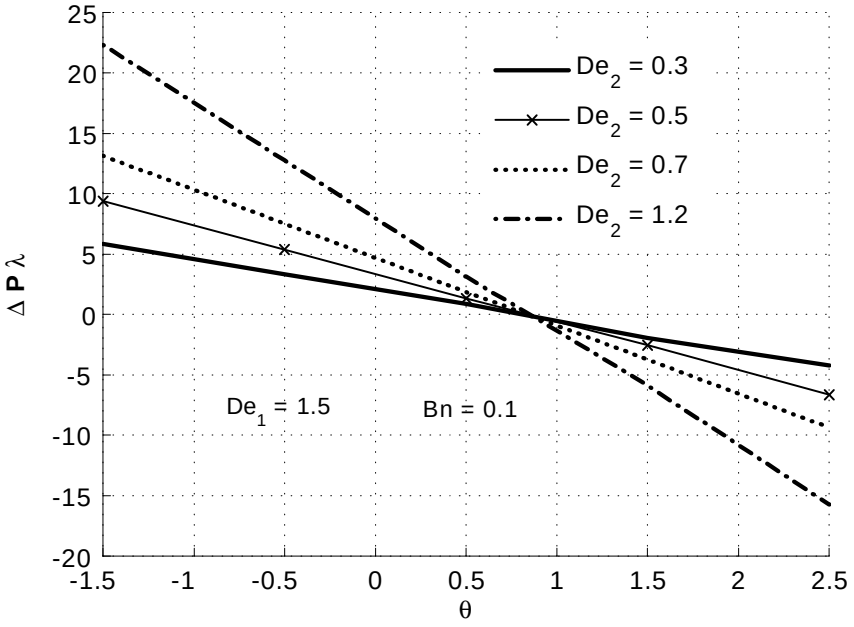

Fig. 2.7: ΔP_λ for De_2 with $\phi = 0.6,\ \xi_1 = 0.8,\ \varepsilon = 0.2$

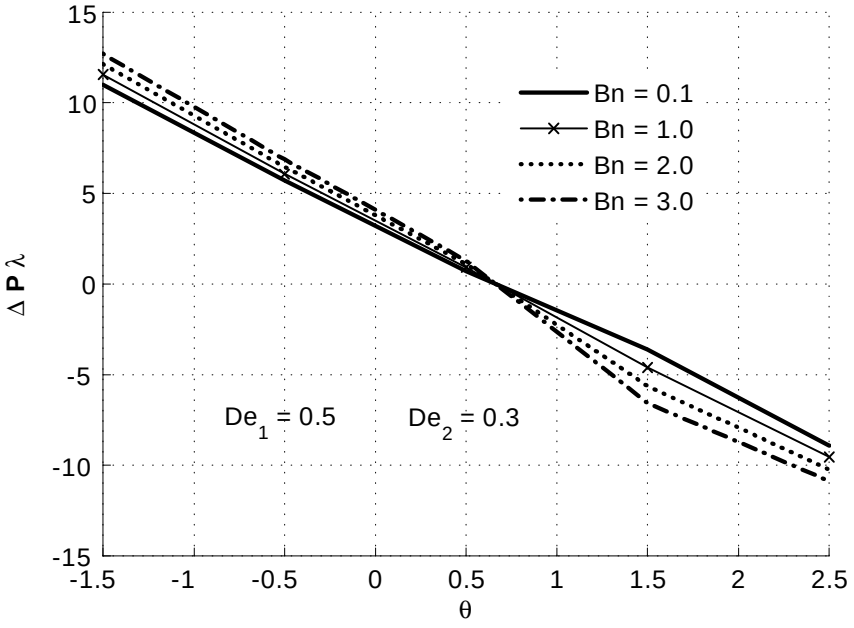

Fig. 2.8: ΔP_λ for De_1 with $\phi = 0.6,\ \xi_1 = 0.8,\ \varepsilon = 0.2$

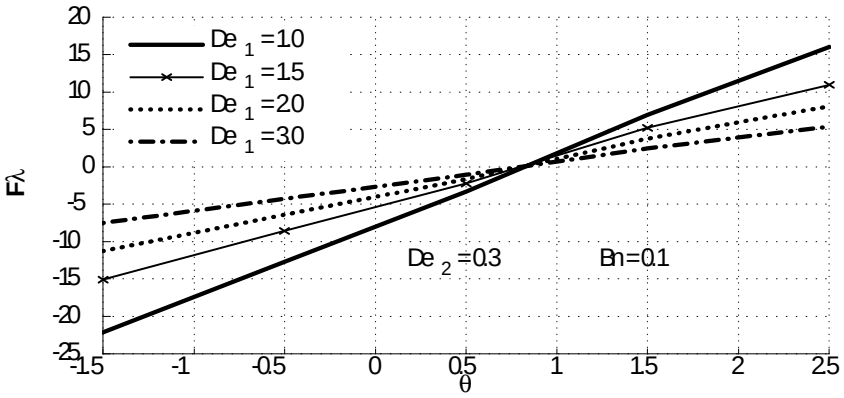

Fig. 2.9: F_λ for De_1 with $\phi = 0.6,\ \xi_1 = 0.8,\ \varepsilon = 0.2$

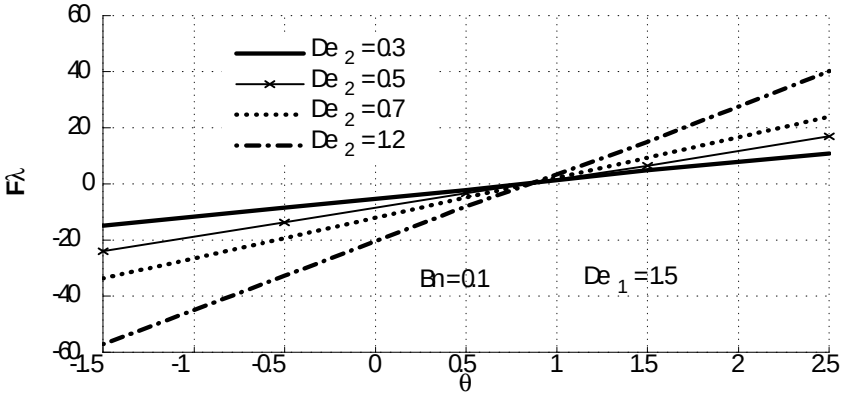

Fig. 2.10: F_λ for De_2 with $\phi = 0.6,\ \xi_1 = 0.8,\ \varepsilon = 0.2$

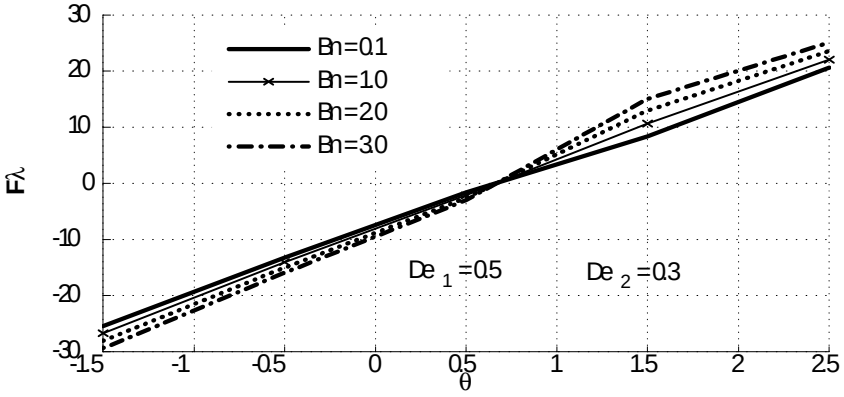

Fig. 2.11: F_λ for De_1 with $\phi = 0.6,\ \xi_1 = 0.8,\ \varepsilon = 0.2$

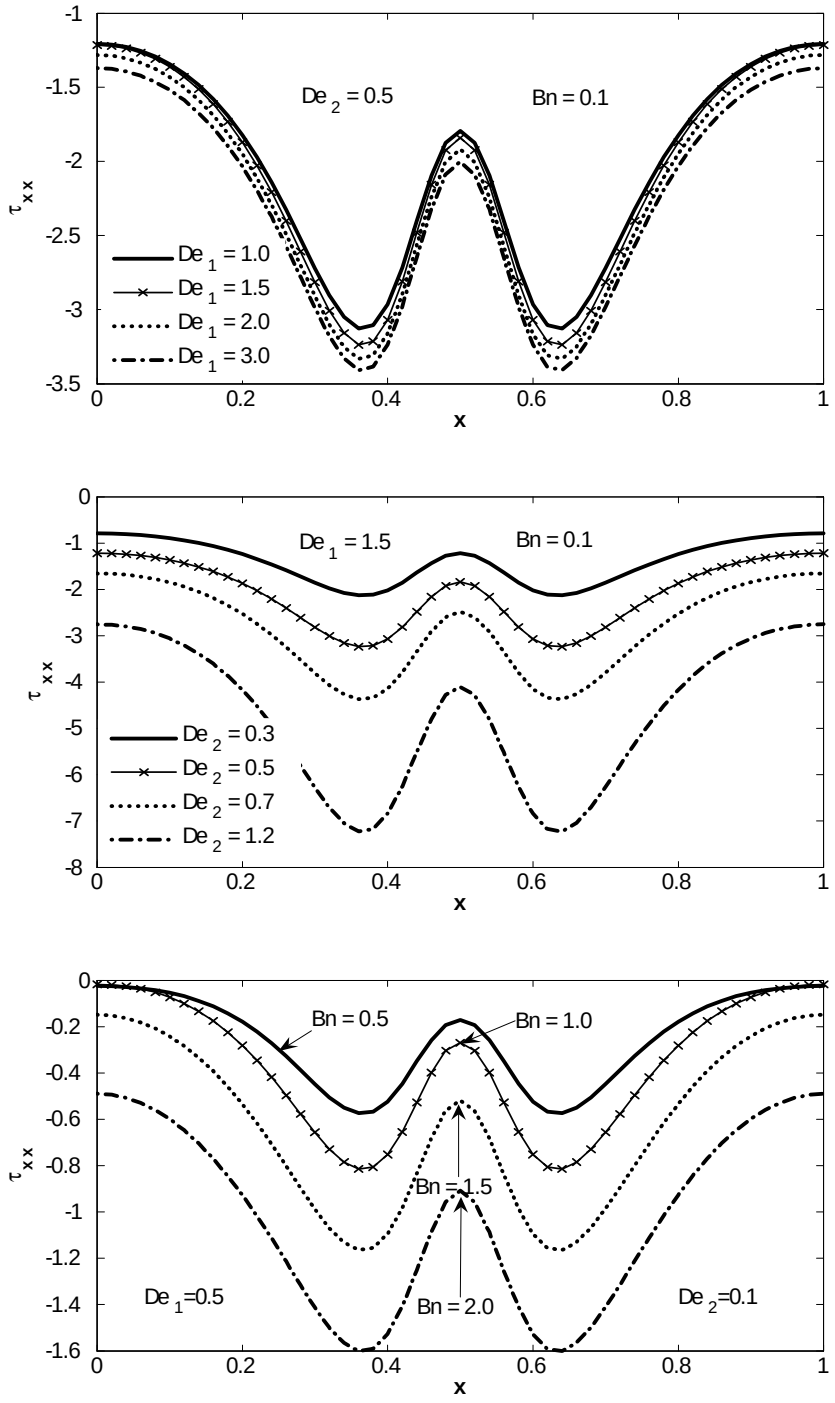

Fig. 2.12: τ_{xx} for different values of $De_1,\ De_2$ and Bn

with $\theta = 1.4, \phi = 0.6,\ \xi_1 = 0.8, \varepsilon = 0.2$

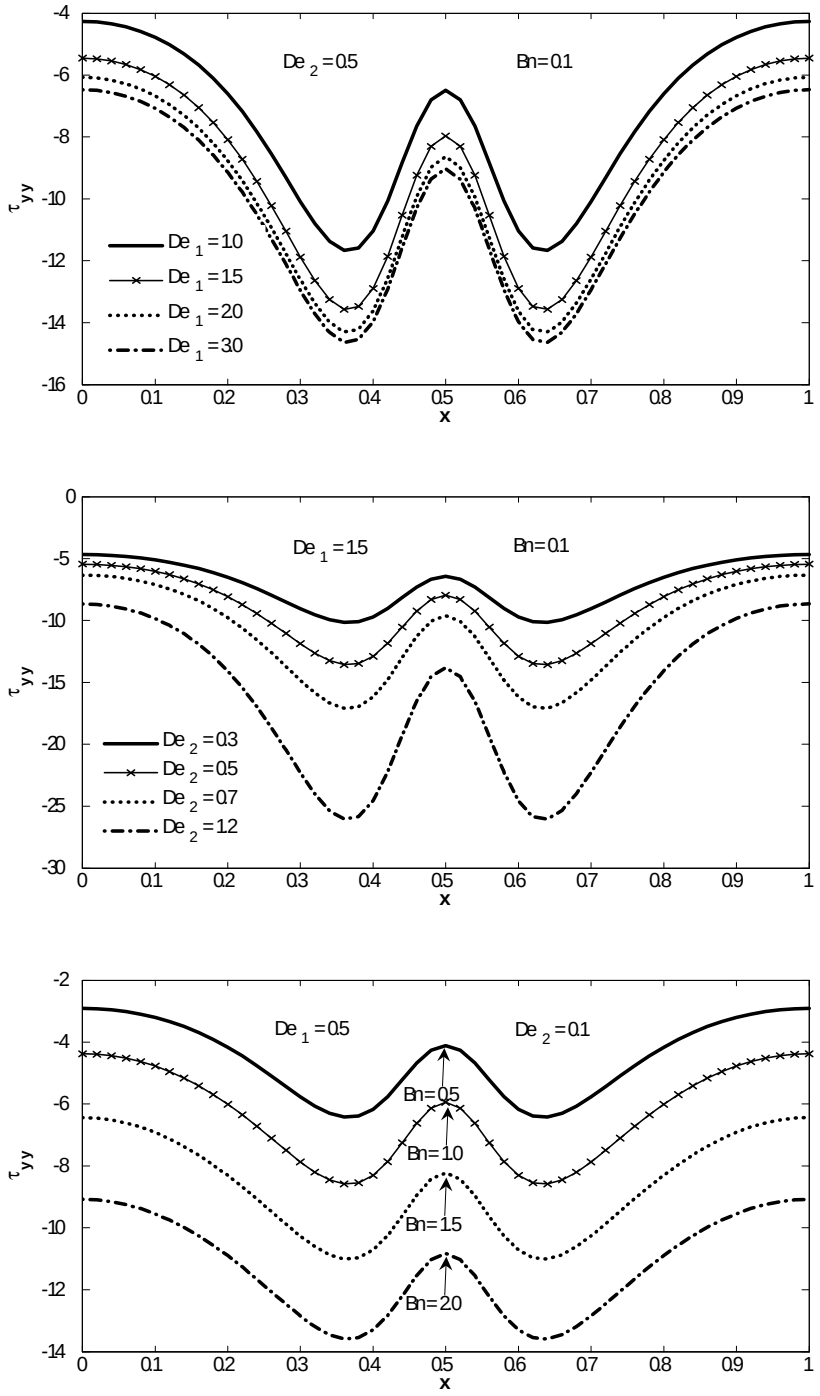

Fig. 2.13: τ_{yy} for different values of $De_1,\ De_2$ and Bn

with $\theta = 1.4, \phi = 0.6,\ \xi_1 = 0.8, \varepsilon = 0.2$

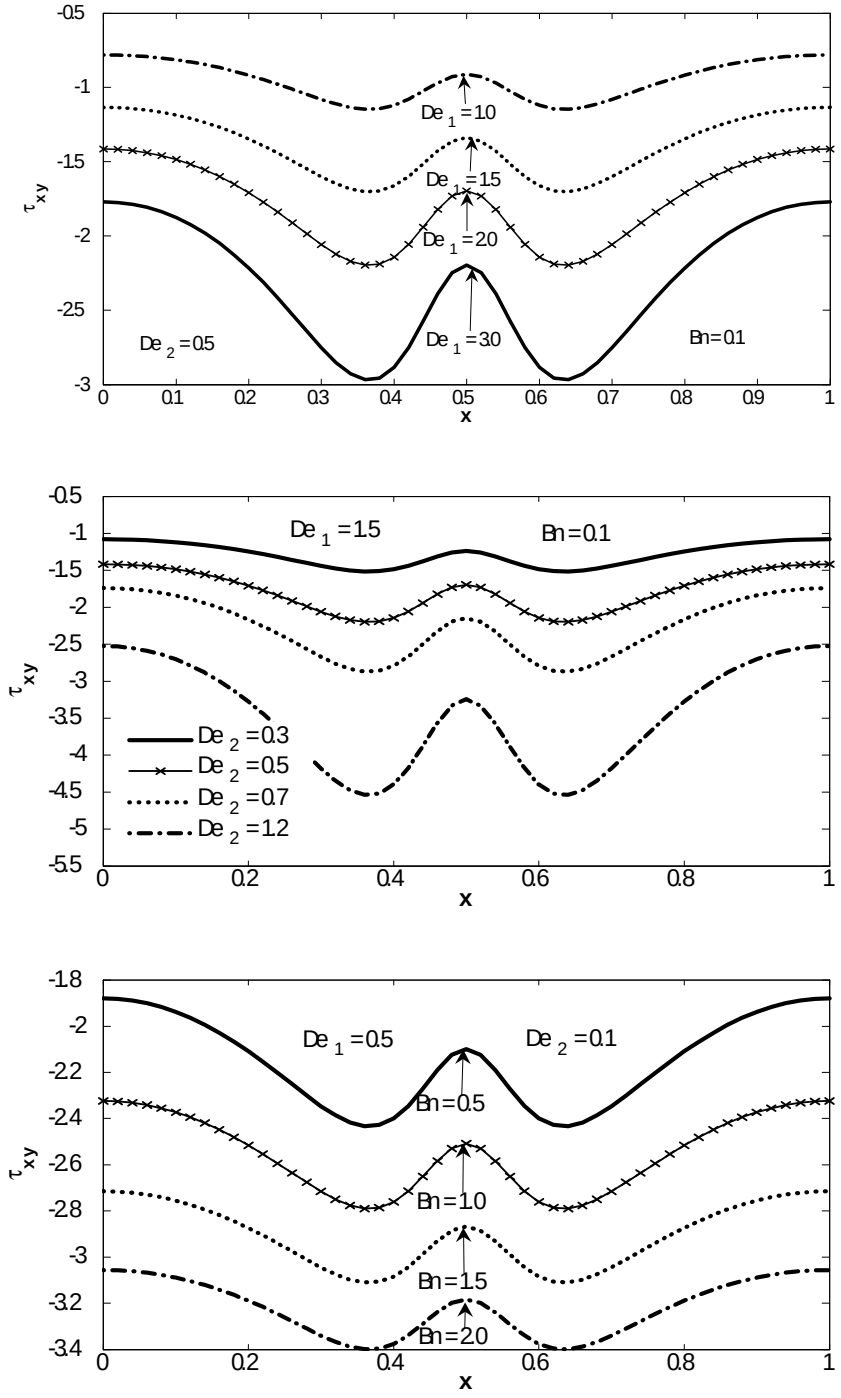

Fig. 2.14: τ_{xy} for different values of $De_1,\ De_2$ and Bn

with $\theta = 1.4, \phi = 0.6,\ \xi_1 = 0.8, \varepsilon = 0.2$

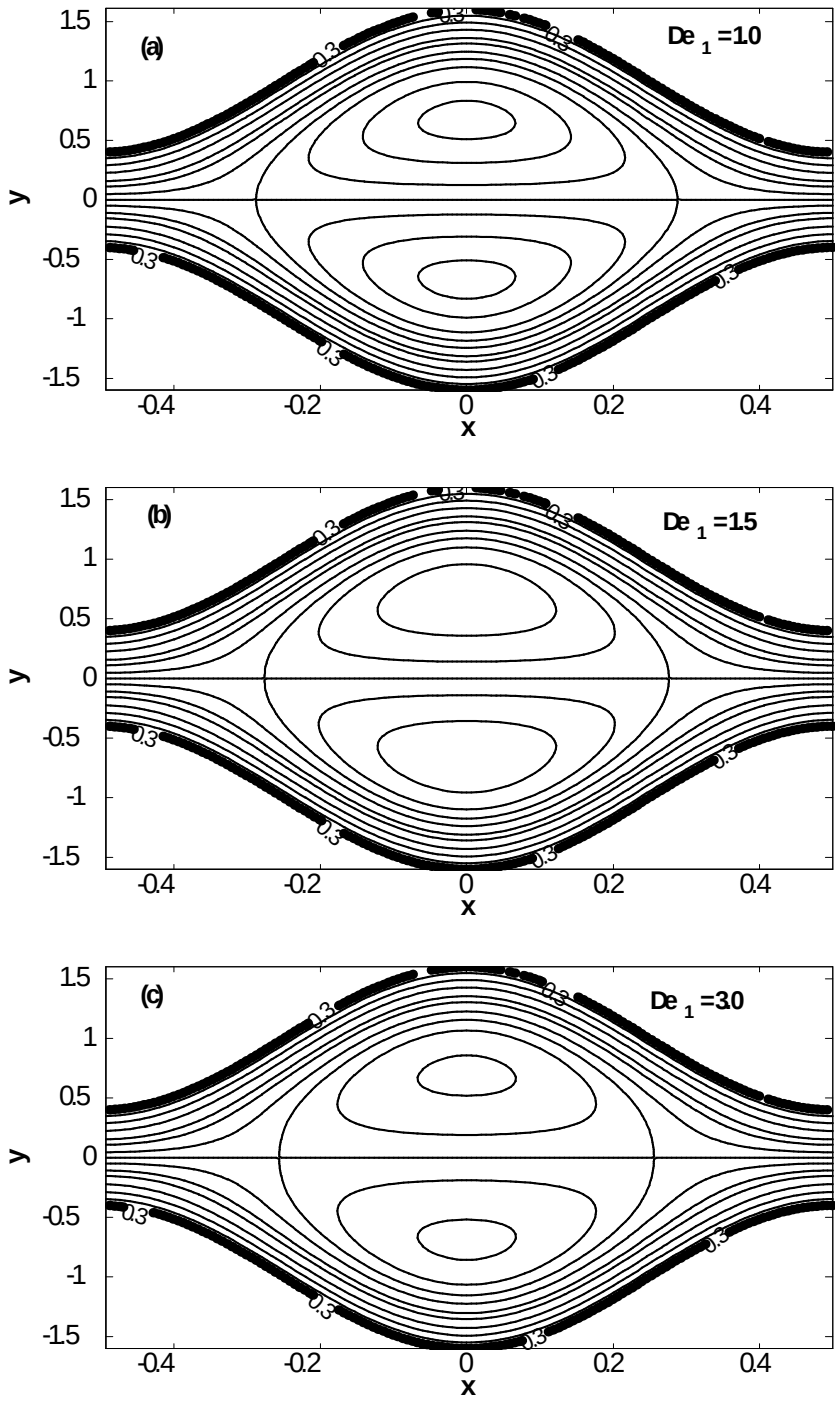

Fig. 2.15: Streamlines for De_1 with $\theta = 1.4,\ \phi = 0.6,\ De_2 = 1.2,\ \varepsilon = 0.2,\ \xi_1 = 0.8,\ Bn = 1.$

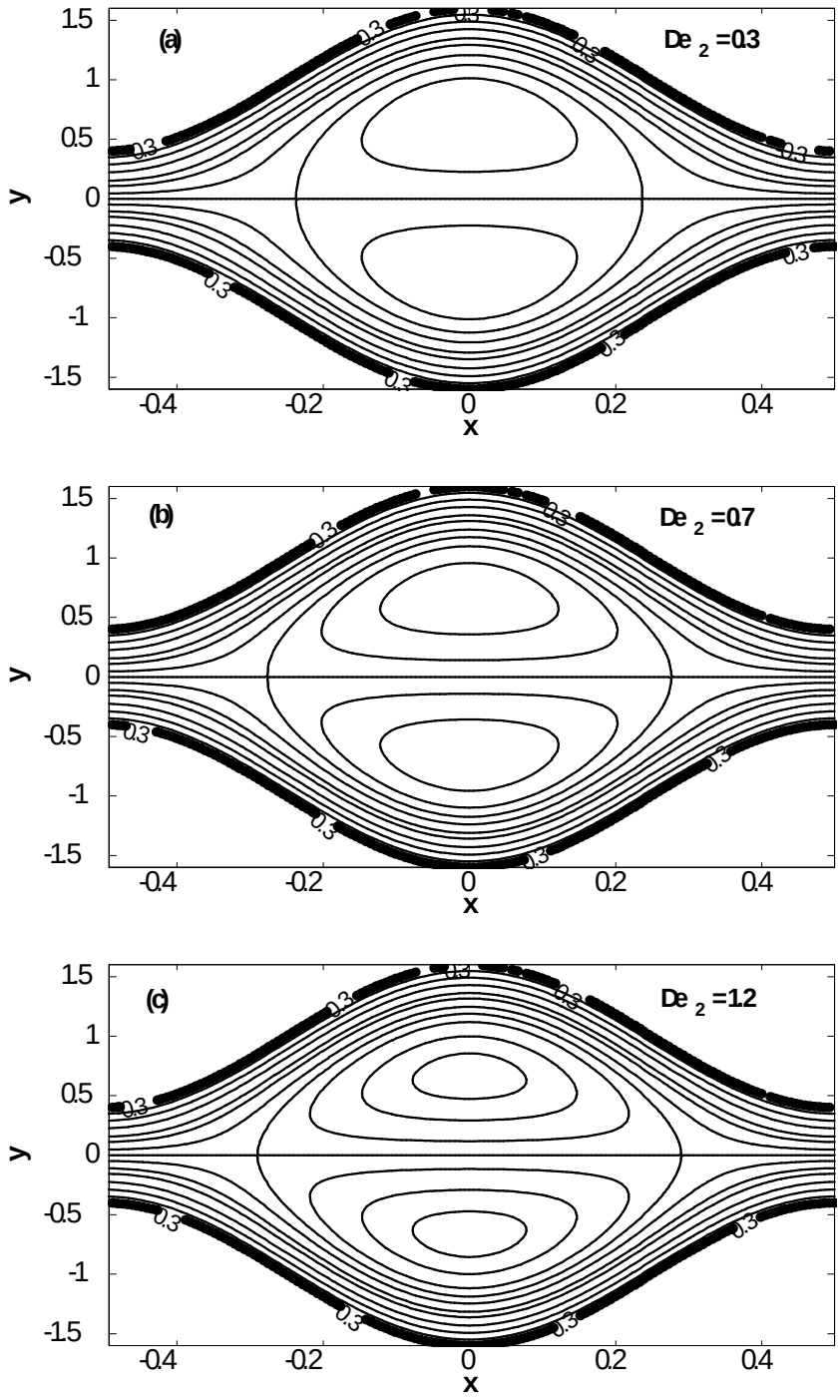

Fig. 2.16: Streamlines for De_2 with $\theta = 1.4,\ \phi = 0.6,\ De_1 = 0.5,\ \varepsilon = 0.2,\ \xi_1 = 0.8,\ Bn = 1.$

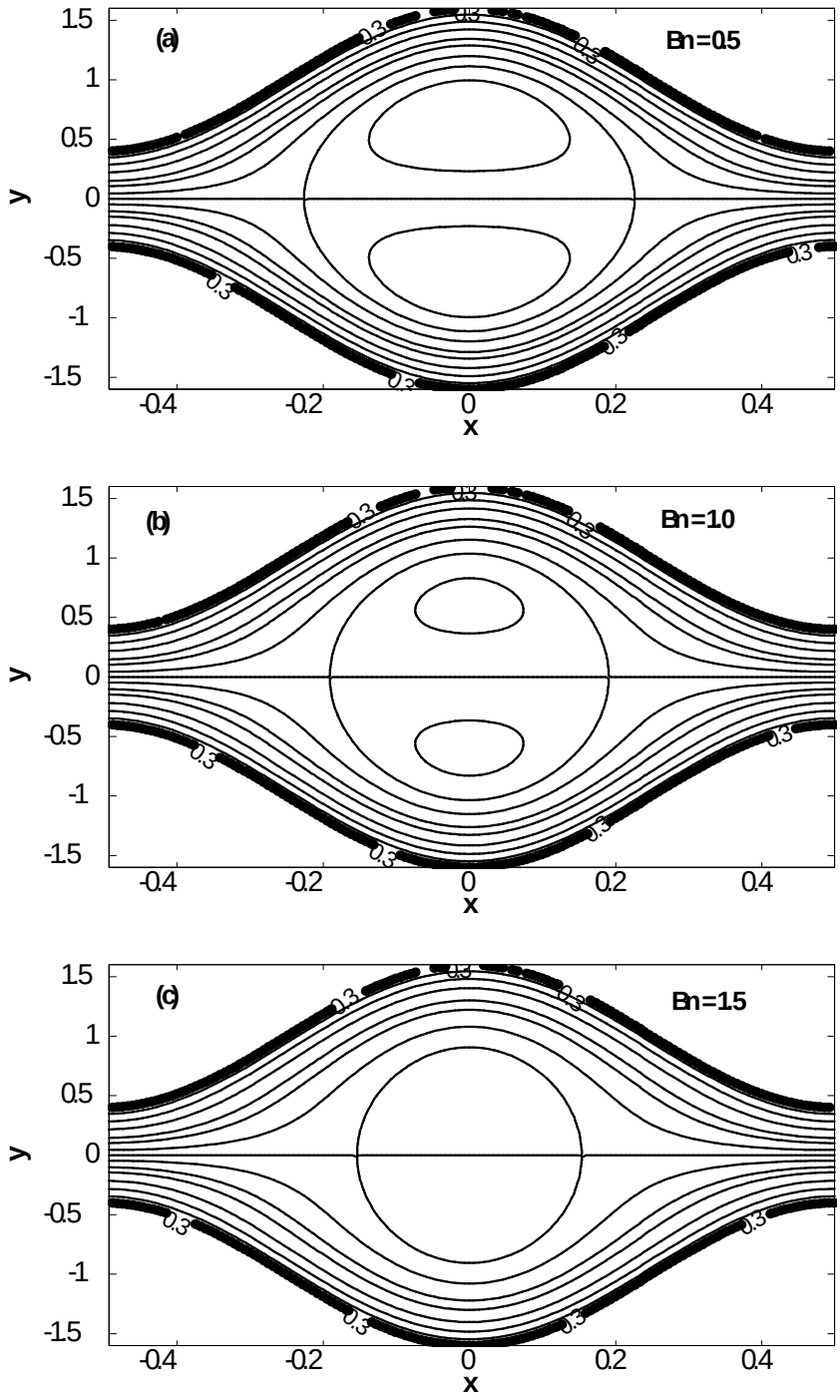

Fig. 2.17: Streamlines for Bn with $\theta = 1.4,\ \phi = 0.6,\ De_2 = 1.2,\ \varepsilon = 0.2,\ \xi_1 = 0.8,\ De_1 = 0.5$.

y	$Vel.\ (BVP4c)$	$Vel.(Shooting\ Method)$	$Vel.(BVP4c)$	$Vel.(Shooting\ Method)$
-1.60	-1.0000	-1.0000	-1.0000	-1.0000
-1.44	-0.7497	-0.7497	-0.7314	-0.7314
-1.28	-0.5353	-0.5353	-0.5041	-0.5041
-1.12	-0.3535	-0.3535	-0.3186	-0.3186
-0.96	-0.2019	-0.2019	-0.1737	-0.1737
-0.80	-0.0782	-0.0782	-0.0649	-0.0650
-0.64	0.0195	0.0195	0.0146	0.0145
-0.48	0.0929	0.0929	0.0710	0.0709
-0.32	0.1438	0.1438	0.1087	0.1087
-0.16	0.1735	0.1735	0.1304	0.1304
0.00	0.1832	0.1832	0.1375	0.1375
0.16	0.1735	0.1735	0.1304	0.1304
0.32	0.1438	0.1437	0.1087	0.1087
0.48	0.0929	0.0929	0.0710	0.0709
0.64	0.0195	0.0195	0.0146	0.0145
0.80	-0.0782	-0.0782	-0.0649	-0.0650
0.96	-0.2019	-0.2019	-0.1737	-0.1737
1.12	-0.3535	-0.3535	-0.3186	-0.3186
1.28	-0.5353	-0.5353	-0.5041	-0.5041
1.44	-0.7497	-0.7497	-0.7314	-0.7314
1.60	-1.0000	-1.0000	-1.0000	-1.0000

Table. 2.1: Comparison of solutions with $\theta = 1.4,\ \phi = 0.6,\ De_1 = 0.5,\ 1.5,$

$De_2 = 0.1, 0.3,\ \varepsilon = 0.2,\ \xi_1 = 0.8, Bn = 0.1.$

2.4 Concluding Remarks

The problem of peristaltic motion is investigated in a planar channel under the assumptions of long wavelength and low Reynolds number. We considered a fairly general constitutive

equation for extra stress tensor that describes the characteristics of viscosity, elasticity and plasticity. Therefore, the governing nonlinear differential equations involve three non-Newtonian parameters characterizing the viscous, elastic and plastic behaviors of the fluid. The analysis reveals the following main observations:

- The velocity profile decreases (increases) at the center (other parts of channel) due to increasing elasticity (De_1) whereas opposite effects are noticed in case of De_2.
- Increasing plasticity (Bn) results in rigidity of material and therefore the velocity profile becomes uniform at the center of channel. In case of strong plasticity the velocity profile becomes uniform in most part of the channel except very close to the wall of channel.
- Normal stress components τ_{xx} and τ_{yy} decrease by increasing De_1, De_2 and Bn.
- τ_{xy} increases (decreases) with De_1 (De_2 and Bn).
- The size and circulation of trapped bolus decrease by increasing elasticity (De_1) and plasticity (Bn). However, the size of bolus increases and it circulates faster by increasing De_2.

Chapter 3

An analysis of peristaltic flow of Finitely Extendable Nonlinear Elastic-Peterlin fluid in a two dimensional planar channel and axisymmetric tube

Peristaltic motion of non-Newtonian fluid characterized by Finitely Extendable Nonlinear Elastic-Peterlin (FENE-P) fluid model is investigated in this chapter. A background for development of the differential constitutive equation of this model has been provided. The flow analysis is carried out both for two-dimensional planar channel and axisymmetric tube. The governing equations have been simplified under the widely used assumptions of long wavelength and low Reynolds number in a frame of reference that moves with constant wave speed. An exact solution is obtained for the stream function and longitudinal pressure gradient with no slip condition. We have portrayed the effects of Deborah number and extensibility parameter on velocity profile, trapping phenomenon and normal stress. It is observed that normal stress is an increasing function of Deborah number and extensibility parameter. As far as the velocity at channel (tube) center is concerned, it decreases (increases) by increasing Deborah number

(extensibility parameter). The non-Newtonian rheology also affect the size of trapped bolus in a sense that the size of trapped bolus decreasses (increases) by increasing Deborah number (extensibility parameter). Further, it is observed through numerical integration that both Deborah number and extensibility parameter have opposite effects on pressure rise per wavelength and frictional forces at the wall. Moreover, it is shown that the results for Newtonian model can be deduced as a special case of FENE-P model. The contents of this chapter are published in the journal of Zeitschrift Fur Naturforschung A, $69a$, $462-472$ (2014).

3.1 Formulation of the Problem

The dumbbell model with the Warner force law and Peterlin approximation for the average spring force is called FENE-P model. This model was rooted in kinetic theory and was initially developed to represent the behavior of dilute polymer solutions. The kinetic theory assumes that the motion of the dumbbells is the combined result of the hydrodynamic force, the Brownian motion force and the connector force. This model leads to a differential constitutive equation that was provided in the form of extra stress tensor in Bird et. al. [135]. Following Chilcott and Rallison [136], we prefer to work with the model given in the form of configuration tensor $\mathbf{A}$, defined by $\mathbf{A} = 3\left\langle \mathbf{RR} \right\rangle / R_e^2$, in which $\mathbf{R}$ is end-to-end vector that connects the dumbbell beads, $\langle \cdot \rangle$ represents an ensemble average over the configuration space and R_e is the characteristic length. The connector force of the spring in the original FENE model follows the expression [137] proposed by Warner

$$\mathbf{F}^{(c)} = \frac{H_0}{1 - \left(\mathbf{R} \cdot \mathbf{R}\right) / R_0^2} \mathbf{R}, \tag{3.1}$$

where H_0 is the Gaussian stiffness in the limit of small molecular extension and R_0 is the maximum allowable dumbbell length. The nonlinearity in (3.1) induces the non-closure problem usually encountered in many areas of statistical physics and a closed form constitutive equation is not possible unless an approximation is made. A well known approximation was made by Peterlin [138]. According to which the configuration dependent nonlinear factor in (3.1) is replaced by a self-consistently averaged term. Thus we can write

$$F^{(c)} \approx \frac{H_0}{1 - \left\langle \mathbf{R}^2 \right\rangle / R_0^2} \mathbf{R} \equiv f H_0 \mathbf{R}, \tag{3.2}$$

where $\left\langle \mathbf{R}^2 \right\rangle$ is already defined and ($\equiv$) means the identically equivalent. After making use of configuration tensor we note that the dimensionless function f gets the form [137],

$$f = f\left(tr\mathbf{A}\right) = \frac{L^2}{L^2 - tr\mathbf{A}}. \tag{3.3}$$

Here L^2 is a measure of the extensibility of the dumbbells and is defined as $L^2 = 3R_0^2/R_e^2$. It is also related to $b(= H_0R_0^2/k_1T)$ by $L^2 = b + 3$ as was used in [135], where k_1 is the Boltzmann constant and T the absolute temperature.

Now the ensemble averaging of equations of motion for dumbbells yield the following evolution equation for $\mathbf{A}$, ([135], [139])

$$\overset{\nabla}{\mathbf{A}} = -\frac{1}{\lambda_1}\left(f\mathbf{A} - a\mathbf{I}\right). \tag{3.4}$$

Eq. (3.4) must be used in conjunction with the Kramer's relation for polymeric stress

$$\overline{\boldsymbol{\tau}} = \frac{\eta_p}{\lambda_1}\left(f\mathbf{A} - a\mathbf{I}\right). \tag{3.5}$$

In above equations, η_p is the zero shear rate polymer viscosity, λ_1 the relaxation time and a is a parameter that depends on extensibility parameter (L^2) by $a = 1/\left(1 - 3/L^2\right)$. The parameter a has the relation with the physical properties by $a = 1 + \left(3k_1T/H_0R_0^2\right)$ and is also related to b by $a = 1 + (3/b)$. On combining (3.4) and (3.5), we get

$$\overset{\nabla}{\mathbf{A}} = -\overline{\boldsymbol{\tau}}/\eta_p \tag{3.6}$$

Generally, the operator $d/d\bar{t}$ satisfies the equation

$$\frac{d}{d\overline{t}}\left(f\mathbf{A}\right) = f\left(\overset{\nabla}{\mathbf{A}}\right) + \mathbf{A}\frac{df}{d\overline{t}} \tag{3.7}$$

for any function f. Here we would like to mention that for axisymmetric case the material derivative $d/d\bar{t}$ is defined by

$$\frac{d}{d\overline{t}} = \frac{\partial}{\partial\overline{t}} + \overline{V}_{\overline{R}}\frac{\partial}{\partial\overline{R}} + \overline{V}_{\overline{Z}}\frac{\partial}{\partial\overline{Z}} \tag{3.8}$$

in which $\overline{V}_{\overline{R}}$ and $\overline{V}_{\overline{Z}}$ are the velocity components in radial and axial directions respectively.

If we apply the upper convected operator $^{\nabla}$ to (3.5), we find

$$\overset{\nabla}{\boldsymbol{\tau}} = \frac{\eta_p}{\lambda_1}\left(\left(f\overset{\nabla}{\mathbf{A}}\right) - a\overset{\nabla}{\mathbf{I}}\right) = \frac{\eta_p}{\lambda_1}\left(\left(f\overset{\nabla}{\mathbf{A}}\right) + 2a\mathbf{D}\right). \tag{3.9}$$

Here we used the result $\overset{\nabla}{\mathbf{I}} = -2\mathbf{D}$ by following [61].

3.1.1 Flow in a planar channel

The geometry of the planar channel is already explained in section 2.1 of the previous chapter. After making use of the transformations (2.18), dimensionless variables (2.24) and definition of stream function (2.41), the form of material derivative (1.11) in terms of stream function becomes

$$\frac{d}{dt} = \delta\left(\frac{\partial\psi}{\partial y}\frac{\partial}{\partial x} - \frac{\partial\psi}{\partial x}\frac{\partial}{\partial y}\right). \tag{3.10}$$

The governing equations for the problem under consideration given Eqs. $(2.25) - (2.27)$. In view of the definition of the stream function (2.41), these equations take the following form

$$\begin{aligned}
\operatorname{Re}\delta\left(\psi_y\frac{\partial}{\partial x} - \psi_x\frac{\partial}{\partial y}\right)\psi_y &= -\frac{\partial p}{\partial x} + \delta\frac{\partial}{\partial x}\tau_{xx} + \frac{\partial}{\partial y}\tau_{xy}, &(3.11)\\
-\operatorname{Re}\delta^3\left(\psi_y\frac{\partial}{\partial x} - \psi_x\frac{\partial}{\partial y}\right)\psi_x &= -\frac{\partial p}{\partial y} + \delta^2\frac{\partial}{\partial x}\tau_{yx} + \delta\frac{\partial}{\partial y}\tau_{yy}. &(3.12)
\end{aligned}$$

Employing the long wavelength approximation [102, 103], the material derivative (3.21) vanishes, i.e., $d/dt = 0$. Using this result in (3.7) and then incorporating the resulting equation in Eq. (3.9), we obtain an equation that yields an explicit relation between $\overset{\nabla}{\boldsymbol{\tau}}$ and $\overset{\nabla}{\mathbf{A}}$ that is

$$\overset{\nabla}{\boldsymbol{\tau}} = \frac{\eta_p}{\lambda_1}\left(f\overset{\nabla}{\mathbf{A}} + 2a\mathbf{D}\right). \tag{3.13}$$

From Eqs. (3.13) and (3.6), we get the constitutive equation of extra stress tensor for the FENE-P model

$$f\overline{\boldsymbol{\tau}} + \lambda_1\overset{\nabla}{\overline{\boldsymbol{\tau}}} = 2a\eta_p\overline{\mathbf{D}}. \tag{3.14}$$

Now it is desired to express f in terms of $\overline{\boldsymbol{\tau}}$, for which we take the trace of (3.5) and get

$$trA = \frac{3a + \frac{\lambda_1}{\eta_p} tr\overline{\boldsymbol{\tau}}}{f}. \tag{3.15}$$

Using above equation in (3.3), we find

$$f = 1 + \frac{3a + (\lambda_1/\eta_p)(tr(\overline{\boldsymbol{\tau}}))}{L^2}. \tag{3.16}$$

Upon making use of (2.6) for the expression of tensor $\overline{\mathbf{D}}$ and the definition of upper convected derivative from (2.7), the component forms of Eq. (3.27) in fixed frame $(\overline{X}, \overline{Y})$ yield

$$\begin{aligned}
& f\overline{\tau}_{\overline{XX}} + \lambda_1 \left\{ \left(\frac{\partial}{\partial \overline{t}} + \overline{U}\frac{\partial}{\partial \overline{X}} + \overline{V}\frac{\partial}{\partial \overline{Y}} \right) \overline{\tau}_{\overline{XX}} - \left(\left(\nabla \overline{\mathbf{V}}\right)^* \overline{\boldsymbol{\tau}} \right)_{\overline{XX}} - \left(\overline{\boldsymbol{\tau}} \left(\nabla \overline{\mathbf{V}}\right) \right)_{\overline{XX}} \right\} \\
= \; & a\eta_p \left(\nabla \overline{\mathbf{V}} + (\nabla \overline{\mathbf{V}})^* \right)_{\overline{XX}}, \qquad (3.17) \\
& f\overline{\tau}_{\overline{XY}} + \lambda_1 \left\{ \left(\frac{\partial}{\partial \overline{t}} + \overline{U}\frac{\partial}{\partial \overline{X}} + \overline{V}\frac{\partial}{\partial \overline{Y}} \right) \overline{\tau}_{\overline{XY}} - \left(\left(\nabla \overline{\mathbf{V}}\right)^* \overline{\boldsymbol{\tau}} \right)_{\overline{XY}} - \left(\overline{\boldsymbol{\tau}} \left(\nabla \overline{\mathbf{V}}\right) \right)_{\overline{XY}} \right\} \\
= \; & a\eta_p \left(\nabla \overline{\mathbf{V}} + (\nabla \overline{\mathbf{V}})^* \right)_{\overline{XY}}, \qquad (3.18) \\
& f\overline{\tau}_{\overline{YY}} + \lambda_1 \left\{ \left(\frac{\partial}{\partial \overline{t}} + \overline{U}\frac{\partial}{\partial \overline{X}} + \overline{V}\frac{\partial}{\partial \overline{Y}} \right) \overline{\tau}_{\overline{YY}} - \left(\left(\nabla \overline{\mathbf{V}}\right)^* \overline{\boldsymbol{\tau}} \right)_{\overline{YY}} - \left(\overline{\boldsymbol{\tau}} \left(\nabla \overline{\mathbf{V}}\right) \right)_{\overline{YY}} \right\} \\
= \; & a\eta_p \left(\nabla \overline{\mathbf{V}} + (\nabla \overline{\mathbf{V}})^* \right)_{\overline{YY}}. \qquad (3.19)
\end{aligned}$$

Invoking Eq. (2.18) and Eq. (2.24), Eqs. (3.16) – (3.19) can be put in the following dimensionless form

$$f = 1 + \frac{3a + (De)\left(tra\left(\tau\right)\right)}{L^2} \tag{3.20}$$

$$\begin{aligned}
& f\tau_{xx} + De\delta \left\{ \left(u\frac{\partial}{\partial x} + v\frac{\partial}{\partial y} \right) \tau_{xx} - 2\left(\tau_{xx}\frac{\partial u}{\partial x} + \delta\tau_{yx}\frac{\partial v}{\partial x} \right) \right\} \\
= \; & 2a\delta\tau_{xx}\frac{\partial u}{\partial x}, \qquad (3.21) \\
& f\tau_{xy} + De\delta \left\{ \left(u\frac{\partial}{\partial x} + v\frac{\partial}{\partial y} \right) \tau_{xy} - \left(\tau_{xy}\frac{\partial u}{\partial x} + \delta^2\frac{\partial v}{\partial x} \right) \right\} \\
= \; & a\left(\delta^2\frac{\partial v}{\partial x} + \frac{\partial u}{\partial x} \right) + De\left(\tau_{xx}\frac{\partial u}{\partial x} + \delta\tau_{yx}\frac{\partial v}{\partial x} \right), \qquad (3.22)
\end{aligned}$$

$$
\begin{aligned}
& f\tau_{yy} + De\left\{\delta\left(u\frac{\partial}{\partial x} + v\frac{\partial}{\partial y}\right)\tau_{yy} - 2\left(\tau_{xy}\frac{\partial u}{\partial y} + \delta\tau_{yy}\frac{\partial v}{\partial y}\right)\right\} \\
= \quad & 2a\delta^2\frac{\partial v}{\partial y}. \qquad (3.23)
\end{aligned}
$$

After using the definition of stream function through (2.41) in (3.20) − (3.23) and then employing the long wavelength and low Reynolds number assumptions on the resulting equations, we have

$$
0 = -\frac{\partial p}{\partial x} + \frac{\partial}{\partial y}\tau_{xy}, \quad 0 = -\frac{\partial p}{\partial y}, \qquad (3.24)
$$

Similarly, Eqs. (3.11) and (3.12) give

$$
f\tau_{xx} = 0, \quad f\tau_{xy} = De\tau_{xx}\psi_{yy} + a\psi_{yy}, \quad f\tau_{yy} = 2De\tau_{xy}\psi_{yy}. \qquad (3.25)
$$

Now on solving Eq. (3.24) and Eq. (3.25) for the components of extra stress tensor and f, we arrive at

$$
f = 1 + \frac{3a + (\frac{2De^2}{a})(\tau_{xy})^2}{L^2},\ \tau_{xy} = \left(y\frac{\partial p}{\partial x} + A_1\right),\ \tau_{yy} = \frac{2De(\tau_{xy})^2}{a} = tra(\boldsymbol{\tau}),\ \tau_{xx} = 0, \qquad (3.26)
$$

where A_1 is a constant of integration. The boundary conditions in the wave frame are same as in [1140]

$$
\begin{aligned}
\psi &= 0, \quad \frac{\partial u}{\partial y} = \frac{\partial^2\psi}{\partial y^2} = 0, \quad at\ y = 0, && (3.27)\\
\psi &= q, \quad \frac{\partial \psi}{\partial y} = -1, \quad at\ y = h, && (3.28)\\
\theta - 1 &= q = \int_0^h \frac{\partial \psi}{\partial y} dy = \psi(h) - \psi(0). && (3.29)
\end{aligned}
$$

By means of (3.26) and the second boundary condition in (3.27), we obtain the following expression of velocity gradient from (3.25):

$$
\frac{\partial^2\psi}{\partial y^2} = \frac{p_x y}{a}\left(1 + \frac{3a + (2De^2/a)p_x^2 y^2}{L^2}\right). \qquad (3.30)
$$

Since $\left(1+\frac{3a}{L^2}\right)/a$ is unity by definition of a, therefore we can write (3.30) as

$$\frac{\partial^2\psi}{\partial y^2}=\frac{\partial u}{\partial y}=p_x y\left(1+\frac{2De^2}{a^2L^2}p_x^2y^2\right). \tag{3.31}$$

Integrating (3.31) and making use of first condition in (3.27) and the second condition in (3.28), we get the following expression of stream function

$$\psi=-y-\frac{dp}{dx}\left((1/2)\left(h^2y-y^3/3\right)+(5B_1/4)(h^4y-y^5/5)\left(\frac{dp}{dx}\right)^2\right). \tag{3.32}$$

Now using the remaining boundary condition in (3.28), i.e., $\psi=q$ at $y=h$, we find

$$\frac{dp}{dx}=\frac{-2\left(2^{1/3}\right)h^8B_1+2^{2/3}\left(-27B_1^2\left(h+q\right)h^{10}+\sqrt{B_1^3h^{20}\left(4h^4+729(h+q)^2B_1\right)}\right)^{2/3}}{6h^5B_1\left(-27B_1^2\left(h+q\right)h^{10}+\sqrt{B_1^3h^{20}\left(4h^4+729(h+q)^2B_1\right)}\right)^{1/3}}, \tag{3.33}$$

where $B_1=2De^2/5a^2L^2$. The pressure rise per wavelength ΔP_λ and frictional forces F_λ on the wall are defined through Eqs. (2.51) and (2.52).

$$\Delta P_\lambda = \int_0^1\left(\frac{dp}{dx}\right)dx, \tag{3.34}$$

$$F_\lambda = \int_0^1 h^2\left(-\frac{dp}{dx}\right)dx \tag{3.35}$$

3.1.2 Flow in an axisymmetric tube

Before proceeding ahead, we mention here that the alternative notations for coordinates, velocity components and stresses will be used for the flow in an axisymmetric tube and rest of the quantities/parameters will be denoted by the same symbols as used in the previous section. Now we consider the peristaltic transport of an incompressible viscoelastic fluid represented by FENE-P model in a flexible axisymmetric tube of radius a_1. In cylindrical coordinates $\left(\overline{R},\overline{Z}\right)$ the shape of tube wall is given as

$$\overline{H}(\overline{Z},\bar{t})=a_1+b_1\left[\cos\left(\frac{2\pi}{\lambda}\left(\overline{Z}-c\,\bar{t}\right)\right)\right]. \tag{3.36}$$

A schematic diagram of the flow geometry is given below.

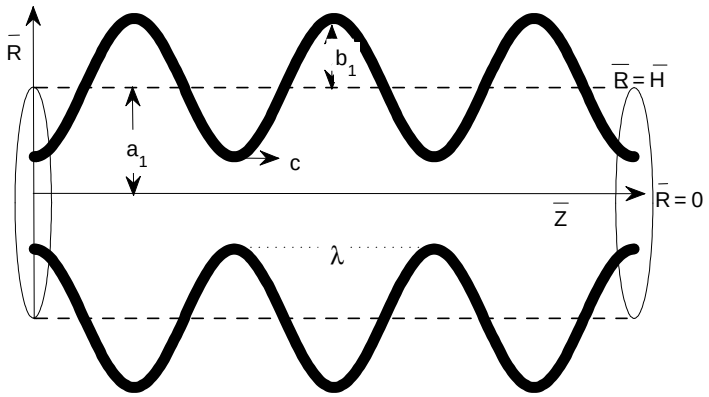

Fig. 3.1 Geometry of the problem for axisymmetric case

The flow is governed by the following equations:

$$\frac{1}{\overline{R}}\frac{\partial}{\partial\overline{R}}\left(\overline{R}\overline{V}_{\overline{R}}\right)+\frac{\partial\overline{V}_{\overline{Z}}}{\partial\overline{Z}}=0, \tag{3.37}$$

$$\rho\frac{d}{d\overline{t}}\overline{V}_{\overline{R}} = -\frac{\partial\overline{P}}{\partial\overline{R}}+\frac{1}{\overline{R}}\frac{\partial}{\partial\overline{R}}\left(\overline{R}\overline{\tau}_{\overline{R}\overline{R}}\right)+\frac{\partial}{\partial\overline{Z}}\overline{\tau}_{\overline{R}\overline{Z}}, \tag{3.38}$$

$$\rho\frac{d}{d\overline{t}}\overline{V}_{\overline{Z}} = -\frac{\partial\overline{P}}{\partial\overline{Z}}+\frac{1}{\overline{R}}\frac{\partial}{\partial\overline{R}}\left(\overline{R}\overline{\tau}_{\overline{Z}\overline{R}}\right)+\frac{\partial}{\partial\overline{Z}}\overline{\tau}_{\overline{Z}\overline{Z}}, \tag{3.39}$$

where $\overline{V}_{\overline{R}}$ and $\overline{V}_{\overline{Z}}$ are radial and axial components of velocity, respectively. The material derivative $d/d\overline{t}$ is defined by

$$\frac{d}{d\overline{t}}=\frac{\partial}{\partial\overline{t}}+\overline{V}_{\overline{R}}\frac{\partial}{\partial\overline{R}}+\overline{V}_{\overline{Z}}\frac{\partial}{\partial\overline{Z}} \tag{3.40}$$

The coordinates, velocities and pressures in the laboratory frame $(\overline{R},\overline{Z})$ and the wave frame

$(\overline{r}, \overline{z})$ are related through the following expressions:

$$\overline{z} = \overline{Z} - c\overline{t}, \quad \overline{r} = \overline{R}, \quad \overline{v}_{\overline{z}} = \overline{V}_{\overline{Z}} - c, \quad \overline{v}_{\overline{r}} = \overline{V}_{\overline{R}}, \quad \overline{p}(\overline{r}, \overline{z}) = \overline{P}(\overline{R}, \overline{Z}, \overline{t}), \tag{3.41}$$

where $\overline{v}_{\overline{z}}$, $\overline{v}_{\overline{r}}$ are the axial and radial components of velocity, respectively and $\overline{p}$ is the pressure in the wave frame. Making use of (3.41), defining the dimensionless variables as

$$z = \frac{\overline{z}}{\lambda}, \; r = \frac{\overline{r}}{a_1}, \; v_z = \frac{\overline{v}_{\overline{z}}}{c}, \; v_r = \frac{\overline{v}_{\overline{r}}}{c\delta}, \; t = \frac{\pi c\overline{t}}{\delta}, \; p = \frac{\delta a_1 \overline{p}}{\eta_p c}, \; h = \frac{\overline{h}}{a_1}, \; \boldsymbol{\tau} = \frac{a_1}{c\eta_p}\overline{\boldsymbol{\tau}} \tag{3.42}$$

and the stream function by

$$v_r = -\frac{1}{r}\frac{\partial \psi}{\partial z}, \qquad v_z = \frac{1}{r}\frac{\partial \psi}{\partial r}, \tag{3.43}$$

the continuity equation (3.37) is identically satisfied whereas Eq. (3.36) and Eqs. (3.38) – (3.40)

$$h\left(z\right) = 1 + \phi_a \cos 2\pi z, \tag{3.44}$$

$$\begin{aligned} \mathrm{Re}\,\delta^3 \left(v_r \frac{\partial}{\partial r} + v_z \frac{\partial}{\partial z} \right) v_r &= -\frac{\partial p}{\partial r} + \frac{\delta}{r}\frac{\partial \left(r\tau_{rr}\right)}{\partial r} + \delta^2 \frac{\partial \tau_{rz}}{\partial z}, & (3.45) \\ \mathrm{Re}\,\delta \left(v_r \frac{\partial}{\partial r} + v_z \frac{\partial}{\partial z} \right) v_z &= -\frac{\partial p}{\partial z} + \frac{1}{r}\frac{\partial \left(r\tau_{zr}\right)}{\partial r} + \delta \frac{\partial \tau_{zz}}{\partial z}, & (3.46) \end{aligned}$$

$$\frac{d}{dt} = \delta \left(v_r \frac{\partial}{\partial r} + v_z \frac{\partial}{\partial z} \right). \tag{3.47}$$

Here $\phi_a = b_1/a_1$ is the amplitude ratio for the axisymmetric case. On using the assumption of long wavelength in Eq. (3.47), we have $d/dt = 0$. The constitutive equation for extra stress is already given in Eq. (3.14). After making use of Eq. (2.6) and the definition of upper convective derivative again, the component form of Eq. (3.14) in fixed frame $\left(\overline{R}, \overline{Z}\right)$ is

$$\begin{aligned} & f\overline{\tau}_{\overline{RR}} + \lambda_1 \left\{ \left(\frac{\partial}{\partial \overline{t}} + \overline{V}_{\overline{R}} \frac{\partial}{\partial \overline{R}} + \overline{V}_{\overline{Z}} \frac{\partial}{\partial \overline{Z}} \right) \overline{\tau}_{\overline{RR}} - \left(\left(\nabla \overline{\mathbf{V}}\right)^* \overline{\boldsymbol{\tau}} \right)_{\overline{RR}} - \left(\overline{\boldsymbol{\tau}} \left(\nabla \overline{\mathbf{V}}\right) \right)_{\overline{RR}} \right\} \\ = \; & a\eta_p \left(\nabla \overline{\mathbf{V}} + \left(\nabla \overline{\mathbf{V}}\right)^* \right)_{\overline{RR}}, \end{aligned} \tag{3.48}$$

$$
\begin{aligned}
& f\overline{\tau}_{\overline{R}\overline{Z}} + \lambda_1 \left\{ \left(\frac{\partial}{\partial \overline{t}} + \overline{V}_{\overline{R}} \frac{\partial}{\partial \overline{R}} + \overline{V}_{\overline{Z}} \frac{\partial}{\partial \overline{Z}} \right) \overline{\tau}_{\overline{R}\overline{Z}} - \left(\left(\nabla \overline{\mathbf{V}} \right)^* \overline{\boldsymbol{\tau}} \right)_{\overline{R}\overline{Z}} - \left(\overline{\boldsymbol{\tau}} \left(\nabla \overline{\mathbf{V}} \right) \right)_{\overline{R}\overline{Z}} \right\} \\
= \; & a\eta_p \left(\nabla \overline{\mathbf{V}} + (\nabla \overline{\mathbf{V}})^* \right)_{\overline{R}\overline{Z}}, \qquad (3.49) \\
& f\overline{\tau}_{\overline{Z}\overline{Z}} + \lambda_1 \left\{ \left(\frac{\partial}{\partial \overline{t}} + \overline{V}_{\overline{R}} \frac{\partial}{\partial \overline{R}} + \overline{V}_{\overline{Z}} \frac{\partial}{\partial \overline{Z}} \right) \overline{\tau}_{\overline{Z}\overline{Z}} - \left(\left(\nabla \overline{\mathbf{V}} \right)^* \overline{\boldsymbol{\tau}} \right)_{\overline{Z}\overline{Z}} - \left(\overline{\boldsymbol{\tau}} \left(\nabla \overline{\mathbf{V}} \right) \right)_{\overline{Z}\overline{Z}} \right\} \\
= \; & a\eta_p \left(\nabla \overline{\mathbf{V}} + (\nabla \overline{\mathbf{V}})^* \right)_{\overline{Z}\overline{Z}}. \qquad (3.50)
\end{aligned}
$$

Incorporating Eq. (3.40) and Eq. (3.41), Eqs. $(3.48) - (3.50)$ in dimensionless form become

$$
\begin{aligned}
& f\tau_{rr} + De \left\{ \delta \left(v_r \frac{\partial}{\partial r} + v_z \frac{\partial}{\partial z} \right) \tau_{rr} - 2 \left(\delta \tau_{rr} \frac{\partial v_r}{\partial r} + \tau_{zr} \frac{\partial v_z}{\partial r} \right) \right\} \\
= \; & a\delta \frac{\partial v_r}{\partial r}, \qquad (3.51) \\
& f\tau_{rz} + De \left\{ \delta \left(v_r \frac{\partial}{\partial r} + v_z \frac{\partial}{\partial z} \right) \tau_{rz} - \left(\delta \tau_{rz} \frac{\partial v_r}{\partial r} + \tau_{zz} \frac{\partial v_z}{\partial r} \right) \right\} \\
= \; & a \left(\delta^2 \frac{\partial v_r}{\partial z} + \frac{\partial v_z}{\partial r} \right) + De\delta \left(\delta^2 \tau_{rr} \frac{\partial v_r}{\partial z} + \delta \tau_{rz} \frac{\partial v_z}{\partial z} \right), \qquad (3.52) \\
& f\tau_{zz} + De \left\{ \delta \left(v_r \frac{\partial}{\partial r} + v_z \frac{\partial}{\partial z} \right) \tau_{zz} - 2 \left(\delta^2 \tau_{rz} \frac{\partial v_r}{\partial z} + \delta \tau_{zz} \frac{\partial v_z}{\partial z} \right) \right\} \\
= \; & a\delta \frac{\partial v_z}{\partial z}. \qquad (3.53)
\end{aligned}
$$

Now on applying the assumptions of long wavelength and low Reynolds number, the scalar momentum equation (3.45) and (3.46) and Eqs. $(3.51) - (3.53)$ yield

$$
\begin{aligned}
0 &= -\frac{\partial p}{\partial r}, \; 0 = -\frac{\partial p}{\partial z} + \frac{1}{r} \frac{\partial \left(r\tau_{zr} \right)}{\partial r}, \qquad (3.54) \\
f\tau_{rr} &= 2De\tau_{zr} \frac{\partial}{\partial r} \left(\frac{1}{r} \frac{\partial \psi}{\partial r} \right), \quad f\tau_{rz} = De\tau_{zz} \frac{\partial}{\partial r} \left(\frac{1}{r} \frac{\partial \psi}{\partial r} \right) + a \frac{\partial}{\partial r} \left(\frac{1}{r} \frac{\partial \psi}{\partial r} \right), \quad f\tau_{zz} = 0 \qquad (3.55)
\end{aligned}
$$

After little algebraic manipulations, we can have

$$
\tau_{rz} = \frac{p_z r}{2} + \frac{A_2}{r}, \; f = 1 + \frac{3a + \left(2De^2/a \right) \left(\tau_{rz} \right)^2}{L^2}, \; \tau_{rr} = \frac{2De \left(\tau_{rz} \right)^2}{a} = tra(\boldsymbol{\tau}), \; \tau_{zz} = 0, \quad (3.56)
$$

where A_2 is the constant of integration. The boundary conditions in the wave frame are defined

as [142]

$$\psi = 0, \quad \frac{\partial}{\partial r}\left(\frac{1}{r}\frac{\partial \psi}{\partial r}\right) = 0, \qquad at\ r = 0, \tag{3.57}$$

$$\psi = q_a, \quad \frac{1}{r}\frac{\partial \psi}{\partial r} = -1, \qquad at\ r = h, \tag{3.58}$$

$$\theta - \frac{1}{2}\left(1 + \frac{\phi_a^2}{2}\right) = q_a = \int_0^h \frac{\partial \psi}{\partial r} dy = \psi(h) - \psi(0). \tag{3.59}$$

Now adopting the same procedure for obtaining stream function and pressure gradient as described for planar case, we arrive at the following expressions:

$$\psi = -\frac{r^2}{2} + \frac{1}{2}\frac{dp}{dz}\left((1/8)\left(2h^2r^2 - r^4\right) + \frac{C}{2}(3h^4r^2 - r^6)\left(\frac{dp}{dz}\right)^2\right), \tag{3.60}$$

$$\frac{dp}{dz} = \frac{-6^{2/3}h^{10}C + 6^{1/3}\left(-144C^2\left(h^2 + 2q_a\right)h^{12} + \sqrt{6}\sqrt{C^3h^{24}\left(h^6 + 3456\left(h^2 + 2q_a\right)^2 C\right)}\right)^{2/3}}{12h^6C\left(-144\beta^2\left(h^2 + 2q_a\right)h^{12} + \sqrt{6}\sqrt{C^3h^{24}\left(h^6 + 3456\left(h^2 + 2q_a\right)^2 C\right)}\right)^{1/3}}, \tag{3.61}$$

where $C = De^2/24a^2L^2$. The pressure rise per wavelength ΔP_λ and frictional forces F_λ are defined through the following formulas:

$$\Delta P_\lambda = \int_0^1 \left(\frac{dp}{dz}\right) dz, \tag{3.62}$$

$$F_\lambda = \int_0^1 h^2 \left(-\frac{dp}{dz}\right) dz. \tag{3.63}$$

3.2 Discussion of the Results

We break up this section into three subsections namely, flow behavior, trapping and pumping phenomena. The detail of these subsections is as follows:

3.2.1 Flow behavior

This part describes the effects of De and (L^2) on the velocity profile and the normal stresses which are depicted in Figs. $(3.2) - (3.4)$. Here we observe that these parameters leave the

opposite effects on the velocity profile but the same effects on the normal stresses. From Figs. 3.2 and 3.3 we observe that the magnitude of the velocity increases at the centre of the channel with the increase of L^2 but decreases by increasing De. We also note that the magnitude of velocity profile is greater for axisymmetric flow compared with the case of planar flow. Here it is important to note that the results for Newtonian fluid can be obtained when either $De \longrightarrow 0$ or $L^2 \longrightarrow \infty$. A departure from Newtonian behavior is observed for small values of L^2 or large values of De. In fact the velocity profile shows shear thinning behavior and become flatter as $L^2 \longrightarrow \infty$ or $De \longrightarrow 0$. We also observe that the velocity field is parabolic for both the Newtonian and FENE-P fluids. Fig. 3.4 highlights the effects of De and L^2 on normal stresses for the axisymmetric case. It is seen that the normal stresses increase by increasing these parameters.

3.2.2 Trapping Phenomenon

This subsection describes the effects of pertinent parameters on trapping phenomenon, through Figs. 3.5 and 3.6. Figs. $3.5a, b$ show the effects of De on trapping for fixed value of L^2. We observe that the size of the trapped bolus decreases by increasing De. Moreover, the size of trapped bolus is greater in the case of axisymmetric flow when compared with the planar flow. From Figs. $3.6a, b$, we observe that L^2 leaves the opposite effects on trapping phenomenon in comparison with De. Thus we may interpret from all these figures that size and circulation of the trapped bolus reduces for a shear-thinning fluid in comparison with Newtonian fluid.

3.2.3 Pumping Phenomenon

Here our focus is to explore the effects of FENE-P model parameters on pressure rise per wavelength ΔP_λ and frictional forces F_λ. For the analysis we have performed numerical integration for the evaluation of integrals appearing in Eqs. (3.34), (3.35), (3.63) and (3.64) using *Mathematica.* The results are shown in Figs. 3.7 and 3.8. We have depicted the results only for axisymmetric case and one can easily observe the same effects for the channel flow only with qualitative differences, i.e., pressure rise attains higher values in the axisymmetric case compared with the planar case.

Fig. 3.7 shows the effects of De and L^2 on ΔP_λ. Since the peristaltic flow shows different

interesting behaviors, therefore Fig. 3.7 is divided into following four sub-regions:

The region in which $\Delta P_\lambda > 0$ and $\theta < 0$ is called retrograde pumping region.

The region where $\Delta P_\lambda > 0$ and $\theta > 0$ is called as peristaltic pumping region.

Third region corresponds to $\Delta P_\lambda = 0$, which is called free pumping region.

The region in which $\Delta P_\lambda < 0$ but $\theta > 0$ is called augmented pumping region.

Fig. 3.7 shows that ΔP_λ decreases by increasing the flow rate θ. Moreover, ΔP_λ shows a linear behavior for Newtonian case whereas nonlinear behavior for the FENE-P fluid. We also note that the De and L^2 leave the opposite effect on ΔP_λ in the retrograde and peristaltic pumping regions i.e., ΔP_λ decreases (increases) by increasing De (L^2). However, in augmented pumping region the situation is reversed. As already mentioned, large values of De or small values of L^2 correspond to shear thinning fluid. Then we may conclude from Figs. 3.7a and b that ΔP_λ in peristaltic pumping region is greater for Newtonian fluid in comparison with the shear thinning fluid. Such observations are also reported in some previous studies [42, 43].

Fig.3.8 presents the variation of frictional force F_λ against the mean flow rate θ for different values of De and L^2. From this figure we see that F_λ increases by increasing θ and show linear behavior for Newtonian case whereas nonlinear behavior for the FENE-P fluid. We observe from Fig. 3.8a that F_λ resists the flow till $\theta \approx 0.3$ and gets weak after this critical value. The resistance provided by F_λ is greater for the Newtonian fluid in comparison with with shear thinning fluid. The effect of De on the frictional forces is opposite to that of L^2 and also with a different value of flow rate $\theta = 0.27$.

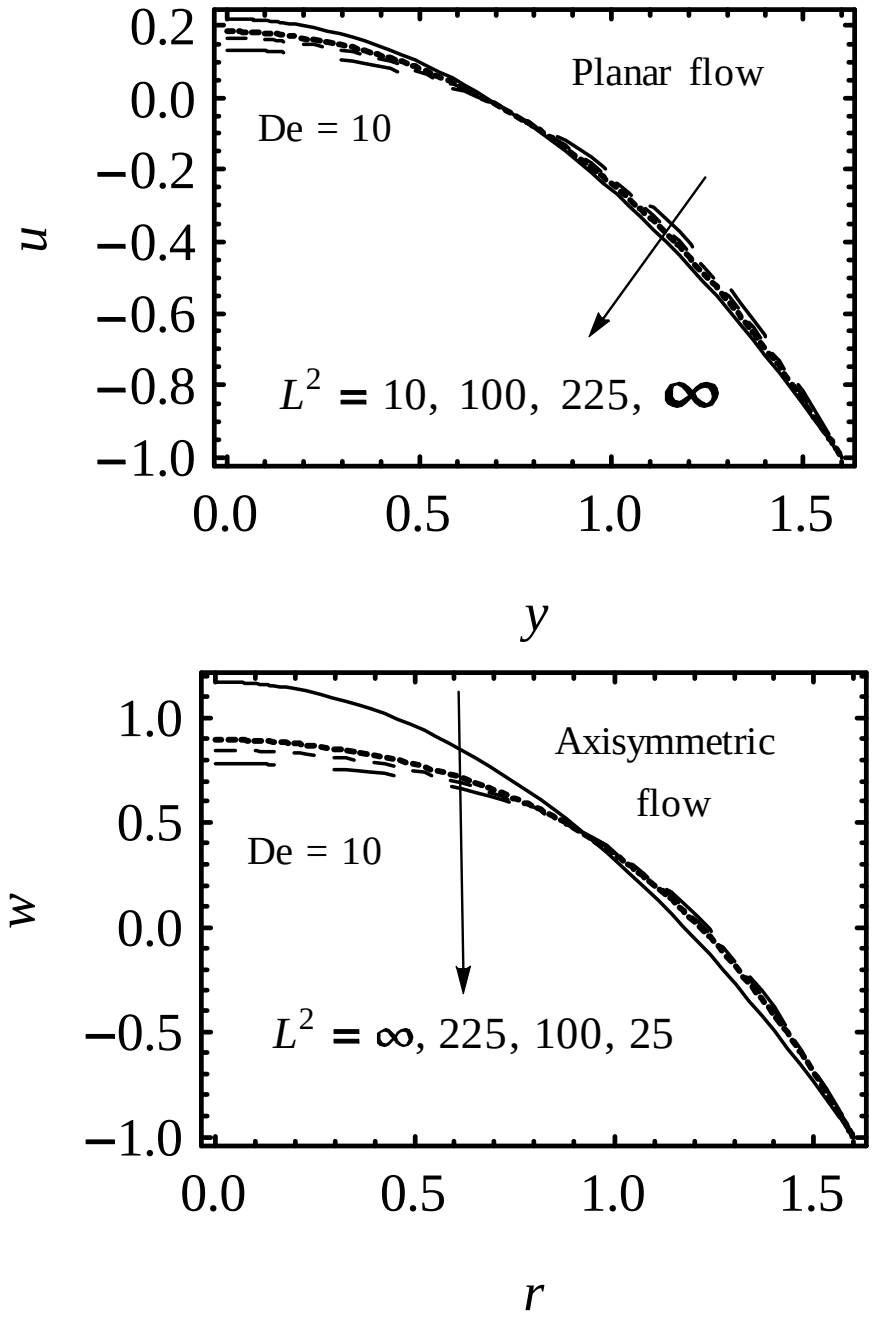

Fig. 3.2: Velocity profile for different values of extensibility parameter with $\theta = 0.7,\ \phi_a = 0.6$.

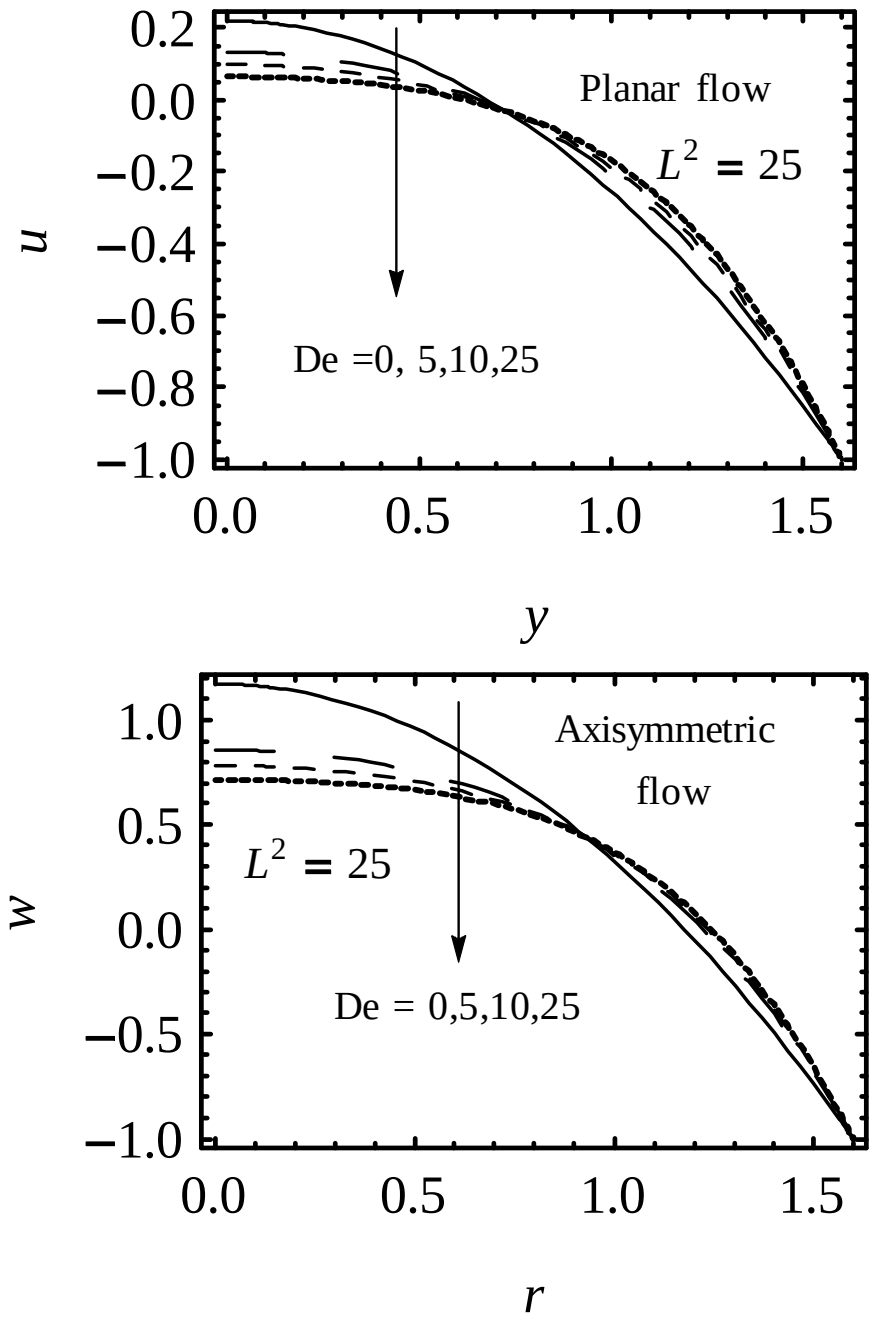

Fig. 3.3: Velocity profile for different values of Deborah number with $\theta = 0.7,\ \phi_a = 0.6$.

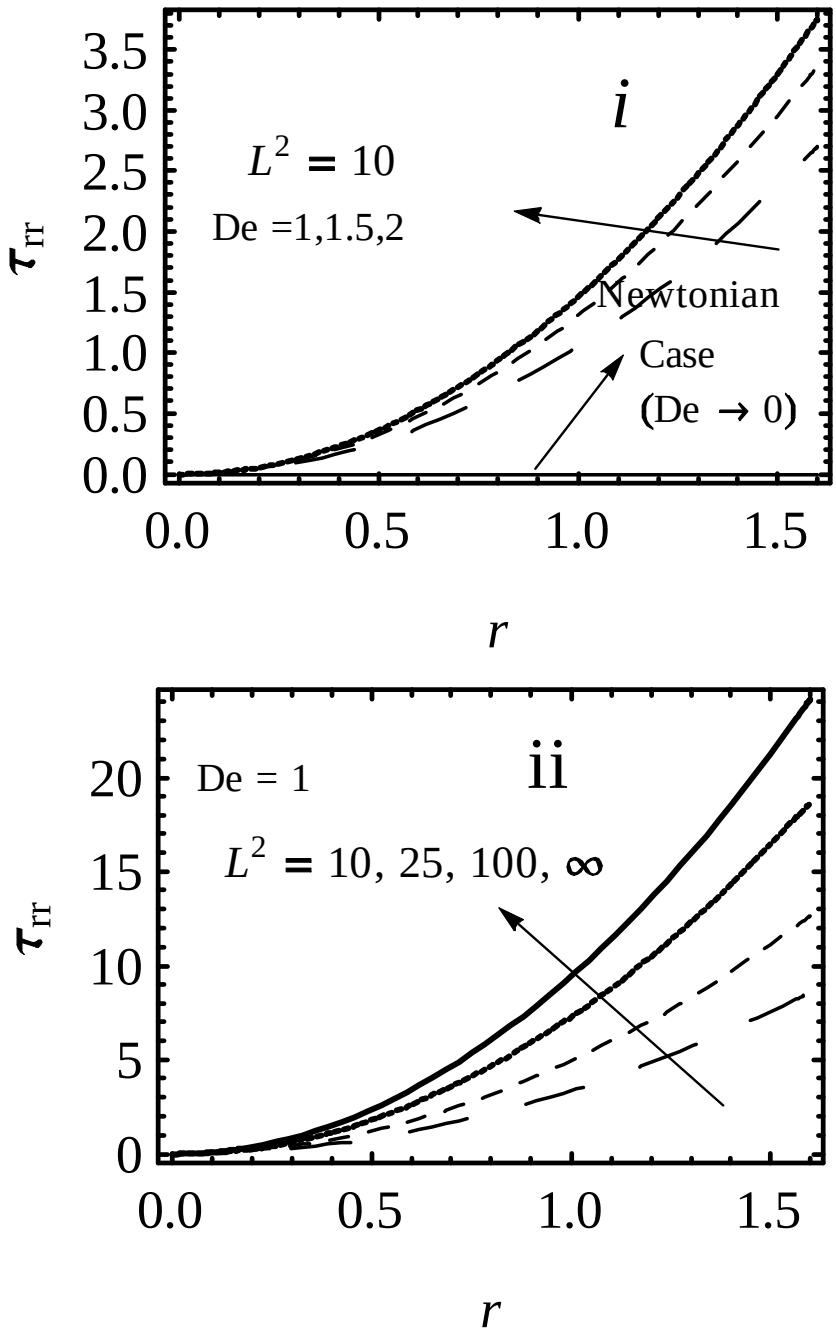

Fig. 3.4: Normal Stress profile in Axisymmetric Case with $\theta = 0.7,\ \phi_a = 0.6$.

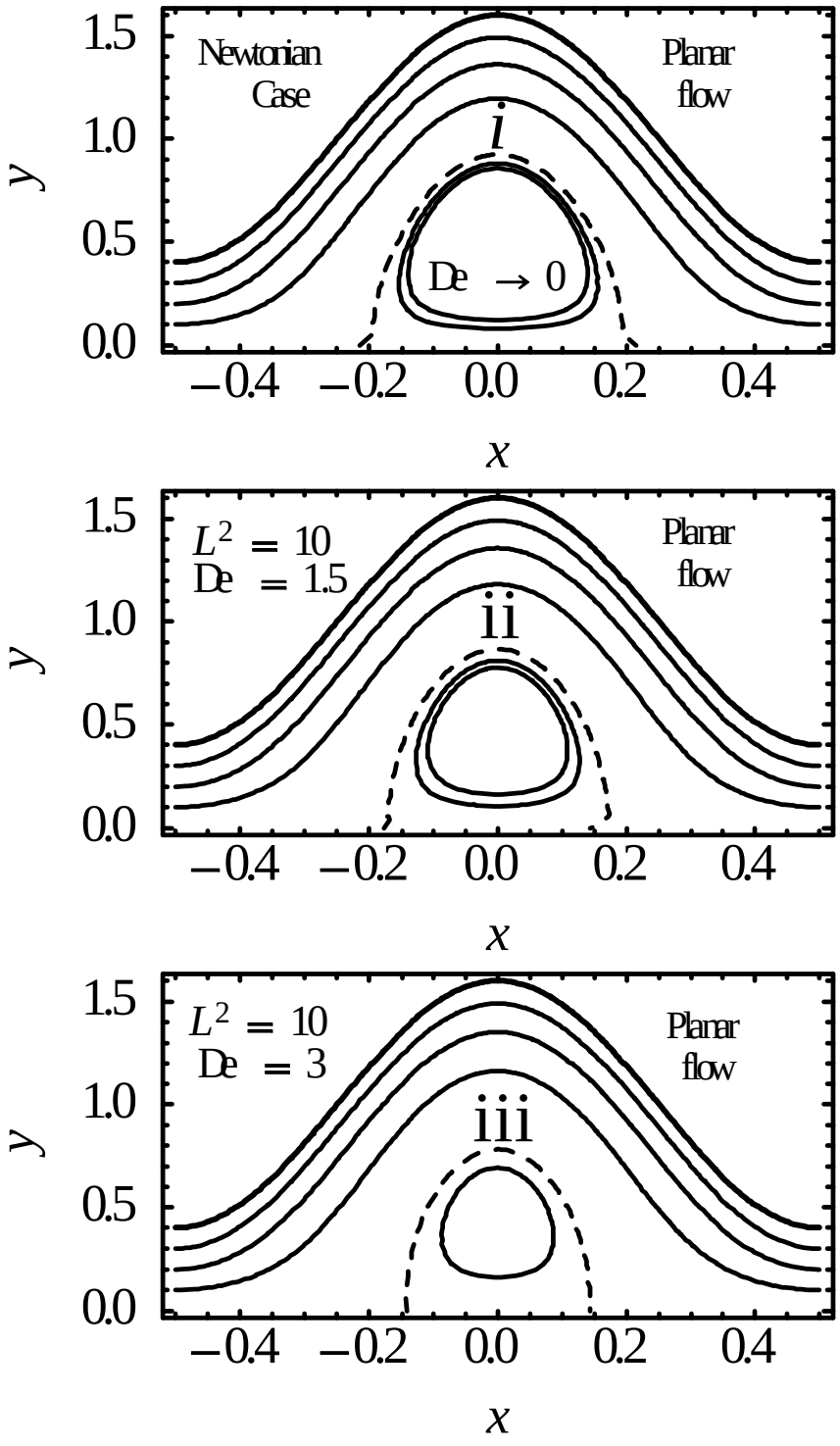

Fig. 3.5(a): Streamlines for the variation of Deborah number with $\theta = 0.6,\ \phi_a = 0.6$.

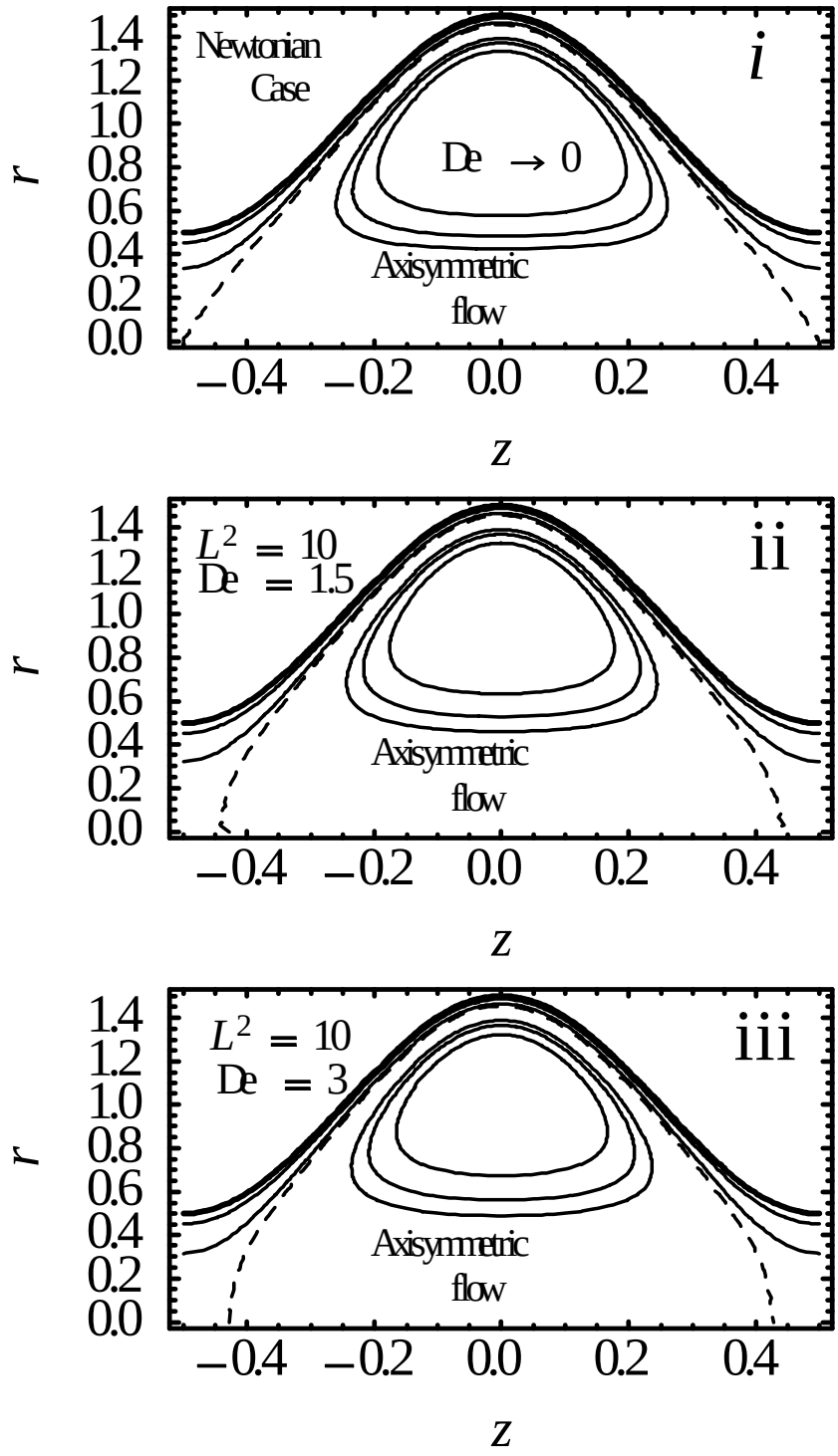

Fig. 3.5(b): Streamlines for the variation of Deborah number with $\theta = 0.5,\ \phi_a = 0.5$.

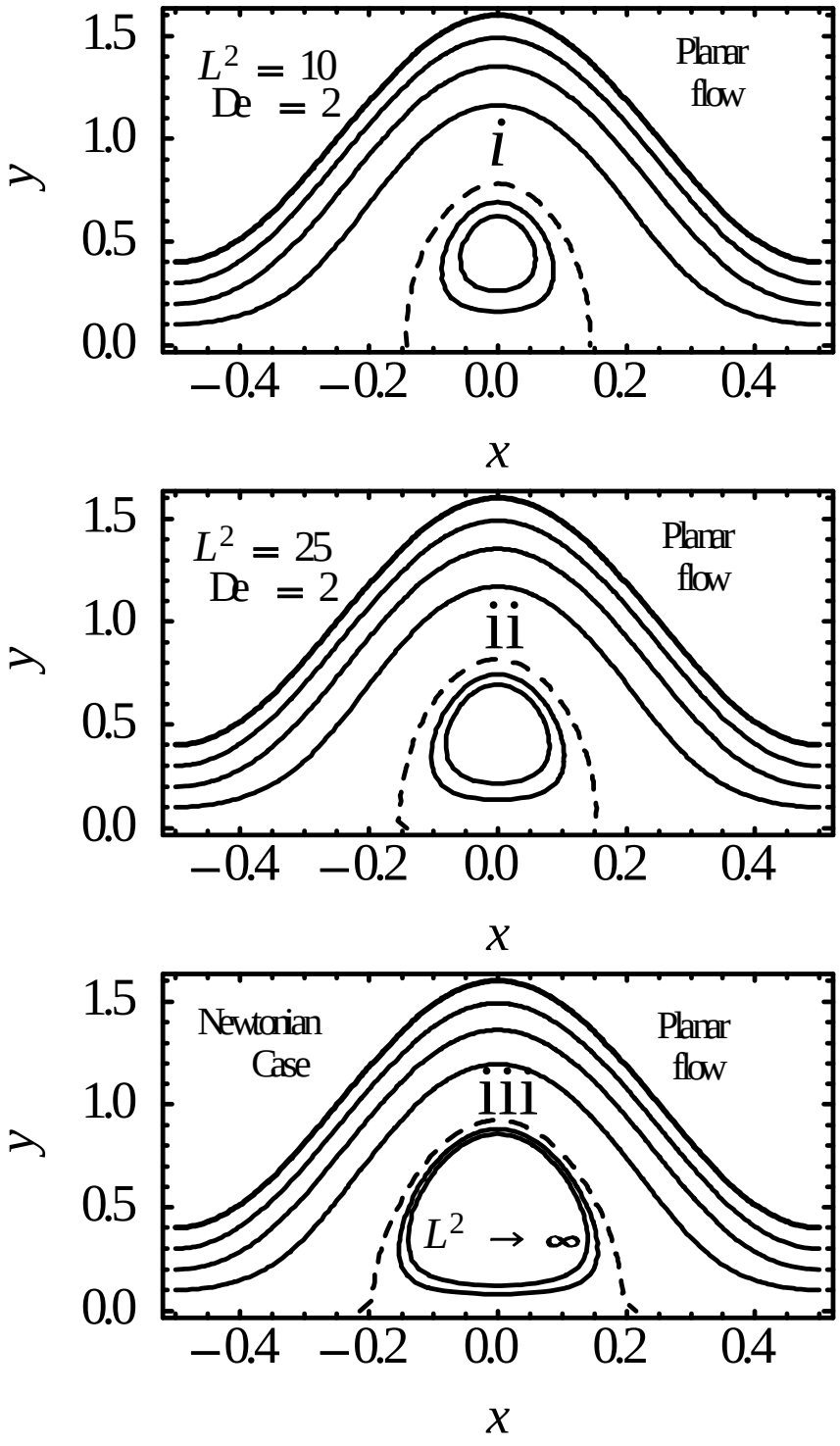

Fig. 3.6(a): Streamlines for the variation of Extensibility parameter with $\theta = 0.6,\ \phi_a = 0.6$.

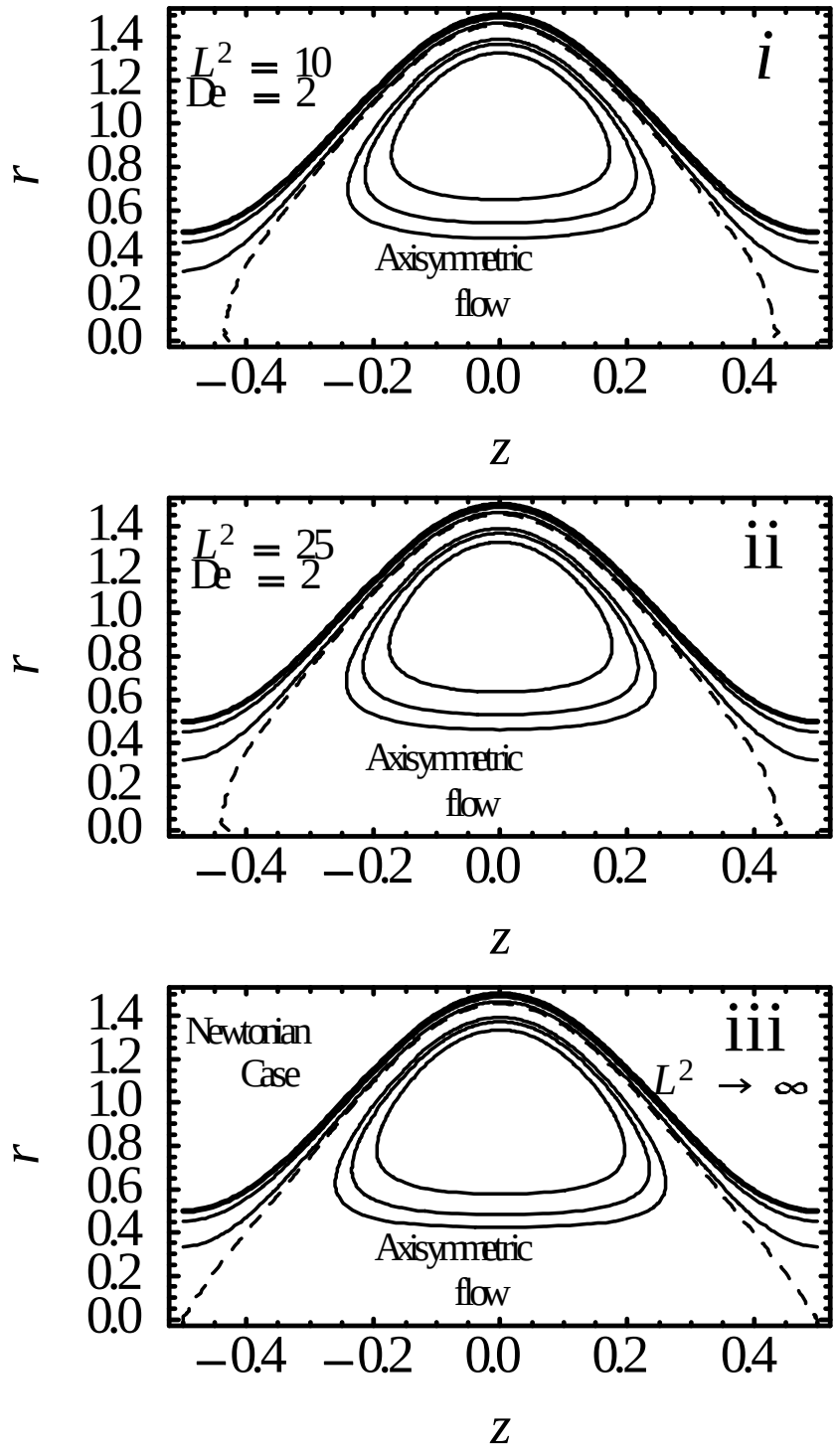

Fig. 3.6(b): Streamlines for the variation of Extensibility parameter with $\theta = 0.5,\ \phi_a = 0.5$.

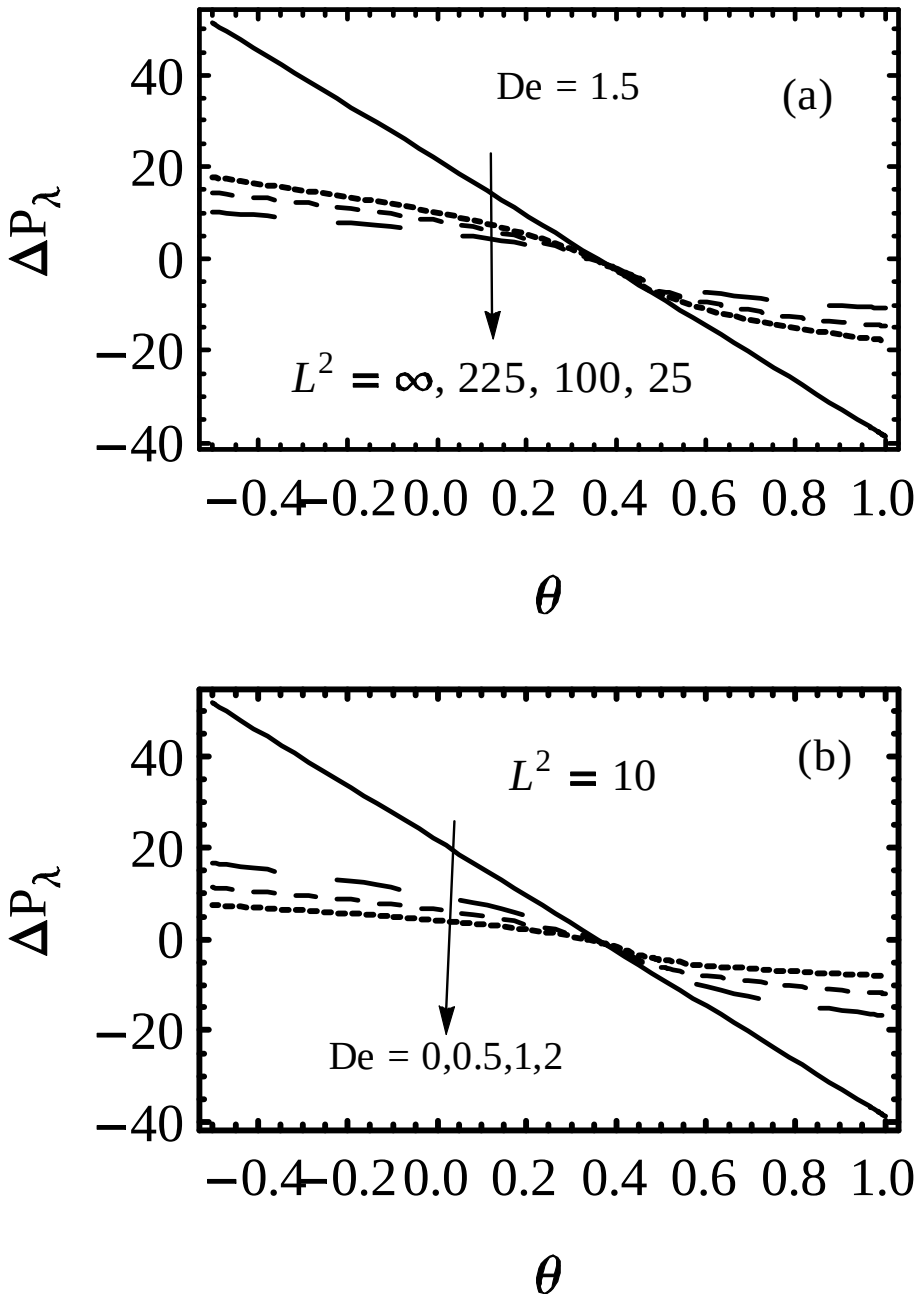

Fig. 3.7: Pressure rise per wavelength (ΔP_λ) with $\phi_a = 0.5$

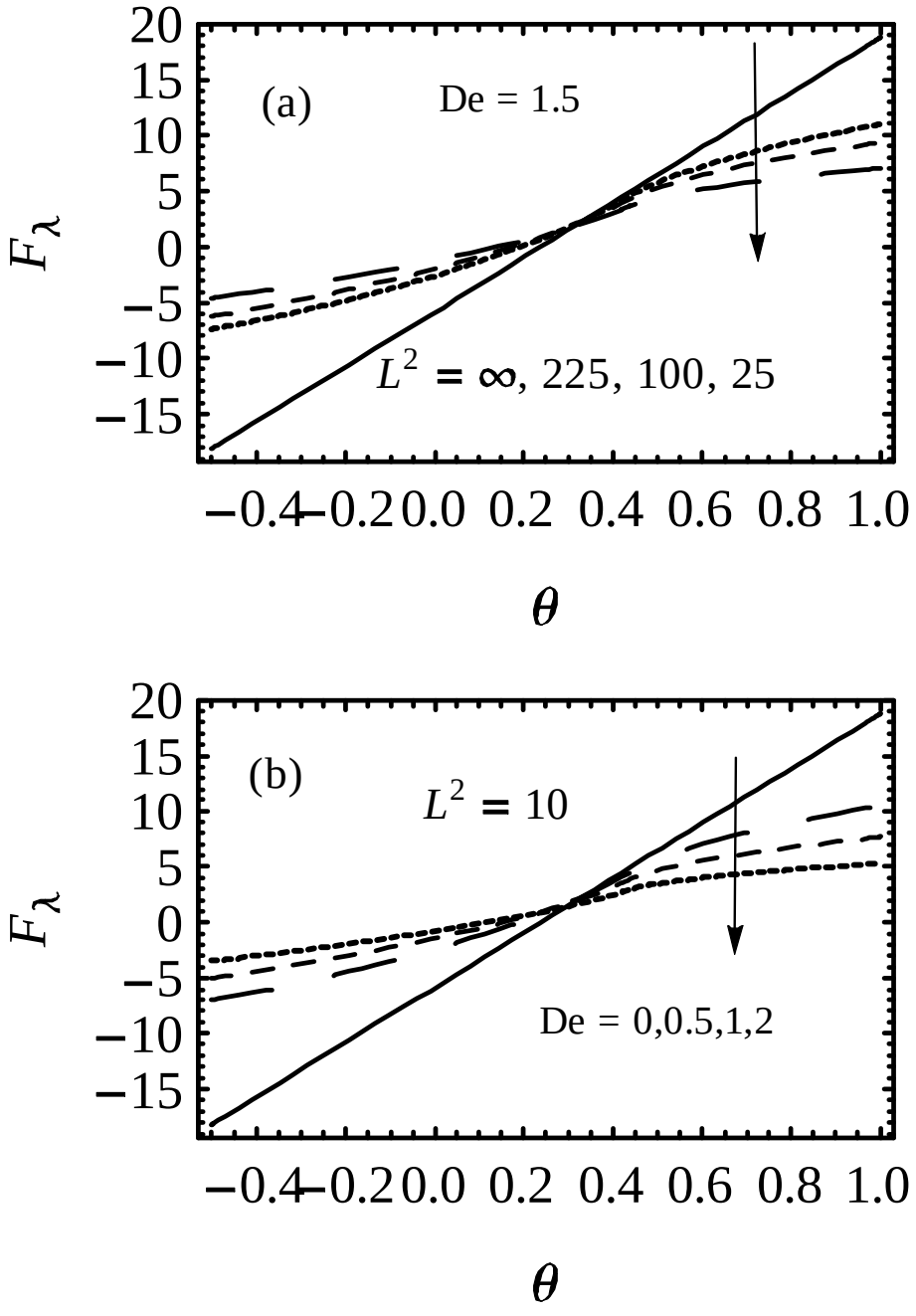

Fig. 3.8: Frictional forces (F_λ) with $\phi_a = 0.5$

3.3 Concluding remarks

From the presented analysis we conclude that Deborah number (De) and extensibility parameter (L^2) leave opposite effects on flow characteristics, trapping and pumping phenomena. Specifically, we find that velocity field attains higher values at the centre of the channel for the case of axisymmetric flow when compared with the planar flow. Moreover, the velocity profile decreases (increases) by increasing De (L^2) at the centre of the channel whereas it shows opposite trend near the walls. The velocity field is parabolic both for Newtonian and FENE-P fluids. As for as normal stress is concerned, it increases by increasing both De and L^2. If we look into the pumping phenomenon we come to know that ΔP_λ increases in the retrograde, peristaltic and free pumping regions, whereas it decreases in the augmented pumping region, by increasing L^2. The effects of De on ΔP_λ are quite opposite to that of L^2. In addition, frictional forces (F_λ) resist the flow below a certain critical value of the flow rate and this resistance increases in going from FENE-P to Newtonian fluid. Furthermore, F_λ shows linear behavior for Newtonian case whereas its behavior is non-linear behavior for FENE-P fluid. Coming on the trapping phenomenon, we infer that the size of trapped bolus reduces by increasing De while it increases by increasing L^2.

Chapter 4

Slip effects on streamline topologies and their bifurcations for peristaltic flows of a viscous fluid

We discuss the effects of the surface slip on streamline patterns and their bifurcations for peristaltic transport of a Newtonian fluid. The flow is in a two-dimensional symmetric channel or an axisymmetric tube. An exact expression for the stream function is obtained in the wave frame under the assumptions of long wavelength and low Reynolds number for both cases. For the discussion of the particle path in wave frame, a system of nonlinear autonomous differential equations is established and the methods of dynamical systems are used to discuss the local bifurcations and their topological changes. Moreover, all types of bifurcations and their topological changes are discussed graphically. Finally, the global bifurcation diagram is used to summarize the bifurcations. The contents of this chapter are published in Chinese Physics B Vol. 23, No. 6 (2014) 064701.

4.1 Problem formulation

4.1.1 Channel Flow

Consider the peristaltic transport of an incompressible viscous fluid in a two dimensional channel of width $2a_1$. The flow is initiated by the sinusoidal wave trains propagating on the channel walls with constant speed c. The shape of the wall surface is characterized by the same expression as in Ref. [133, 143]

$$\overline{H}(\overline{X},\overline{t}) = a_1 - b_1\left[1-\cos^2\left(\frac{\pi}{\lambda}(\overline{X}-c\overline{t})\right)\right], \tag{4.1}$$

The geometry of the problem is given below.

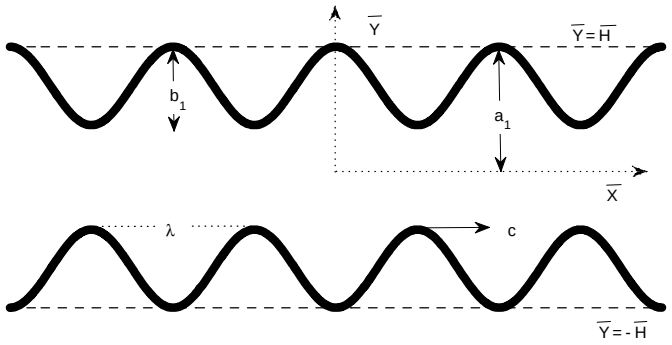

*Fig.*4.1 Geometry for planar case

It is interesting to note that expression (4.1) describes only a wave of contraction at the channel wall. Here the governing equations of the problem are the same as considered in last chapter. The difference comes through the constitutive equation of extra stress tensor. We have considered the case of Newtonian fluid therefore the constitutive equation for extra stress tensor is given by

$$\overline{\tau} = 2\eta D. \tag{4.2}$$

The mass conservation equation for present scenario does not differ from the corresponding

equation in chapter 2. However, the component form of momentum equations (2.14) and (2.15) in view of Eq. (2.6) and Eq. (4.2) becomes

$$\rho\left(\frac{\partial}{\partial\overline{t}}+\overline{U}\frac{\partial}{\partial\overline{X}}+\overline{V}\frac{\partial}{\partial\overline{Y}}\right)\overline{U} = -\frac{\partial\overline{P}}{\partial\overline{X}}+\eta\left(\frac{\partial^2\overline{U}}{\partial\overline{X}^2}+\frac{\partial^2\bar{U}}{\partial\overline{Y}^2}\right), \tag{4.3}$$

$$\rho\left(\frac{\partial}{\partial\overline{t}}+\overline{U}\frac{\partial}{\partial\overline{X}}+\overline{V}\frac{\partial}{\partial\overline{Y}}\right)\overline{V} = -\frac{\partial\overline{P}}{\partial\overline{Y}}+\eta\left(\frac{\partial^2\overline{V}}{\partial\overline{X}^2}+\frac{\partial^2\overline{V}}{\partial\overline{Y}^2}\right). \tag{4.4}$$

Now after making use of well known transformations between the laboratory $\left(\overline{X},\overline{Y}\right)$ and moving $(\overline{x},\overline{y})$ frames, non-dimensionalizing using Eq. (2.24), introducing the stream function through (2.41) and eliminating the pressure gradient from the resulting forms of the Eq. (4.3) and Eq. (4.4) , we get the following equation

$$\mathrm{Re}\,\delta\left[\psi_y\nabla^2\psi_x-\psi_x\nabla^2\psi_y\right]=\nabla^2(\nabla^2\psi). \tag{4.5}$$

In non-dimensional form, equation (4.1) reduces to

$$h(x)=1-\phi\ \left(1-\cos^2\pi x\right). \tag{4.6}$$

The modified Laplacian ∇^2 is defined by the relations

$$\nabla^2=\delta^2\frac{\partial^2}{\partial x^2}+\frac{\partial^2}{\partial y^2} \tag{4.7}$$

After taking into account the long wavelength and low Reynolds number assumptions, Eq. (4.5) reduce to a similar equation as obtained in Ref. [133]

$$\frac{\partial^4\psi}{\partial y^4}=0. \tag{4.8}$$

The dimensionless volume flow rate and boundary conditions in the wave frame are

$$\psi = 0,\quad \frac{\partial^2\psi}{\partial y^2}=0,\ \ at\ \ y=0, \tag{4.9a}$$

$$\psi = q,\quad \frac{\partial\psi}{\partial y}+\beta\frac{\partial^2\psi}{\partial y^2}=-1,\ \ at\ \ y=h, \tag{4.9b}$$

$$q = \int_0^h \frac{\partial \psi}{\partial y} dy = \psi(h) - \psi(0). \tag{4.10}$$

Here β ($= \beta_1/a_1$, β_1 is the dimensional slip parameter) is the dimensionless slip parameter. Since the flow is symmetric with respect to centerline, therefore we shall discuss the problem in the domain $y \in [0, h]$.

Solution of the problem

The solution of Eq. (4.8) subject to boundary conditions (4.9a) and (4.9b) is

$$\psi = \frac{1}{h}\left(\frac{3qh + h^2 + 6\beta q}{2h + 6\beta}\right) y - \left(\frac{q + h}{2h^3 + 6\beta h^2}\right) y^3. \tag{4.11}$$

Three different flow situations, namely, backward flow, trapping and augmented flow occur. Backward flow refers to the case in which the whole flow goes in the direction opposite to the travelling wave. Trapping is the situation where the streamline splits to enclose an amount of fluid, called a bolus. The augmented flow occurs when the trapped bolus splits and there exist some flow going in the forward direction.

Flow Field as a Nonlinear Dynamical System

In this section, we employ the idea of the qualitative theory of dynamical systems. At a particular instant, say t_0, the motion of individual particles moving in paths defined by $\dot{\mathbf{x}} = [u(x, y, t), v(x, y, t), 0]$ is identical to instantaneous streamlines, in other words, we have $\dot{\mathbf{x}} = [u(x, y, t_0), v(x, y, t_0), 0]$. The present problem can be written as a system of following nonlinear differential equations by using the definition of stream function (2.41) and Eq. (4.11):

$$\dot{x} = \frac{3qh + h^2 + 6\beta q}{2h^2 + 6\beta h} - \frac{(3y^2)(q + h)}{2h^3 + 6\beta h^2} = f(x, y, \boldsymbol{\alpha}), \tag{4.12}$$

$$\dot{y} = y\frac{\partial h}{\partial x}\frac{1}{h(2h^2 + 6\beta h)^2}\left[6qh(h^2 - y^2) - 4h^2y^2 - 6\beta h(h^2 + y^2) + 12\beta q(2h^2 - y^2)\right]$$

$$+36\beta^2 qh = g(x, y, \boldsymbol{\alpha}), \tag{4.13}$$

where $\boldsymbol{\alpha} = [\phi, q, \beta]$, $-\infty < x < \infty$, $-h < y < h$ and the amplitude ratio ϕ lies between 0 and 1.

To obtain the critical points we set $f(x, y, \boldsymbol{\alpha}) = 0 = g(x, y, \boldsymbol{\alpha})$ by following Ref. [133] and

then use the Hartman-Grobman theorem according to which the nature of the critical point can be found using the Jacobian at the critical point. If the determinant of the Jacobian at certain critical point is zero, the critical point is degenerate. There are two subclasses namely simple and non-simple degeneracies. The simple degeneracy corresponds to the case when eigen values of the Jacobian are zero and for non-simple degeneracy, Jacobian is a zero matrix. We shall use the notation [144] to classify the critical points, where trace: $p_{12} = \lambda_1 + \lambda_2$ and the Jacobian: $d_{12} = \lambda_1\lambda_2$, which are based on eigen values λ_1, λ_2 are used to classify the phase portraits.

According to [145] a bifurcation point with respect to parameter $\boldsymbol{\alpha}$ is a solution $(x, y, \boldsymbol{\alpha})$, where the number of equilibria, periodic or quasi-periodic solutions change when $\boldsymbol{\alpha}$ passes through $\boldsymbol{\alpha}_c$, with α_c as a critical value.

The critical points are given by

1. $\{x_{1,2}, y_{1,2}\} = \left\{n\pi, \pm\sqrt{\frac{3q+1+6\beta q}{3(q+1)}}\right\}$
2. $\{x_{3,4}, y_{3,4}\} = \left\{\pm\cos^{-1}\sqrt{\frac{\phi-1-\frac{3q}{2}-\frac{1}{2}\sqrt{9q^2-24\beta q}}{\phi}}, 0\right\}$
3. $\{x_{5,6}, y_{5,6}\} = \left\{\frac{(2n-1)\pi}{2}, \pm\sqrt{\frac{(3q+1-\phi)(1-\phi)^2+6\beta q(1-\phi)}{3(q+1-\phi)}}\right\}$

In the coming sections we present the qualitative classification and discussion of the critical points. We will also discuss the critical values of the parameters and graphical representation of the local and global bifurcations of the critical points.

Classification and Bifurcation of the critical points

The critical points $\{x_{1,2}, y_{1,2}\} = \left\{n\pi, \pm\sqrt{\frac{3q+1+6\beta q}{3(q+1)}}\right\}$ where $n \in \mathbb{Z}$, lie on the vertical below the wave crests. The Jacobian at these critical points is

$$J|_{\{x_{1,2},y_{1,2}\}} = \begin{bmatrix} 0 & \mp\frac{3(q+1)}{1+3\beta}\sqrt{\frac{3q+1+6\beta q}{3(q+1)}} \\ \left(\begin{array}{c} \pm\frac{\phi(3q+2+3\beta+6\beta q)}{(1+3\beta)^2}\left(\sqrt{\frac{3q+1+6\beta q}{3(q+1)}}\right)^3\mp \\ \frac{\phi(3q-3\beta+12\beta q+18\beta^2 q)}{(1+3\beta)^2}\left(\sqrt{\frac{3q+1+6\beta q}{3(q+1)}}\right) \end{array}\right) & 0 \end{bmatrix} \tag{4.14}$$

and the eigenvalues of the Jacobian are given by

$$\lambda_{1,2} = \pm \frac{\sqrt{6\phi(q+1)(3q+1+6\beta q)(1+3\beta)(1+6\beta-9\beta q^2-18\beta^2 q)}}{3(q+1)\left(1+3\beta\right)^2}. \tag{4.15}$$

Since eigen values vary with q by fixing the values of ϕ and β, therefore, the nature and stability of critical points change with the value of flow rate q, and the values of the flow rate are taken between -1 and 1. Qualitative changes are divided into two cases which take place as follows:
Case-1 (*for* $0 < \beta \leq 1/6$)

- As $p_{12} = 0$ and $d_{12} < 0$ when $-1 < q < \frac{-1}{3+6\beta}$, therefore the critical point is co-dimension two saddle as it depends on β and q; see Fig.4.3(a).

- An isolated critical point occurs at $q = q_{c_1} = \frac{-1}{3+6\beta}$, which is also known as a degenerate point but is non-hyperbolic as defined in [146], because both the eigen values and Jacobian matrix are zero. Moreover the critical point with $q = \frac{-1}{3+6\beta}$ corresponds to non-simple degeneracy because $J|_{\{x_{1,2},y_{1,2}\}} = 0$ for $q = q_{c_1} = \frac{-1}{3+6\beta}$, see Fig. 4.3($a$).

- As $p_{12} = 0$ and $d_{12} > 0$ when $q > \frac{-1}{3+6\beta}$, therefore each critical point is a center; see Fig. 4.3(a).

A bifurcation diagram in the $q-y$ plane depending on the definition of a bifurcation which crop up on the vertical situated at the wave crest at $x = n\pi$ for $n \in \mathbb{Z}$, is traced in Fig. 4.3(a). This bifurcation is also of co-dimension two as it depends on q and β.

Case-2 (*for* $\beta > 1/6$)

- As $p_{12} = 0$ and $d_{12} < 0$ when $-1 < q < \frac{-1}{3+6\beta}$ or $-\beta + \frac{1}{3}\sqrt{\frac{1+6\beta+9\beta^3}{\beta}} < q < 1$, therefore the critical point is co-dimension two saddle as it depends on β and q; see Fig.4.3(b).
- Isolated critical points occur when $q = q_{c_1} = \frac{-1}{3+6\beta}$ and $q = q_{c_2} = -\beta + \frac{1}{3}\sqrt{\frac{1+6\beta+9\beta^3}{\beta}}$. These are also known as a degenerate points but the degeneracy is non-simple. Critical points are also non-hyperbolic, see Fig. 4.3(b).
- As $p_{12} = 0$ and $d_{12} > 0$ when $\frac{-1}{3+6\beta} < q < -\beta + \frac{1}{3}\sqrt{\frac{1+6\beta+9\beta^3}{\beta}}$ therefore, each critical point is a center; see Fig. 4.3(b).

A bifurcation diagram in the $q - y$ plane is traced in Fig. 4.3(b). This bifurcation is of co-dimension two as it also depends on q and β.

Classification and Bifurcation of the Stagnation Points (for $\beta \leq 0$)

Consider $\{x_{3,4}, y_{3,4}\} = \left\{ \pm \cos^{-1} \sqrt{\frac{\phi - 1 - \frac{3q}{2} - \frac{1}{2}\sqrt{9q^2 - 24\beta q}}{\phi}}, 0 \right\}$. These critical points lie along the longitudinal axis. The Jacobian at these critical points is $J|_{\{x_{3,4}, y_{3,4}\}} = \begin{bmatrix} \frac{\partial f}{\partial x} & 0 \\ 0 & -\frac{\partial f}{\partial x} \end{bmatrix}$ where

$$\begin{aligned} \frac{\partial f}{\partial x} \quad = \quad & \left(\frac{3\phi}{\left(\frac{3q}{2} + \frac{1}{2}\sqrt{9q^2 - 24\beta q}\right)^2 \left(3\beta - \frac{3q}{2} - \frac{1}{2}\sqrt{9q^2 - 24\beta q}\right)^2} \right) \times \\ & \left(\sqrt{\frac{\phi - 1 - \frac{3q}{2} - \frac{1}{2}\sqrt{9q^2 - 24\beta q}}{\phi}} \right) \times \left(\sqrt{\frac{1 + \frac{3q}{2} + \frac{1}{2}\sqrt{9q^2 - 24\beta q}}{\phi}} \right) \times \\ & \left((q - \beta) \left(\frac{3q}{2} + \frac{1}{2}\sqrt{9q^2 - 24\beta q} \right)^2 - 4\beta q \left(\frac{3q}{2} + \frac{1}{2}\sqrt{9q^2 - 24\beta q} \right) + 6\beta^2 q \right) \end{aligned}$$

and the eigen values are given by

$$\begin{aligned}\lambda_{3,4} &= \pm\frac{3}{\left(\frac{3q}{2}+\frac{1}{2}\sqrt{9q^2-24\beta q}\right)^2\left(3\beta-\frac{3q}{2}-\frac{1}{2}\sqrt{9q^2-24\beta q}\right)^2}\times \\ &\sqrt{\phi\left(1+\frac{3q}{2}+\frac{1}{2}\sqrt{9q^2-24\beta q}\right)-\left(1+\frac{3q}{2}+\frac{1}{2}\sqrt{9q^2-24\beta q}\right)^2}\times \\ &\left((q-\beta)\left(\frac{3q}{2}+\frac{1}{2}\sqrt{9q^2-24\beta q}\right)^2-4\beta q\left(\frac{3q}{2}+\frac{1}{2}\sqrt{9q^2-24\beta q}\right)+6\beta^2 q\right) \quad (4.16)\end{aligned}$$

From (4.16) we note that a discussion about these critical points is only possible for negative values of β and since negative values of β are of no interest physically therefore we will not proceed further.

Classification and Bifurcation of the critical points

$x=\frac{(2n-1)\pi}{2}$ with $q>-\frac{1}{3}\left(\frac{(1-\phi)^2}{1-\phi+2\beta}\right)$ where $n\in\mathbb{Z}$,

Likewise in previous section, a degenerate fixed point bifurcates to saddle nodes on the longitudinal axis for $-1+\phi<q<-\frac{1}{3}\frac{(1-\phi)^2}{1-\phi+2\beta}$. The case when q approaches $q_{c_2}=-\frac{1}{3}\frac{(1-\phi)^2}{1-\phi+2\beta}$ saddle nodes of adjacent waves join together below the wave troughs, therefore the critical points merge on $x=\frac{(2n-1)\pi}{2}$ for $q=q_{c_2}$. This join of critical points produce degenerate points with six heteroclinic connections. The degenerate points bifurcates on the $y-$branch at $x=\frac{(2n-1)\pi}{2}$ with $q>q_{c_2}$ and change stability to saddle nodes.

Critical points $\{x_{5,6},y_{5,6}\}=\left\{\frac{(2n-1)\pi}{2},\pm\sqrt{\frac{(3q+1-\phi)(1-\phi)^2+6\beta q(1-\phi)}{3(q+1-\phi)}}\right\}$ lie on the vertical below the wave troughs. The Jacobian is given by $J|_{\{x_{5,6},y_{5,6}\}}=\begin{bmatrix}0 & \frac{\partial f}{\partial y}\\ \frac{\partial g}{\partial x} & 0\end{bmatrix}$ where

$$\frac{\partial f}{\partial y}=\pm\frac{(q+1-\phi)}{((\phi-1)^3-3\beta(\phi-1)^2)}\sqrt{\frac{3(3q+1-\phi)(\phi-1)^2-18\beta q(\phi-1)}{q+1-\phi}}$$

and

$$\begin{aligned}\frac{\partial g}{\partial x} &= \mp\frac{\phi}{3(1-\phi)^2(3\beta+1-\phi)^2(q+1-\phi)}\sqrt{\frac{(3q+1-\phi)(\phi-1)^2+6\beta q(1-\phi)}{3(q+1-\phi)}}\\ &[2h^4-18\beta^2q^2+12\beta h^3-36\beta^2 qh]\end{aligned}$$

with eigen values

$$\lambda_{5,6} = \pm\left(\frac{\sqrt{6\phi(q+1-\phi)(1-\phi)\left[(3q+1-\phi)(1-\phi)^2+6\beta q(1-\phi)\right]}}{3(1-\phi)^{5/2}\left(3\beta+1-\phi\right)^{3/2}\left(q+1-\phi\right)}\right) \times\sqrt{(1-\phi)^4-9\beta^2q^2+6\beta(1-\phi)^3-18\beta^2q(1-\phi)}. \quad (4.17)$$

Qualitative changes of critical points for $q \geq -\frac{(1-\phi)^2}{3[1-\phi+2\beta]}$ on $x = \frac{(2n-1)\pi}{2}$ take place as follows:

- $P_{56} = 0$ and $d_{56} = 0$ when $q = q_{c_2}$, therefore the critical point is degenerate. And since $J|_{\{x_{5,6},y_{5,6}\}} = 0$ with $q = q_{c_2}$, therefore degeneracy non-simple; see Fig. 4.4(b).
- $P_{56} = 0$ and $d_{56} < 0$ when $q > -\frac{(1-\phi)^2}{3[1-\phi+2\beta]}$, therefore the critical points are saddle nodes; see Fig. 4.4(c)

A bifurcation diagram for the $y-q$ plane with the variation of β is portrayed in Fig. 4.4.

Global bifurcation and streamline patterns

The vector field associated with $y = 0$ is $\{\dot{x}, \dot{y}\} = \left\{\frac{3qh+h^2+6\beta q}{2h^2+6\beta h}, 0\right\}$, from which $\zeta = q + \frac{h^2}{(3h+6\beta)}$. Critical conditions crop up at the wave crests $x = n\pi$ and troughs $x = \frac{(2n-1)\pi}{2}$. Global bifurcation curves are given by $f(\mathbf{x}, \boldsymbol{\alpha}) = \zeta = 0$, so we have

$$\begin{aligned} \zeta|_{(x=n\pi)} &= q + \frac{1}{(3+6\beta)} = 0, \\ \zeta|_{(x=\frac{(2n-1)\pi}{2})} &= q + \frac{(1-\phi)^2}{(3(1-\phi)+6\beta)} = 0. \end{aligned}$$

The global bifurcation diagram in the parameters space $\phi - q$ with the variation of β contains the following set of curves:

$$M = \left\{(\phi, q)|0 < \phi < 1, q = \frac{-1}{(3+6\beta)}\right\}, \quad (4.18)$$

$$N = \left\{(\phi, q)|0 < \phi < 1, q = \frac{(1-\phi)^2}{(3(1-\phi)+6\beta)}\right\}. \quad (4.19)$$

Along the bifurcation curve M, an isolated non-hyperbolic degenerate point exists below the wave crest which is also non-simple. Whereas along the bifurcation curve N, the associated

critical points join together below the wave troughs and form connections of non-simple degenerate points. Critical points that amalgamate on N produce a degenerate saddle having six heteroclinic paths. Bifurcation curves are shown in Fig. 4.5.

The region of peristaltic flow is divided as follows:

Region I: backward flow, where all the flow going in an opposite direction to the flow.

Region II: trapping,where saddles are connected by heteroclinic connections and the interaction of two vortices with opposite rotations exist in the flow.

RegionIII : Augmented flow, where the eddies below wave crests merge and form heteroclinic connections with their neighbors,

and part of the fluid is able to flow through the centerline in the flow direction.

4.1.2 Axisymmetric flow

Now we consider the peristaltic motion of an incompressible Newtonian fluid in an axisymmetric tube with flexible walls. The tube wall in cylindrical coordinates $\left(\overline{R}, \overline{Z}\right)$ is expressed by

$$\overline{H}(\overline{Z}, \bar{t}) = a_1 - b_1 \left[1 - \cos^2\left(\frac{\pi}{\lambda}\left(\overline{Z} - c\bar{t}\right)\right)\right], \tag{4.20}$$

in which a_1 is the tube radius in this case. In the governing equations in laboratory frame $(\overline{R}, \overline{Z})$, the momentum equations in view of (2.6) and (4.2) can be written as

$$\rho\left(\frac{\partial}{\partial \bar{t}} + \overline{V}_{\overline{R}}\frac{\partial}{\partial \overline{X}} + \overline{V}_{\overline{Z}}\frac{\partial}{\partial \overline{Y}}\right)\overline{V}_{\overline{R}} = -\frac{\partial \overline{P}}{\partial \overline{R}} + \eta\left(\frac{\partial}{\partial \overline{R}}\left(\frac{1}{\overline{R}}\frac{\partial}{\partial \overline{R}}(\overline{R}\overline{V}_{\overline{R}})\right) + \frac{\partial^2 \overline{V}_{\overline{R}}}{\partial \overline{Z}^2}\right), \tag{4.21}$$

$$\rho\left(\frac{\partial}{\partial \bar{t}} + \overline{V}_{\overline{R}}\frac{\partial}{\partial \overline{X}} + \overline{V}_{\overline{Z}}\frac{\partial}{\partial \overline{Y}}\right)\overline{V}_{\overline{Z}} = -\frac{\partial \overline{P}}{\partial \overline{Z}} + \eta\left(\frac{1}{\overline{R}}\frac{\partial}{\partial \overline{R}}\left(\overline{R}\frac{\partial \overline{V}_{\overline{Z}}}{\partial \overline{R}}\right) + \frac{\partial^2 \overline{V}_{\overline{Z}}}{\partial \overline{Z}^2}\right), \tag{4.22}$$

The flow geometry is illustrated in the following figure.

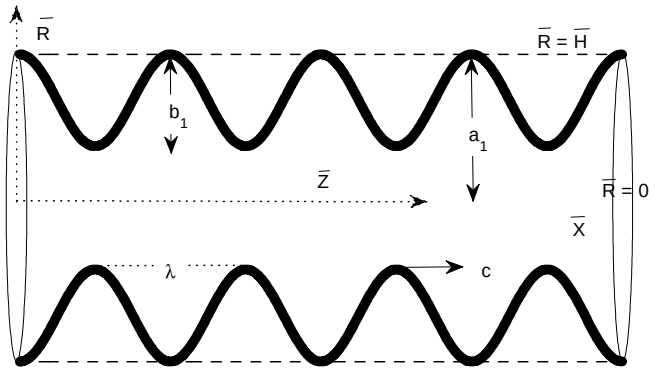

*Fig.*4.2 Geometry for axisymmetric case

Now following a similar procedure as done for planar case, the counter-part of Eq. (4.5) is the present case is [130]

$$\delta \,\mathrm{Re}\left[\frac{\partial\left(\psi, \nabla^2\psi/r^2\right)}{\partial(r,z)}\right] = \frac{1}{r}\nabla^2(\nabla^2\psi). \tag{4.23}$$

The dimensionless form of the tube surface is

$$h(z) = 1 - \phi_a \ \left(1 - \cos^2 \pi z\right). \tag{4.24}$$

The modified Laplacian ∇^2 is defined by the relations

$$\nabla^2 = \delta^2 \frac{\partial^2}{\partial z^2} + \frac{\partial^2}{\partial r^2} - \frac{1}{r}\frac{\partial}{\partial r}. \tag{4.25}$$

Employing long wavelength and low Reynolds number assumptions Eq. (4.32) reduces to the similar form as obtained in [133] i.e.

$$\nabla^2(\nabla^2\psi) = 0. \tag{4.26}$$

The dimensionless volume flow rate and boundary conditions in the wave frame are

$$\psi = 0, \quad \frac{\partial}{\partial r}\left(\frac{1}{r}\frac{\partial \psi}{\partial r}\right) = 0, \quad at\ r = 0, \tag{4.27a}$$

$$\psi = q_a, \quad \frac{1}{r}\frac{\partial \psi}{\partial r} + \beta \frac{\partial}{\partial r}\left(\frac{1}{r}\frac{\partial \psi}{\partial r}\right) = -1, \quad at\ r = h, \tag{4.27b}$$

$$q_a = \int_0^h \frac{\partial \psi}{\partial r} dr = \psi(h) - \psi(0). \tag{4.28}$$

Solution of the problem

The solution of the equation (4.26) subject to boundary conditions $(4.27a, b)$ is

$$\psi = \frac{1}{(h+4\beta)}\left[\left(\frac{2q_a}{h} + \frac{h}{2} + \frac{4q_a\beta}{h^2}\right) r^2 - \left(\frac{q_a}{h^3} + \frac{1}{2h}\right) r^4\right]. \tag{4.29}$$

Dynamical System approach to the flow field

We can write the present problem as a system of nonlinear differential equations by using the relation $\overset{\bullet}{z} = v_z = \frac{1}{r}\frac{\partial \psi}{\partial r}$ and $\overset{\bullet}{r} = v_r = -\frac{1}{r}\frac{\partial \psi}{\partial z}$ and invoking Eq. (4.29) as

$$\overset{\bullet}{z} = \frac{1}{h^3\,(h+4\beta)}\left[h^4 - 4q_a r^2 + h^2\left(4q_a - 2r^2\right) + 8hq_a\beta\right] = l(z, r, \boldsymbol{\alpha}), \tag{4.30}$$

$$\overset{\bullet}{r} = r\frac{\partial h}{\partial z}\frac{1}{h^4\,(h+4\beta)^2}[4h^3 q_a - h\left(h^2 + 4q_a\right) r^2 - 2(h^4 + 6q_a r^2 + h^2\left(-10q_a + r^2\right))\beta$$

$$+32\beta^2 q_a h] = m(z, r, \boldsymbol{\alpha}), \tag{4.31}$$

where $-\infty < z < \infty$ and $-h < r < h$.

For the critical points we set $l(z, r, \boldsymbol{\alpha}) = 0 = m(z, r, \boldsymbol{\alpha})$ and use the same technique as applied for the planar flow. The critical points are given by

1. $\{z_{1,2}, r_{1,2}\} = \left\{n\pi, \pm\sqrt{\frac{4q_a(2\beta+1)+1}{2(2q_a+1)}}\right\}$
2. $\{z_{3,4}, r_{3,4}\} = \left\{\pm\cos^{-1}\sqrt{\frac{\phi_a - 1 - \frac{3q_a}{2} - \frac{1}{2}\sqrt{9q_a^2 - 24\beta q_a}}{\phi_a}}, 0\right\}$
3. $\{z_{5,6}, r_{5,6}\} = \left\{\frac{(2n-1)\pi}{2}, \pm\sqrt{\frac{\left(4q_a + (\phi_a - 1)^2\right)(\phi_a - 1)^2 - 8\beta q_a(\phi_a - 1)}{2(2q_a + (\phi_a - 1)^2)}}\right\}$

Next we present the qualitative classification and discussion of the critical points. We also present the discussion about the critical values and local and global bifurcation diagrams for the critical points.

Classification and Bifurcation of the critical points

Consider $\{z_{1,2}, r_{1,2}\} = \left\{n\pi, \pm\sqrt{\frac{4q_a(2\beta+1)+1}{2(2q_a+1)}}\right\}$ where $n \in \mathbb{Z}$. These critical points lie on a vertical line below the wave crests. The Jacobian at these critical points is

$$J|_{\{z_{1,2},r_{1,2}\}} = \begin{bmatrix} 0 & \frac{\partial l}{\partial r} \\ \frac{\partial m}{\partial z} & 0 \end{bmatrix} \tag{4.32}$$

where

$$\begin{aligned} \frac{\partial l}{\partial r} &= \mp\frac{4}{4\beta+1}\left(2q_a+1\right)\sqrt{\frac{4q_a(2\beta+1)+1}{2(2q_a+1)}}, \\ \frac{\partial m}{\partial z} &= \mp\frac{\phi_a\left[-1+2(-3+4q_a+8q_a^2)\beta+8q_a(7+10q_a)\beta^2\right]}{\left(2q_a+1\right)\left(4\beta+1\right)^2}\sqrt{\frac{4q_a\left(2\beta+1\right)}{2(2q_a+1)}} \end{aligned}$$

and the eigen values are given by

$$\begin{aligned} \lambda_{1,2} &= \pm\left(\frac{\sqrt{-(4q_a+2)(4q_a(2\beta+1)+1)(4\beta+1)\phi_a}}{\left(2q_a+1\right)\left(4\beta+1\right)^2}\right) \\ &\quad\times\left(\sqrt{1-2(-3+4q_a+8q_a^2)\beta-8q_a(7+10q_a)\beta^2}\right). \end{aligned} \tag{4.33}$$

For discussion of the qualitative changes we again take $-1 < q_a < 1$ and these changes occur in the following way:

- $p_{12} = 0$ and $d_{12} < 0$ when $-\frac{1}{2} < q_a < \frac{-1}{4+8\beta}$. The critical point is co-dimension two saddle as it depends on β and q_a; see Fig.4.6(a).

- $p_{12} = 0$ and $d_{12} = 0$ at $q_a = q_{c_1}^a = \frac{-1}{4+8\beta}$ and the critical point is non-simple degenerate point because $J|_{\{z_{1,2},r_{1,2}\}} = 0$, see Fig. 4.6($b$).

- $p_{12} = 0$ and $d_{12} > 0$ when $q_a > \frac{-1}{4+8\beta}$, therefore each critical point is a center; see Fig. 4.6(c).

Classification and Bifurcation of the critical points ($\beta \leq 0$)

The critical points

$$\{z_{3,4}, r_{3,4}\} = \left\{ \pm \cos^{-1} \left(\sqrt{ \frac{2^{1/3}\sqrt{q_a}\left(\sqrt{q_a}+\sqrt{3}\sqrt{-q_a}\right)}{\left(-9q_a\beta+\sqrt{3}\sqrt{4q_a^3+27q_a^2\beta^2}\right)^{1/3}} - 1 + \phi_a - \frac{\left(\sqrt{q_a}-\sqrt{3}\sqrt{-q_a}\right)\left(-9q_a\beta+\sqrt{3}\sqrt{4q_a^3+27q_a^2\beta^2}\right)^{1/3}}{18^{1/3}\sqrt{q_a}} } \right), 0 \right\}.$$

lie along the longitudinal axis. The Jacobian at these critical points is $J|_{\{z_{3,4},r_{3,4}\}} = \begin{bmatrix} \frac{\partial l}{\partial z} & 0 \\ 0 & -\frac{1}{2}\frac{\partial l}{\partial z} \end{bmatrix}$ where

$$\frac{\partial l}{\partial z} = 4\frac{\partial h}{\partial z}\left(\frac{-2q_a h^2 + h^3\beta - 10q_a h\beta - 16q_a\beta^2}{h^3\left(h+4\beta\right)^2}\right)$$

and the eigen values are given by

$$\lambda_3 = \frac{\partial l}{\partial z}, \qquad \lambda_4 = -\frac{1}{2}\frac{\partial l}{\partial z} \tag{4.34}$$

Here we would again mention that existence of these critical points is subject to negative values of β and therefore these critical points are of no physical interest.

Classification and Bifurcation of the critical points

Now take $z = \frac{(2n-1)\pi}{2}$ with $q_a \geq -\frac{(1-\phi_a)^3}{4(1-\phi_a)+8\beta}$ where $n \in \mathbb{Z}$.

As previously mentioned, a degenerate fixed point bifurcates to saddle nodes on the longitudinal axis for $-\frac{1}{4+8\beta} < q_a < -\frac{(1-\phi_a)^3}{4(1-\phi_a)+8\beta}$. As q_a approaches $q_{c_2}^a = -\frac{(1-\phi_a)^3}{4(1-\phi_a)+8\beta}$, saddle nodes of contiguous waves coalesce below the wave troughs. Critical points merge on $z = \frac{(2n-1)\pi}{2}$ with $q_a = q_{c_2}^a$, this produce degenerate points with six heteroclinic connections. For $q_a > q_{c_2}^a$ the degenerate points bifurcates on the $r-$branch at $z = \frac{(2n-1)\pi}{2}$ and changes stability to saddle nodes.

Critical points $\{z_{5,6}, r_{5,6}\} = \left\{\frac{(2n-1)\pi}{2}, \pm\sqrt{\frac{(4q_a+(\phi_a-1)^2)(\phi_a-1)^2-8\beta q_a(\phi_a-1)}{2(2q_a+(\phi_a-1)^2)}}\right\}$ lie on the vertical

below the wave trough. The Jacobian is given by $J|_{\{z_{5,6},r_{5,6}\}} = \begin{bmatrix} 0 & \frac{\partial l}{\partial r} \\ \frac{\partial m}{\partial z} & 0 \end{bmatrix}$ where

$$\begin{aligned}
\frac{\partial l}{\partial r} &= \pm\frac{4\left(2q_a+(\phi_a-1)^2\right)}{(1-\phi_a+4\beta)(\phi_a-1)^3}\sqrt{\frac{\left(4q_a+(\phi_a-1)^2\right)(\phi_a-1)^2-8q_a\beta(\phi_a-1)}{2\left(2q_a+(\phi_a-1)^2\right)}}, \\
\frac{\partial m}{\partial z} &= \pm\left(\frac{2\phi_a\left[-16q_a\beta^2\left(2q_a+3(\phi_a-1)^2\right)+2\beta\left(2q_a-3(\phi_a-1)^2\right)(\phi_a-1)^3+(\phi_a-1)^6\right]}{2\left(2q+(\phi_a-1)^2\right)(\phi_a-1)^3(\phi_a-1-4\beta)}\right) \\
&\quad\times\left(\sqrt{\frac{\left(4q+(\phi_a-1)^2\right)(\phi_a-1)^2-8q_a\beta(\phi_a-1)}{2\left(2q_a+(\phi_a-1)^2\right)}}\right)
\end{aligned}$$

with eigenvalues

$$\begin{aligned}
\lambda_{5,6} &= \pm\left(\frac{\sqrt{2\phi_a\left(2q_a+(\phi_a-1)^2\right)\left\{\left(4q_a+(\phi_a-1)^2\right)(\phi_a-1)^2-8q_a\beta(\phi_a-1)\right\}}}{(\phi_a-1)^3(4\beta+1-\phi_a)^{3/2}\left(2q_a+(\phi_a-1)^2\right)}\right) \\
&\quad\sqrt{(\phi_a-1)^6-16\beta^2q_a\left(2q_a+3(\phi_a-1)^2\right)+2\beta\left(2q_a-3(\phi_a-1)^2\right)(\phi_a-1)^3} \quad (4.35)
\end{aligned}$$

Qualitative changes of critical points takes place as follows:

- $P_{56}=0$ and $d_{56}=0$ at $q_a=q_{c_2}^a$ and the critical point is non-simple degenerate because $J|_{\{z_{5,6},r_{5,6}\}}=0$; look at Fig. 4.7$(b)$.
- For, $P_{56}=0$ and $d_{56}<0$ when $q>-\frac{(1-\phi_a)^3}{4(1-\phi_a)+8\beta}$ therefore the critical points are saddle nodes; see Fig. 4.7(c)

A bifurcation diagram for the $r-q_a$ plane is traced keeping ϕ_a and β fixed; see Fig. 4.7.

Global bifurcation and streamline patterns

The associated vector field for $r=0$ is $\{\mathbf{v}_z,\mathbf{v}_r\}=\left\{\frac{h^3+4hq_a+8q_a\beta}{h^2(h+4\beta)},0\right\}$, from which $\zeta=q_a+\frac{h^3}{4(h+2\beta)}$. Critical conditions occur at the wave crests $z=n\pi$ and troughs $z=\frac{(2n-1)\pi}{2}$. Bifurcation

curves are given by $l(\overline{\mathbf{z}}, \boldsymbol{\alpha}) = \zeta = 0$, so we have

$$\begin{aligned} \zeta|_{(z=n\pi)} &= q_a + \frac{1}{4\,(1+2\beta)} = 0, \\ \zeta|_{\left(z=\frac{(2n-1)\pi}{2}\right)} &= q_a + \frac{(1-\phi_a)^3}{4\,(1-\phi_a+2\beta)} = 0. \end{aligned}$$

The global bifurcation diagram in the parameter space $\phi - q$ by keeping β fixed, contains of the following curves :

$$O = \left\{ (\phi_a, q_a) | 0 < \phi_a < 1, q_a = \frac{-1}{4\,(1+2\beta)} \right\}, \tag{4.36}$$

$$P = \left\{ (\phi_a, q_a) | 0 < \phi_a < 1, q_a = -\frac{(1-\phi_a)^3}{4\,(1-\phi_a+2\beta)} \right\}. \tag{4.37}$$

Along the bifurcation curve O, an isolated non-hyperbolic degenerate point exists below the wave crest which is also non-simple. Whereas along the bifurcation curve P, the associated critical points join together below the wave troughs and form connections of non-simple degenerate points. Critical points that amalgamate on P produce a degenerate saddle having six heteroclinic paths. Bifurcation curves are shown in Fig. 4.8. Figs. 4.8 $(a) - (e)$ highlight the transitions between different values of q_a with fixed values of ϕ_a and β. In Fig. 4.8, panels (a), (b), panels (c), (d) and (e) corresponds to backward flow, trapping and forward flow, respectively.

4.2 Results and discussion

Different flow formations which occur in peristaltic motion are discussed through Figs. $4.3 - 4.8$. Fig. 4.3 is prepared to show the bifurcation that occurs corresponding to the critical points $\{x_{1,2}, y_{1,2}\}$ for different values of slip parameter. Here we observe that with the increase in slip parameter β, the bifurcation point occurs for the larger values of flow rate. Moreover, vortices spread along the vertical. Similar observation is made from Fig. 4.4. Global bifurcation diagram is presented in Fig. 4.5. From this figure we observe that with an increase in slip parameter, backward flow region expands whereas the trapping region narrows down. However, no change occurs in the augmented region by increasing slip parameter. This explains the

vanishing trapped bolus with an increase in slip parameter. In fact, if one keeps increasing β for a fixed value of q_a, then the backward flow region expands and encloses the chosen value of q_a. Thus this chosen value of q_a, which was initially in trapping region, now falls in backward flow region where trapping phenomenon is not possible.

Figs. $4.6 - 4.8$ are plotted for the axisymmetric case and the observations in Figs. 4.6 and 4.7 are similar to those noticed in Figs. 4.3 and 4.4. Fig. 4.8 shows the global bifurcation curves and the streamline patterns for different values of slip parameter β. In order to show the streamline patterns in different flow regions, we take values of the flow rate (q_a) both from inside the regions (I-III) and on the lines that separate them, and then the streamlines are drawn for the five selected values of flow rate, which are shown in Fig. 4.6.

The whole analysis provides the bifurcation points and the parametric ranges for different flow situations (backward flow, trapping and augmented flow). We draw a consequence from this analysis that if peristaltic walls are made slippery, then the trapping could be reduced and as a result, the damage of the internal parts due to contamination, if the fluid is a chemical, could be avoided.

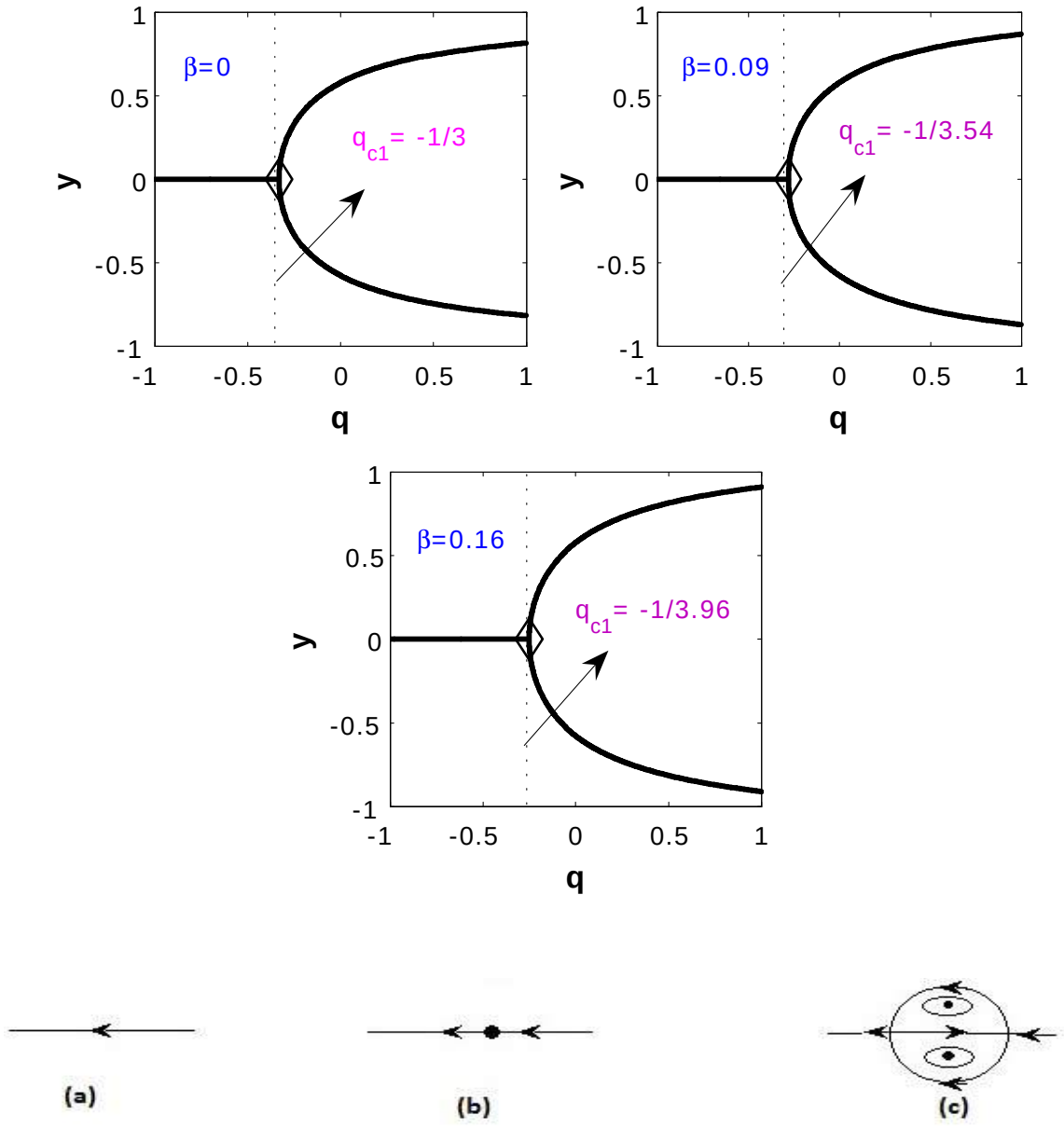

Fig. 4.3(a): Bifurcation diagram for $x = n\pi$, $n \in \mathbb{Z}$ and pictorial topological changes with the variation of β for $0 \leq \beta \leq \frac{1}{6}$ (a) $q < \frac{-1}{3+6\beta}$, (b) $q = \frac{-1}{3+6\beta}$, (c) $q > \frac{-1}{3+6\beta}$.

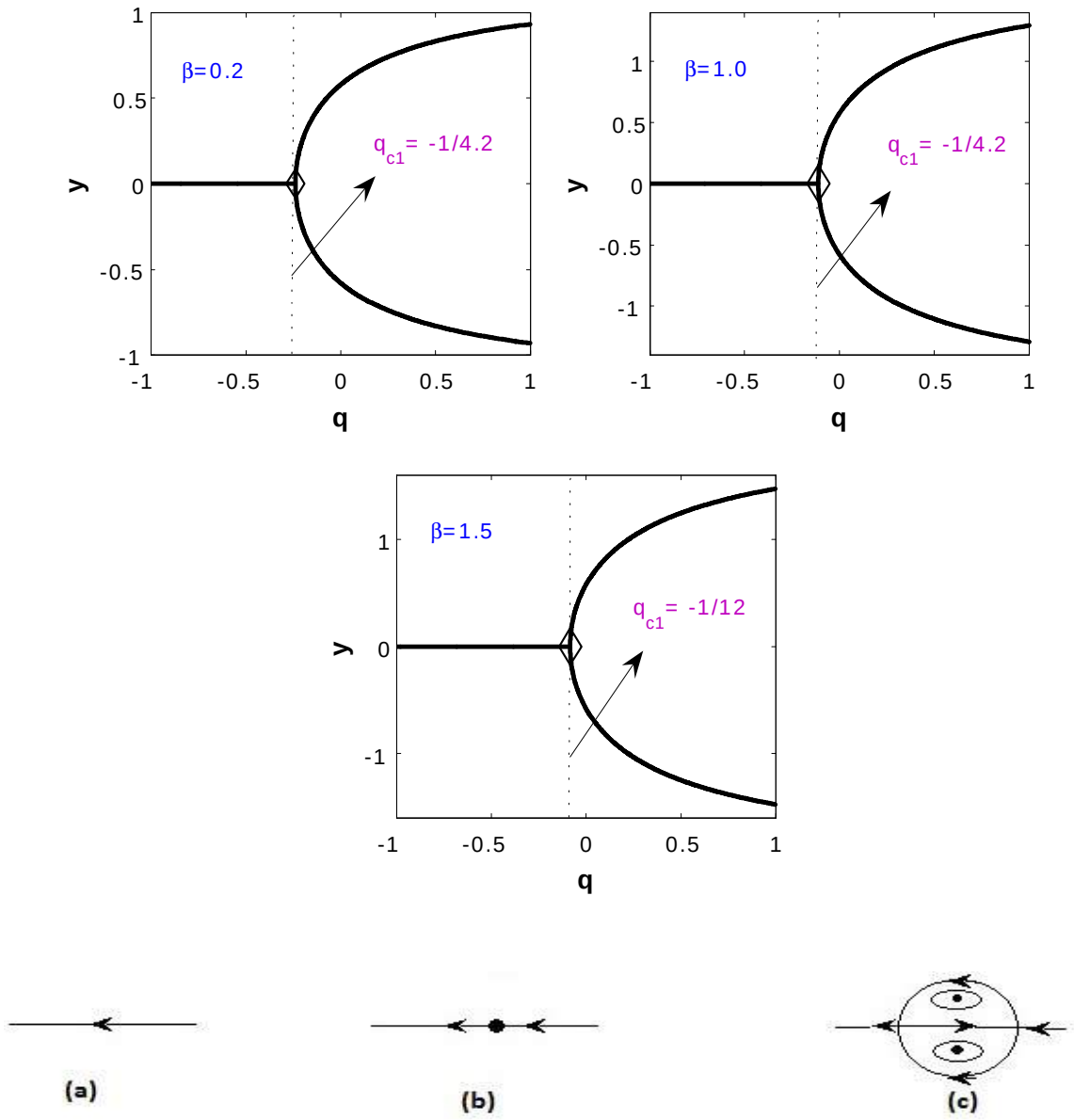

Fig. 4.3(b): Bifurcation diagram for $x = n\pi$, $n \in \mathbb{Z}$ and pictorial topological changes with the variation of β for $\beta > \frac{1}{6}$ (a) $q < \frac{-1}{3+6\beta}$, (b) $q = \frac{-1}{3+6\beta}$, (c) $q > \frac{-1}{3+6\beta}$.

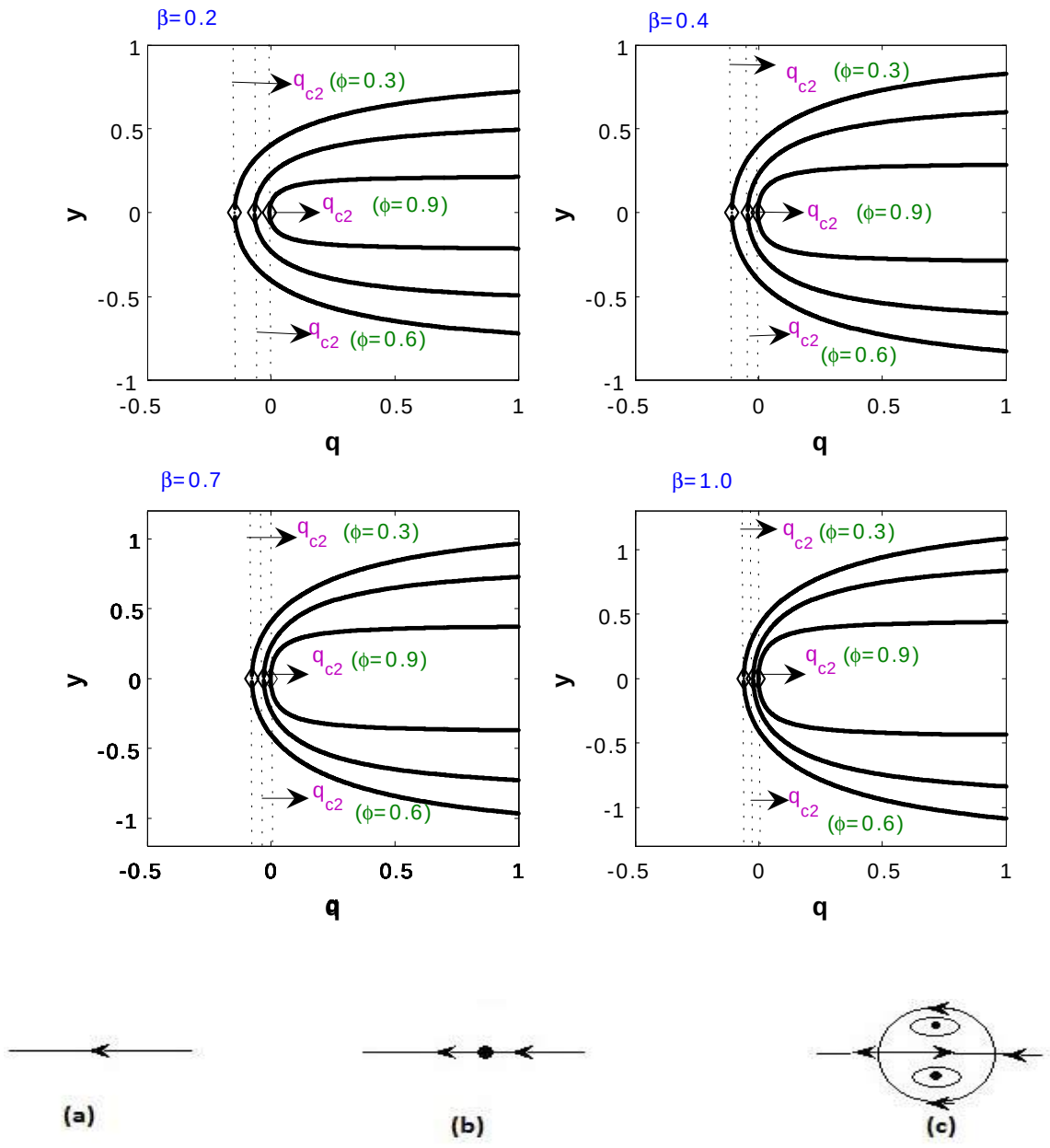

Fig. 4.4: Local bifurcation for wave troughs at $x = (2n-1)\pi/2$ with $q > -\frac{(1-\phi)^2}{3[1-\phi+2\beta]}$ for different values of ϕ and pictorial changes: (a) $q < -\frac{(1-\phi)^2}{3[1-\phi+2\beta]}$, (b) $q = -\frac{(1-\phi)^2}{3[1-\phi+2\beta]}$, (c) $q > -\frac{(1-\phi)^2}{3[1-\phi+2\beta]}$.

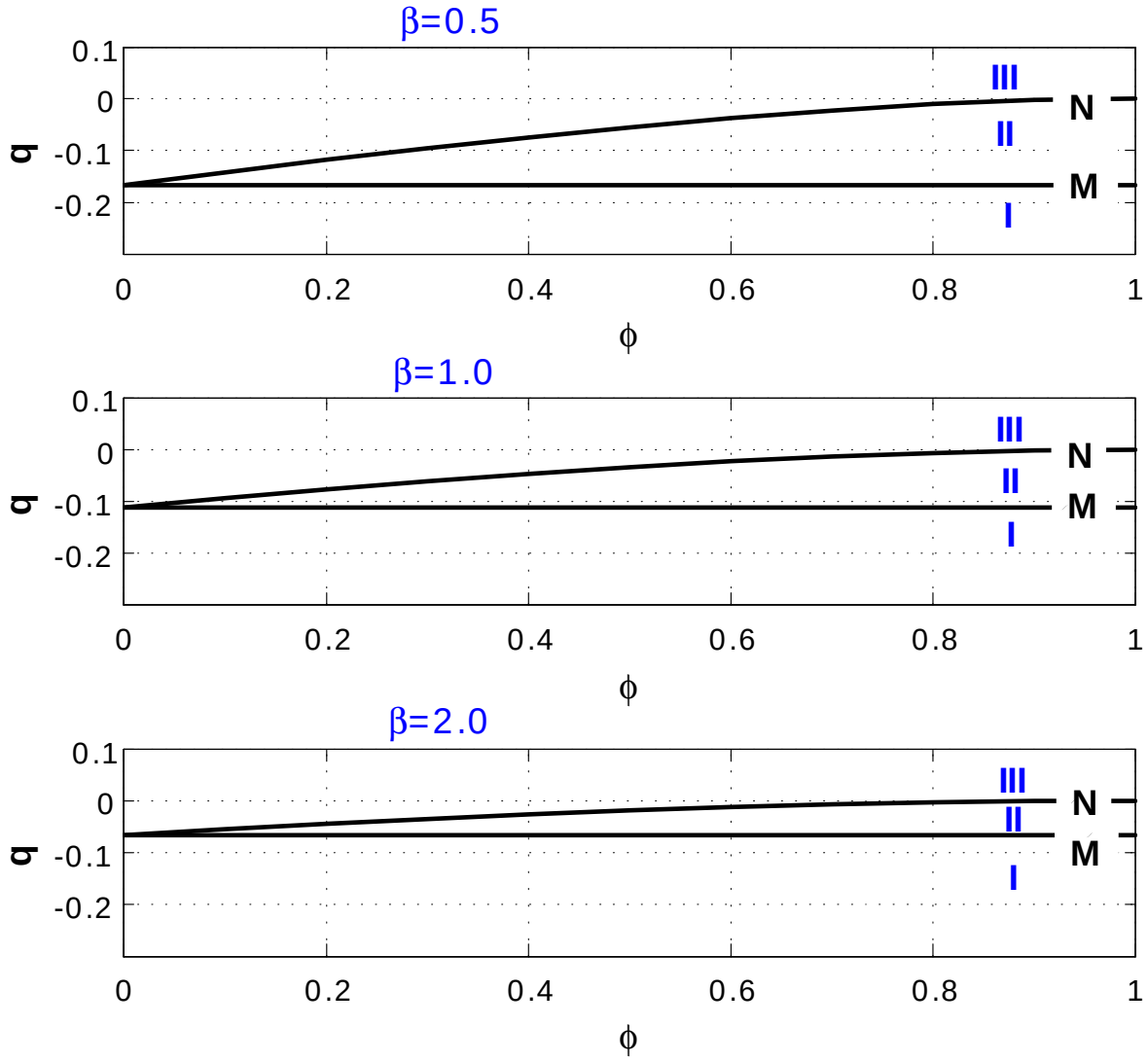

Fig. 4.5: Global bifurcation for planar flow with the variation of β; region I: backward flow, region II: trapping, region III: augmented flow

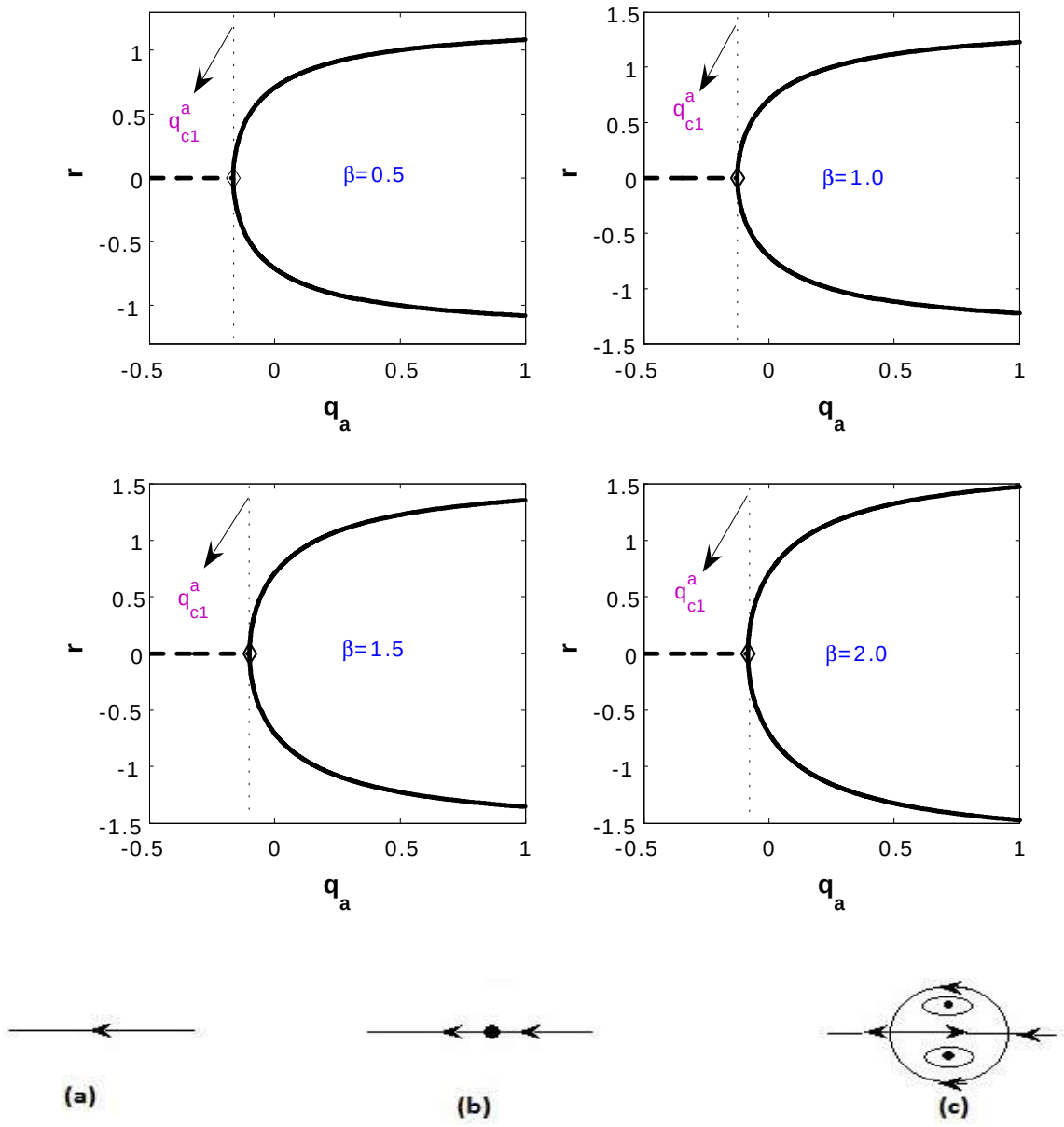

Fig. 4.6: Local bifurcation for wave crest $z = n\pi$, $n \in \mathbb{Z}$ and pictorial topological changes (a) $q_a < \frac{-1}{4+8\beta}$, (b) $q_a = \frac{-1}{4+8\beta}$, (c) $q_a > \frac{-1}{4+8\beta}$.

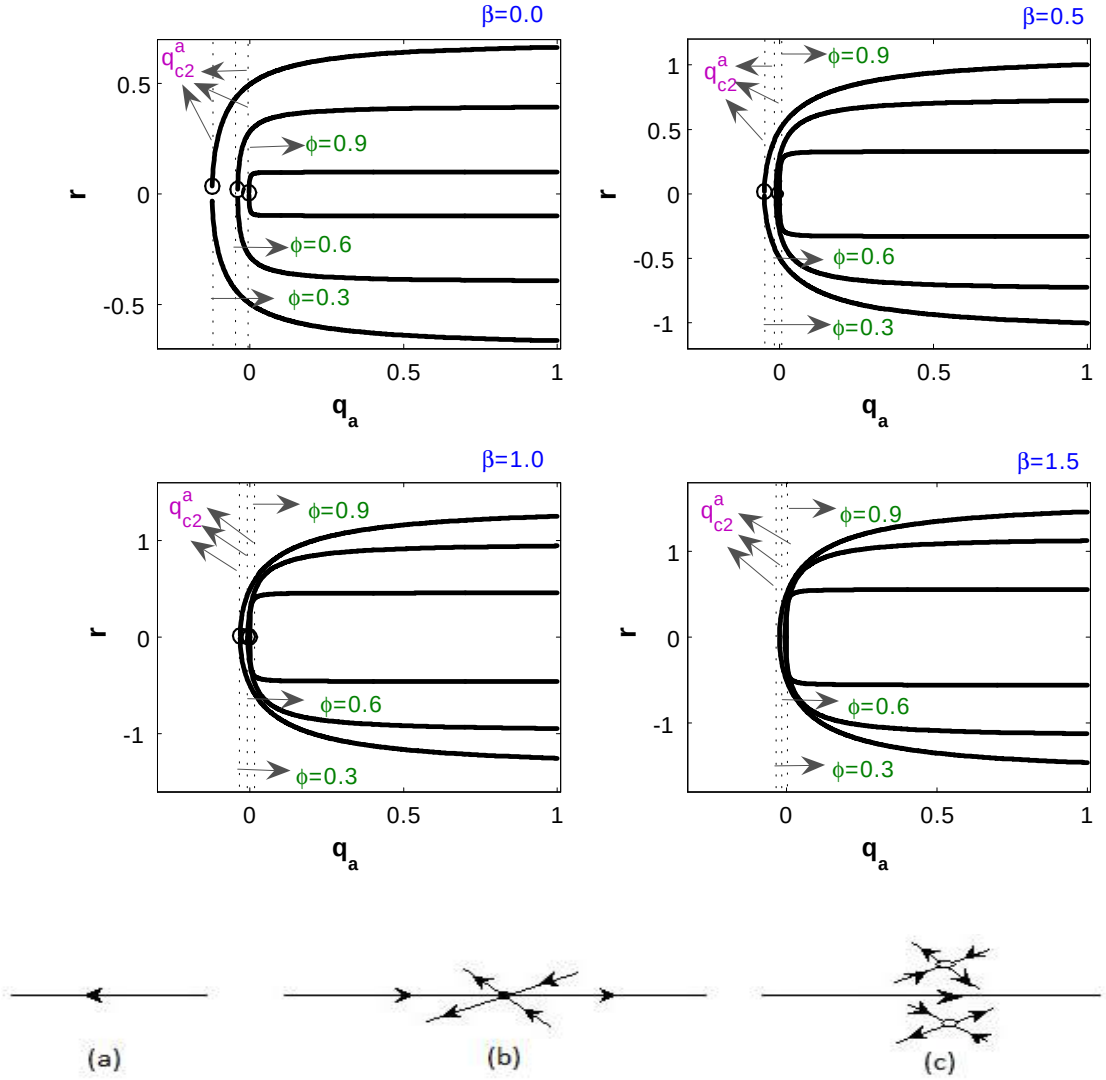

Fig. 4.7: Local bifurcation for wave troughs $z = (2n-1)\pi/2$ with $q_a > -\frac{(1-\phi_a)^3}{4(1-\phi_a)+8\beta}$ with different values of ϕ_a and pictorial changes: (a) $q_a < -\frac{(1-\phi_a)^3}{4(1-\phi_a)+8\beta}$, (b) $q_a = -\frac{(1-\phi_a)^3}{4(1-\phi_a)+8\beta}$, (c) $q_a > -\frac{(1-\phi_a)^3}{4(1-\phi_a)+8\beta}$.

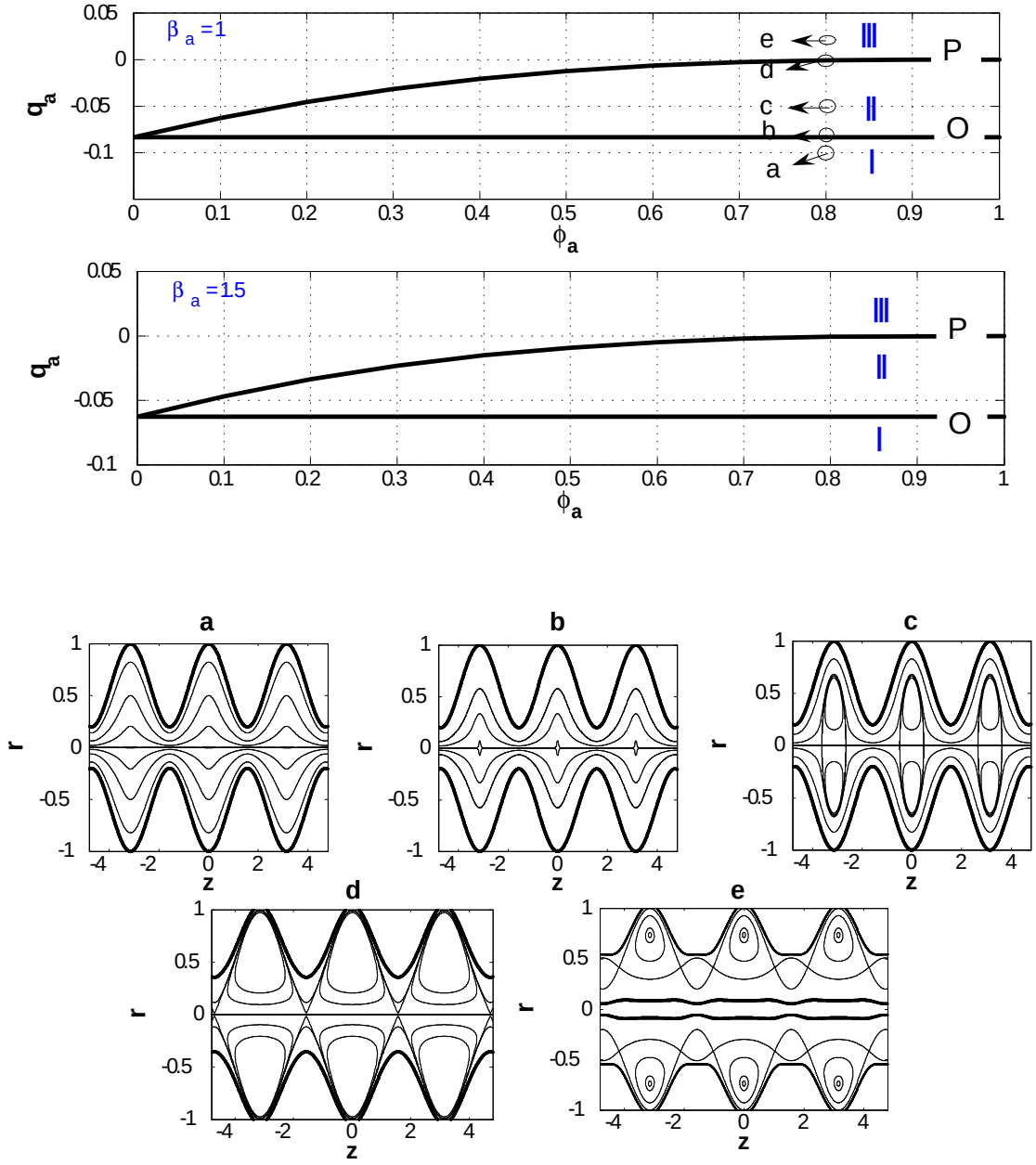

Fig. 4.8: Global bifurcation diagram for axisymmetric flow, $(a)-(e)$ corresponds to $\phi_a = 0.6$ with different values of q_a; region I: backward flow, region II: trapping,region III: augmented flow, (a) $q_a = -0.1$, (b) $q_a = -0.08$, (c) $q_a = -0.05$, (d) $q_a = -0, (e)$ $q_a = 0.02$.

4.3 Concluding remarks

An analysis is performed to investigate the streamline topologies and their bifurcations for peristaltic flow of viscous incompressible fluid in the presence of slip at the wall of channel/tube. The main findings are:

- Trapping region narrows down by increasing the slip parameter.
- The backward flow region expands, whereas no changes occur in the augmented flow region by increasing β.
- The location of bifurcation point changes with the variation of slip parameter.
- Transitions between backward flow to trapping and trapping to the augmented flow corresponds to bifurcations of co-dimension two.
- An increase in slip parameter accelerates the lift off of the centerline and also accelerates the flow through the center.

Chapter 5

Streamline topologies and their bifurcations for mixed convective peristaltic flow

In this chapter, our focus is on streamlines patterns and their bifurcations for mixed convective peristaltic flow of Newtonian fluid with heat transfer. It is assumed that all the fluid properties, except the density are constant. The Boussinesq approximation which relates density change to temperature changes is used in formulating buoyancy force term in the momentum equation. The flow is considered in a two dimensional symmetric channel and the governing equations are simplified under widely taken assumptions of large wavelength and low Reynolds number in a wave frame of reference. In order to study the streamlines patterns, a system of nonlinear autonomous differential equations are established and dynamical systems approach is used to discuss the local bifurcations and their topological changes. We have discussed all types of bifurcations and their topological changes are presented graphically. We found that the vortices contract along the vertical direction whereas they expand along horizontal direction. A global bifurcations diagram is used to summarize the bifurcations. The trapping and backward flow regions are mainly affected by increasing Grashof number and constant heat source parameter in such a way that trapping region increases whereas backward flow region shrinks. The contents of this chapter are published in AIP Advances 5 (9) (2015) 097142.

5.1 Problem formulation

We consider the flow of an incompressible viscous fluid in a two-dimensional vertical channel of width $2a_1$ initiated due to sinusoidal wave trains travelling on the channel walls with speed c. In contrast to previous chapter, we have considered buoyant force in this case. Due to this consideration, an additional term in the $x-$component of momentum equation (4.3) will appear. The expression for the shape of wall surface is same as considered in previous chapter for the planar case. Additionally, it is assumed that the walls are maintained at a constant temperature $\overline{T}_0$. The geometry of the problem is explained in Fig. 5.1.

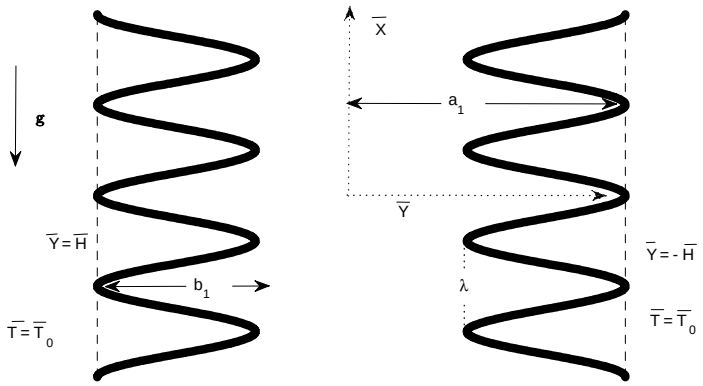

Fig.5.1 Geometry of the problem

For the problem under consideration are continuity equation is given by Eq. (2.13). The scalar momentum equations and energy equation after ignoring dissipation term and taking

into account the source term in fixed frame of reference $\left(\overline{X}, \overline{Y}\right)$ are:

$$\rho\left(\frac{\partial}{\partial \overline{t}}+\overline{U}\frac{\partial}{\partial \overline{X}}+\overline{V}\frac{\partial}{\partial \overline{Y}}\right)\overline{U} = -\frac{\partial \overline{P}}{\partial \overline{X}}+\eta\left(\frac{\partial^2 \overline{U}}{\partial \overline{X}^2}+\frac{\partial^2 \bar{U}}{\partial \overline{Y}^2}\right)+\rho g\alpha(\overline{T}-\overline{T}_0), \tag{5.1}$$

$$\rho\left(\frac{\partial}{\partial \overline{t}}+\overline{U}\frac{\partial}{\partial \overline{X}}+\overline{V}\frac{\partial}{\partial \overline{Y}}\right)\overline{V} = -\frac{\partial \overline{P}}{\partial \overline{Y}}+\eta\left(\frac{\partial^2 \overline{V}}{\partial \overline{X}^2}+\frac{\partial^2 \overline{V}}{\partial \overline{Y}^2}\right), \tag{5.2}$$

$$\rho C_p\left(\frac{\partial}{\partial \overline{t}}+\overline{U}\frac{\partial}{\partial \overline{X}}+\overline{V}\frac{\partial}{\partial \overline{Y}}\right)\overline{T} = k\left(\frac{\partial^2 \overline{T}}{\partial \overline{X}^2}+\frac{\partial^2 \overline{T}}{\partial \overline{Y}^2}\right)+Q. \tag{5.3}$$

In view of the channel symmetry, the problem is considered only in the upper half of the channel. The appropriate boundary conditions on temperature field are:

$$\frac{\partial \overline{T}}{\partial \overline{Y}} = 0 \quad \text{at } \overline{Y}=0, \tag{5.4}$$

$$\overline{T} = \overline{T}_0 \quad \text{at } \overline{Y}=\overline{H}. \tag{5.5}$$

Making use of the transformations (2.18), dimensionless quantities (2.24) and stream function (2.41) in Eqs. (5.1) and Eq. (5.2) and eliminating pressure gradient from the resulting equations, we get

$$\mathrm{Re}\,\delta\left[\psi_y\nabla^2\psi_x-\psi_x\nabla^2\psi_y\right]=\nabla^2\left(\nabla^2\psi\right)+Gr_t\theta^*_y. \tag{5.6}$$

Similarly Eq. (5.3) becomes

$$\mathrm{Re}\,\mathrm{Pr}\,\delta\left[\psi_y\theta^*_x-\psi_x\theta^*_y\right]=\nabla^2\theta+E_1, \tag{5.7}$$

where the Grashof number Gr_t, dimensionless temperature θ^*, constant heat generation E_1 and Prandtl number (Pr) are respectively defined as below

$$Gr_t=\frac{g\alpha a^3\overline{T}_0}{\nu^2},\quad \theta^*=\frac{\overline{T}-\overline{T}_0}{\overline{T}_0},\quad E=\frac{Qa^2}{k\overline{T}_0},\quad P_r=\frac{\mu C_p}{k}. \tag{5.8}$$

Now under the assumptions of long wavelength and low Reynolds number, Eqs. (5.6) and (5.7) yield

$$0 = \frac{\partial^4 \psi}{\partial y^4} + Gr_t \frac{\partial \theta^*}{\partial y}, \tag{5.9}$$

$$0 = \frac{\partial^2 \theta^*}{\partial y^2} + E. \tag{5.10}$$

The dimensionless volume flow rate and boundary conditions in the wave frame are [39]

$$\psi = 0, \quad \frac{\partial^2 \psi}{\partial y^2} = 0, \quad \frac{\partial \theta^*}{\partial y} = 0, \quad at\ y = 0, \tag{5.11a}$$

$$\psi = q, \quad \frac{\partial \psi}{\partial y} = -1, \quad \theta^* = 0, \quad at\ y = h, \tag{5.11b}$$

$$\theta - 1 = q = \int_0^h \frac{\partial \psi}{\partial y} dy, \tag{5.12}$$

where q and F are dimensionless mean flow rates in the laboratory and wave frames respectively.

5.2 Solution of the problem

The solution of the Eq. (5.9) and Eq. (5.10) subject to boundary conditions $(5.11a, b)$ is

$$\psi = \frac{y(60q(3h^2 - y^2) + h(h^2 - y^2)(60 + \xi h^2(h^2 - y^2)))}{120h^2}, \tag{5.13}$$

where $\xi = Gr_t E$.

5.3 Flow Field as a Nonlinear Dynamical System

Here we follow the idea of the qualitative theory of dynamical systems. At a particular instant, say t_0, the motion of individual particles moving in paths defined by $\overline{V} = [u(x, y, t), v(x, y, t), 0]$ is identical to instantaneous streamlines, or we have $\overline{V} = [u(x, y, t_0), v(x, y, t_0), 0] = [u(x, y), v(x, y), 0]$. The present problem will reduce to as a system of nonlinear autonomous differential equations

by using the relation $u(x,y)=\frac{\partial\psi}{\partial y}$ and $v(x,y)=-\frac{\partial\psi}{\partial x}$. Using Eq. (5.13) we have

$$u = \frac{-180hy^2+180q(h^2-y^2)+h^7\xi-6h^5y^2\xi+5h^3(12+y^4\xi)}{120h^3}=f(x,y,\boldsymbol{\alpha}), \quad (5.14)$$

$$v = \frac{\partial h}{\partial x}\left[\frac{30hy^3-45qy(h^2-y^2)+h^5y\xi(h^2-y^2)}{30h^4}\right]=g(x,y,\boldsymbol{\alpha}), \quad (5.15)$$

where $\boldsymbol{\alpha}=[\phi,q,\xi]$, $-\infty<x<\infty$, $-h<y<h$ and $0<\phi<1$.

For the equilibrium points we set $f(x,y,\boldsymbol{\alpha})=0=g(x,y,\boldsymbol{\alpha})$ by following [133] and use the Hartman-Grobman theorem according to which the nature of the equilibrium point for the nonlinear autonomous system can be found by the Jacobian at the equilibrium point. If the determinant of the Jacobian at certain equilibrium point is zero, the equilibrium point is degenerate. There are two subcases of degeneracy namely Simple and Non-Simple. The simple degeneracy corresponds to the case when eigenvalues of the Jacobian are zero and for non-simple degeneracy, Jacobian is a zero matrix. We used the notation of [144] to classify the equilibrium points, where trace: $p_{ij}=\lambda_i+\lambda_j$ and the Jacobian: $d_{ij}=\lambda_i\lambda_j$, which are based on eigen values λ_i,λ_j, and are used to classify the phase space. Here i and j represent arbitrary indices.

According to Seydel [145]: a bifurcation point w.r.t. parameter $\boldsymbol{\alpha}$ is a solution $(x,y,\boldsymbol{\alpha})$, where the number of equilibria, periodic or quasi-periodic solutions change when $\boldsymbol{\alpha}$ passes through $\boldsymbol{\alpha}_c$, with $\boldsymbol{\alpha}_c$ as a critical value.

The equilibrium points are given by

I. $\{x_{1,2},y_{1,2}\}=\left\{n\pi,\pm\sqrt{\frac{90(q+1)+3\xi-2\sqrt{A_1}}{5\xi}}\right\}$

II. $\{x_{3,4},y_{3,4}\}=\left\{n\pi,\pm\sqrt{\frac{90(q+1)+3\xi+2\sqrt{A_1}}{5\xi}}\right\}$

III. $\{x_{5,6},y_{5,6}\}=\left\{\frac{(2n-1)\pi}{2},\pm\sqrt{\frac{-90q-3(30+\xi(1-\phi)^4)(1-\phi)+2\sqrt{B_1}}{5\xi(-1+\phi)^3}}\right\}$

IV. $\{x_{7,8},y_{7,8}\}=\left\{\frac{(2n-1)\pi}{2},\pm\sqrt{\frac{-90q-3(30+\xi(1-\phi)^4)(1-\phi)-2\sqrt{B_1}}{5\xi(-1+\phi)^3}}\right\}$

V. $\{x_{9,10},y_{9,10}\}=\left\{\cos^{-1}\left[\pm\sqrt{\frac{\left(\left(-3q+\frac{81(q-1)^5}{20}\xi\right)-1+\phi\right)}{\phi}}\right],0\right\}$

where

$$\begin{aligned} A_1 &= 2025\,(q+1)^2 - 15(35 + 6\,(q+1))\xi + \xi^2, \\ B_1 &= 2025(q+1-\phi)^2 + \xi^2(1-\phi)^{10} - 30\xi(1-\phi)^5(-5 + 3\,(1+q) + 2\phi). \end{aligned}$$

Here it is important to remember that critical points $\{x_{9,10}, y_{9,10}\}$ are calculated by taking ξ small and terms $O(\xi^2)$ are neglected. The nature of the critical points, critical ranges for the parameters and local and global bifurcations of the critical points will be discussed in coming sections.

5.3.1 Classification and bifurcation of the critical points $\{x_{1,2}, y_{1,2}\}$

The equilibrium points $\{x_{1,2}, y_{1,2}\} = \left\{ n\pi, \pm\sqrt{\frac{90(q+1)+3\xi-2\sqrt{A_1}}{5\xi}} \right\}$ with $n \in \mathbb{Z}$, lie on the vertical below the wave crests. The Jacobian at these equilibrium points is

$$J|_{\{x_{1,2},y_{1,2}\}} = \begin{bmatrix} 0 & \frac{\partial f}{\partial y}|_{\{x_{1,2},y_{1,2}\}} \\ \frac{\partial g}{\partial x}|_{\{x_{1,2},y_{1,2}\}} & 0 \end{bmatrix} \tag{5.16}$$

where

$$\begin{aligned} \frac{\partial f}{\partial y}|_{\{x_{1,2},y_{1,2}\}} &= \mp\frac{1}{30}\left(\sqrt{\frac{90\,(q+1)+3\xi-2\sqrt{A_1}}{5\xi}}\right)\left(90\,(q+1)+3\xi-\left(90\,(q+1)+3\xi-2\sqrt{A_1}\right)\right), \\ \frac{\partial g}{\partial x}|_{\{x_{1,2},y_{1,2}\}} &= \pm\frac{1}{15}\phi\left(\sqrt{\frac{90\,(q+1)+3\xi-2\sqrt{A_1}}{5\xi}}\right)\begin{pmatrix} -45((q+1)-1)+\xi+\left(\frac{-15+45(q+1)-\xi}{5\xi}\right) \\ \times\left(90\,(q+1)+3\xi-2\sqrt{A_1}\right) \end{pmatrix}, \end{aligned}$$

and the eigenvalues of the Jacobian are given by

$$\lambda_{1,2} = \pm\frac{1}{15\sqrt{5}}\left(\sqrt{\left(-\frac{1}{\xi}\sqrt{A_1}\left(90\,(q+1)+3\xi-2\sqrt{A_1}\right)\begin{pmatrix} -45((q+1)-1)+\xi+\left(\frac{-15+45(q+1)-\xi}{5\xi}\right) \\ \times\left(90\,(q+1)+3\xi-2\sqrt{A_1}\right) \end{pmatrix}\phi\right)}\right). \tag{5.17}$$

Here the eigenvalues vary with θ by fixing the values of ϕ and ξ, therefore, the nature and stability of equilibrium points change with the value of flow rate θ. All the discussion will be made by taking the values of flow rate between -1 and 1. Qualitative changes are divided into

four cases which are as follows:

Case-1 (*for* $0 < \xi < 21/64$)

- $p_{12} = 0$ and $d_{12} < 0$ when $\left(-1 < q < \frac{\xi}{45} - \frac{1}{3}\sqrt{\frac{7\xi}{3}}\right)$ OR $\left(\frac{\xi}{45} + \frac{1}{3}\sqrt{\frac{7\xi}{3}} < q < \frac{-1}{27}\sqrt{1-3\xi} + \frac{1}{135}(40+3\xi)\right)$, therefore the equilibrium points are co-dimension two saddle as they depend on ξ and q.

- Equilibrium points occur at $q = q_{c_{1,2}} = \frac{\xi}{45} \pm \frac{1}{3}\sqrt{\frac{7\xi}{3}}$ and $q = q_{c_3} = \frac{-1}{27}\sqrt{1-3\xi} + \frac{1}{135}(40+3\xi)$, with the variations of ξ. They are degenerate and non-hyperbolic [146], because both the Jacobian matrix and eigenvalues are zero respectively. Moreover the critical points with $q = q_{c_{1,2,3}}$ correspond to non-simple degeneracy because $J|_{\{x_{1,2},y_{1,2}\}} = 0$ for $q = q_{c_{1,2,3}}$.

- $p_{12} = 0$ and $d_{12} > 0$ when $\frac{-1}{27}\sqrt{1-3\xi} + \frac{1}{135}(40+3\xi) < q < 1$, therefore each equilibrium point is a center for these value of parameters.

  This whole case is presented in Fig. 5.1(a).

Case-2 $\left(for\ \frac{21}{64} \leq \xi < \frac{1}{2}\left(615 - 15\sqrt{1645}\right)\right)$

- $p_{12} = 0$ and $d_{12} < 0$ when $-1 < q < \frac{\xi}{45} - \frac{1}{3}\sqrt{\frac{7\xi}{3}}$, therefore the equilibrium point is co-dimension two saddle as it depends on ξ and θ.

- $p_{12} = 0$ and $d_{12} > 0$ when $\frac{\xi}{45} + \frac{1}{3}\sqrt{\frac{7\xi}{3}} < q < 1$, therefore, each equilibrium point is a center.

- Equilibrium points occur at $q = q_{c_1} = \frac{\xi}{45} \pm \frac{1}{3}\sqrt{\frac{7\xi}{3}}$, which are also known as a degenerate point but are non-hyperbolic.

  This whole case is presented in Fig. 5.1(b).

Case-3 $\left(for\ \frac{1}{2}\left(435 + 15\sqrt{805}\right) < \xi < \frac{1}{2}\left(615 + 15\sqrt{1645}\right)\right)$

- $p_{12} = 0$ and $d_{12} > 0$ when $-1 < q < \frac{\xi}{45} - \frac{1}{3}\sqrt{\frac{7\xi}{3}}$, therefore, each equilibrium point is a center.

- An isolated equilibrium point occurs at $q = q_{c_1} = \frac{\xi}{45} - \frac{1}{3}\sqrt{\frac{7\xi}{3}}$, which is also degenerate point but is non-hyperbolic [146]. Moreover the equilibrium point with $q = \frac{\xi}{45} - \frac{1}{3}\sqrt{\frac{7\xi}{3}}$ corresponds to non-simple degeneracy because $J|_{\{x_{1,2},y_{1,2}\}} = 0$ for $q = q_{c_1} = \frac{\xi}{45} - \frac{1}{3}\sqrt{\frac{7\xi}{3}}$. This whole case is presented in Fig. 5.1(c).

  Case-4 $\left(for\ \xi \geq \frac{1}{2}\left(615 + 15\sqrt{1645}\right)\right)$

- $p_{12} = 0$ and $d_{12} > 0$ when $-1 < q < 1$, therefore, each equilibrium point is a center; see Fig. 5.1(d).

Based on the definition of a bifurcation, one occurs on the vertical situated at the wave crest at $x = n\pi$. Bifurcation diagram in the $q - y$ plane is traced for each $Case - (1 - 4)$; see Figs. 5.1$(a) - (d)$ respectively. All these bifurcations are of co-dimension two as these depend on q and ξ.

5.3.2 Classification and bifurcation of the critical points $\{x_{3,4}, y_{3,4}\}$

The equilibrium points $\{x_{3,4}, y_{3,4}\} = \left\{n\pi, \pm\sqrt{\frac{90q+3\xi+2\sqrt{A_1}}{5\xi}}\right\}$ lie on the vertical below the wave crests. The Jacobian at these equilibrium points is

$$J|_{\{x_{3,4},y_{3,4}\}} = \begin{bmatrix} 0 & \frac{\partial f}{\partial y}|_{\{x_{3,4},y_{3,4}\}} \\ \frac{\partial g}{\partial x}|_{\{x_{3,4},y_{3,4}\}} & 0 \end{bmatrix} \tag{5.18}$$

where

$$\begin{aligned} \frac{\partial f}{\partial y}|_{\{x_{3,4},y_{3,4}\}} &= \mp\frac{1}{30}\left(\sqrt{\frac{90q+3\xi+2\sqrt{A_1}}{5\xi}}\right)\left(90q+3\xi-\left(90q+3\xi+2\sqrt{A_1}\right)\right) \\ \frac{\partial g}{\partial x}|_{\{x_{3,4},y_{3,4}\}} &= \pm\frac{1}{15}\phi\left(\sqrt{\frac{90q+3\xi+2\sqrt{A_1}}{5\xi}}\right)\begin{pmatrix} -45(q-1)+\xi+\left(\frac{-15+45q-\xi}{5\xi}\right) \\ \times\left(90q+3\xi+2\sqrt{A_1}\right) \end{pmatrix} \end{aligned}$$

and the eigenvalues of the Jacobian are given by

$$\lambda_{3,4} = \pm\frac{1}{15\sqrt{5}}\left(\sqrt{\left(\frac{1}{\xi}\sqrt{A_1}\left(90q+3\xi+2\sqrt{A_1}\right)\begin{pmatrix} -45(q-1)+\xi+\left(\frac{-15+45q-\xi}{5\xi}\right) \\ \times\left(90q+3\xi+2\sqrt{A_1}\right) \end{pmatrix}\phi\right)}\right). \tag{5.19}$$

Since eigenvalues vary with q by fixing the values of ϕ, ξ, therefore, the nature and stability of critical points change with the value of flow rate q. Qualitative changes are divided into four cases which take place as follows:

Case-1 (*for* $0 < \xi \leq 21/64$)

- $p_{34} = 0$ and $d_{34} < 0$ when
  $\left(\frac{\xi}{45} + \frac{1}{3}\sqrt{\frac{7\xi}{3}} < q < \frac{-1}{27}\sqrt{1-3\xi} + \frac{1}{35}(40+3\xi)\right)$ OR
  $\left(\frac{1}{27}\sqrt{1-3\xi} + \frac{1}{135}(40+3\xi) < q < 1\right)$, therefore the equilibrium points are co-dimension two saddle as they depend on ξ and q.

- Equilibrium points occur at $q = q_{c_{1,2}} = \frac{\xi}{45} \pm \frac{1}{3}\sqrt{\frac{7\xi}{3}}$, $q = q_{c_{3,4}} = \pm\frac{1}{27}\sqrt{1-3\xi} + \frac{1}{135}(40+3\xi)$, which are also known as degenerate points but are non-hyperbolic. Moreover these equilibrium points correspond to non-simple degeneracy because $J|_{\{x_{3,4}, y_{3,4}\}} = 0$ for $q = q_{c_{1,2,3,4}}$.

- $p_{34} = 0$ and $d_{34} > 0$ when $\left(-1 < q < \frac{\xi}{45} - \frac{1}{3}\sqrt{\frac{7\xi}{3}}\right)$ OR $\frac{\xi}{45} + \frac{1}{3}\sqrt{\frac{7\xi}{3}} < q < \frac{1}{27}\sqrt{1-3\xi} + \frac{1}{135}(40+3\xi)$ OR $(-\frac{1}{27}\sqrt{1-3\xi} + \frac{1}{35}(40+3\xi) < q < \frac{1}{27}\sqrt{1-3\xi} + \frac{1}{35}(40+3\xi))$, therefore each equilibrium point is a center.

  This whole case is portrayed in Fig. 5.2(a).

Case-2 $\left(\textit{for } 1/3 < \xi < \frac{1}{2}\left(615 - 15\sqrt{1645}\right)\right)$

- $p_{34} = 0$ and $d_{34} < 0$ when $\frac{\xi}{45} + \frac{1}{3}\sqrt{\frac{7\xi}{3}} < q < 1$, therefore, each equilibrium point is a co-dimension two saddle as it depends on ξ and q.

- Isolated equilibrium points occur at $q = q_{c_{1,2}} = \frac{\xi}{45} \pm \frac{1}{3}\sqrt{\frac{7\xi}{3}}$, which are also known as degenerate point but are non-hyperbolic. Moreover the equilibrium points $q = q_{c_{1,2}}$ corresponds to non-simple degeneracy because $J|_{\{x_{3,4}, y_{3,4}\}} = 0$ for $q = q_{c_{1,2}}$.

- $p_{34} = 0$ and $d_{34} > 0$ when $-1 < q < \frac{\xi}{45} - \frac{1}{3}\sqrt{\frac{7\xi}{3}}$, therefore, each equilibrium point is a center.

  This whole case is portrayed in Fig. 5.2(b).

Case-3 $\left(\textit{for } \frac{1}{2}\left(435 + 15\sqrt{805}\right) < \xi < \frac{1}{2}\left(615 + 15\sqrt{1645}\right)\right)$

- $p_{34} = 0$ and $d_{34} < 0$ when $-1 < q < \frac{\xi}{45} - \frac{1}{3}\sqrt{\frac{7\xi}{3}}$, therefore, each equilibrium point is a co-dimension two saddle.

- An isolated equilibrium point occur at $q = q_{c_1} = \frac{\xi}{45} - \frac{1}{3}\sqrt{\frac{7\xi}{3}}$, which is also known as a degenerate point but is non-hyperbolic. Moreover the equilibrium point with $q = q_{c_1}$ corresponds to non-simple degeneracy because $J|_{\{x_{3,4}, y_{3,4}\}} = 0$ for $q = q_{c_1}$.

  This whole case is presented in Fig. 5.2(c).

  Case-4 $\left(for\ \xi \geq \frac{1}{2}\left(615 + 15\sqrt{1645}\right)\right)$

- $p_{34} = 0$ and $d_{34} < 0$ when $-1 < q < 1$, therefore, each equilibrium point is a center; see Fig. 5.2(d).

Based on the definition of a bifurcation, one occurs on the vertical situated at the wave crest at $x = n\pi$. Bifurcation diagram in the $q - y$ plane is traced for each $Case - (1 - 4)$; see Figs. 5.2$(a) - (d)$ respectively. All these bifurcations are of co-dimension two as these depend on q and ξ.

5.3.3 Classification and bifurcation of the critical points $\{x_{5,6}, y_{5,6}\}$

Now we consider $x = \frac{(2n-1)\pi}{2}$ with $q > q_a$ where $q_a = \frac{1}{180}(120 - \xi + 60\phi + 5\xi\phi - 10\xi\phi^2 + 10\xi\phi^3 - 5\xi\phi^4 + \xi\phi^5)$ and $0 < \xi < \frac{-300-60\phi}{-1+5\phi-10\phi^2+10\phi^3-5\phi^4+\phi^5}$. Likewise in previous section, a degenerate fixed point bifurcates to saddle nodes on the longitudinal axis for $q_a < q < 1$. The case when q approaches $q_{c_1} = q_a$ saddle nodes of adjacent waves join together below the wave troughs, therefore the equilibrium points merge on $x = \frac{(2n-1)\pi}{2}$ for $q = q_{c_1}$. This join of equilibrium points produce degenerate points with six heteroclinic connections. The degenerate points bifurcate on the $y-$branch at $x = \frac{(2n-1)\pi}{2}$ with $q > q_{c_1}$ and change stability to saddle nodes.

Equilibrium points $\{x_{5,6}, y_{5,6}\} = \left\{\frac{(2n-1)\pi}{2}, \pm\sqrt{\frac{-90(q-1)-3(30+\xi(1-\phi)^4)(1-\phi)+2\sqrt{B_1}}{5\xi(-1+\phi)^3}}\right\}$ lie on the vertical below the wave troughs. The Jacobian is given by

$$J|_{\{x_{5,6}, y_{5,6}\}} = \begin{bmatrix} 0 & \frac{\partial f}{\partial y}|_{\{x_{5,6}, y_{5,6}\}} \\ \frac{\partial g}{\partial x}|_{\{x_{5,6}, y_{5,6}\}} & 0 \end{bmatrix} \tag{5.20}$$

where

$$\frac{\partial f}{\partial y}|_{\{x_{5,6},y_{5,6}\}} = \frac{-1}{30\left(1-\phi\right)^3} \pm \sqrt{\frac{-90(q-1)-3(30+\xi(1-\phi)^4)(1-\phi)+2\sqrt{B_1}}{5\xi(-1+\phi)^3}} \times \left(\begin{array}{c} 90(q-1)-90(-1+\phi)-3\xi\left(-1+\phi\right)^5+5\xi\left(-1+\phi\right)^3 \\ \times\left(\frac{-90(q-1)-3(30+\xi(1-\phi)^4)(1-\phi)+2\sqrt{B_1}}{5\xi(-1+\phi)^3}\right) \end{array} \right)$$

and

$$\frac{\partial g}{\partial x}|_{\{x_{5,6},y_{5,6}\}} = \pm\frac{\phi}{15\left(1-\phi\right)^4}\left(\sqrt{\frac{-90(q-1)-3(30+\xi(1-\phi)^4)(1-\phi)+2\sqrt{B_1}}{5\xi(-1+\phi)^3}}\right) \times \left(\begin{array}{c} \left(45(q-1)+\xi\left(-1+\phi\right)^5\right)\left(-1+\phi\right)^2+(-45(q-1) \\ -(-30+\xi\left(-1+\phi\right)^4)\left(-1+\phi\right)) \times \left(\frac{-90(q-1)+3(30+\xi(1-\phi)^4)(1-\phi)+2\sqrt{B_1}}{5\xi(-1+\phi)^3}\right) \end{array} \right)$$

with eigenvalues

$$\lambda_{5,6} = \pm\frac{1}{\sqrt{15}}\left(\sqrt{\left(\begin{array}{c} \frac{\phi}{(1-\phi)^4}(\left(45(q-1)+\xi\left(-1+\phi\right)^5\right)\left(-1+\phi\right)^2+\frac{1}{5\xi(-1+\phi)^3} \\ \times(45(q-1)+(-30+\xi\left(-1+\phi\right)^4)\left(-1+\phi\right))\times \\ \left(90(q-1)-3(30+\xi\left(-1+\phi\right)^4)\left(-1+\phi\right)-2\sqrt{B_1}\right) \\ \left(\pm\sqrt{\frac{90(q-1)+3(30+\xi(1-\phi)^4)(1-\phi)-2\sqrt{B_1}}{5\xi(1-\phi)^3}}\right) \end{array} \right)}\right) \times \sqrt{\left(\frac{-1}{30\left(1-\phi\right)^3} \pm \frac{2}{\sqrt{5}}\sqrt{B_1}\sqrt{\frac{1}{\xi\left(1-\phi\right)^3}\left(\begin{array}{c} 90(q-1)-2\sqrt{B_1}+ \\ 3(30+\xi\left(-1+\phi\right)^4)\left(-1+\phi\right) \end{array} \right)}\right)} \quad (5.21)$$

Qualitative changes of critical points for $q \geq q_a$ on $x = \frac{(2n-1)\pi}{2}$ takes place as follows:

Case $\left(for\ 0 < \xi < \frac{-300-60\phi}{-1+5\phi-10\phi^2+10\phi^3-5\phi^4+\phi^5}\right)$

- $P_{56} = 0$ and $d_{56} = 0$ when $q = q_{c_1}$, therefore the equilibrium point is degenerate. And since $J|_{\{x_{5,6},y_{5,6}\}} = 0$ with $q = q_{c_1}$, therefore degeneracy is non-simple.

- $P_{56} = 0$ and $d_{56} < 0$ when $q > q_a$, therefore the equilibrium points are saddle nodes.

A bifurcation diagram for the $y - q$ plane with the variation of ξ is traced as Fig. 5.3.

5.3.4 Classification and bifurcation of the critical points $\{x_{7,8}, y_{7,8}\}$

$x = \frac{(2n-1)\pi}{2}$ and $0 < \xi < \frac{-40-20\phi}{-1+5\phi-10\phi^2+10\phi^3-5\phi^4+\phi^5}$

Likewise in previous section, a degenerate fixed point bifurcates to saddle nodes on the longitudinal axis for $-1 < q < q_b$ where $q_b = \frac{1}{30}\left(10 - \xi + 20\phi + 5\xi\phi - 10\xi\phi^2 + 10\xi\phi^3 - 5\xi\phi^4 + \xi\phi^5\right)$ and $q_b < q < 1$. The case when q approaches $q_{c_2} = q_b$ saddle nodes of adjacent waves join together below the wave troughs, therefore the equilibrium points merge on $x = \frac{(2n-1)\pi}{2}$ for $q = q_{c_1}$. This join of equilibrium points produce degenerate points with six heteroclinic connections. The degenerate points bifurcates on the $y-$branch at $x = \frac{(2n-1)\pi}{2}$ with $q > q_{c_2}$ and change stability to saddle nodes.

Equilibrium points $\{x_{7,8}, y_{7,8}\} = \left\{\frac{(2n-1)\pi}{2}, \pm\sqrt{\frac{-90(q-1)-3(30+\xi(1-\phi)^4)(1-\phi)+2\sqrt{B_1}}{5\xi(-1+\phi)^3}}\right\}$ lie on the vertical below the wave troughs. The Jacobian is given by

$$J|_{\{x_{7,8},y_{7,8}\}} = \begin{bmatrix} 0 & \frac{\partial f}{\partial y}|_{\{x_{7,8},y_{7,8}\}} \\ \frac{\partial g}{\partial x}|_{\{x_{7,8},y_{7,8}\}} & 0 \end{bmatrix} \tag{5.22}$$

where

$$\begin{aligned} \frac{\partial f}{\partial y}|_{\{x_{7,8},y_{7,8}\}} &= \frac{-1}{30\left(1-\phi\right)^3} \pm \sqrt{\frac{-90(q-1)-3(30+\xi(1-\phi)^4)(1-\phi)-2\sqrt{B_1}}{5\xi(-1+\phi)^3}} \\ &\times \begin{pmatrix} 90(q-1)-90(-1+\phi)-3\xi\left(-1+\phi\right)^5+5\xi\left(-1+\phi\right)^3 \\ \times\left(\frac{-90(q-1)-3(30+\xi(1-\phi)^4)(1-\phi)-2\sqrt{B_1}}{5\xi(-1+\phi)^3}\right) \end{pmatrix} \end{aligned}$$

and

$$\begin{aligned} \frac{\partial g}{\partial x}|_{\{x_{7,8},y_{7,8}\}} &= \pm\frac{\phi}{15\left(1-\phi\right)^4}\left(\sqrt{\frac{-90(q-1)-3(30+\xi(1-\phi)^4)(1-\phi)-2\sqrt{B_1}}{5\xi(-1+\phi)^3}}\right) \\ &\times \begin{pmatrix} \left(45(q-1)+\xi\left(-1+\phi\right)^5\right)\left(-1+\phi\right)^2+\left(-45(q-1)\right. \\ -\left(-30+\xi\left(-1+\phi\right)^4\right)\left(-1+\phi\right))\times\left(\frac{-90(q-1)+3(30+\xi(1-\phi)^4)(1-\phi)-2\sqrt{B_1}}{5\xi(-1+\phi)^3}\right) \end{pmatrix} \end{aligned}$$

with eigenvalues

$$\lambda_{7,8} = \pm\frac{1}{\sqrt{15}}\left(\sqrt{\left(\begin{array}{c}\frac{\phi}{(1-\phi)^4}\left(\left(45(q-1)+\xi\left(-1+\phi\right)^5\right)\left(-1+\phi\right)^2+\frac{1}{5\xi(-1+\phi)^3}\right.\\ \times(45(q-1)+(-30+\xi\left(-1+\phi\right)^4)\left(-1+\phi\right))\times\\ \left(90(q-1)-3(30+\xi\left(-1+\phi\right)^4)\left(-1+\phi\right)+2\sqrt{B_1}\right)\\ \left(\pm\sqrt{\frac{90(q-1)+3(30+\xi(1-\phi)^4)(1-\phi)+2\sqrt{B_1}}{5\xi(1-\phi)^3}}\right)\end{array}\right)}\right)$$
$$\times\sqrt{\left(\frac{-1}{30\left(1-\phi\right)^3}\pm\frac{2}{\sqrt{5}}\sqrt{B_1}\sqrt{\frac{1}{\xi\left(1-\phi\right)^3}\left(\begin{array}{c}90(q-1)+2\sqrt{B_1}+\\ 3(30+\xi\left(-1+\phi\right)^4)\left(-1+\phi\right)\end{array}\right)}\right)} \quad (5.23)$$

Qualitative changes of equilibrium points for $q \geq q_b$ on $x = \frac{(2n-1)\pi}{2}$ takes place as follows:

Case $\left(for\ 0 < \xi < \frac{-40-20\phi}{-1+5\phi-10\phi^2+10\phi^3-5\phi^4+\phi^5}\right)$

- $P_{78} = 0$ and $d_{78} = 0$ when $q = q_{c_2}$, therefore the equilibrium point is degenerate. And since $J|_{\{x_{7,8},y_{7,8}\}} = 0$ with $q = q_{c_2}$, therefore degeneracy is non-simple.
- $P_{78} = 0$ and $d_{78} < 0$ when $-1 < q < q_b$, therefore the equilibrium points are saddle nodes.
- $P_{78} = 0$ and $d_{78} > 0$ when $q_b < q < 1$, therefore the equilibrium points are centers.

A bifurcation diagram for the $y - q$ plane with the variation of ξ is traced as Fig. 5.4.

Classification and Bifurcation of the critical points The equilibrium points $\{x_{9,10}, y_{9,10}\} = \left\{\cos^{-1}\left[\pm\sqrt{\frac{\left(\left(-3(q-1)+\frac{81(q-1)^5}{20}\xi\right)-1+\phi\right)}{\phi}}\right], 0\right\}$ lie along the longitudinal axis. The Jacobian at these equilibrium points is

$$J|_{\{x_{9,10},y_{9,10}\}} = \left[\begin{array}{cc}\frac{\partial f}{\partial x}|_{\{x_{9,10},y_{9,10}\}} & 0\\ 0 & -\frac{\partial f}{\partial x}|_{\{x_{9,10},y_{9,10}\}}\end{array}\right] \quad (5.24)$$

where

$$\frac{\partial f}{\partial x} = -\frac{\phi\left(-45(q-1)h^2+\xi h^7\right)\cos x\sin x}{15h^4}$$

with eigenvalues

$$\begin{aligned} \lambda_{9,10} &= \pm\sqrt{\left(\frac{2+C_1+\phi}{225\,(3+C_1)}\right)(2+C_1)\left(\xi\,(3+C_1)^5-45\,(-1+q)\right)^2}, \\ with\ C_1 &= \frac{81}{20}\xi(-1+q)^5-3q \end{aligned} \tag{5.25}$$

The further classification is based on the solution of the inequality $d_{910} < 0$. In previous cases we were fortunate to classify such equilibrium points by giving general ranges for ξ and q. However, in this case due to complicated nature of d_{910}, we are only able to find general ranges for ξ. But unfortunately corresponding ranges of q cannot be obtained in general. Therefore by taking some specific values of ξ from these ranges one can classify the critical points. We have done it only for the case when $0 < \xi \leq 25/648$. In this case due to occurrence of twelfth degree term in d_{910}, we are not able to find general ranges for flow rate q.

Qualitative changes of equilibrium points take place as follows:

Case-1 (*for* $0 < \xi \leq 25/648$)

- $p_{910} = 0$ and $d_{910} < 0$ when

  (i) $(-1 < q < q_1)$ OR $(q_2 < q < 1)$ with $q_1 = 0.666611, q_2 = 0.866666$ and $\xi = 0.01$

  (ii) $(-1 < q < q_3)$ OR $(q_2 < q < 1)$ with $q_3 = 0.666555$ and $\xi = 0.02$

  (iii) $(-1 < q < q_4)$ OR $(q_5 < q < 1)$ with $q_4 = 0.6665, q_5 = 0.866665$ and $\xi = 0.03$,

  therefore the critical point is co-dimension two saddle as it depends on ξ and q.

- Critical points occur at $q = q_{c_{1,2,3,4,5}} = q_1,\ q_2,\ q_3,\ q_4,\ q_5$ for $\xi = 0.01, 0.02, 0.03$, which is also known as a degenerate point but is non-hyperbolic. Moreover these critical points correspond to non-simple degeneracy because $J|_{\{x_{9,10}, y_{9,10}\}} = 0$ for $q = q_{c_{1,2,3,4,5}}$. A set of infinitely many such critical points with the variation of ξ can be obtained but very few are discussed in order to avoid to present lengthy calculations.

- $p_{910} = 0$ and $d_{910} > 0$ when

  (i) $(q_1 < q < q_2)$ with $\xi = 0.01$

  (ii) $(q_3 < q < q_2)$ with $\xi = 0.02$

(iii) $(q_4 < q < q_5)$ with $\xi = 0.03$

therefore each critical point is a center.

This whole case is depicted in Fig. 5.5(a). For other cases in which critical points of co-dimension three appear, the ranges of ξ are $\frac{25}{648} < \xi < \frac{1}{648}(25 + 5\phi)$ and $\frac{1}{648}(25 + 5\phi) < \xi < \frac{3072}{625}$. Their pictorial representation are given in Figs. 5.5(b) and 5.5(c) respectively.

Global bifurcation and streamline patterns The vector field associated with $y = 0$ is $\{\dot{x}, \dot{y}\} = \left\{\frac{180q+\xi h^5+60h}{12h^3}, 0\right\}$, from which $\zeta = q + \frac{\xi h^5+60h}{180}$. Critical conditions occur at the wave crests and troughs. Global bifurcation curves are given by $f(\mathbf{x}, \boldsymbol{\alpha}) = \zeta = 0$, so we have

$$\begin{aligned} \zeta|_{(x=n\pi)} &= q + \frac{\xi + 60}{180} = 0, \\ \zeta|_{(x=\frac{(2n-1)\pi}{2})} &= q + \frac{\xi(1-\phi)^5 + 60(1-\phi)}{180} = 0. \end{aligned}$$

The global bifurcation diagram in the parameters space $\phi - q$ with the variation of ξ contains the following set of curves:

$$M = \left\{(\phi, q)|0 < \phi < 1, q = -\frac{\xi + 60}{180}\right\}, \tag{5.26}$$

$$N = \left\{(\phi, q)|0 < \phi < 1, q = -\frac{\xi(1-\phi)^5 + 60(1-\phi)}{180}\right\}. \tag{5.27}$$

Along the bifurcation curve M, isolated non-hyperbolic degenerate points exist below the wave crests which are also non-simple. Whereas along the bifurcation curve N, the associated critical points join together below the wave troughs and form connections of non-simple degenerate points. Critical points that merge on N produce a degenerate saddles having six heteroclinic paths. Bifurcation curves are shown in Fig. 6. The region of peristaltic flow is divided as follows:

Region$I$: backward flow, where all the flow going in an opposite direction to the flow.

RegionII : trapping, where saddles are connected by heteroclinic connections and the interaction of two vortices with opposite rotations exist in the flow.

RegionIII : Augmented flow, where the eddies below wave crests merge and form heteroclinic connections with their neighbors, and part of the fluid is able to flow through the centerline in

the flow direction.

5.4 Results

Different types of flow topologies and bifurcations in the mixed convective peristaltic flow have been portrayed in Figs. $5.1-5.6$. Fig. $5.1(a)$ discloses the bifurcations that occur corresponding to the critical points $\{x_{1,2}, y_{1,2}\}$ for different values of parameter ξ. The bifurcation points for negative values of flow rate move in the backward direction, whereas those with positive values of flow rates move forward. This translation of bifurcation points result in narrowing down the eddying/circulation region. In this way circulation will remain in control. Same observations are made in Fig. $5.1(b)$. An opposite observation is made from Fig. $5.1(c)$ that the region of eddying motion increases due to which more vortices will arise. Fig. $5.2(a)$ shows that the region of eddying motion decreases and the region where separatrices are generated also decreases. Same results are noted from Fig. $5.2(b)$. In Fig. $5.2(c)$ we note that the region where separatrices are formed increases. In Fig. $5.2(d)$ it is observed that the whole region becomes eddying motion region. Fig. 5.3 shows that there is no bifurcation point for which vortices or eddying motion will occur. In Fig. 5.4 eddying motion region decreases means that vortices reduce along the vertical. In all Figs. $5.5\ (a)-(c)$, we note that eddying motion region expands by increasing ξ. This means that vortices spread along the longitudinal direction.

The global bifurcation diagram is presented in Fig. 5.6. We note that the backward flow region decreases whereas trapping region increases by increasing ξ. This means that there will be more trapping by increasing ξ. Increasing ξ means increasing Grashof number and this observation was made by many researchers that trapping increases by increasing Grashof number. Streamlines are depicted in Fig. 5.7. These streamlines are drawn by taking the values of flow rate from bifurcations curves and different regions. From this figure we note that the behavior of streamlines are quite according to different flow regions, i.e., there is no trapping in backward flow region and on bifurcation curve between backward flow and trapping regions. We also observe that a volume of fluid is observed to be trapped for the values of flow rate $q = 0.8, 1.3$ which basically correspond to trapping and augmented flow regions respectively. Different ranges of parameters are calculated for different types of bifurcations. There are many

bifurcation points where circulations occur. We have prepared Fig. 5.8 and Fig. 5.9 to verify the case-4 of circulation for the critical points $\{x_{3,4}, y_{3,4}\}$. The constructed figures are quite agreed with the calculations. That's why we observed circulations both for the variations of ξ and flow rate.

By the topological fluid dynamics approach one can easily find the range(s) of flow rate for different regions corresponding to different values of involved parameters. If one discusses trapping by choosing values of flow rates in backward flow region, then he will observe no trapping. Similarly if another researcher workout same problem and take values of flow rate from trapping region then he will surely observe trapping. Now there will arise two different opinions for a single work regarding trapping. This is the qualitative approach which enables to fix ranges for flow rate to avoid ambiguities.

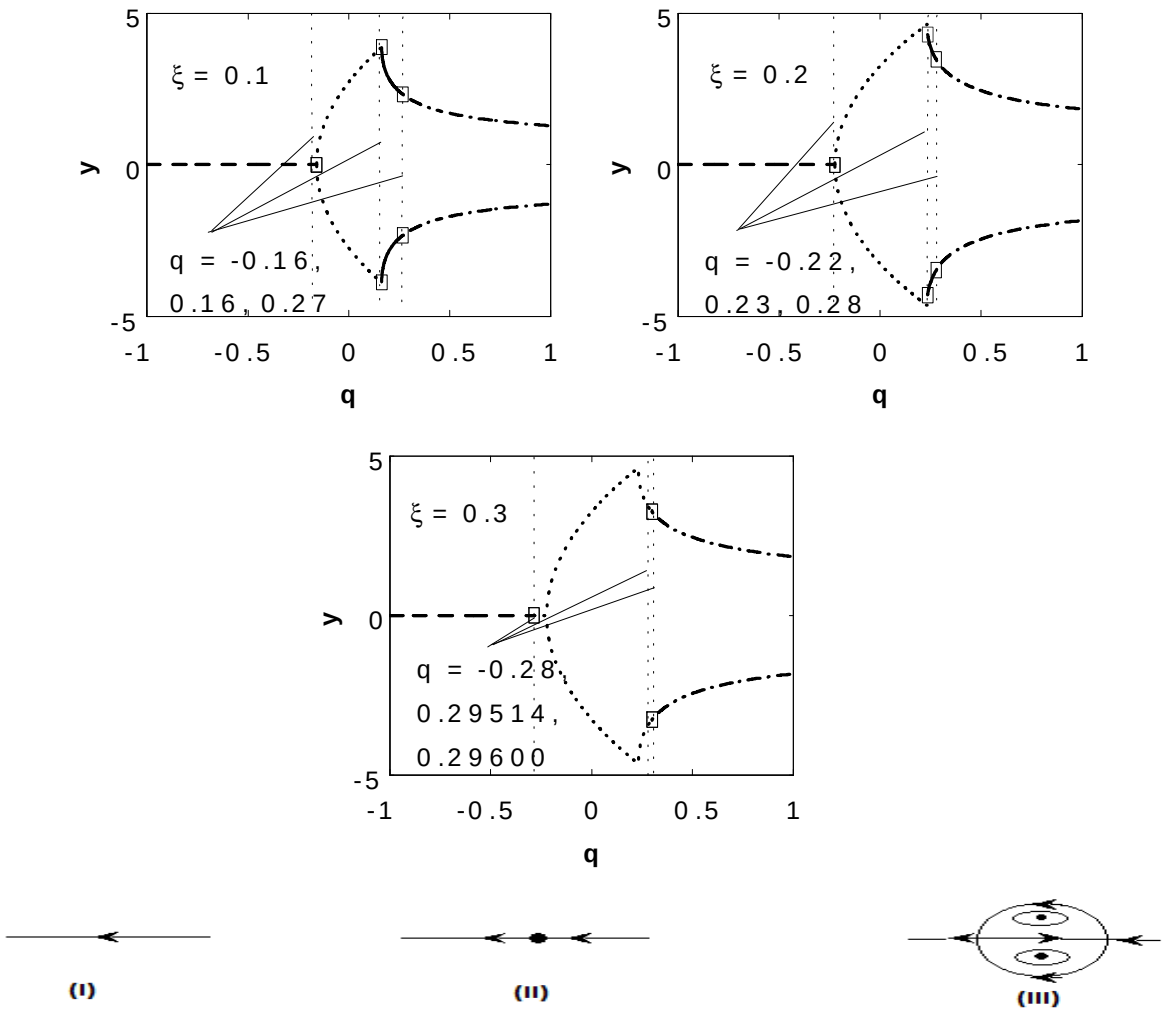

Fig.5.1(a):Localbifurcation for wave crests $x = n\pi, n \in \mathbb{Z}$ and pictorial topological changes with the variation of ξ for $0 < \xi \leq \frac{21}{64}$ $(a)q < \frac{\xi}{45} - \frac{1}{3}\sqrt{\frac{7\xi}{3}}$, $(b)q = \frac{\xi}{45} - \frac{1}{3}\sqrt{\frac{7\xi}{3}}, (c)q > \frac{1}{27}\sqrt{1-3\xi} - \frac{1}{135}(40+3\xi)$.

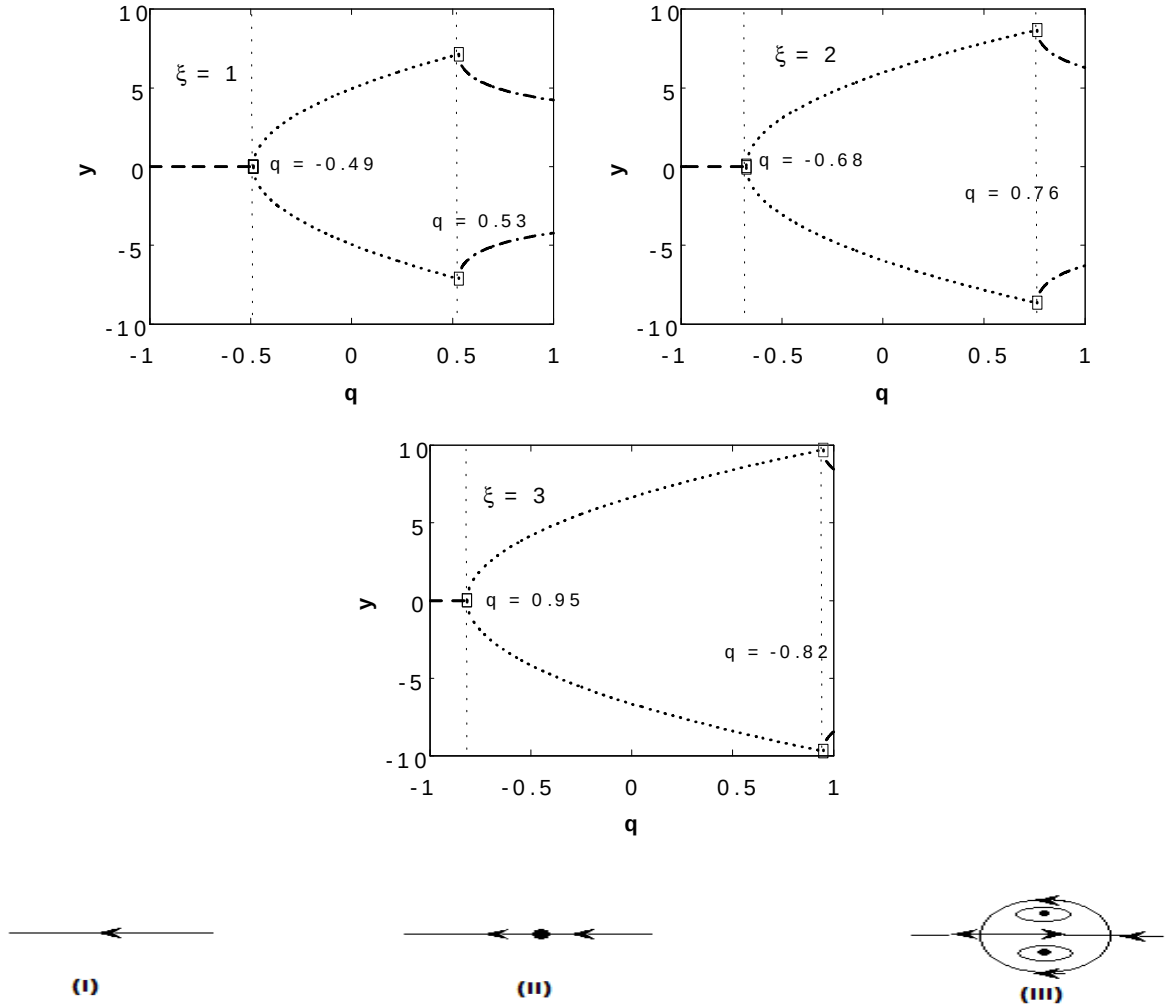

Fig. 5.1(b): Local bifurcation for wave crests $x = n\pi, n \in \mathbb{Z}$ and pictorial topological changes with the variation of ξ for $\frac{21}{64} < \xi \leq \frac{1}{2}\left(615 - 15\sqrt{1645}\right)$
$(a) q < \frac{\xi}{45} - \frac{1}{3}\sqrt{\frac{7\xi}{3}}, (b) q = \frac{\xi}{45} - \frac{1}{3}\sqrt{\frac{7\xi}{3}}, (c) q > \frac{\xi}{45} + \frac{1}{3}\sqrt{\frac{7\xi}{3}}$.

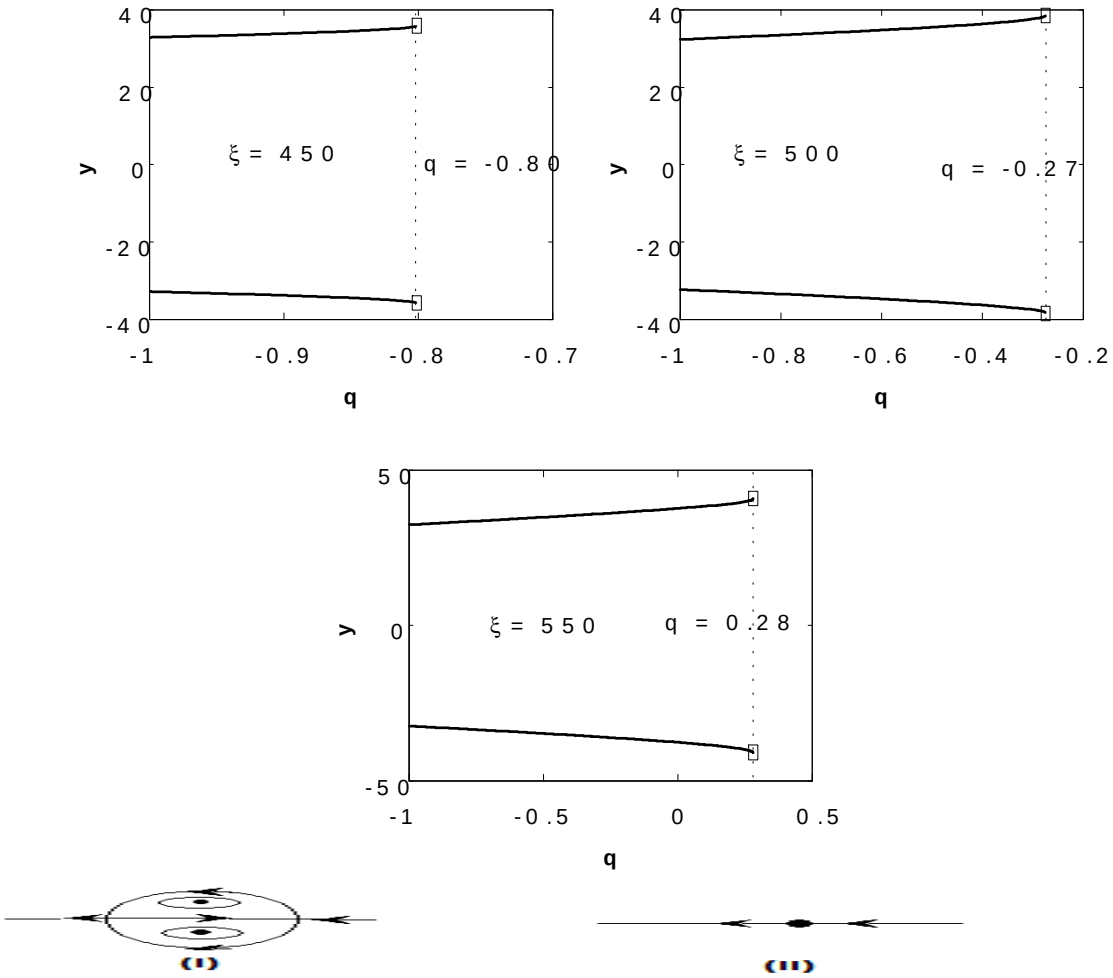

Fig. 5.1(c): Local bifurcation for wave crests $x = n\pi, n \in \mathbb{Z}$ and pictorial topological changes with the variation of ξ for $\frac{1}{2}\left(435 + 15\sqrt{805}\right) < \xi \leq \frac{1}{2}\left(615 + 15\sqrt{1645}\right)$ $(a) q < \frac{\xi}{45} - \frac{1}{3}\sqrt{\frac{7\xi}{3}}, (b) q = \frac{\xi}{45} - \frac{1}{3}\sqrt{\frac{7\xi}{3}}, (c) q > \frac{\xi}{45} + \frac{1}{3}\sqrt{\frac{7\xi}{3}}$.

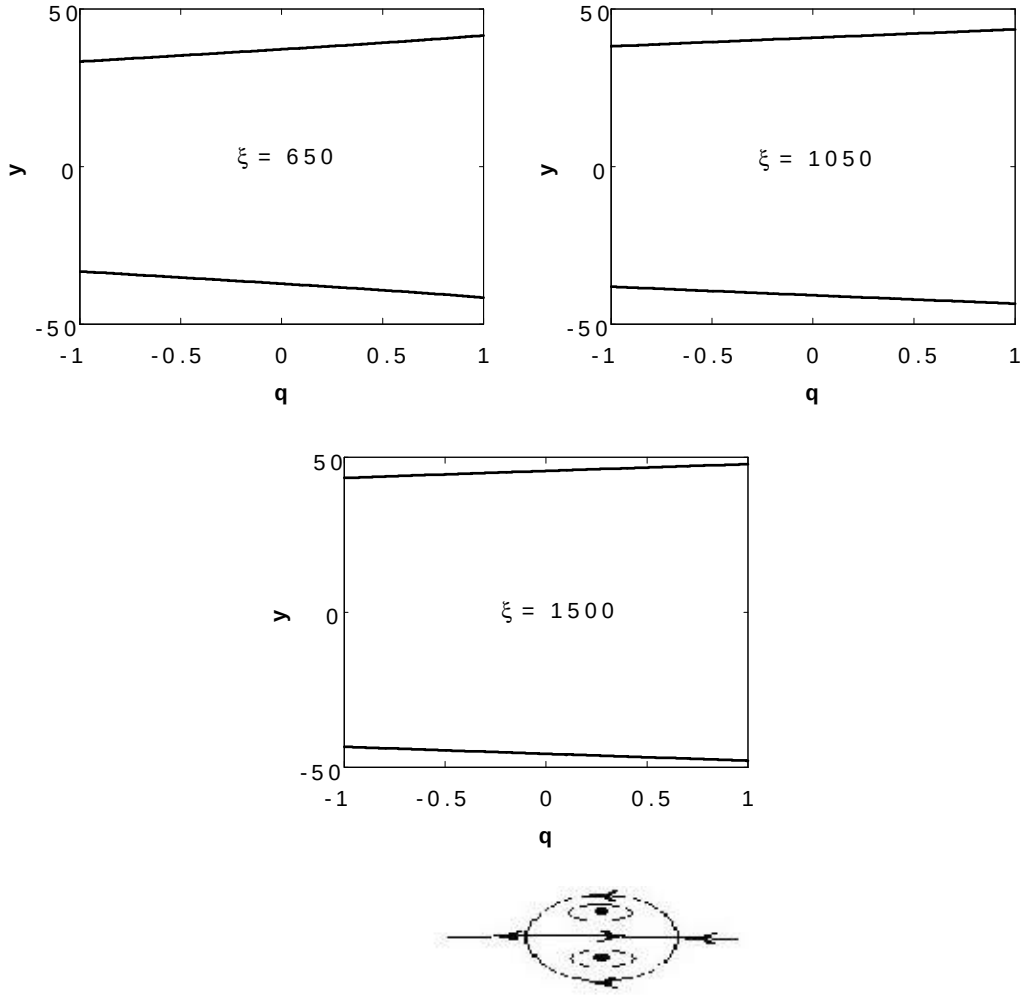

Fig. 5.1(d): Local bifurcation for wave crests $x = n\pi, n \in \mathbb{Z}$ and pictorial topological changes with the variation of ξ for $\xi \geq \frac{1}{2}\left(615 + 15\sqrt{1645}\right)$ and $|q| < 1$.

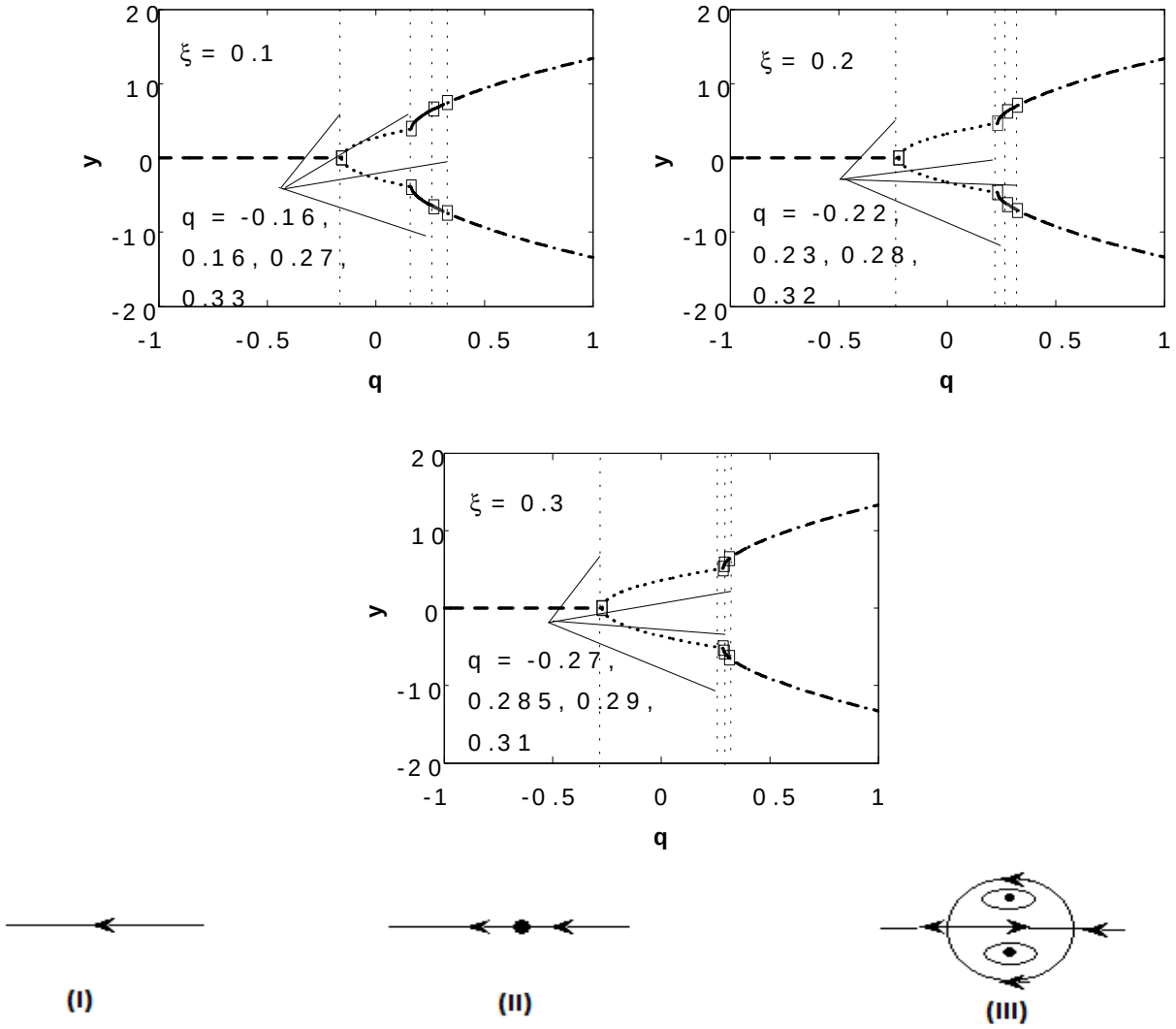

Fig. 5.2(a): Local bifurcation for wave crests $x = n\pi$ for different values of ϕ and qualitative changes for ξ for $0 < \xi \leq \frac{21}{64}$ $(a) q > \frac{\xi}{45} - \frac{1}{3}\sqrt{\frac{7\xi}{3}}$, $(b) q = \frac{\xi}{45} \pm \frac{1}{3}\sqrt{\frac{7\xi}{3}}, (c) q < \frac{\xi}{45} - \frac{1}{3}\sqrt{\frac{7\xi}{3}}$.

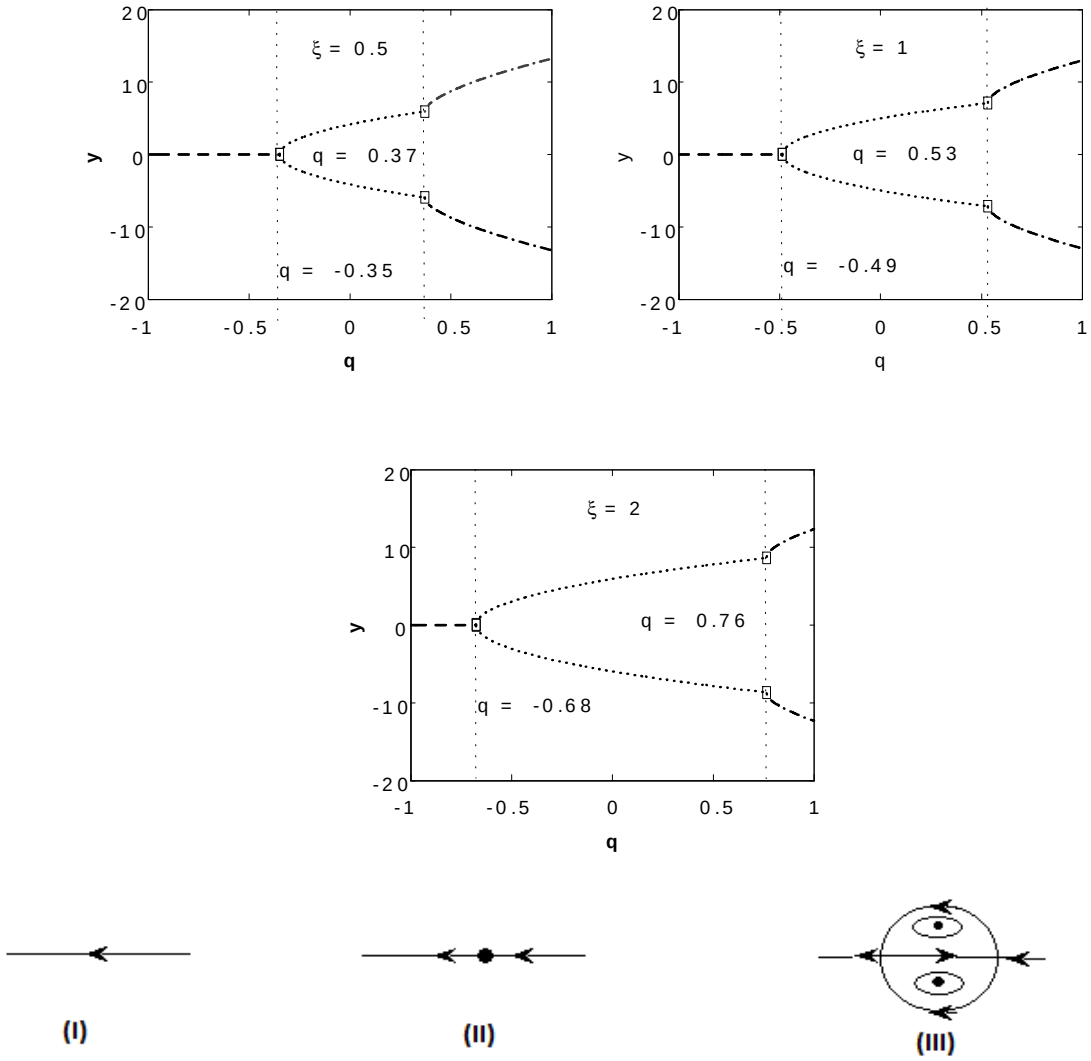

Fig. 5.2(b). Local bifurcation for wave crests $x = n\pi$ for different values of ϕ and pictorial changes for ξ for $\frac{1}{3} < \xi \leq \frac{1}{2}\left(615 - 15\sqrt{1645}\right)$ (a) $q > \frac{\xi}{45} + \frac{1}{3}\sqrt{\frac{7\xi}{3}}$, (b) $q = \frac{\xi}{45} \pm \frac{1}{3}\sqrt{\frac{7\xi}{3}}, (c)$ $q < \frac{\xi}{45} - \frac{1}{3}\sqrt{\frac{7\xi}{3}}$.

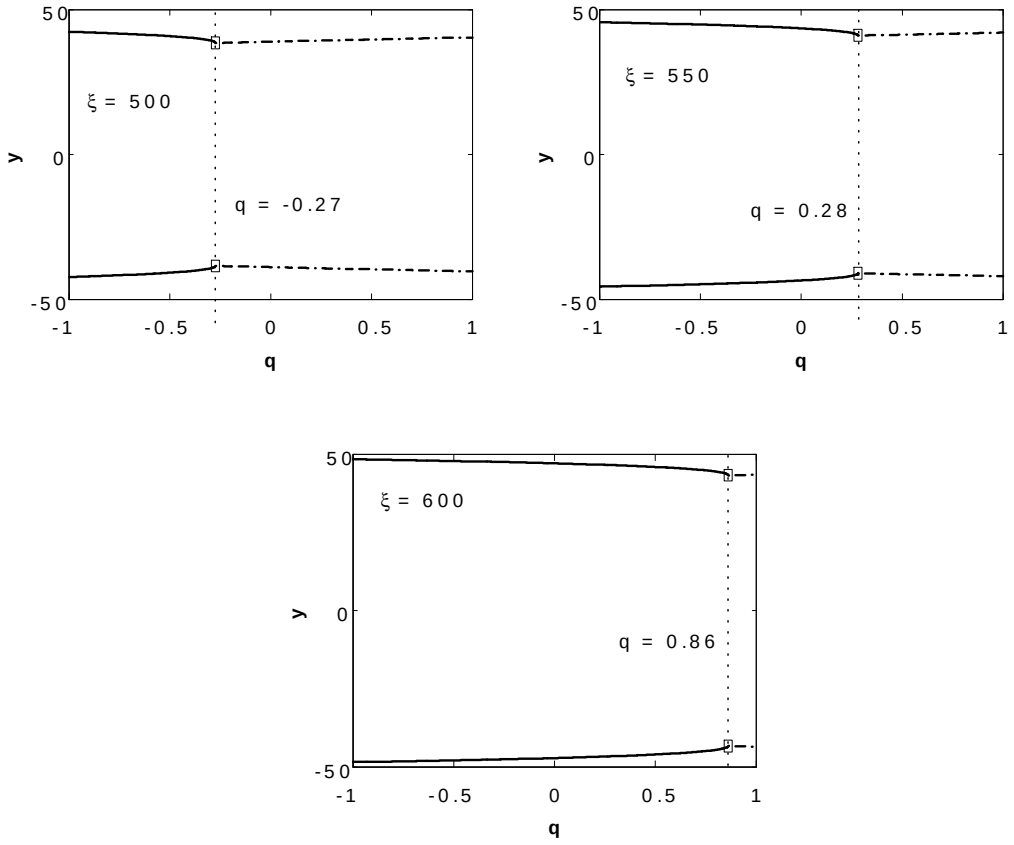

Fig. 5.2(c): Local bifurcation for wave crests $x = n\pi$ with different values of ϕ and pictorial changes for ξ for $\frac{1}{2}\left(435 + 15\sqrt{805}\right) < \xi \leq \frac{1}{2}\left(615 + 15\sqrt{1645}\right)$ $(a)\ q < \frac{\xi}{45} - \frac{1}{3}\sqrt{\frac{7\xi}{3}}, (b)\ q = \frac{\xi}{45} - \frac{1}{3}\sqrt{\frac{7\xi}{3}}$.

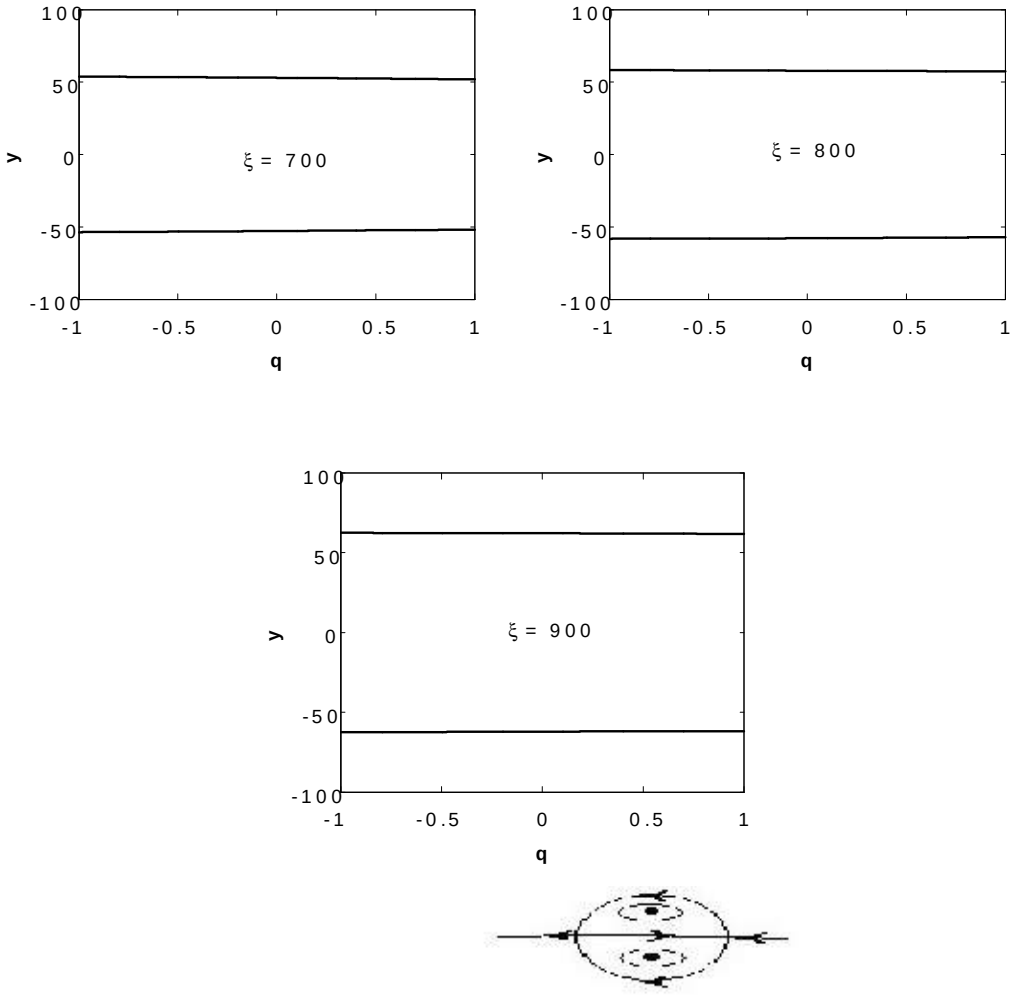

Fig. 5.2(d): Local bifurcation for wave crests $x = n\pi, n \in \mathbb{Z}$ and pictorial topological changes with the variation of ξ for $\xi \geq \frac{1}{2}\left(615 + 15\sqrt{1645}\right)$ and $|q| < 1$.

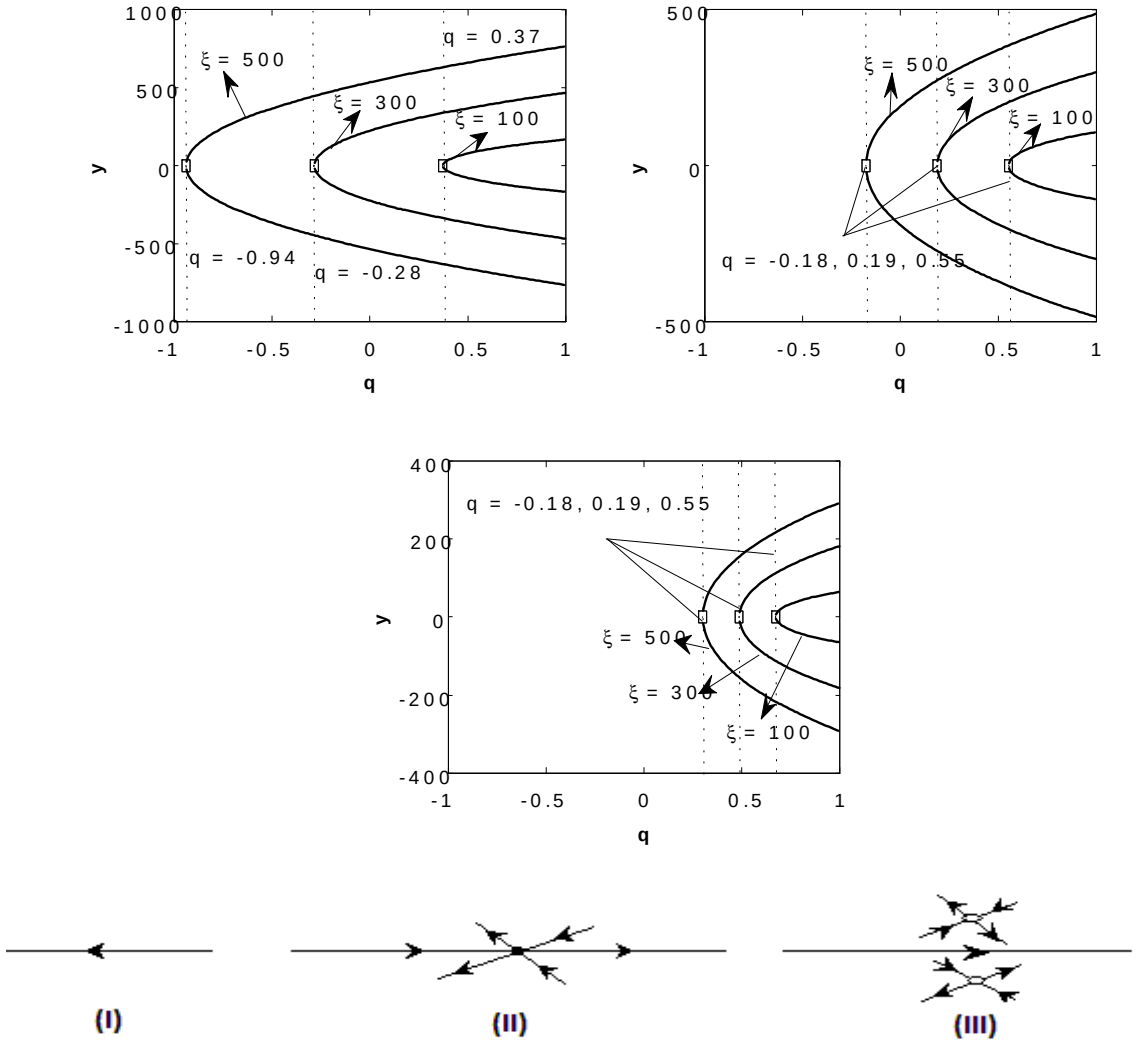

Fig. 5.3: Local bifurcation for wave troughs $z = (2n-1)\pi/2$ for$q > q_a$ and variation of ξ, $0 < \xi < \frac{-300-60\phi}{-1+5\phi-10\phi^2+10\phi^3-5\phi^4+\phi^5}$ with different values of ϕ and pictorial changes: $(a)q < q_a$, $(b)q = q_a$, $(c)q > q_a$.

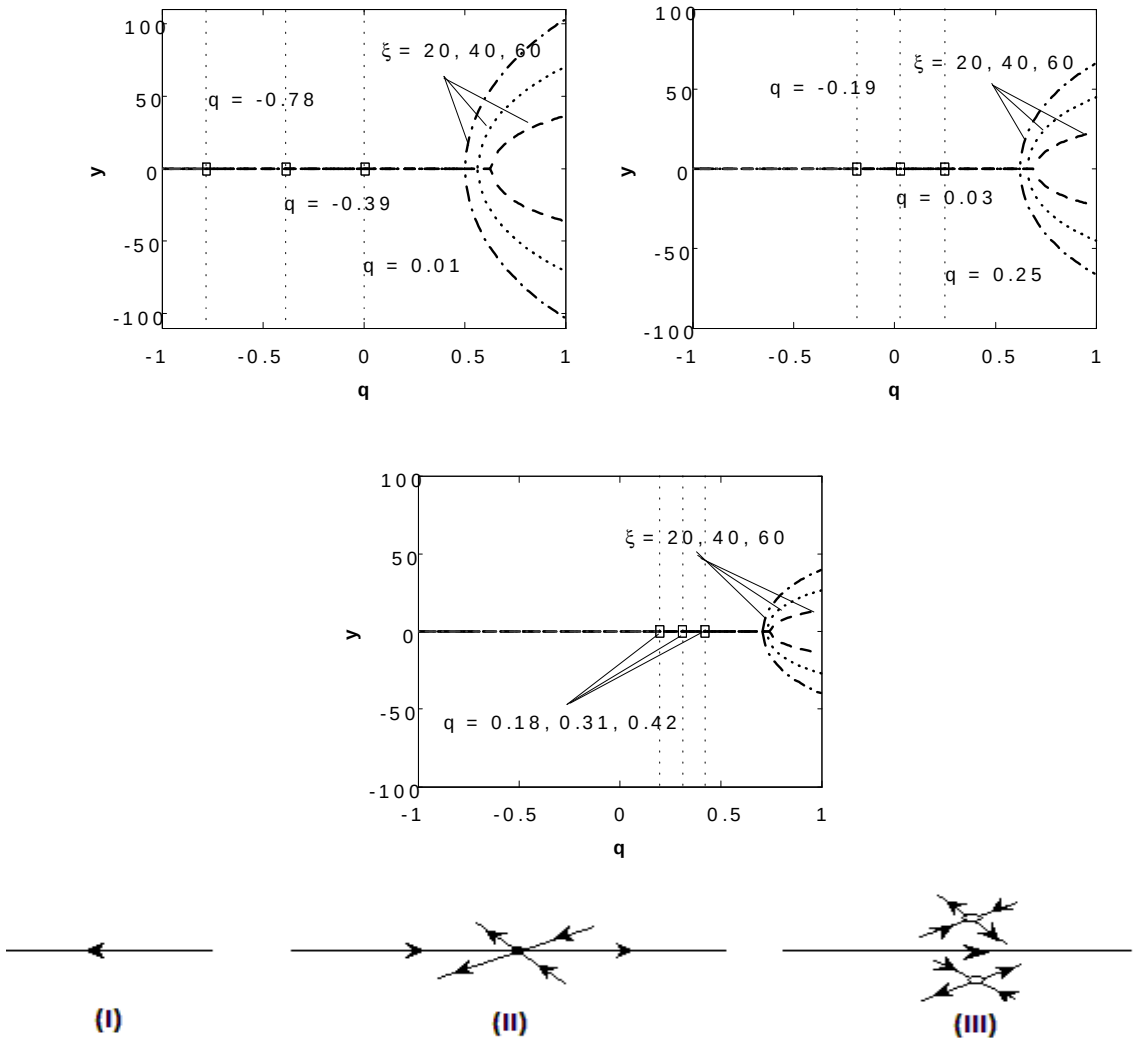

Fig. 5.4: Local bifurcation for wave troughs $z = (2n-1)\pi/2$ for $q > q_b$ and variation of ξ, $0 < \xi < \frac{-40-20\phi}{-1+5\phi-10\phi^2+10\phi^3-5\phi^4+\phi^5}$ with different values of ϕ and pictorial changes: $(a) q < q_b$, $(b) q = q_b$, $(c) q > q_b$.

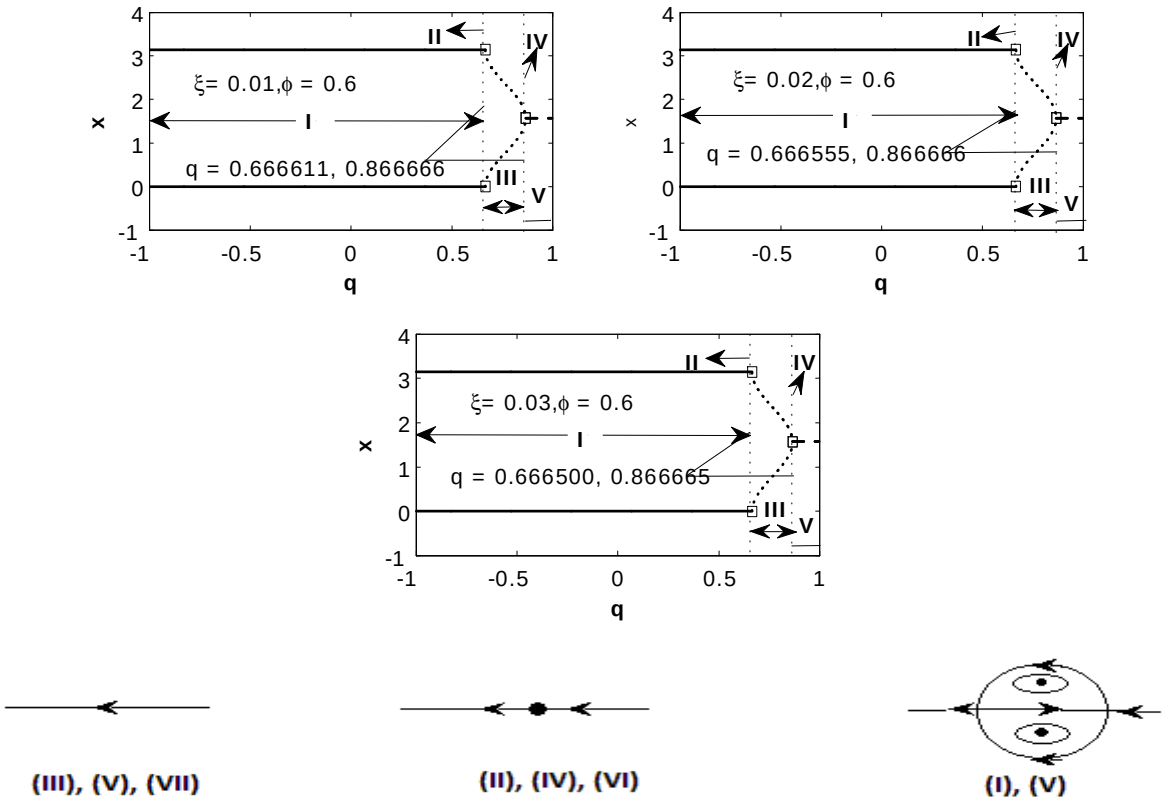

Fig. 5.5(a): Local bifurcation for $y = 0$ and pictorial topological changes with the variation of ξ for $0 < \xi \leq \frac{25}{648}$ and $\phi = 0.6$.

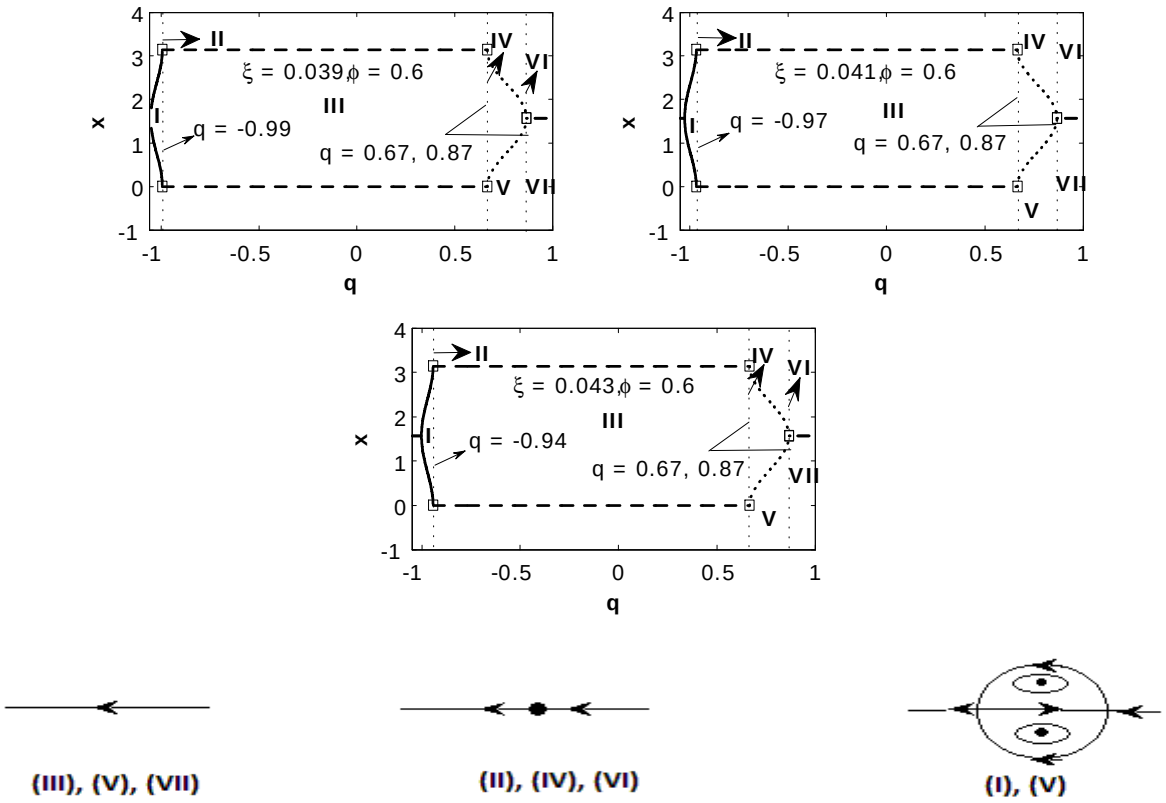

Fig. 5.5(b): Local bifurcation for $y = 0$ and pictorial topological changes with

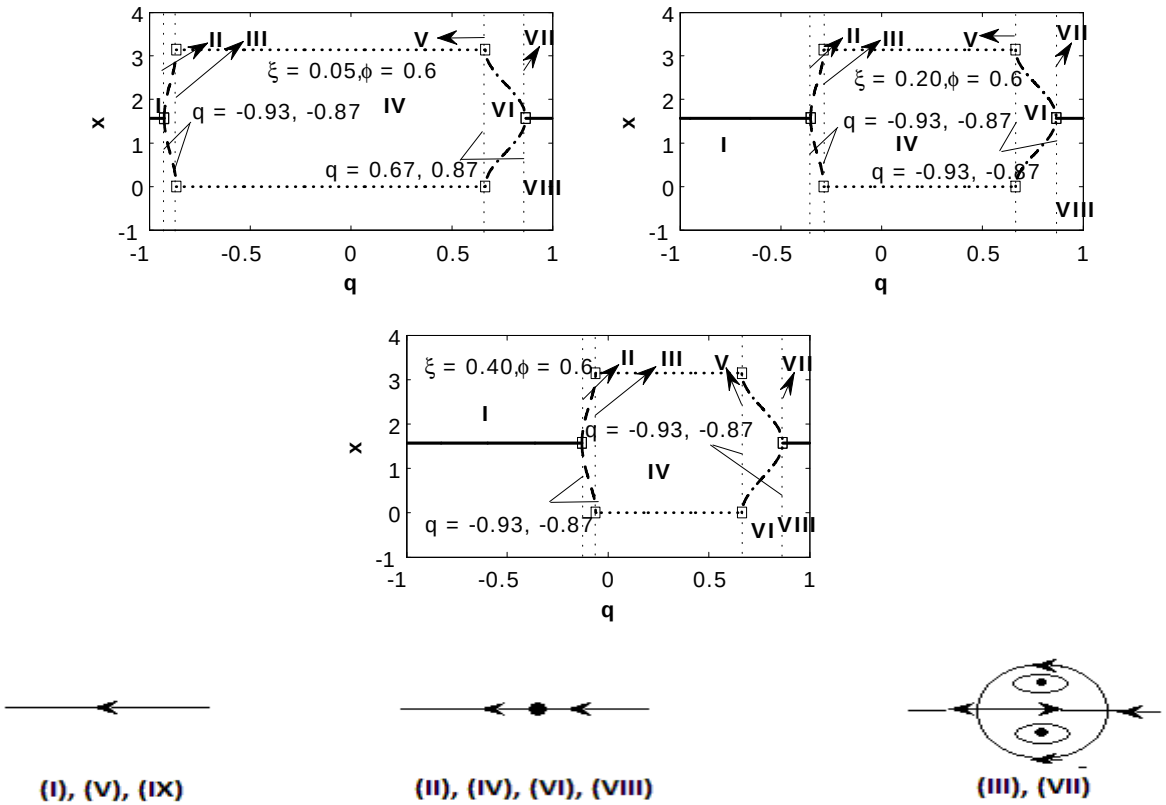

Fig. 5.5(c): Local bifurcation for $y = 0$ and pictorial topological changes with the variation of ξ for $\frac{1}{648}(25 + 5\phi) < \xi \leq \frac{3072}{625}$ and $\phi = 0.6$.

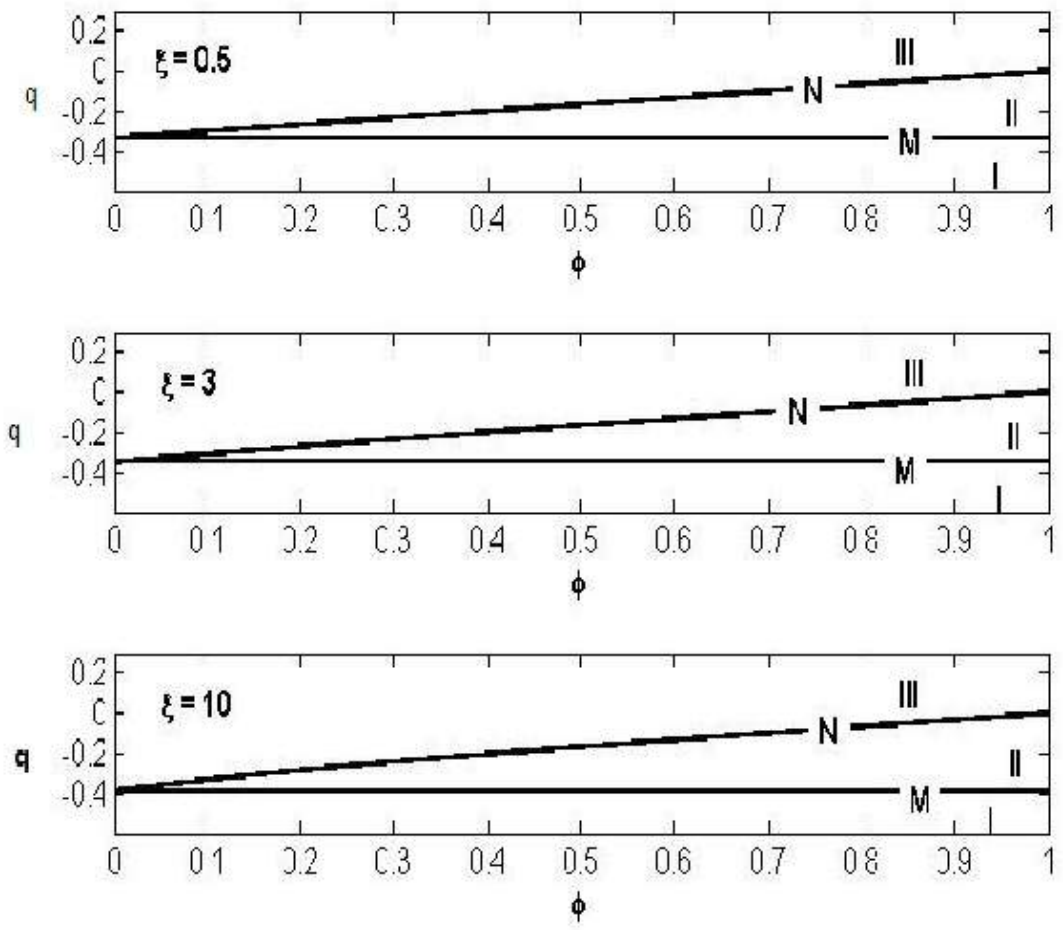

Fig. 5.6: Global bifurcation for the variation of ξ with Region I : Backward flow region, Region II : Trapping region, Region III : Augmented flow region.

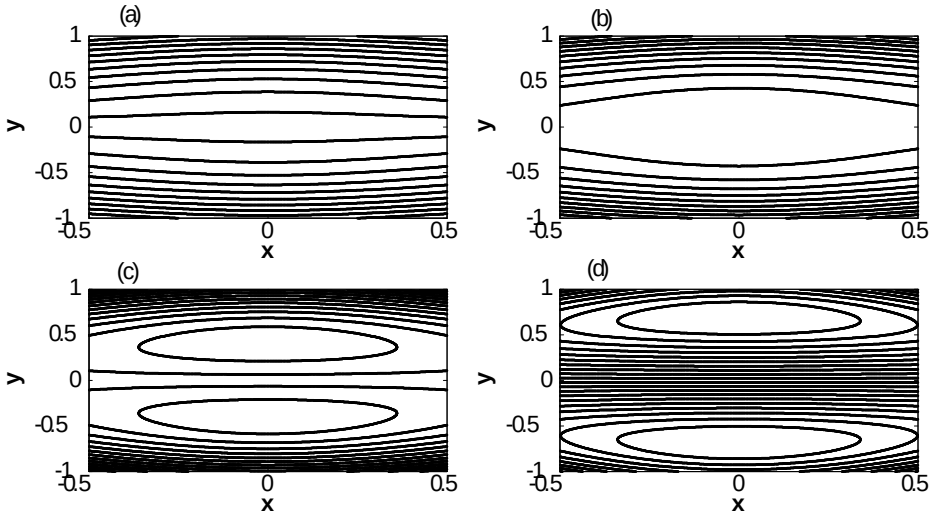

Fig. 5.7: Streamlines for different regions corresponding to $\phi = 0.6$ and $\xi = 4$ with different values of q; region I: backward flow, region II: trapping region, III: augmented flow, $(a)\ q = 0.55, (b)\ q = 0.66, (c)\ q = 0.8, (d)\ q = 1.3$.

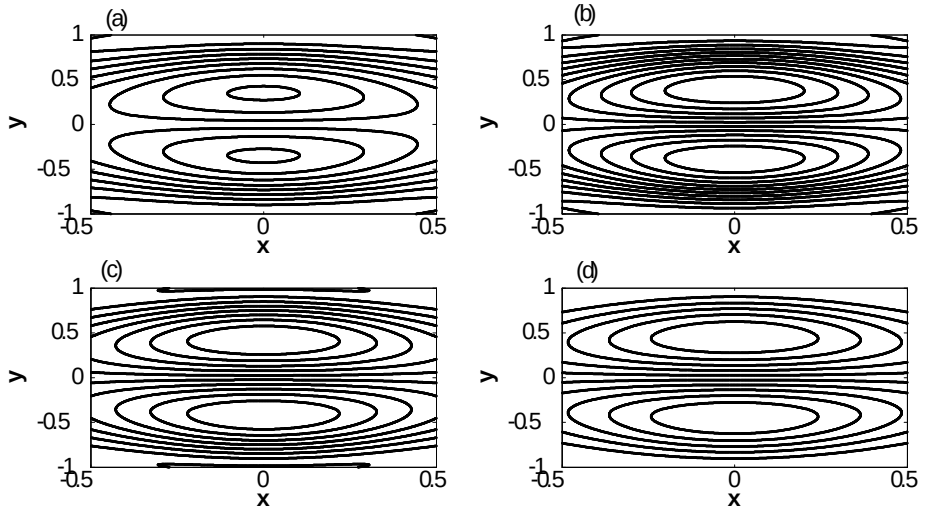

Fig. 5.8: Streamlines for verification of the occurrence of circulation corresponding to $\phi = 0.6$ and $\xi = 615$ with $(a)\ q = -0.55, (b)\ q = 0, (c)\ q = 0.4, (d)\ q = 0.9$.

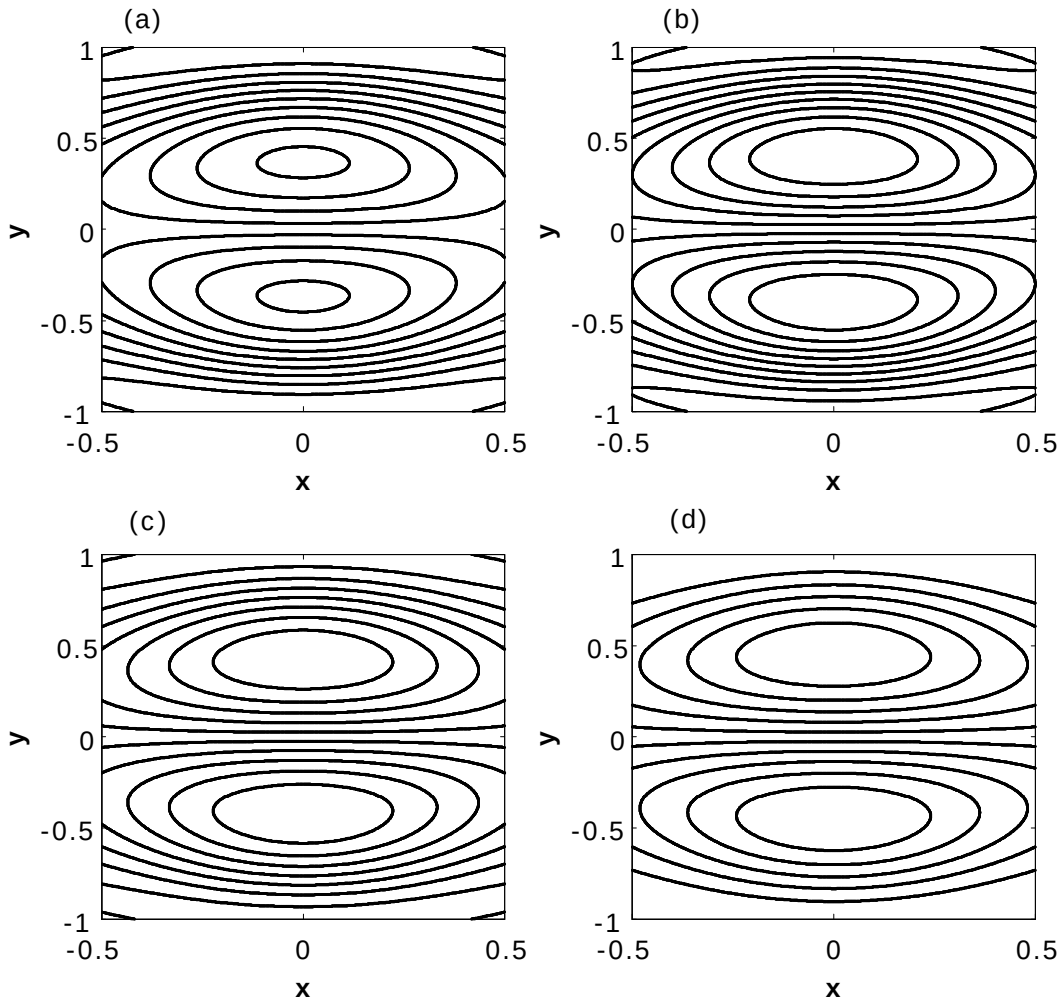

Fig. 5.9: Streamlines for verification of the occurrence of circulation corresponding to $\phi = 0.6$ and $\xi = 750$ with (a) $q = -0.55, (b)$ $q = 0, (c)$ $q = 0.4, (d)$ $q = 0.9$.

5.5 Concluding remarks

We have performed the analysis for mixed convective peristaltic flow of viscous fluid in the presence of heat transfer to discuss the streamline topologies and all possible bifurcations. The flow is considered in a two dimensional channel therefore the possible nature of critical points were either saddle or center. The region where vortices occur shrinks by increasing ξ

(i.e. Grashof number or constant (Gr_t) source (β)) in the vertical direction whereas the region of eddying motion expands along longitudinal direction by increasing ξ. The trapping region expands by increasing either Gr_t or β. The backward flow region shrinks while augmented flow region remains conserved by increasing either Gr_t or β. Transition between the backward flow to trapping and trapping to the augmented flow regions corresponds to bifurcations of co-dimension two and three respectively.

Chapter 6

Analysis of mixed convective heat and mass transfer on peristaltic flow of FENE-P fluid with chemical reaction

This study presents the influence of heat and mass transfer on peristaltic transport of Finitely Extensible Nonlinear Elastic Peterlin (FENE-P) fluid in the presence of chemical reaction. This chapter is basically the extension of chapter 3. It is assumed that all the fluid properties, except the density are constant. The Boussinesq approximation which relates density change to temperature and concentration changes is used in formulating buoyancy force terms in the momentum equation. Moreover, we neglect viscous dissipation and include diffusion-thermal (Dufour) and thermal-diffusion (Soret) effects in the present analysis. By the consideration of such important aspects the flow equations become highly nonlinear and coupled. In order to make the problem tractable we have adopted widely used assumptions of long wave length and low Reynolds number. An exact solution of the simplified coupled linear equations for the temperature and concentration has been obtained whereas numerical solution is obtained for dimensionless stream function and pressure gradient. The effects of different parameters on velocity field, temperature and concentration fields and trapping phenomenon are highlighted

through various graphs. Numerical integration has been performed to analyze pressure rise per wavelength. The contents of this chapter are published in the Journal of Mechanics (2015) 1−10.

6.1 Formulation of the Problem

We consider the peristaltic transport of an incompressible viscoelastic fluid in a two-dimensional symmetric channel of width $2a_1$. The flow geometry is similar to that given in previous chapter. However, the walls of the channel here are maintained at different temperature. Moreover, the concentration of species at both the walls is also assumed to be different.

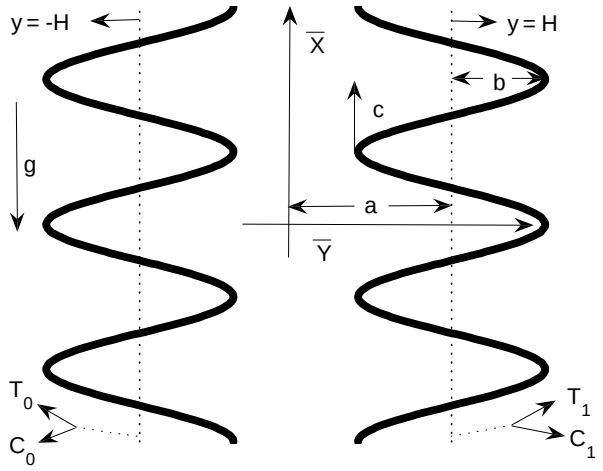

Fig. 6.1: Geometry of the Problem

The flow is governed by the four coupled non-linear partial differential equations namely; continuity (2.13), momentum, energy and mass diffusion equations which in the frame $(\overline{X}, \overline{Y})$ are expressed by

$$\rho\left(\frac{\partial}{\partial \overline{t}}+\overline{U}\frac{\partial}{\partial \overline{X}}+\overline{V}\frac{\partial}{\partial \overline{Y}}\right)\overline{U} = -\frac{\partial \overline{P}}{\partial \overline{X}}+\frac{\partial}{\partial \overline{X}}\overline{\tau}_{\overline{XX}}+\frac{\partial}{\partial \overline{Y}}\overline{\tau}_{\overline{XY}}+\rho g\alpha_1\left(T-T_0\right) + \rho g\alpha_2\left(C-C_0\right), \tag{6.1}$$

$$\rho\left(\frac{\partial}{\partial \overline{t}}+\overline{U}\frac{\partial}{\partial \overline{X}}+\overline{V}\frac{\partial}{\partial \overline{Y}}\right)\overline{V} = -\frac{\partial \overline{P}}{\partial \overline{Y}}+\frac{\partial}{\partial \overline{X}}\overline{\tau}_{\overline{YX}}+\frac{\partial}{\partial \overline{Y}}\overline{\tau}_{\overline{YY}}, \tag{6.2}$$

$$\rho C_p\left(\frac{\partial}{\partial \overline{t}}+\overline{U}\frac{\partial}{\partial \overline{X}}+\overline{V}\frac{\partial}{\partial \overline{Y}}\right)T = k\left(\frac{\partial^2 T}{\partial \overline{X}^2}+\frac{\partial^2 T}{\partial \overline{Y}^2}\right)+\frac{\rho D^* k_T}{c_s}\left(\frac{\partial^2 C}{\partial \overline{X}^2}+\frac{\partial^2 C}{\partial \overline{Y}^2}\right), \quad (6.3)$$

$$\rho\left(\frac{\partial}{\partial \overline{t}}+\overline{U}\frac{\partial}{\partial \overline{X}}+\overline{V}\frac{\partial}{\partial \overline{Y}}\right)C = \rho D^*\left(\frac{\partial^2 C}{\partial \overline{X}^2}+\frac{\partial^2 C}{\partial \overline{Y}^2}\right)+\frac{\rho D^* k_T}{(T_1-T_0)}\left(\frac{\partial^2 T}{\partial \overline{X}^2}+\frac{\partial^2 T}{\partial \overline{Y}^2}\right) - \rho k_2(C-C_0), \quad (6.4)$$

in which g is the acceleration due to gravity, α_1 and α_2 are the coefficients of thermal and concentration expansion respectively, T the temperature, C the concentration, T_0 and C_0 are the temperature and concentration at lower wall, D^* the coefficient of mass diffusivity, k_T is the thermal diffusion ratio, c_s is the concentration susceptibility and k_2 is the chemical reaction parameter. Now we use the same transformations (2.13) and dimensionless variables (2.24) as considered in previous chapters in Eqs. $(6.1)-(6.4)$ to get

$$\mathrm{Re}\,\delta\left(u\frac{\partial}{\partial x}+v\frac{\partial}{\partial y}\right)u = -\frac{\partial p}{\partial x}+\delta\frac{\partial}{\partial x}\tau_{xx}+\frac{\partial}{\partial y}\tau_{xy}+Gr_t\theta^*+Gr_c\phi^*, \quad (6.5)$$

$$\mathrm{Re}\,\delta^3\left(u\frac{\partial}{\partial x}+v\frac{\partial}{\partial y}\right)v = -\frac{\partial p}{\partial y}+\delta^2\frac{\partial}{\partial x}\tau_{yx}+\delta\frac{\partial}{\partial y}\tau_{yy}, \quad (6.6)$$

$$\mathrm{Re}\,\delta\left(u\frac{\partial}{\partial x}+v\frac{\partial}{\partial y}\right)\theta^* = \frac{1}{\mathrm{Pr}}\left(\delta^2\frac{\partial^2\theta^*}{\partial x^2}+\frac{\partial^2\theta^*}{\partial y^2}\right)+D_f\left(\delta^2\frac{\partial^2\phi^*}{\partial x^2}+\frac{\partial^2\phi^*}{\partial y^2}\right), \quad (6.7)$$

$$\mathrm{Re}\,\delta\left(u\frac{\partial}{\partial x}+v\frac{\partial}{\partial y}\right)\phi^* = \frac{1}{S_c}\left(\delta^2\frac{\partial^2\phi^*}{\partial x^2}+\frac{\partial^2\phi^*}{\partial y^2}\right)+S_r\left(\delta^2\frac{\partial^2\theta^*}{\partial x^2}+\frac{\partial^2\theta^*}{\partial y^2}\right)-\gamma\phi^*. \quad (6.8)$$

The dimensionless numbers, Gr_t and Gr_c (local Grashof numbers for temperature and concentration), Pr (Prandtl number), D_f (Dufour number), S_c (Schmidt number), S_r (Soret number) and γ the chemical reaction parameter for the present flow situation are given by

$$Gr_t = \frac{\rho g\alpha_1 a_1^2(T_1-T_0)}{\eta_p c},\ Gr_c=\frac{\rho g\alpha_2 a_1^2(C_1-C_0)}{\eta_p c},\ D_f=\frac{\rho D^* k_T(C_1-C_0)}{c_s C_p(T_1-T_0)\eta_p},\ \theta^*=\frac{T-T_0}{T_1-T_0},$$
$$S_c = \frac{\eta_p}{\rho D^*},\ S_r=\frac{\rho D^* k_T}{(C_1-C_0)\eta_p},\ \gamma=\frac{\rho k_1 a_1^2}{\eta_p},\quad \mathrm{Pr}=\frac{C_p\eta_p}{k},\ \phi^*=\frac{C-C_0}{C_1-C_0}. \quad (6.9)$$

Our objective is to extend the results of chapter 3 by carrying out heat and mass transfer analysis. Therefore, the constitutive equation for extra stress will remain the same and hence the components of extra stress in Eqs. (6.5) and (6.6) are given through Eqs. $(3.20)-(3.23)$.

Employing long wavelength and low Reynolds number assumption Eqs. (6.5) and (6.8) become

$$0 = -\frac{\partial p}{\partial x} + \frac{\partial}{\partial y}\tau_{xy} + Gr_t\theta^* + Gr_c\phi^*, \tag{6.10}$$

$$0 = -\frac{\partial p}{\partial y}, \tag{6.11}$$

$$0 = \frac{1}{\mathrm{Pr}}\left(\frac{\partial^2\theta^*}{\partial y^2}\right) + D_f\left(\frac{\partial^2\phi^*}{\partial y^2}\right), \tag{6.12}$$

$$0 = \frac{1}{S_c}\left(\frac{\partial^2\phi^*}{\partial y^2}\right) + S_r\left(\frac{\partial^2\theta^*}{\partial y^2}\right) - \gamma\phi^*. \tag{6.13}$$

The dimensionless volume flow rate and boundary conditions in the wave frame are taken by following [38]

$$\psi = \frac{q}{2}, \quad \frac{\partial\psi}{\partial y} = -1, \quad \theta^* = 1, \quad \phi^* = 1, \quad at \;\; y = h, \tag{6.14}$$

$$\psi = -\frac{q}{2}, \quad \frac{\partial\psi}{\partial y} = -1, \quad \theta^* = 0, \quad \phi^* = 0, \quad at \; y = -h, \tag{6.15}$$

$$\theta - 2 = q = \int_{-h}^{h}\frac{\partial\psi}{\partial y}dy = \psi(h) - \psi(-h). \tag{6.16}$$

It is remarked here that due to non-symmetric nature of temperature and concentration fields it is necessary to solve the flow problem in domain $y \in [-h, h]$. On solving Eqs. (6.12) and (6.13) with the boundary conditions given in Eqs. (6.14) and (6.15), we obtain the following expressions of dimensionless temperature and concentration fields

$$\theta^* = -\mathrm{Pr}\, D_f\phi^* + \left(\frac{1 + \mathrm{Pr}\, D_f}{2}\right)\left(\frac{y}{h} + 1\right), \tag{6.17}$$

$$\phi^* = \frac{\sinh\left(\sqrt{\alpha}\,(y + h)\right)}{\sinh\left(2\sqrt{\alpha}h\right)}. \tag{6.18}$$

Using the above expressions for θ^* and ϕ^* in Eq. (6.10) and then integrating the resulting equation, we get

$$\tau_{xy} = A_3 + p_x y + A_4\cosh\left(\sqrt{\alpha}\,(h + y)\right) + A_5\left(\frac{y^2}{2h} + y\right) \tag{6.19}$$

where

$$\alpha = \gamma \diagup (1 - \Pr D_f S_c S_r), \quad A_4 = (Gr_t \Pr D_f - Gr_c) / \sqrt{\alpha_1}, \quad A_5 = -\frac{1}{2} Gr_t (1 + \Pr D_f),$$

From Eq. (3.25) the expression for transverse component of velocity gradient is

$$\frac{\partial u}{\partial y} = \frac{\tau_{xy}}{a} \left(1 + \frac{3a + (2De^2/a) (\tau_{xy})^2}{L^2} \right). \tag{6.20}$$

Invoking the definition of stream function, we can write

$$\frac{\partial^2 \psi}{\partial y^2} = \frac{\partial u}{\partial y} = \tau_{xy} \left(1 + A_6 (\tau_{xy})^2 \right),$$

where $A_6 = 2De^2/a^2L^2$. Now integrating Eq. (6.20), we get

$$\frac{\partial \psi}{\partial y} = \int_{-h}^{y} \tau_{xy} (\varphi) \, d\varphi + A_6 \int_{-h}^{y} \tau_{xy}^3 (\varphi) \, d\varphi + A_1. \tag{6.21}$$

Another integration yields

$$\psi = \int_{-h}^{y} \int_{-h}^{\varphi} \tau_{xy} (\eta) \, d\eta d\varphi + A_6 \int_{-h}^{y} \int_{-h}^{\varphi} \tau_{xy}^3 (\eta) \, d\eta d\varphi + A_1 y + A_2. \tag{6.22}$$

A further simplification gives

$$\psi = \int_{-h}^{y} (y - \varphi) \, \tau_{xy} (\varphi) \, d\varphi + A_6 \int_{-h}^{y} (y - \varphi) \, \tau_{xy}^3 (\varphi) \, d\varphi + A_1 y + A_2 \tag{6.23}$$

where A_1 and A_2 are contents of integrations. The utilization of boundary conditions (6.14) and (6.15) gives $A_1 = -1$ and $A_2 = -\frac{q}{2} - h$. Inserting the values of A_1 and A_2 in (6.23) and making use of remaining two boundary conditions, we get

$$\int_{-h}^{h} (h - \varphi) \, \tau_{xy} (\varphi) \, d\varphi + A_6 \int_{-h}^{h} (h - \varphi) \, \tau_{xy}^3 (\varphi) \, d\varphi - 2h - q = 0, \tag{6.24}$$

$$\int_{-h}^{h} \tau_{xy}(\varphi)\, d\varphi + A_6 \int_{-h}^{h} \tau_{xy}^3(\varphi)\, d\varphi = 0 \tag{6.25}$$

Eqs. (6.24) and (6.25) are nonlinear algebraic equations which can be solved numerically for a given set of parameter at each cross-section x to get the values of A_3 and p_x by using any computational software like Mathematica. Once A_3 and p_x are known, ψ is given by

$$\psi = \int_{-h}^{y} (y-\varphi)\, \tau_{xy}(\varphi)\, d\xi + A_6 \int_{-h}^{y} (y-\varphi)\, \tau_{xy}^3(\varphi)\, d\varphi - y - \frac{q}{2} - h. \tag{6.26}$$

The pressure rise per wavelength (ΔP_λ) is defined through the following integrals given via Eq. (2.51).

6.2 Results and Discussion

This section provides the discussion of the effects of different parameters such as Pr (Prandtl number), S_r (Soret number), D_f (Dufour number), S_c (Schmidt number), Gr_t (local Grashof number), Gr_c (Grashof number for concentration) and γ (chemical reaction parameter) on velocity profile, pressure rise per wavelength, temperature profile, concentration profile, and trapping phenomenon.

The effects of above mentioned parameters on longitudinal velocity at a cross-section $x = 0$ are in Fig. 6.2. The value of flow rate in Fig. 6.2 is kept fixed i.e. $q = -0.6$. As an implication, the velocity at this cross-section adjust itself i.e. it may increase or decrease in lower or upper half of the channel by increasing a particular parameter to maintain the same flux. Interestingly, the axial velocity profiles are not symmetric about the centerline $y = 0$.

In general the shape of streamlines is similar to that of the boundary wall in the wave frame. However, some of the streamlines split and enclose an amount of fluid called *bolus* which is pushed ahead along with the wave speed. This phenomenon of enclosing the *bolus* is called trapping phenomenon.

The effects of above mentioned parameters on velocity profile are depicted in Fig. 6.2. We observe that parameters Pr, D_f, Gr_t and Gr_c leave the same effects on the velocity profile in such a way that it decreases near the lower wall of the channel whereas its behavior reverses

near the upper wall of the channel. Previous studies on peristalsis report that asymmetric velocity profiles in a straight channel result due to asymmetric waves propagating along the channel wall. By asymmetric waves we mean that waves which are out of phase or have different amplitudes. However, in this case the asymmetry in velocity profiles is not due to nature of the waves propagating at wall, rather it is due to coupling between momentum, energy and concentration equations. A close examination of Eqs. $(6.24) - (6.27)$ reveals that a strong coupling between energy and momentum equations is expected for higher values of Grashof number for temperature. Similarly higher values of Grashof number for concentration may result in a strong coupling between momentum and concentration equations. Graphical results presented in Fig. 6.2 indicate that velocity profile is not symmetric about the centerline of channel for non-zero values of Gr_t and Gr_c. In addition to that a flow reversal in lower half of the channel is observed for non-zero large values of Grashof numbers for temperature and concentration. It is observed that flow reversal increases by increasing Prandtl number, Grashof numbers and Dufour number while it decreases by increasing Schmidt number, Soret number and chemical reaction parameter.

In Fig. 6.3 the profiles of pressure rise per wavelength ΔP_λ are shown for various values of the parameters of interest. The complicated integral appearing in Eq. (6.40) is evaluated numerically using MATHEMATICA. Each panel in Fig. 6.3 can be divided into two sub-regions: (I) peristaltic pumping region that corresponds to $\Delta P_\lambda > 0$ and $q > 0$ and (II) augmented pumping region which corresponds to $\Delta P_\lambda < 0$ and $q > 0$. It is observed that ΔP_λ in peristaltic pumping region increases by increasing Prandtl number, Grashof numbers (Gr_t and Gr_c) and Dufour number. However, it decreases by increasing chemical reaction parameter, Schmidt number and Soret number. The increase in ΔP_λ in peristaltic pumping region by increasing Pr, Gr_t, Gr_c and D_f may be due to increased flow reversal caused by increasing these parameters. Similarly a decrease in flow reversal by increasing S_r, S_c and γ results in decrease of ΔP_λ in peristaltic pumping region by increasing these parameters. A reduction in pressure rise per wavelength by increasing the rheological properties of fluid is already reported in the literature. However, the above results suggest another possible way to reduce the pressure rise per wavelength in addition to the already available remedy i.e. by altering the rheological properties of the fluid. Thus heat transfer characteristics may also be

exploited to our use to reduce the pressure rise per wavelength in the peristaltic pumping region without altering the rheological features of the fluid. Another interesting observation from Fig. 6.3 is the expansion of peristaltic pumping region i.e. ΔP_λ is positive over a quite large range of F. Thus the prescribed flow rate F must be large for the pressure to assist the flow. In almost all cases considered in Fig. 6.3 the prescribed flow rate F must be greater than 3 for ΔP_λ to be negative. The expansion of peristaltic pumping region may be due to the choice of larger values for Gr_t and Gr_c. However, it can be reduced by altering the rheological properties of the fluid i.e. by altering the parameter De and L^2. In fact the larger values of De results in contraction of peristaltic pumping region.

The effects of Prandtl number, Dufour number, Schmidt number, Soret number and chemical reaction parameter on temperature and concentration field are shown through Figs. 6.4 and 6.5. It is evident from Fig. 6.4 that temperature inside the channel increases by increasing all the above mentioned parameters. On contrary the concentration profiles follow a reverse trend by increasing either of these parameters. This is perhaps inherited property of solutions of temperature and concentration fields. In fact the following relation holds for temperature and concentration fields

$$\theta^* = -\operatorname{Pr} D_f \phi^* + \left(\frac{1+\operatorname{Pr} D_f}{2}\right)\left(\frac{y}{h}+1\right).$$

Now the profiles of ϕ^* (Fig. 6.5) show that it is positive but a decreasing function of each of the parameters Pr, D_f, S_r, Sc and γ. This implies its derivative with respect to either of these parameter is always negative and hence strictly less then the value of ϕ^* itself. Now let us differentiate above equation with respect to Pr i.e.

$$\frac{\partial \theta^*}{\partial \operatorname{Pr}} = -D_f \phi^* - \operatorname{Pr} D_f \frac{\partial \phi^*}{\partial \operatorname{Pr}} + \frac{D_f}{2}\left(\frac{y}{h}+1\right)$$

The second term of above expression is positive and greater than the first term. Similarly third term is also positive. Therefore $\partial\theta^*/\partial \operatorname{Pr} > 0$ for all values of Pr . This illustrates that temperature is an increasing function of Pr . The above argument also holds for other parameters. In this way the behavior of temperature field for increasing values of each of the parameters Pr, D_f, S_r, Sc and γ is opposite to the behavior of concentration field for these parameters.

In general it is expected that in the wave frame behavior of streamlines is similar to that of boundary wall. However, under specific conditions some of the streamlines split and enclose a bolus of fluid which moves as a whole with the wave speed. This phenomenon is known as trapping. It has been reported in various available studies on peristaltic transport that trapping is largely dependent on the magnitude of flow rate [21]. In fact one can find the values of flow rate for which trapping occurs near the boundary, centerline or nowhere. In the present study, we have chosen a specific value of flow rate for which circulating region emerges in the center of the channel. It has been observed through Figs. 6.6 and 6.7 that for small values of Grashof numbers (Gr_t and Gr_c), the trapped bolus of fluid is almost asymmetric about centerline. However the bolus becomes asymmetric by increasing the values of Gr_t or Gr_c. In such case the size of the bolus in lower half of the channel increases while it decreases in upper half of the channel. A further reduction in the size of bolus in upper half of the channel is observed for larger values of Gr_t and Gr_c. These results may be justified with similar reasons as given for velocity profiles. In fact asymmetry is due to strong coupling between energy, momentum and concentration equations. For smaller values of Grashof numbers the coupling effects are weak and in that case the bolus of fluid is symmetric about the centerline. The streamline patterns by increasing the values of other parameters such as Pr, D_f, S_r, S_c and γ are not shown here because these parameters do not affect the streamlines pattern to an appreciable extent. This is perhaps due to implicit dependence of stream function on these parameters.

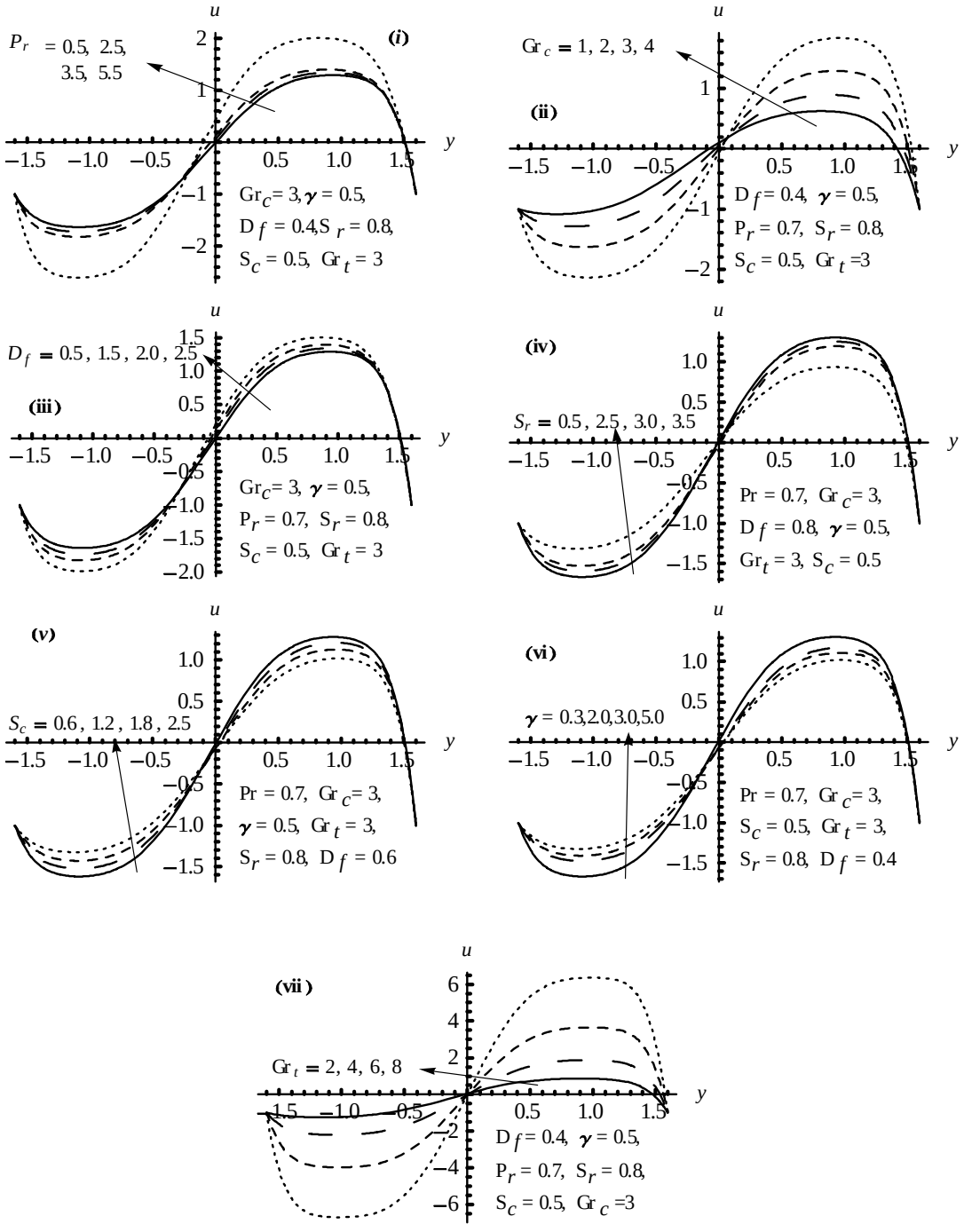

*Fig.*6.2: Velocity profile with $L = 3.5, \phi = 0.6, \theta = 0.7, De = 5$.

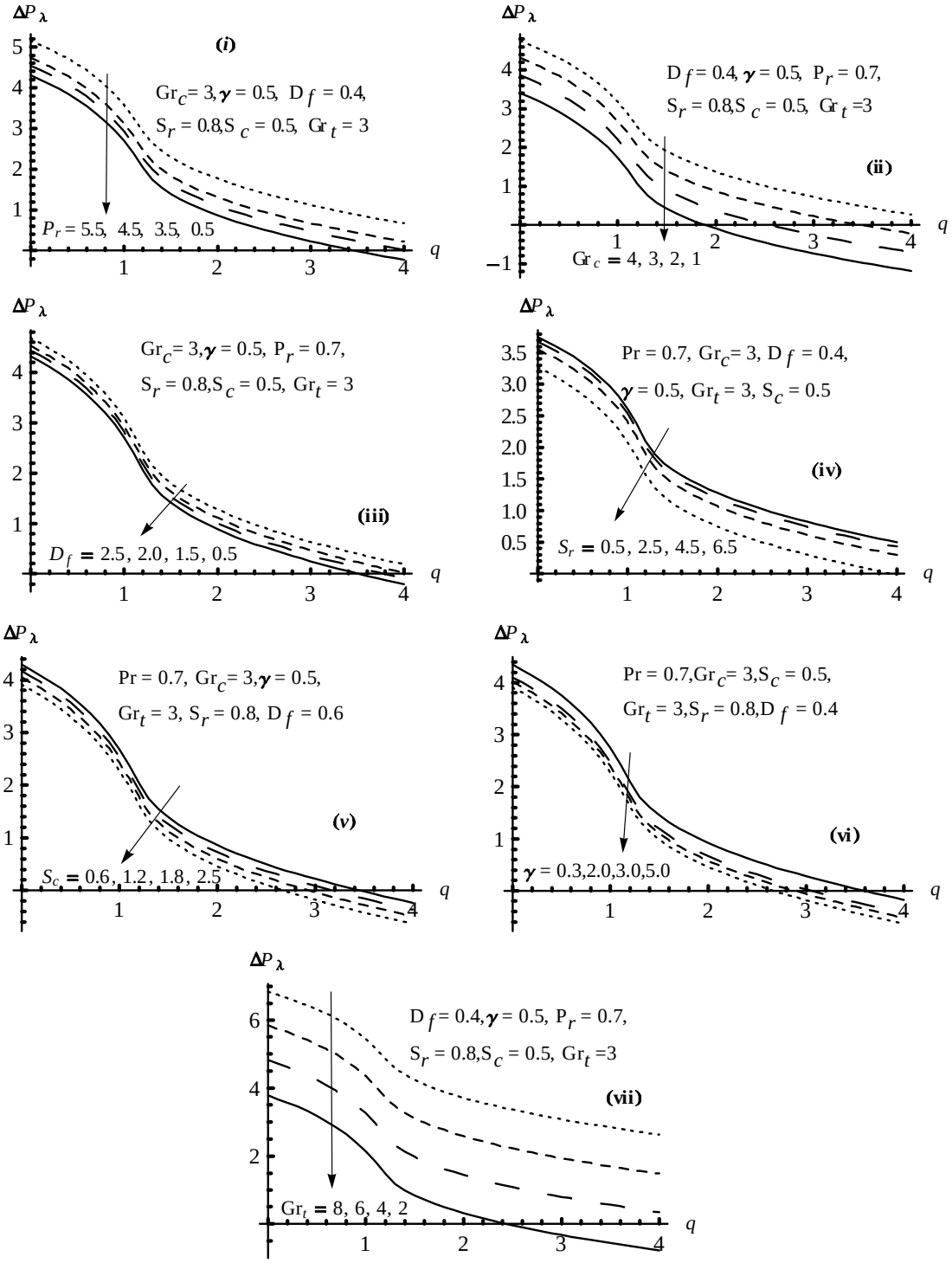

*Fig.*6.3: Pressure rise per wavelength versus flow rate q with $L = 3.5, De = 5, \phi = 0.6$.

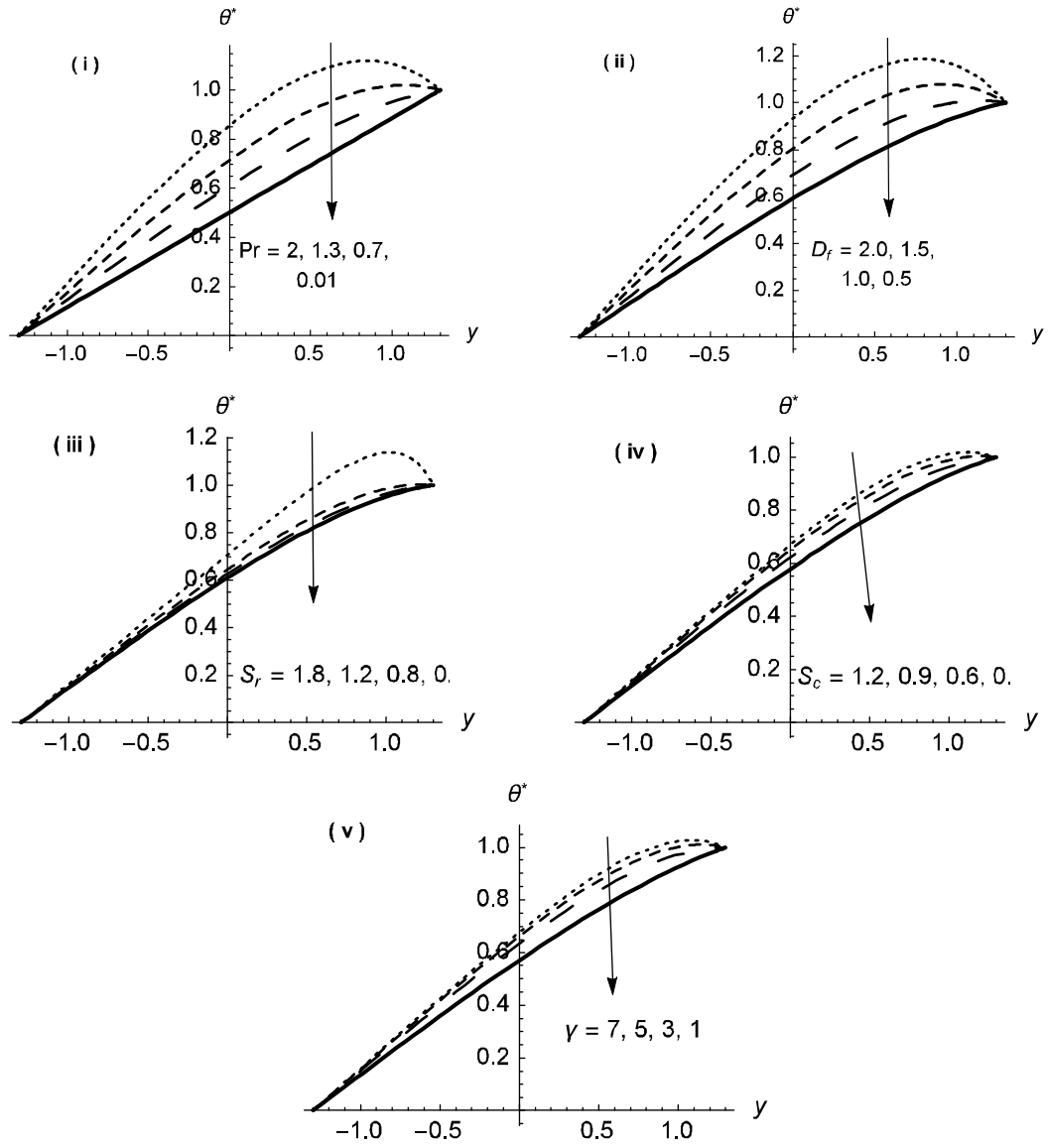

Fig.6.4: Temperature Profile for $\phi = 0.6, x = 1/6$ and (i) $D_f = 0.6, S_r = 0.5, S_c = 0.5, \gamma = 2$, (ii) $\mathrm{Pr} = 0.7, S_r = 0.5, S_c = 0.5, \gamma = 2$ (iii) $\mathrm{Pr} = 0.7, D_f = 0.6, S_c = 0.5, \gamma = 2$, (iv) $\mathrm{Pr} = 0.7, D_f = 0.6, S_r = 0.5, \gamma = 2$, (v) $\mathrm{Pr} = 0.7, D_f = 0.6, S_r = 0.5, S_c = 0.5$.

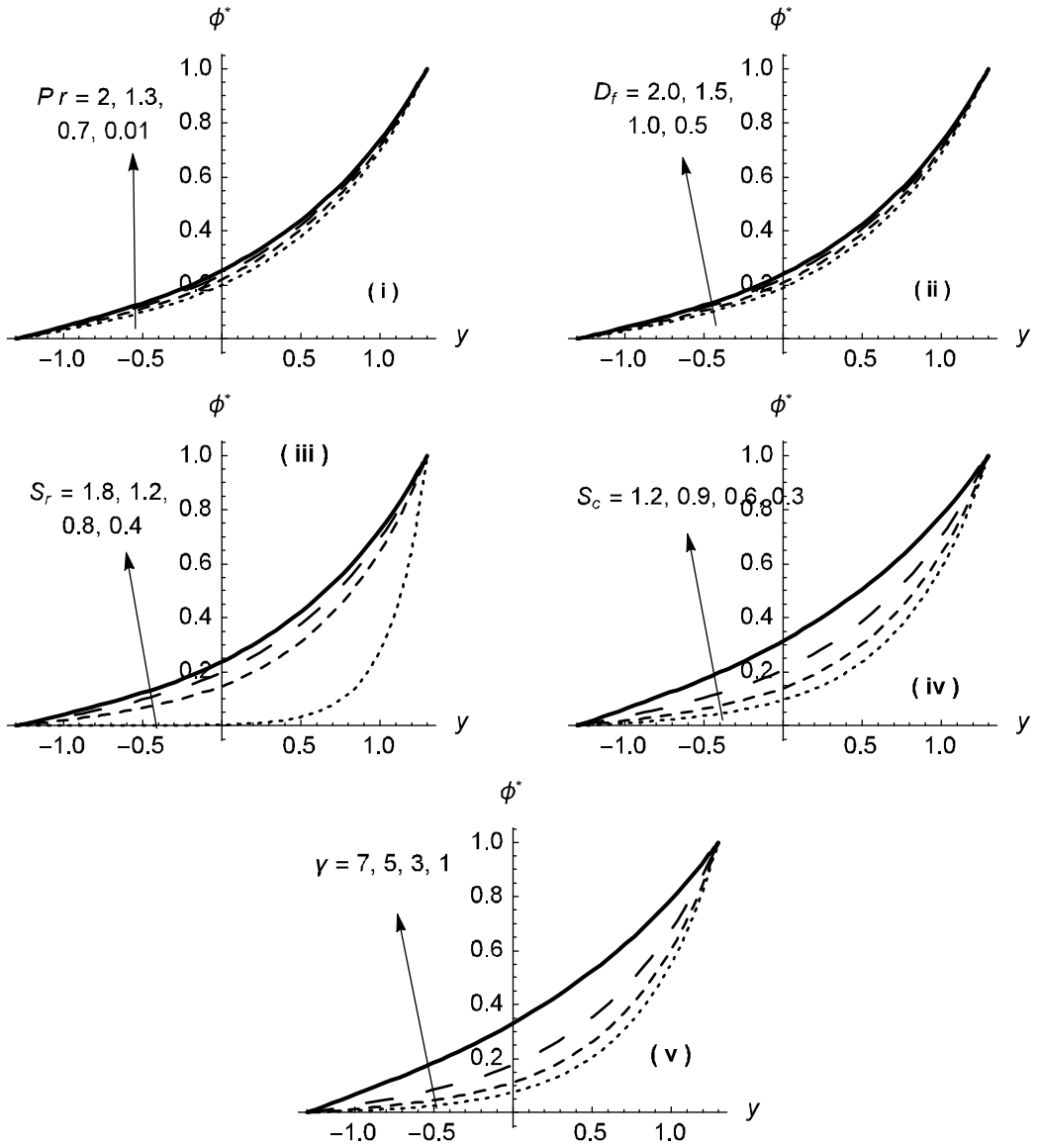

*Fig.*6.5: Concentration Profile for $\phi = 0.6, x = 1/6$ and (i) $D_f = 0.6, S_r = 0.5, S_c = 0.5, \gamma = 2$, (ii) $\mathrm{Pr} = 0.7, S_r = 0.5, S_c = 0.5, \gamma = 2$, (iii) $\mathrm{Pr} = 0.7, D_f = 0.6, S_c = 0.5, \gamma = 2$, (iv) $\mathrm{Pr} = 0.7, D_f = 0.6, S_r = 0.5, \gamma = 2$, (v) $\mathrm{Pr} = 0.7, D_f = 0.6, S_r = 0.5, S_c = 0.5$.

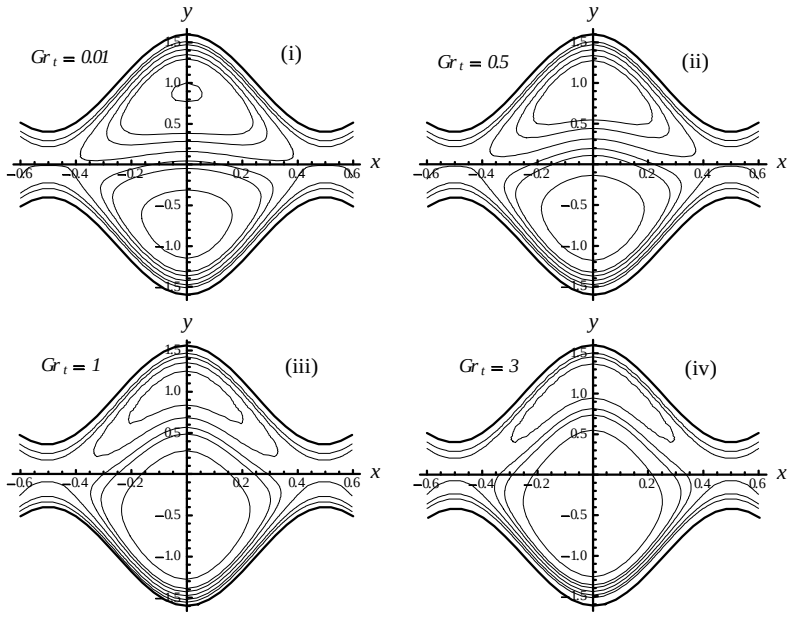

Fig. 6.6: Streamlines for the variation in Gr_t with $\theta = 1.7$, $\phi = 0.6$, $D_e = 1$, $S_r = 0.5$, $S_c = 0.5$, $D_f = 0.5$, $\gamma = 0.1$, $Gr_c = 0.5$, Pr $= 0.5$.

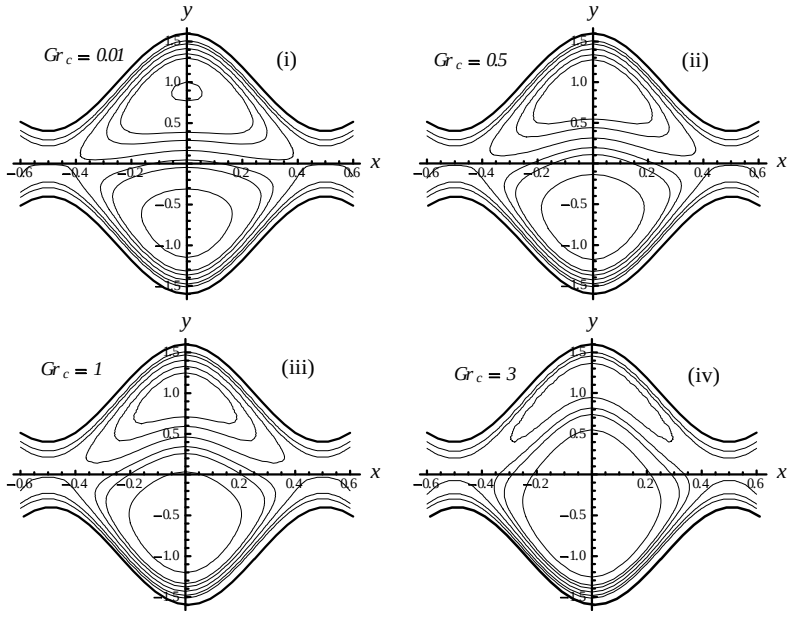

Fig. 6.7: Streamlines for the variation in Gr_c with $\theta = 1.7$, $\phi = 0.6$, $D_e = 1$, $S_r = 0.5$, $S_c = 0.5$, $D_f = 0.5$, Pr $= 0.5$, $Gr_t = 0.5$, $\gamma = 0.1$.

6.3 Concluding remarks

Peristaltic flow of a FENE-P fluid is analyzed in presence of chemically reactive species in a channel whose walls are maintained at different temperatures. The coupling between momentum, energy and concentration equations is achieved by using Boussinesq approximation. The equations governing the flow are modeled under long wavelength and low Reynolds number assumptions. Closed form solutions are reported for temperature and concentration fields. However, stream function and pressure gradient are evaluated numerically. The striking observations of the present analysis are: the existence of non-symmetric velocity profiles and asymmetric shape of circulating bolus of fluid for non-zero values of Grashof numbers for temperature and concentration. The buoyancy effects induced by non-zero values of Grashof numbers are also responsible for increase in pressure rise per wavelength in the peristaltic pumping region. It is further observed that an increase in either of the parameters Pr, D_f, S_r, S_c and γ increases the temperature inside the channel. On contrary the concentration field is found to follow an opposite trend.

Chapter 7

Mixed convective heat transfer analysis for the peristaltic transport of viscoplastic fluid

This chapter present the analysis of mixed convective peristaltic flow of incompressible viscoplastic fluid in a two-dimensional symmetric channel. The rheology of viscoplastic fluid is characterized by the constitutive equation for Bingham plastic model. The coupling between momentum and energy equations is done through Boussinesq approximation. The coupled nonlinear partial differential equations are transformed in wave frame using Galilean transformation and then simplified under realistic assumptions of long wavelength and low Reynolds number. Approximate solution is obtained using regular perturbation method which is restricted for the smaller values of Grashof and Bingham numbers. The validity of approximate solution is established by comparing it with the numerical solution obtained via Matlab built-in routine bvp4c. Based on the numerical solution an extensive analysis is performed in order to analyze the effects of various parameters of interest on flow characteristics, pumping and trapping phenomena. It is found that velocity decreases at the center by increasing Bingham number showing a boundary layer character for large values. However, it increases by increasing Brinkman and Grashof numbers. Moreover, pressure rise per wavelength increases with Bingham number, Brinkman number and Grashof number, in the pumping region. The trapping phenomenon is

also discussed in detail. The contents of this chapter are submitted for possible publication in International Journal of Heat and Mass Transfer.

7.1 Formulation of the Problem

We consider the peristaltic transport of an incompressible viscoplastic fluid in a two-dimensional symmetric channel of width $2a_1$. The flow is generated by continuously moving sinusoidal waves of speed c along the walls of the channel. The geometry of the problem is similar to that considered in chapter 5. In contrast to previous chapter, here the channel walls are maintained at same temperature T_0. The equations governing the flow and heat transfer in the peristaltic channel in the fixed frame $\left(\overline{X}, \overline{Y}\right)$ are

$$\rho\left(\frac{\partial}{\partial\overline{t}}+\overline{U}\frac{\partial}{\partial\overline{X}}+\overline{V}\frac{\partial}{\partial\overline{Y}}\right)\overline{U} = -\frac{\partial\overline{P}}{\partial\overline{X}}+\frac{\partial}{\partial\overline{X}}\overline{\tau}_{\overline{XX}}+\frac{\partial}{\partial\overline{Y}}\overline{\tau}_{\overline{XY}}+\rho g\alpha_1\left(T-T_0\right), \quad (7.1)$$

$$\rho\left(\frac{\partial}{\partial\overline{t}}+\overline{U}\frac{\partial}{\partial\overline{X}}+\overline{V}\frac{\partial}{\partial\overline{Y}}\right)\overline{V} = -\frac{\partial\overline{P}}{\partial\overline{Y}}+\frac{\partial}{\partial\overline{X}}\overline{\tau}_{\overline{YX}}+\frac{\partial}{\partial Y}\overline{\tau}_{\overline{YY}}, \quad (7.2)$$

$$\rho C_p\left(\frac{\partial}{\partial\overline{t}}+\overline{U}\frac{\partial}{\partial\overline{X}}+\overline{V}\frac{\partial}{\partial\overline{Y}}\right)T = k\left(\frac{\partial^2 T}{\partial\overline{X}^2}+\frac{\partial^2 T}{\partial\overline{Y}^2}\right)+\mathbf{T}\cdot(\boldsymbol{\nabla}\overline{\mathbf{V}}). \quad (7.3)$$

where

$$\overline{\boldsymbol{\tau}} = 2\eta\mathbf{D}+2\tau_0\hat{\mathbf{D}} \quad (7.4)$$

and the term $\mathbf{T}\cdot(\boldsymbol{\nabla}\overline{\mathbf{V}})$ is the well known viscous dissipation term. The definition of dot product of arbitrary tensors $\mathbf{A}_1$ and $\mathbf{B}_1$, i.e., $\mathbf{A}\cdot\mathbf{B} = tra(\mathbf{AB})$ enables us to write energy equation (7.3) as

$$\rho C_p\left(\frac{\partial}{\partial\overline{t}}+\overline{U}\frac{\partial}{\partial\overline{X}}+\overline{V}\frac{\partial}{\partial\overline{Y}}\right)T = k\left(\frac{\partial^2 T}{\partial\overline{X}^2}+\frac{\partial^2 T}{\partial\overline{Y}^2}\right)+\overline{\tau}_{\overline{XX}}\left(\frac{\partial\overline{U}}{\partial\overline{X}}\right)+\overline{\tau}_{\overline{XY}}\left(\frac{\partial\overline{V}}{\partial\overline{X}}\right) +\overline{\tau}_{\overline{XY}}\left(\frac{\partial\overline{U}}{\partial\overline{Y}}\right)+\overline{\tau}_{\overline{YY}}\left(\frac{\partial\overline{V}}{\partial\overline{Y}}\right). \quad (7.5)$$

In view of Eqs. (7.4) and (2.6), the components of extra stress tensor in the laboratory frame become

$$\begin{aligned}\overline{\tau}_{\overline{XX}} &= 2\eta D_{\overline{XX}} + \frac{2\tau_0 D_{\overline{XX}}}{\sqrt{\varepsilon_1 + 2tr\mathbf{D}^2}}, \quad \overline{\tau}_{\overline{XY}} = 2\eta D_{\overline{XY}} + \frac{2\tau_0 D_{\overline{XY}}}{\sqrt{\varepsilon_1 + 2tr\mathbf{D}^2}}, \\ \overline{\tau}_{\overline{YY}} &= 2\eta D_{\overline{YY}} + \frac{2\tau_0 D_{\overline{YY}}}{\sqrt{\varepsilon_1 + 2tr\mathbf{D}^2}}. \end{aligned} \tag{7.6}$$

In view of Eq. (2.18), Eq. (2.24), Eq. (2.32) and Eq. (5.8), components of momentum equation (7.1) and (7.2) and the energy equation (7.3) reduce to

$$\mathrm{Re}\,\delta\left(u\frac{\partial}{\partial x} + v\frac{\partial}{\partial y}\right)u = -\frac{\partial p}{\partial x} + \delta\frac{\partial}{\partial x}\tau_{xx} + \frac{\partial}{\partial y}\tau_{xy} + Gr_t\theta^*, \tag{7.7}$$

$$\mathrm{Re}\,\delta^3\left(u\frac{\partial}{\partial x} + v\frac{\partial}{\partial y}\right)v = -\frac{\partial p}{\partial y} + \delta^2\frac{\partial}{\partial x}\tau_{xy} + \delta\frac{\partial}{\partial y}\tau_{yy}, \tag{7.8}$$

$$\begin{aligned}\mathrm{Re}\,\delta\left(u\frac{\partial}{\partial x} + v\frac{\partial}{\partial y}\right)\theta^* &= \frac{1}{\mathrm{Pr}}\left(\delta^2\frac{\partial^2\theta^*}{\partial x^2} + \frac{\partial^2\theta^*}{\partial y^2}\right) + Ec\delta\tau_{xx}\left(\frac{\partial u}{\partial y}\right) \\ &\quad + Ec\tau_{xy}\left(\frac{\partial u}{\partial y} + \delta\frac{\partial v}{\partial x}\right) + Ec\tau_{yy}\left(\frac{\partial v}{\partial y}\right), \end{aligned} \tag{7.9}$$

The components of extra stress tensor (7.6) in non-dimensional form transform to

$$\tau_{xx} = 2\delta\frac{\partial u}{\partial x} + \frac{2\delta Bn\left(\frac{\partial u}{\partial x}\right)}{\sqrt{\varepsilon + 2\delta^2\left(\frac{\partial u}{\partial x}\right)^2 + 2\left(\frac{\partial v}{\partial y}\right)^2 + \left(\frac{\partial u}{\partial y} + \delta\frac{\partial v}{\partial x}\right)^2}}, \tag{7.10}$$

$$\tau_{xy} = \left(\frac{\partial u}{\partial y} + \delta\frac{\partial v}{\partial x}\right) + \frac{Bn\left(\frac{\partial u}{\partial y} + \delta\frac{\partial v}{\partial x}\right)}{\sqrt{\varepsilon + 2\delta^2\left(\frac{\partial u}{\partial x}\right)^2 + 2\left(\frac{\partial v}{\partial y}\right)^2 + \left(\frac{\partial u}{\partial y} + \delta\frac{\partial v}{\partial x}\right)^2}}, \tag{7.11}$$

$$\tau_{yy} = 2\frac{\partial v}{\partial y} + \frac{2Bn\left(\frac{\partial v}{\partial y}\right)}{\sqrt{\varepsilon + 2\delta^2\left(\frac{\partial u}{\partial x}\right)^2 + 2\left(\frac{\partial v}{\partial y}\right)^2 + \left(\frac{\partial u}{\partial y} + \delta\frac{\partial v}{\partial x}\right)^2}}. \tag{7.12}$$

The Eckert number Ec and the Brinkman number are defined by

$$Ec = \frac{c^2}{C_p T_0}, \quad B_r = \mathrm{Pr}\,Ec. \tag{7.13}$$

Defining the stream function (ψ) through (2.41), Eqs. (7.7) – (7.9) take the following form

$$\begin{aligned}
\mathrm{Re}\,\delta\left(\psi_y\frac{\partial}{\partial x}-\psi_x\frac{\partial}{\partial y}\right)\psi_y &= -\frac{\partial p}{\partial x}+\delta\frac{\partial}{\partial x}\tau_{xx}+\frac{\partial}{\partial y}\tau_{xy}+Gr_t\theta^*, && (7.14)\\
-\mathrm{Re}\,\delta^3\left(\psi_y\frac{\partial}{\partial x}-\psi_x\frac{\partial}{\partial y}\right)\psi_x &= -\frac{\partial p}{\partial y}+\delta^2\frac{\partial}{\partial x}\tau_{xy}+\delta\frac{\partial}{\partial y}\tau_{yy}, && (7.15)\\
\mathrm{Re}\,\delta\left(\psi_y\frac{\partial}{\partial x}-\psi_x\frac{\partial}{\partial y}\right)\theta^* &= \left(\delta^2\frac{\partial^2\theta^*}{\partial x^2}+\frac{\partial^2\theta^*}{\partial y^2}\right)+B_r\delta\tau_{xx}\psi_{yy}\\
&\quad +B_r\tau_{xy}\left(\psi_{yy}-\delta^2\psi_{xx}\right)-\delta B_r\tau_{yy}\psi_{xy} && (7.16)
\end{aligned}$$

whereas the components of extra stress tensor in terms of stream function become

$$\begin{aligned}
\tau_{xx} &= 2\delta\psi_{xy}+\frac{2\delta Bn\psi_{xy}}{\sqrt{\varepsilon+2\delta^2\left(\psi_{xy}\right)^2+2\delta^2\left(\psi_{xy}\right)^2+\left(\psi_{yy}-\delta^2\psi_{xx}\right)^2}}, && (7.17)\\
\tau_{xy} &= \left(\psi_{yy}-\delta^2\psi_{xx}\right)+\frac{Bn\left(\psi_{yy}-\delta^2\psi_{xx}\right)}{\sqrt{\varepsilon+2\delta^2\left(\psi_{xy}\right)^2+2\delta^2\left(\psi_{xy}\right)^2+\left(\psi_{yy}-\delta^2\psi_{xx}\right)^2}}, && (7.18)\\
\tau_{yy} &= -2\delta\psi_{xy}+\frac{-2\delta Bn\psi_{xy}}{\sqrt{\varepsilon+2\delta^2\left(\psi_{xy}\right)^2+2\delta^2\left(\psi_{xy}\right)^2+\left(\psi_{yy}-\delta^2\psi_{xx}\right)^2}}. && (7.19)
\end{aligned}$$

Employing long wavelength and low Reynolds number assumptions, the Eqs. (7.14) – (7.16) reduce to the following coupled equations

$$\begin{aligned}
0 &= -\frac{\partial p}{\partial x}+\frac{\partial}{\partial y}\tau_{xy}+Gr_t\theta^*, && (7.20)\\
0 &= -\frac{\partial p}{\partial y}, && (7.21)\\
0 &= \frac{\partial^2\theta^*}{\partial y^2}+B_r\tau_{xy}\psi_{yy} && (7.22)
\end{aligned}$$

where

$$\tau_{xy}=\psi_{yy}+\frac{Bn\psi_{yy}}{\sqrt{\varepsilon+\left(\psi_{yy}\right)^2}}. \qquad (7.23)$$

Eliminating pressure between (7.20) and (7.21), one can write

$$0=\frac{\partial^2}{\partial y^2}\tau_{xy}+Gr_t\frac{\partial\theta^*}{\partial y}. \qquad (7.24)$$

Invoking the component of extra stress tensor in Eqs. (7.22) and (7.24), one gets the following coupled nonlinear differential equations

$$0 = \frac{\partial^2}{\partial y^2}\left(\psi_{yy} + Bn\psi_{yy}/\sqrt{\varepsilon + \left(\psi_{yy}\right)^2}\right) + Gr_t\frac{\partial\theta^*}{\partial y}, \tag{7.25}$$

$$0 = \frac{\partial^2\theta^*}{\partial y^2} + B_r\left(\psi_{yy}^2 + Bn\psi_{yy}^2/\sqrt{\varepsilon + \left(\psi_{yy}\right)^2}\right). \tag{7.26}$$

The dimensionless volume flow rate and boundary conditions in the wave frame are [149]

$$\psi = -\frac{q}{2}, \quad \frac{\partial\psi}{\partial y} = -1, \quad \theta^* = 0, \quad at \quad y = -h, \tag{7.27}$$

$$\psi = \frac{q}{2}, \quad \frac{\partial\psi}{\partial y} = -1, \quad \theta^* = 0, \quad at \quad y = h, \tag{7.28}$$

$$\theta - 2 = q = \int_{-h}^{h}\frac{\partial\psi}{\partial y}dy = \psi(h) - \psi(-h). \tag{7.29}$$

7.2 Solution of the Problem

The perturbation method is adopted for the analytical solution of the problem. To this end, the dependent variables ψ and θ^* are expressed as

$$\psi = \sum_{i=0}^{\infty}\psi_{0i}\left(Gr_t\right)^i + Bn\sum_{i=0}^{\infty}\psi_{1i}\left(Gr_t\right)^i + O(Bn^2), \tag{7.30}$$

$$\theta^* = \sum_{i=0}^{\infty}\theta_{0i}^*\left(Gr_t\right)^i + Bn\sum_{i=0}^{\infty}\theta_{1i}^*\left(Gr_t\right)^i + O(Bn^2). \tag{7.31}$$

Substituting the above expressions in the Eqs. $(7.25) - (7.29)$ and equating the various power Bn, one get the following systems:

Zeroth Order System:

$$\frac{\partial^4\psi_{00}}{\partial y^4} = 0, \quad \frac{\partial^2\theta_{00}^*}{\partial y^2} + B_r\left(\frac{\partial^2\psi_{00}}{\partial y^2}\right)^2 = 0, \tag{7.32}$$

$$\frac{\partial^4\psi_{01}}{\partial y^4} + \theta_{00}^* = 0, \quad \frac{\partial^2\theta_{01}^*}{\partial y^2} + 2B_r\left(\frac{\partial^2\psi_{00}}{\partial y^2}\right)\left(\frac{\partial^2\psi_{01}}{\partial y^2}\right) = 0, \tag{7.33}$$

$$\psi_{00}(\pm h) = \pm\frac{q}{2}, \quad \psi_{00y}(\pm h) = -1, \quad \psi_{01}(\pm h) = 0, \tag{7.34}$$

$$\psi_{01y}(\pm h) = 0, \quad \theta_{00}^*(\pm h) = 0 = \theta_{01}^*(\pm h). \tag{7.35}$$

First Order System:

$$0 = \psi_{10yyyy} + \frac{3\left(\psi_{00yy}\right)^3\left(\psi_{00yyy}\right)^2}{\left(\varepsilon+\left(\psi_{00yy}\right)^2\right)^{5/2}} - \frac{3\left(\psi_{00yy}\right)\left(\psi_{00yyy}\right)^2}{\left(\varepsilon+\left(\psi_{00yy}\right)^2\right)^{3/2}}, \tag{7.36}$$

$$\begin{aligned} 0 = {} & \psi_{11yyyy} + \frac{18\left(\psi_{00yy}\right)^2\left(\psi_{01yy}\right)\left(\psi_{00yyy}\right)^2 + 6\left(\psi_{00yy}\right)^3\left(\psi_{00yyy}\right)\left(\psi_{01yyy}\right)}{\left(\varepsilon+\left(\psi_{00yy}\right)^2\right)^{5/2}} \\ & - \frac{15\left(\psi_{00yy}\right)^4\left(\psi_{01yy}\right)\left(\psi_{00yyy}\right)^2}{\left(\varepsilon+\left(\psi_{00yy}\right)^2\right)^{7/2}} - \frac{6\left(\psi_{01yy}\right)\left(\psi_{00yyy}\right)\left(\psi_{01yyy}\right)}{\left(\varepsilon+\left(\psi_{00yy}\right)^2\right)^{3/2}} \\ & + \frac{\left(\psi_{01yyyy}\right)}{\sqrt{\varepsilon+\left(\psi_{00yy}\right)^2}} + \frac{\left(\psi_{00yy}\right)^2\left(\psi_{01yyyy}\right) - 3\left(\psi_{01yy}\right)\left(\psi_{00yyy}\right)^2}{\left(\varepsilon+\left(\psi_{00yy}\right)^2\right)^{3/2}} + \theta^*_{10}, \end{aligned} \tag{7.37}$$

$$0 = \theta^*_{10yy} + \frac{B_r\left(\psi_{00yy}\right)^2}{\sqrt{\varepsilon+\left(\psi_{00yy}\right)^2}} + 2B_r\left(\psi_{00yy}\right)\left(\psi_{10yy}\right), \tag{7.38}$$

$$\begin{aligned} 0 = {} & \theta^*_{11yy} - \frac{B_r\left(\psi_{00yy}\right)^3\left(\psi_{01yy}\right)}{\left(\varepsilon+\left(\psi_{00yy}\right)^2\right)^{3/2}} + \frac{2B_r\left(\psi_{00yy}\right)\left(\psi_{01yy}\right)}{\sqrt{\varepsilon+\left(\psi_{00yy}\right)^2}} + 2B_r\psi_{01yy}\psi_{10yy}, \\ & + 2B_r\psi_{00yy}\psi_{11yy}, \end{aligned} \tag{7.39}$$

$$0 = \psi_{10}(\pm h), \quad 0 = \psi_{10y}(\pm h), \quad 0 = \psi_{11}(\pm h), \tag{7.40}$$

$$0 = \psi_{11y}(\pm h), \quad 0 = \theta^*_{10}(\pm h), \quad 0 = \theta^*_{11}(\pm h). \tag{7.41}$$

The solution of the zeroth order system is

$$\psi_{00} = yC_2 + y^3C_4, \qquad \psi_{01} = (1/70)\,B_rC_4^2y^7 + yC_8 + y^3C_{10}, \qquad \theta^*_{00} = -3B_rC_4^2y^4 + C_5,$$
$$\theta^*_{01} = -6B_rC_{10}C_4y^4 - (9/70)\,B_r^2C_4^3y^8 + C_{11}.$$

On solving the first order system, one gets

$$
\begin{aligned}
\psi_{10} &= T_1 + yT_2 + y^3T_4 - \left(6C_4y\sqrt{L} + \varepsilon \ln\left|2C_4\left(6C_4y + \sqrt{L}\right)\right|\right)/72C_4^2, \\
\psi_{11} &= T_7 + yT_8 + y^2T_9 + y^3T_{10} + \left(1/(104509440C_4^5)\right)(35\varepsilon(82944C_{10}C_4^2 \\
&\quad + Br(10368C_4^4y^4 + 864C_4^2y^2\varepsilon + 17\varepsilon^2))\ln\left|2\left(6C_4y + \sqrt{L}\right)\right| \\
&\quad + 18C_4y(165888BrC_4^5T_4y^6 - 8792B_rC_4^2y^2\varepsilon\sqrt{L} + 399B_r\varepsilon^2\sqrt{L} \\
&\quad - 8064(C_4^4)(y^3)(30T_6 + B_ry\sqrt{L}) - 4200B_rC_4y\varepsilon^2\ln\left|2C_4\left(6C_4y + \sqrt{L}\right)\right|)), \\
\theta_{10}^* &= B_r(-6C_4T_4y^4 + (T_4\varepsilon^2)/(216C_4^3) + (1/6)(y^2)\sqrt{L} + \varepsilon\sqrt{L}/54C_4^2) + T_5 \\
&\quad + yT_6 - B_ry\varepsilon\ln\left|2\left(6C_4y + \sqrt{L}\right)\right|/12C_4, \\
\theta_{11}^* &= T_{11} + yT_{12} + \left(1/4354560C_4^4\right)B_r(-26127360C_4^4(C_4T_{10} + C_{10}T_4)y^4 \\
&\quad + 1306368C_4^5T_6y^5 - 1679616B_rC_4^6T_4y^8 + (1/15C_4)(2\sqrt{L}(604800C_{10} \\
&\quad (9C_4^4y^2 - 2C_4^2\varepsilon) + B_r(466560C_4^6y^6 + 329184C_4^4y^4\varepsilon - 3267C_4^2y^2\varepsilon^2 - 256\varepsilon^3)).
\end{aligned}
$$

The various constants appearing in above expressions are listed in below.

$$
\begin{aligned}
L &= 36C_4^2y^2+\varepsilon, \quad ,M=36C_4^2h^2+\varepsilon, \quad C_2=(3F+2h)/(4h), \quad C_4=-((F+2h)/(4h^3)),\\
C_5 &= 3B_rC_4^2h^4, \quad C_8=(B_rC_4^2h^6)/35, \;\; C_{10}=(-3/70)\,(B_rC_4^2h^6),\\
C_{11} &= (3/70)\,(140B_rC_{10}C_4h^4+3B_r^2C_4^3h^8), \qquad T_1=\varepsilon\ln\left(4C_4^2\varepsilon\right)/144C_4^2,\\
T_2 &= (144C_4^3h^3+4C_4h\varepsilon)/\sqrt{M}+\varepsilon\ln\left(\left(6C_4h+\sqrt{M}\right)^2/\varepsilon\right),\\
T_4 &= \left(432C_4^3h^3+12C_4h\varepsilon\right)/\sqrt{M}+\varepsilon\ln\left(\left(-6C_4h+\sqrt{M}\right)^2/\varepsilon\right)/288C_4^2h^3,\\
T_5 &= -(1/(216C_4^3))B_r(-1296C_4^4h^4T_4+T_4\varepsilon^2+36C_4^3h^2\sqrt{M}+4C_4\varepsilon\sqrt{M}\\
&\quad +9C_4^2h\varepsilon\ln\left(\left(-6C_4h+\sqrt{M}\right)^2/\varepsilon\right),\\
T_6 &= \left(B_r\varepsilon\ln(4\varepsilon)\right)/24C_4, \quad T_7=(-1/5971968C_4^5)(248832C_4^5h^4T_6+\varepsilon(-10368C_4^2\\
&\quad \times(-8C_{10}+B_rC_4^2h^4)+17Br\varepsilon^2)\ln(4\varepsilon),\\
T_8 &= (1/139345920C_4^5h\sqrt{M})(4C_4h(2903040C_{10}C_4^2\varepsilon+1990656B_r(C_4^5)(h^6)T_4\sqrt{M}\\
&\quad -7B_r(373248C_4^6h^6+90720C_4^4h^4\varepsilon+12636C_4^2h^2\varepsilon^2+257\varepsilon^3))+35\varepsilon\sqrt{M}\\
&\quad ((82944C_{10}C_4^2+B_r(-3456C_4^4h^4+288C_4^2h^2\varepsilon+17\varepsilon^2))\ln\left(\left(-6C_4h+\sqrt{M}\right)^2/\varepsilon\right)\\
&\quad +720B_rC_4^2h^2\varepsilon\ln\left(\left(6C_4h+\sqrt{M}\right)^2/\varepsilon\right)),\\
T_9 &= (1/13824C_4^3)(1152C_4^3h^2T_6+B_r\varepsilon(5\varepsilon\ln\left(4C_4^2\varepsilon\right)-2(24C_4^2h^2+\varepsilon)\ln(4\varepsilon))),\\
T_{10} &= (1/418037760C_4^5h^3\sqrt{M})(12C_4h(4354560B_rC_4^6h^6+2582496B_rC_4^4h^4\varepsilon-595B_r\varepsilon^3\\
&\quad -2985984BrC_4^5h^6T_4\sqrt{M}+420C_4^2\varepsilon(-6912C_{10}+131B_rh^2\varepsilon))-35\varepsilon\sqrt{M}\\
&\quad \times((10368C_4^2(8C_{10}-3B_rC_4^2h^4)-864B_rC_4^2h^2\varepsilon+17B_r\varepsilon^2)\ln\left(\left(-6C_4h+\sqrt{M}\right)^2/\varepsilon\right)\\
&\quad +2160B_rC_4^2h^2\varepsilon\ln\left(\left(-6C_4h+\sqrt{M}\right)^2/\varepsilon\right),\\
T_{11} &= (B_r/130636800C_4^5)(4(195955200C_{10}C_4^5h^4T_4+12597120BrC_4^7h^8T_4+256B_r\varepsilon^3\sqrt{M}\\
&\quad +27C_4^2\varepsilon\sqrt{M}(44800C_{10}+121Brh^2\varepsilon)-2592C_4^2h^2\sqrt{M}(2100C_{10}+127Brh^2\varepsilon)\\
&\quad -466560C_4^6(-420h^4T_{10}B_rh^6\sqrt{M}))+105C_4h\varepsilon((51840C_{10}C_4^2-B_r(216C_4^2h^2-5\varepsilon)\\
&\quad \times(72C_4^2h^2+5\varepsilon))\ln\left(\left(-6C_4h+\sqrt{M}\right)^2/\varepsilon\right)+1800B_rC_4^2h^2\varepsilon\ln\left(\left(-6C_4h+\sqrt{M}\right)^2/\varepsilon\right)\\
T_{12} &= (B_r/1244160C_4^4)(-124416C_4^5h^2(3h^2T_6-40T_9)-\varepsilon(1800B_rC_4^2h^2\varepsilon\ln\left(4C_4^2\varepsilon\right)\\
&\quad +(51840C_{10}C_4^2-B_r(216C_4^2h^2-5\varepsilon)(72C_4^2h^2+5\varepsilon))\ln(4\varepsilon).
\end{aligned}
$$

With the above expressions in hand, the approximate solution of Eqs. (7.25) and (7.26) is known up to first order of Grashof and Bingham numbers. Numerical solution of the problem is also obtained using Matlab built-in routine bvp4c without any restriction on parameters being small. The comparison of the numerical and analytical solutions is presented in Table. 7.1 and Fig. 7.2. It is observed that both the solutions are in excellent agreement for smaller values of Gr_t and Bn. For further discussion regarding the influence of parameters of interest on flow characteristics, pumping and trapping phenomena, we have preferred numerical solution over perturbation solution.

7.3 Results and Discussion

In this section, graphical results are displayed in order to see the effects of various emerging parameters such as Bn, Gr_t and B_r on velocity and temperature profiles, pressure rise per wavelength, frictional forces and trapping phenomenon.

The effects of parameters Bn, Gr_t and B_r, on velocity profile are shown in the Figs. 7.3. In these parameters Bn shows the effects of plasticity. We observe that increasing plasticity (Bn) results in decrease of velocity at the center and for the larger values of Bn i.e., for higher values of yield stress, fluid behaves like a solid. In that case the velocity shows a uniform behavior over most part of the channel cross-section and changes only in a thin layer near the walls which may be due to frictional forces. From Fig. 7.3 we also note that the velocity profile increases near the channel whereas it decreases in the vicinity of the walls with increasing both the Grashof number (Gr_t) and Brinkman number (B_r).

Fig. 7.4 and Fig. 7.5 are prepared to see the influence of parameters Bn, Gr_t and B_r on pumping phenomenon. Fig. 7.4 highlights the variation of pressure rise per wavelength (ΔP_λ) for different values of Bn, Gr_t and B_r. From this figure it is observed that Gr_t and B_r have the similar effects on ΔP_λ i.e., ΔP_λ increases with increasing these parameters in all three regions namely: retrograde pumping region ($q < 0$ and $\Delta P_\lambda > 0$), peristaltic pumping region ($q > 0$ and $\Delta P_\lambda > 0$) and augmented pumping region ($q > 0$ and $\Delta P_\lambda < 0$). From Fig. 7.4 we also observe that ΔP_λ increases by increasing plasticity (Bn) in retrograde and peristaltic pumping regions but decreases in augmented pumping region. We also note that

ΔP_λ shows a nonlinear behavior due to presence of plasticity. It is interesting to note that ΔP_λ decreases by increasing flow rate up to a certain critical value and above that critical value it starts to increase. Moreover, this increase is more prominent for large values of Gr_t and B_r. Fig. 7.5 shows that the effects of all the involved parameters on frictional forces are quite opposite to effects of these parameters on ΔP_λ. In retrograde and peristaltic pumping regions, frictional forces resist the flow due to peristalsis and the magnitude of resistance increases by increasing Bn, Gr_t and B_r. However, in augmented pumping region they assist the flow and again the magnitude of assistance increases by increasing Bn while it decreases with Gr_t and B_r. The results reported above which depict the effects of Gr_t and B_r on ΔP_λ and F_λ are quite interesting and new addition in the literature.

Fig. 7.6 illustrates the variation in temperature profile for different values of involved parameters. From this figure it is observed that the temperature profile increases with increasing all the involved parameters. As expected, increasing the plasticity parameter (Bn) result in the hampering of fluid motion and in consequence more work is done on the fluid to maintain the flow rate. As a result more heat is generated and eventually a rise in the temperature is observed. Similarly an increase in temperature with increasing Grashof number Gr_t is attributed to large temperature gradients within the fluid for larger values of Gr_t.means that the buoyant force is higher than the viscous force as a result of which the larger temperature difference between the fluid particles will occur and therefore the temperature increases. The rise in temperature for larger values of Brinkman number is due to the fact that higher values of B_r results in lesser conduction of heat produced by viscous dissipation.

Finally we report some results about the phenomenon of trapping. In this phenomenon an amount of fluid called *bolus* is trapped due to contraction of walls. To see the influence of parameters Bn, Gr_t and B_r on trapping, we have plotted Figs. $7.7 - 7.9$. From Fig. 7.7 we note that an increase in Bn decreases the size and circulation of the bolus. Figs. 7.8 and 7.9 show that though the size of bolus is independent of the Gr_t and B_r but it circulate faster for large values of Gr_t and B_r.

Comparison of velocity profile		
y	*Solution by Perturbation*	*Solution by bvp4c*
−1.60	−1.0000000000	−1.0000000000
−1.44	−0.7430926598	−0.7436599899
−1.28	−0.5139202503	−0.5149601267
−1.12	−0.3136751353	−0.3150914599
−0.96	−0.1431066839	−0.1447877193
−0.80	−0.0025892965	−0.0043712754
−0.64	0.1078613554	0.1062768005
−0.48	0.1886819834	0.1879071792
−0.32	0.2411262419	0.2423347756
−0.16	0.2682421882	0.2727034296
0.00	0.2758974988	0.2823523318
0.16	0.2682421882	0.2727034296
0.32	0.2411262419	0.2423347756
0.48	0.1886819834	0.1879071792
0.64	0.1078613554	0.1062768005
0.80	−0.0025892965	−0.0043712753
0.96	−0.1431066839	−0.1447877192
1.12	−0.3136751353	−0.3150914599
1.28	−0.5139202503	−0.5149601299
1.44	−0.7430926598	−0.7436599899
1.60	−1.0000000000	−1.0000000000

Comparison of temperature profile		
y	*Solution by Perturbation*	*Solution by bvp4c*
−1.60	0.0000000000	0.0000000000
−1.44	0.1384192059	0.1381180352
−1.28	0.2369391566	0.2362746361
−1.12	0.3037895776	0.3027716022
−0.96	0.3464959763	0.3451889360
−0.80	0.3716937695	0.3701971323
−0.64	0.3850083576	0.3834324157
−0.48	0.3909827722	0.3894185762
−0.32	0.3930388860	0.3915266088
−0.16	0.3934692382	0.3919897535
0.00	0.3934953567	0.3920196670
0.16	0.3934692382	0.3919897535
0.32	0.3930388860	0.3915266088
0.48	0.3909827722	0.3894185762
0.64	0.3850083576	0.3834324156
0.80	0.3716937695	0.3701971322
0.96	0.3464959763	0.3451889359
1.12	0.3037895776	0.3027716021
1.28	0.2369391566	0.2362746404
1.44	0.1384192059	0.1381180352
1.60	0.0000000000	0.0000000000

Table 7.1: Comparison of solutions of velocity and temperature profiles

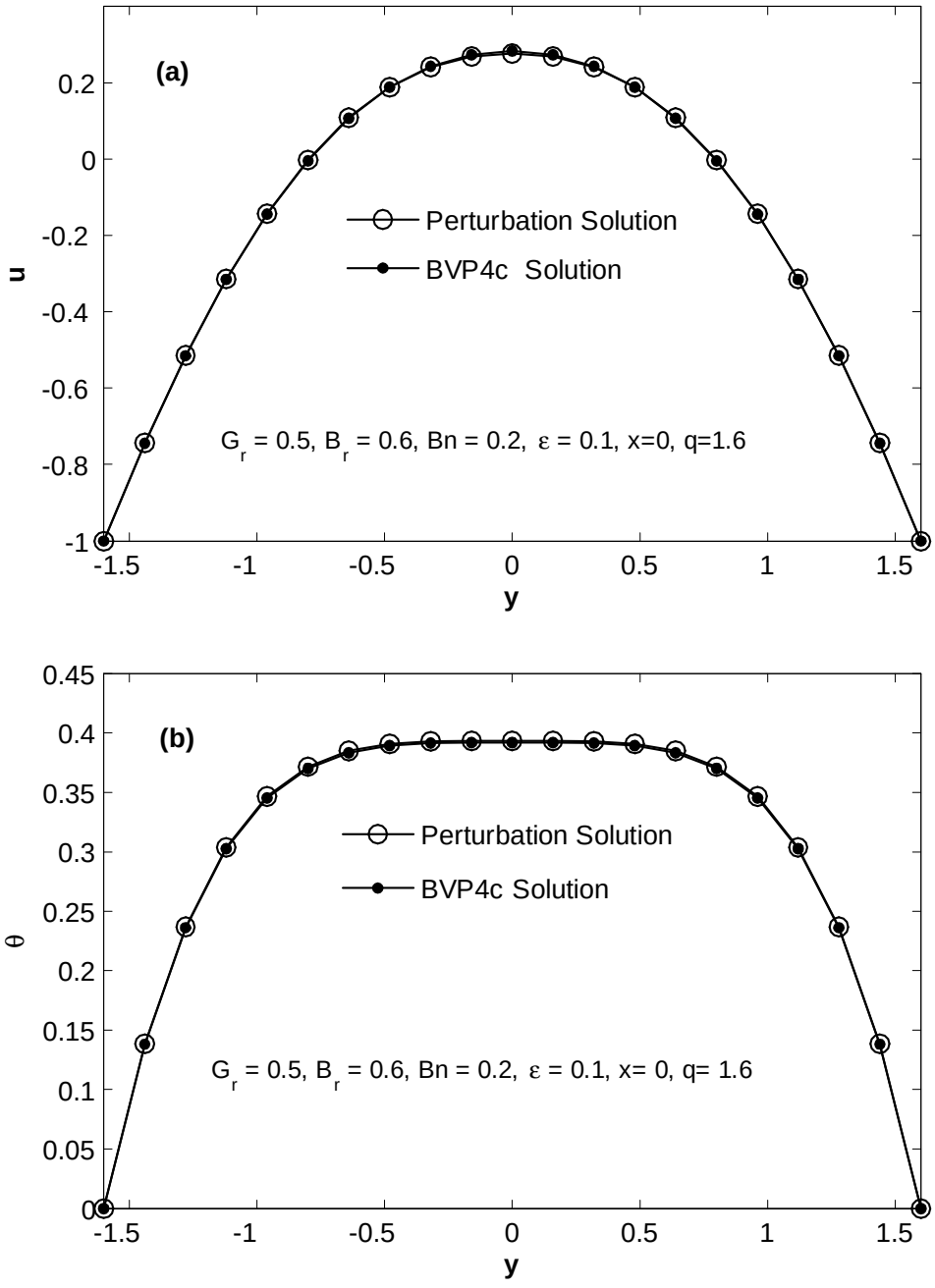

Fig.7.2: Comparison of perturbation and numerical solutions

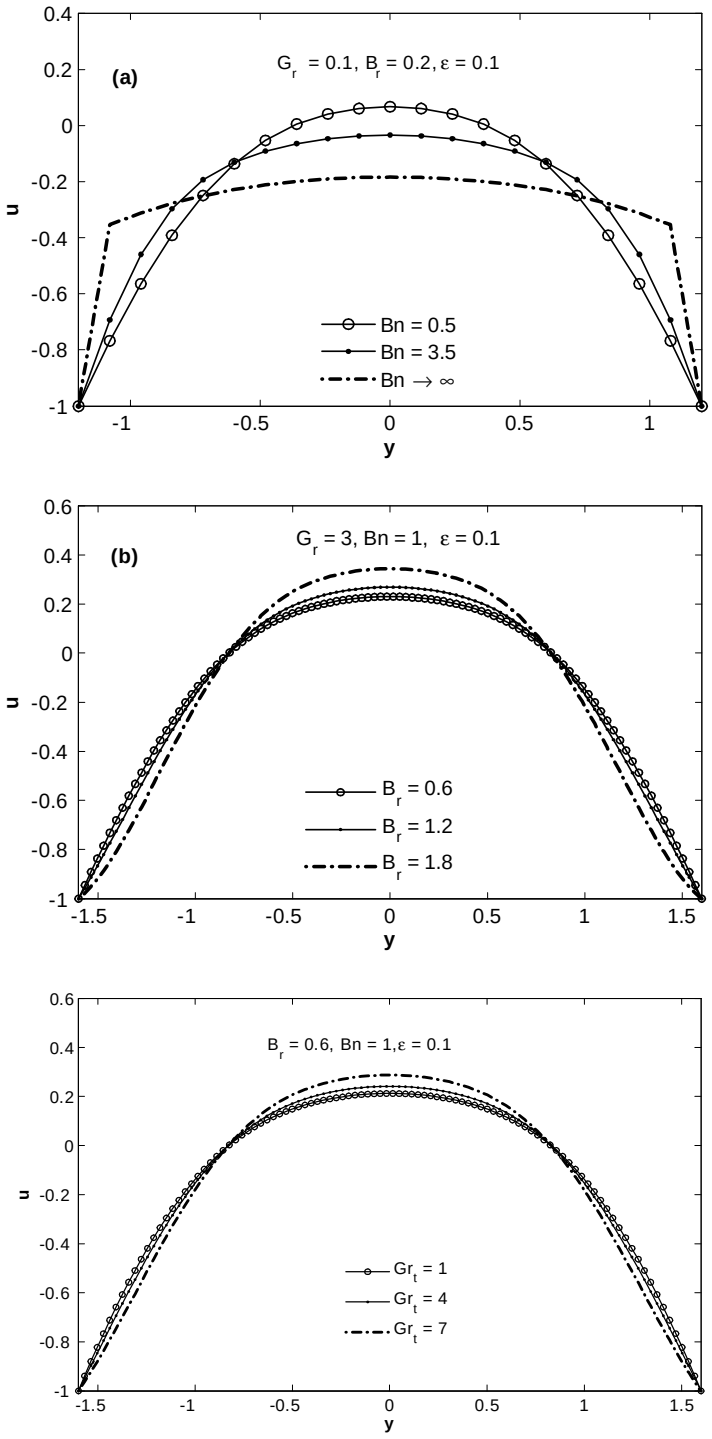

Fig.7.3: Velocity profile with $x = 0$, $q = 1.4$, $\phi = 0.6$.

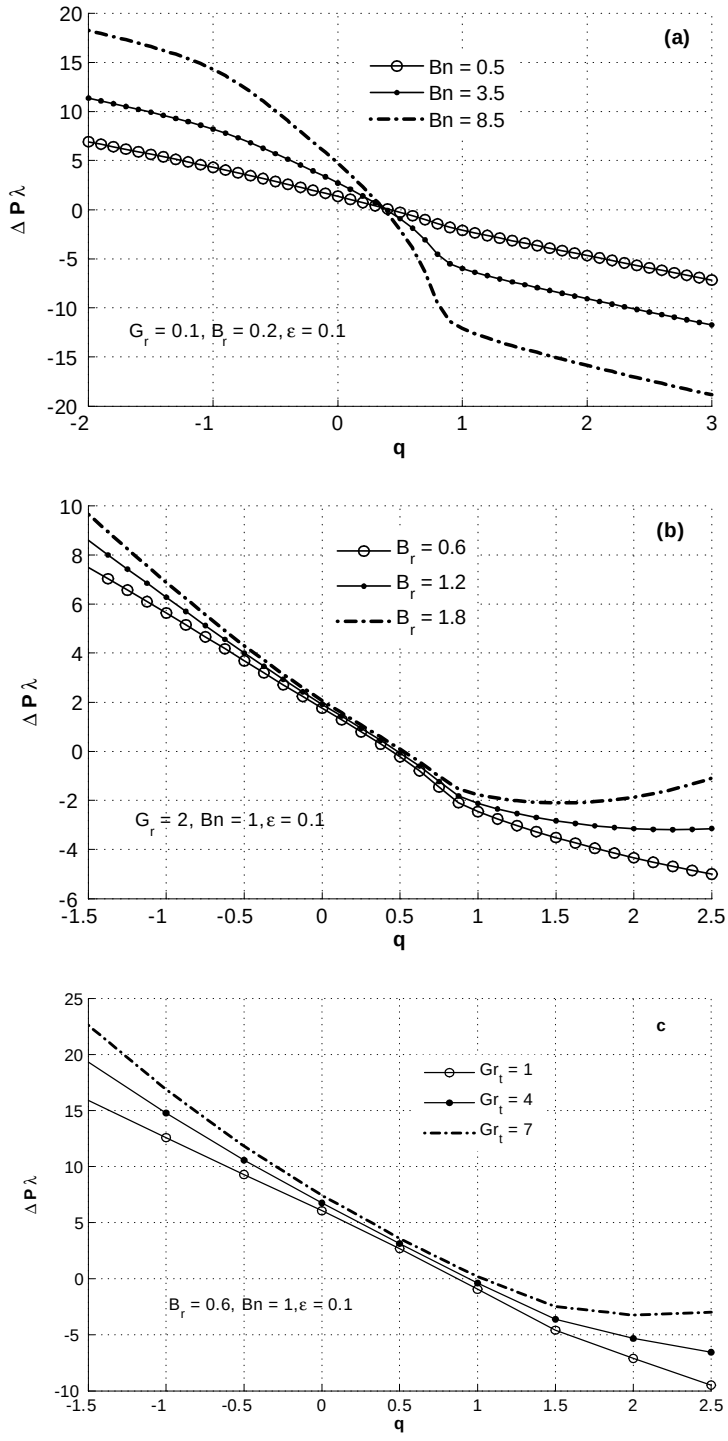

*Fig.*7.4: Pressure rise per wavelength versus flow rate q with $\phi = 0.4$.

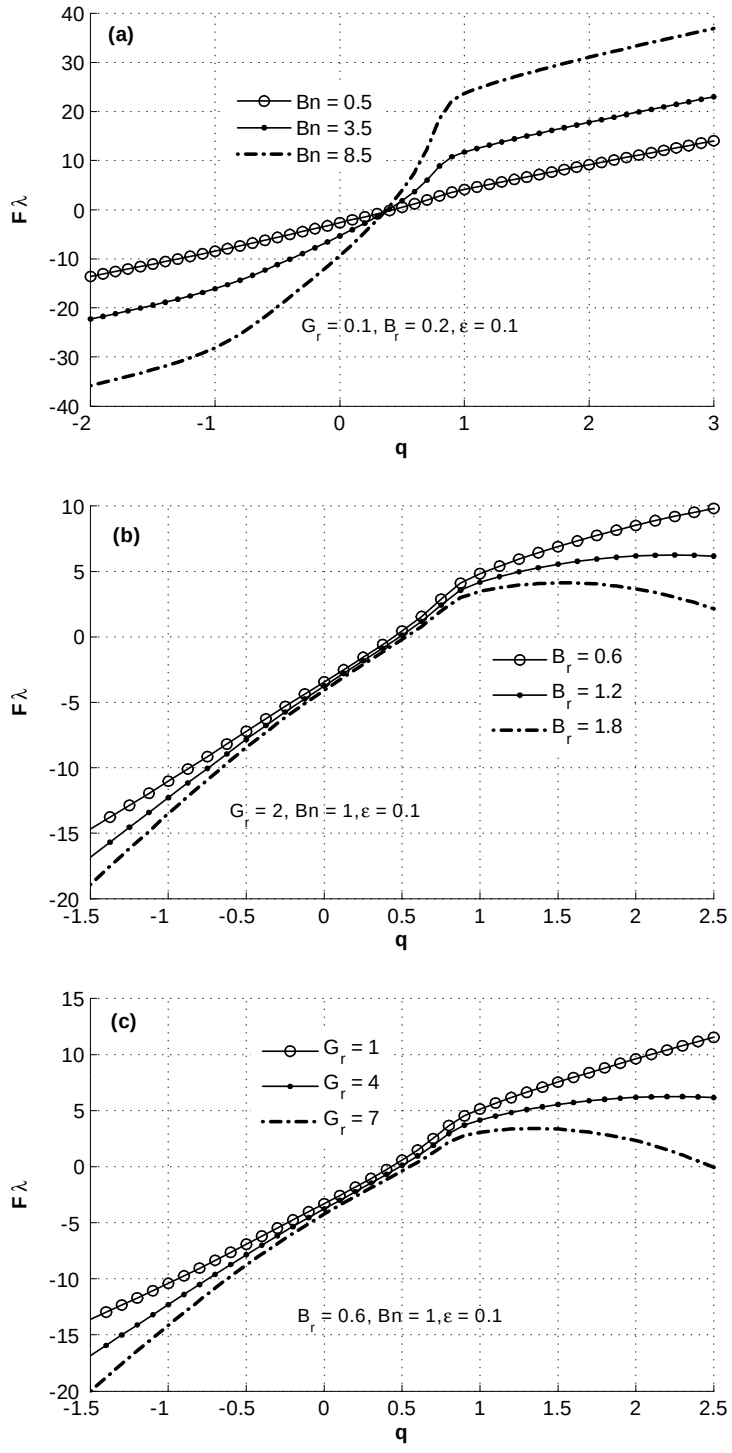

Fig.7.5: Frictional forces versus flow rate q with $\phi = 0.4$.

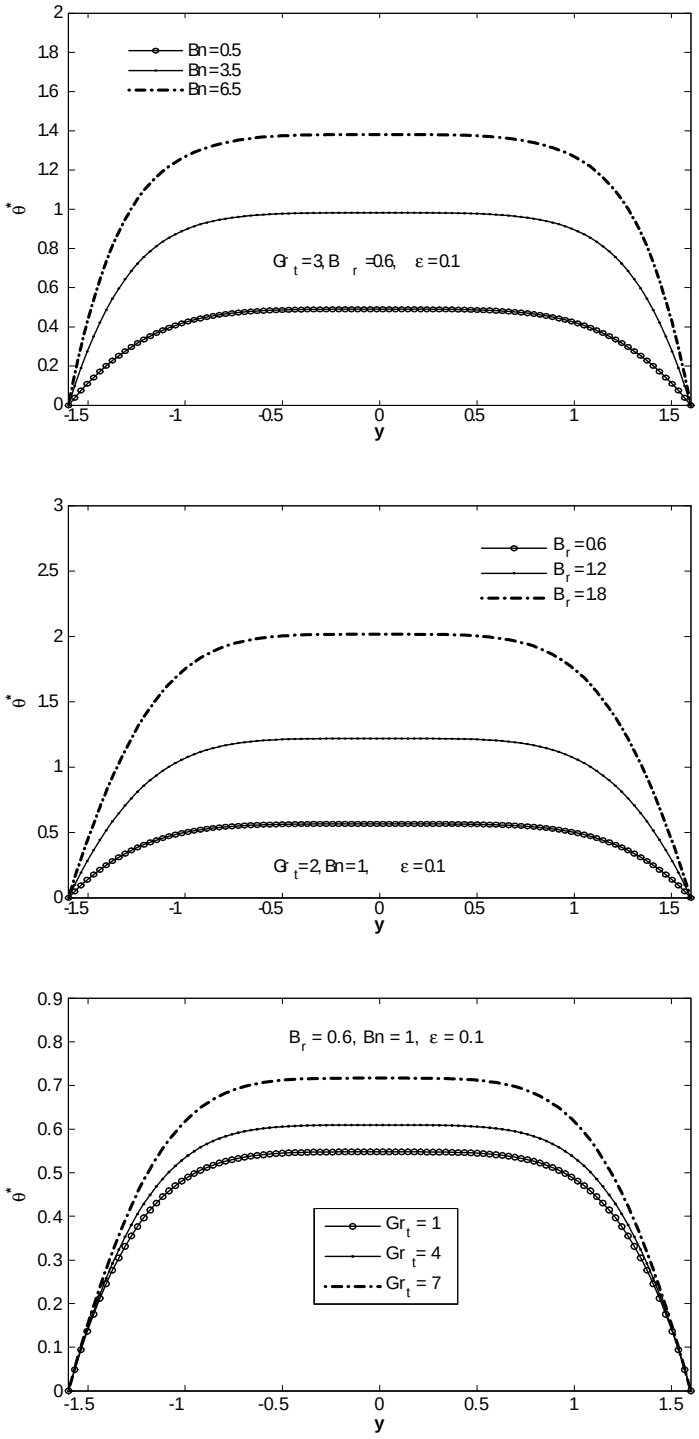

*Fig.*7.6: Temperature profile with $x = 0$, $q = 1.4$, $\phi = 0.6$.

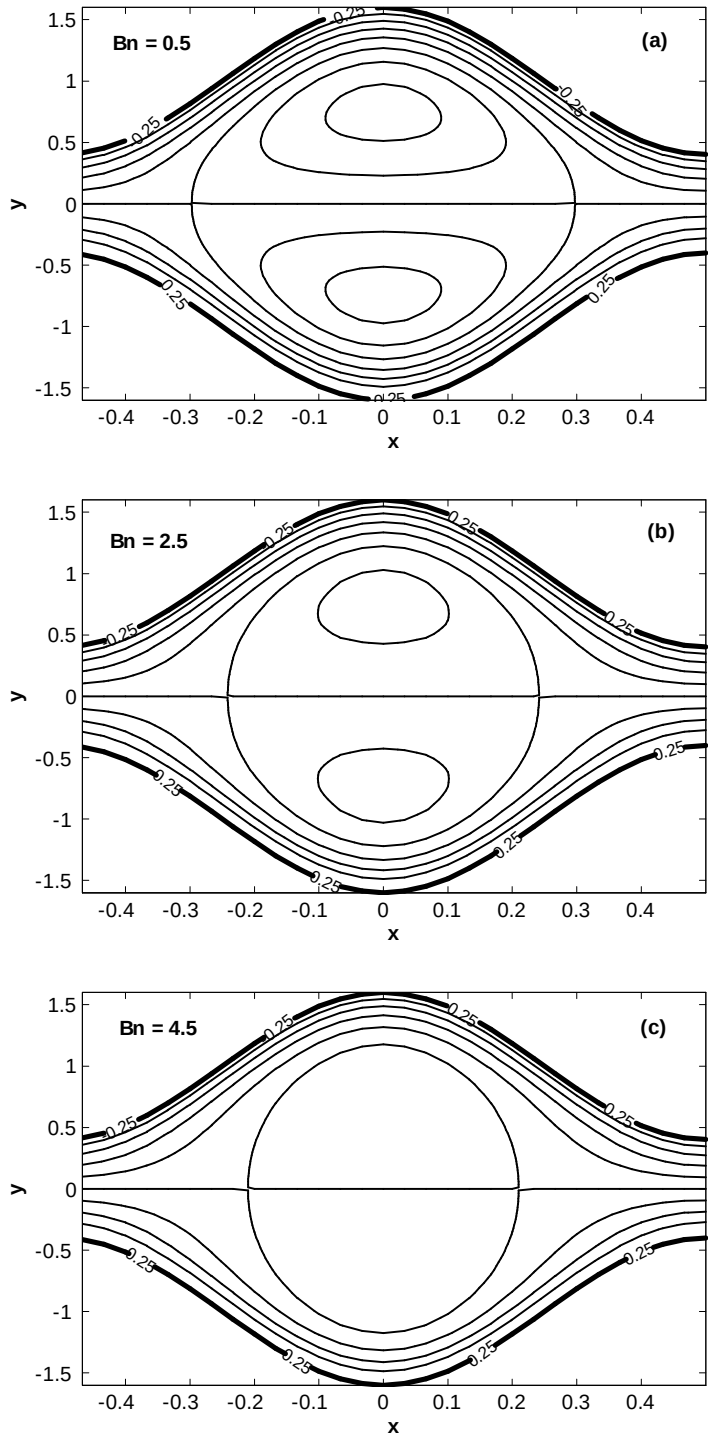

*Fig.*7.7: Streamlines for various values of Bn with $B_r = 0.6$, $Gr_t = 3$, $q = 1.5$, $\phi = 0.6$.

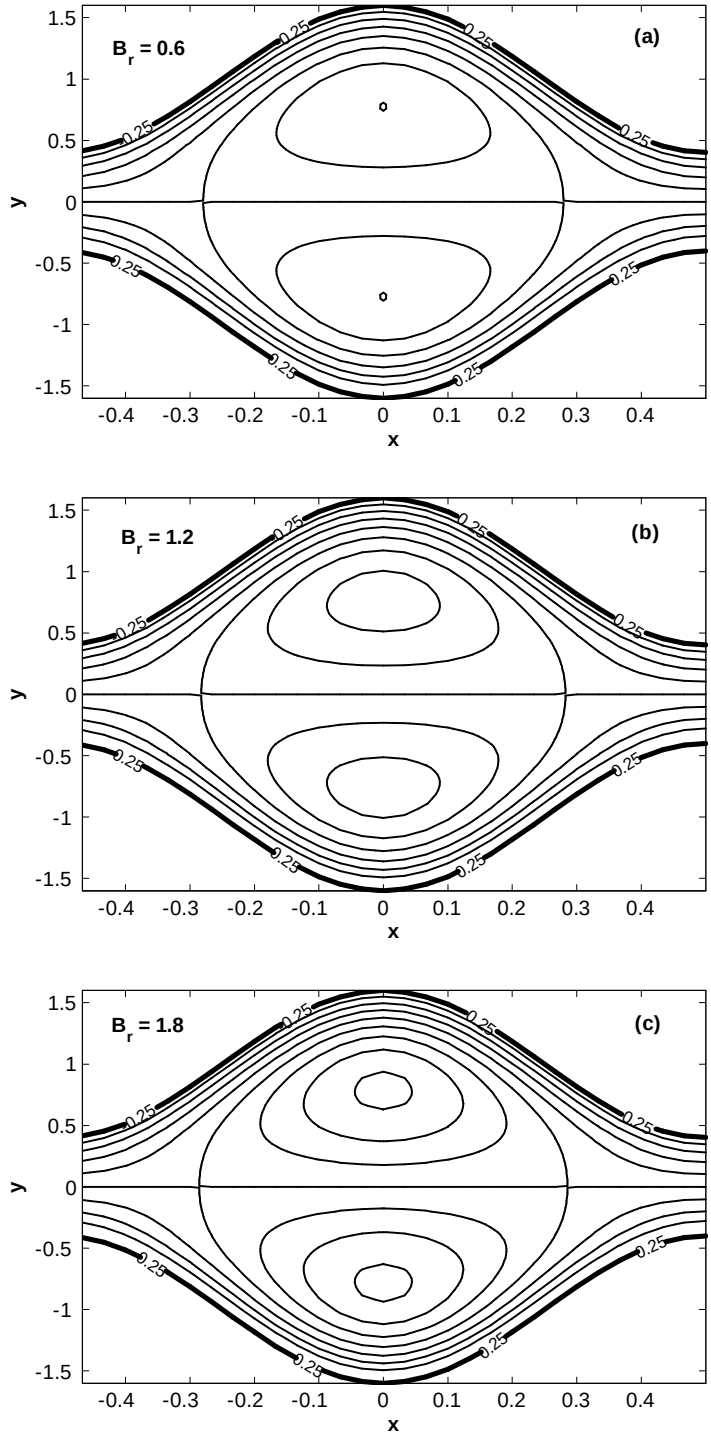

*Fig.*7.8: Streamlines for various values of B_r with $Gr_t = 3$, $Bn = 1$, $q = 1.5$, $\phi = 0.6$.

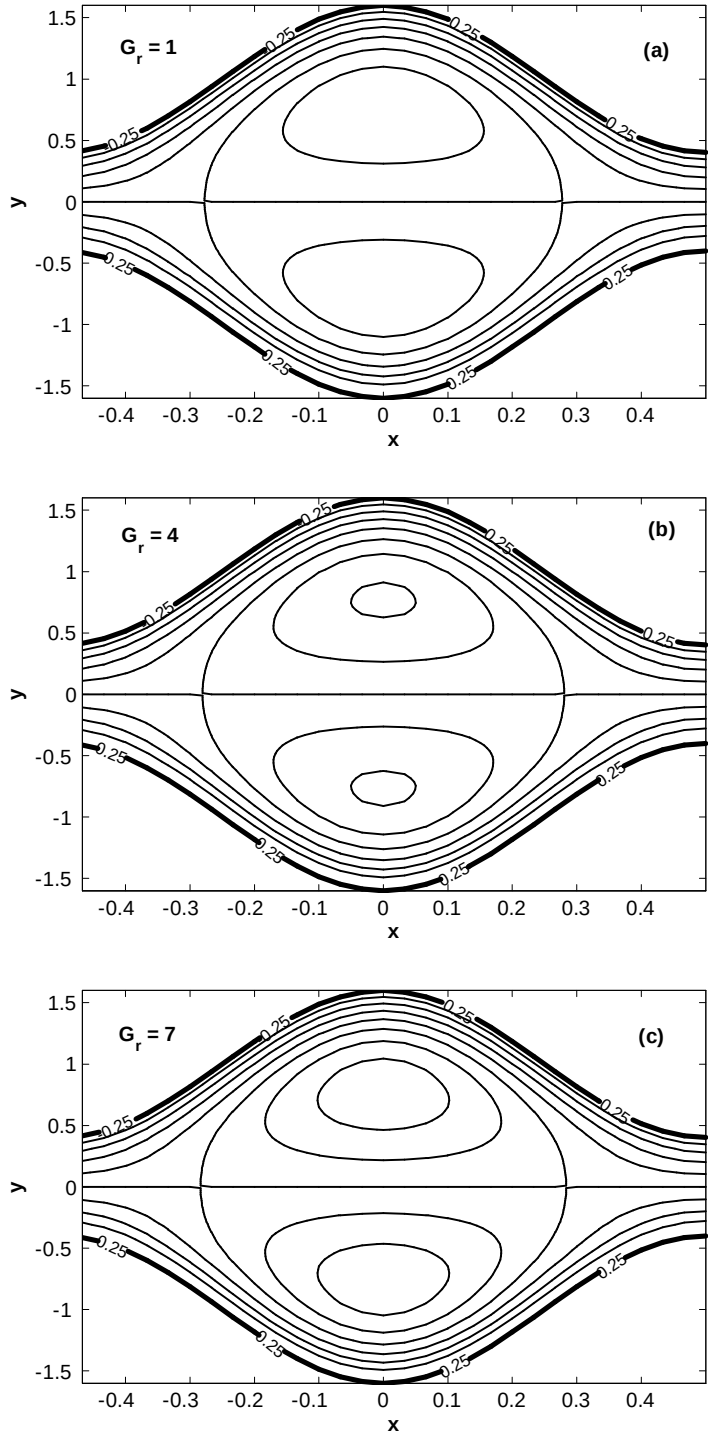

Fig.7.9: Streamlines for values of Gr_t with $B_r = 0.6$, $Bn = 1$, $q = 1.5$, $\phi = 0.6$.

7.4 Concluding remarks

Heat transfer analysis is performed for peristaltic flow of a viscoplastic fluid in presence of buoyant forces and viscous dissipation. The problem is modeled under long wavelength and low Reynolds number assumptions in form of few coupled nonlinear ordinary differential equations. The solution of these equations is obtained analytically and numerically. A quantitative analysis is performed through various plots. It is observed that the velocity of fluid shows uniformity over the whole cross-section except near the boundaries, with the increase in plasticity (Bn). However, it increases near the center of channel while decreases near the boundaries by increasing Gr_t and B_r. The pressure rise per wavelength increases in the retrograde and peristaltic pumping regions but decreases in the augmented pumping region with the increase in plasticity. While it increases in all the three regions by increasing Gr_t and B_r. It is further observed that effects of Bn, Gr_t and B_r on temperature field are similar. The trapping phenomenon is also affected with the increase of Bn, Gr_t and B_r. In fact the size and circulation of bolus decreases by increasing Bn while its size remain unchanged with an increase in Gr_t and B_r.

Bibliography

1. T. W. Latham, Fluid motion in peristaltic pump, M. S. Thesis, MIT, Cambridge, M A, 1966.

2. A. H. Shapiro, Pumping and retrograde diffusion in peristaltic waves, *Proceedings. Workshop on ureteral reflux in children. National Academy of Science (Natural Research Council)*, 3 (1967) 109 – 126.

3. A. H. Shapiro and T. W. Latham, "On peristaltic pumping" *(abstract). Proc. Ann. Conf. Engng Med. Bio. San Francisco, Cal.*, 8 (1966) p. 147.

4. S. L. Weinberg, A theoretical and experimental treatment of peristaltic pumping and its relation to ureteral function. *Ph.D. Thesis, M.I.T. Cambridge, Mass* (1970).

5. A. H. Shapiro, M. Y. Jaffrin and S. L. Weinberg, Peristaltic pumping with long wavelength at low Reynolds number. *J. Fluid Mech.* 37 (1969) 799 – 825.

6. M. Y. Jaffrin, Inertia and streamline curvature effects in peristaltic pumping. *Int. J. Engng Sci.* 11 (1973) 681 – 699.

7. P. S. Lykoudis, Peristaltic pumping a bioengineering model. *Proc. Workshop Hydrodynam. Upper Urinary tract. National Academy of Science, Wash. D. C.* (1971).

8. S. L. Weinberg, M. Y. Jaffrin and A. H. Shapiro, An hydro dynamical model of ureteral function. *Proc. Workshop Hydrodynam. Upper urinary tract. National Academy of Science, Wash. D. C.* (1971).

9. Y. C. Fung and C. S. Yih, Peristaltic transport, *J. Appl. Mech.* 35 (1968) 669 – 675.

10. Y. C. Fung, Peristaltic pumping; a bioengineering model. *Proc. Workshop Hydrodynam. Upper urinary tract. National Academy of Science, Wash. D. C.* (1971).

11. M. Y. Jaffrin and A. H. Shapiro, Peristaltic pumping, *Ann. Rev. Fluid Mech.* 3 (1997) 13 – 36.

12. T. D. Brown and T. K. Hung, Computational and experimental investigations of two dimensional nonlinear peristaltic flows. *J. Fluid Mech.* 83 (1977) 249 – 272.

13. S. Takabatake and K. Ayukawa, Numerical study of two-dimensional peristaltic waves. *J. Fluid Mech.* 122 (1982) 439 – 465.

14. S. Takabatake, K. Ayukawa and A. Mori, Peristaltic pumping in circular cylindrical tubes: a numerical study of fluid transport and its efficiency. *J. Fluid Mech.* 193 (1988) 267−283.

15. B. V. R. Kumar and K. B. Naidu, A numerical study of peristaltic flows, *Computers & Fluids* 24 (1995) 161 – 176.

16. L. M. Srivastava and V. P. Srivastava, Interaction of peristaltic flow with pulsatile flow in a circular cylindrical tube. *J. Biomech.* 18 (1985) 247 – 253.

17. N. A. S. Afifi and N. S. Gad, Interaction of peristaltic flow with pulsatile magneto-fluid through a porous medium. *Acta Mech.* 149 (2001) 229 – 237.

18. K. De Vries, E. A. Lyons, J. Ballard, C. S. Levi and D. J. Lindsay, Contractions of the inner third of the myometrial. *Am J. Obstetrics Gynecol.* 102 (1990) 679 – 682.

19. O. Eytan, A. J. Jaffa, J. H. Toov, E. Dalach and D. Elad, Dynamics of the intra-uterine fluid-wall interface. *Annals Biomed. Engng.* 27 (1999) 372 – 379.

20. O. Eytan and D. Elad, Analysis of intra-uterine fluid motion induced by uterine contractions. *Bull. Math. Biology* 61 (1999) 221 – 238.

21. M. Mishra and A. R. Rao, Peristaltic transport of a Newtonian fluid in an asymmetric channel, *ZAMP* 53 (2003) 532 – 550.

22. A. E. H. Abd El Naby and A. E. M. El Misery, Effects of an endoscope and generalized Newtonian fluid on peristaltic motion, *J. Appl. Math. Comput.* 128 (2002) 19−.

23. T. Hayat and N. Ali, Effect of variable viscosity on the peristaltic transport of a Newtonian fluid in an asymmetric channel. *Appl. Math. Model.* 32 (2008) 761 – 774.

24. M. A. Abd Elnaby and M. H. Haroun, A new model for study the effect of wall properties on peristaltic transport of a viscous fluid, *Commun. Nonlinear Sci. Numer. Simulat.* 13 (2008) 752 – 762.

25. E. F. Elshehawey, N. T. Eldabe, E. M. Elghazy and A. Ebaid, Peristaltic transport in an asymmetric channel through a porous medium, *Appl. Math. Comput.*182 (2006) 140−150.

26. A. Ebaid, Effects of magnetic field and wall slip conditions on the peristaltic transport of a Newtonian fluid in an asymmetric channel, *Phys. Letts. A*, 372 (2008) 4493 – 4499.

27. N. Ali, Q. Hussain, T. Hayat and S. Asghar, Slip effects on the peristaltic transport of MHD fluid with variable viscosity, *Phys. Letters A* 372 (2008) 1477 – 1489.

28. S. Srinivas and V. Pushparaj, Non-linear peristaltic transport in an inclined asymmetric channel, *Commun. Nonlinear Sci. Numer. Simulat.*, 13 (2008) 1782 – 1795.

29. H. Sato, T. Kawai, T. Fujita and M. Okabe, Two dimensional peristaltic flow in curved channels. *Trans. Japan. Soc. Mech. Eng. B* 66 (2000) 679 – 685.

30. N. Ali, M. Sajid and T. Hayat, Long wavelength flow analysis in a curved channel, *Z. Naturforsch.* 65*a* (2010) 191 – 196.

31. J. V. Ramanamurthy, K. M. Prasad and V. K. Narla, Unsteady peristaltic transport in curved channels, *Phys. Fluid* 25 (2013) 091903.

32. K. Vajravelua, G. Radhakrishnamacharya and V. Radhakrishnamurty, Peristaltic flow and heat transfer in a vertical porous annulus, with long wave approximation, *Int. J. Non-Linear Mech.* 42 (2007) 754 – 759.

33. S. Srinivas, R. Gayathri and M. Kothandapani, The influence of slip conditions, wall properties and heat transfer on MHD peristaltic transport, *Comp. Phys. Commun.* 180 (2009) 2115 – 2122.

34. T. Hayat, M. U. Qureshi and Q. Hussain, Effect of heat transfer on the peristaltic flow of an electrically conducting fluid in a porous space, *Appl. Math. Model.* 33 (2009) 1862 – 1873.

35. Kh. S. Mekheimer and Y. Abd elmaboud, The influence of heat transfer and magnetic field on peristaltic transport of a Newtonian fluid in a vertical annulus: Application of an endoscope, *Phys. Letts. A* 372 (2008) 1657 – 1665.

36. S. Nadeem and N. S. Akbar, Influence of temperature dependent viscosity on peristaltic transport of a Newtonian fluid: Application of an endoscope, *Appl. Math. Comput.* 216 (2010) 3606 – 3619.

37. S. Hina, T. Hayat, S. Asghar and A. A. Hendi, Influence of compliant walls on peristaltic motion with heat/mass transfer and chemical reaction, *Int. J. Heat Mass Trans.*, 55 (2012) 3386 – 3394.

38. M. Mustafa, S. Hina, T. Hayat and A. Alsaedi, Influence of wall properties on the peristaltic flow of a nanofluid: analytic and numerical solutions, *Int. J. Heat Mass Trans.*, 55 (2012) 4871 – 4877.

39. T. Hayat and Z. Asghar, Heat Transfer Analysis on the Peristaltic Motion with Slip Effects, *Z. Naturforschung.* 65*a* (2010) 697 – 704.

40. S. Srinivas, R. Gayathri and M. Kothandapani, The influence of slip conditions, wall properties and heat transfer on MHD peristaltic transport, *Comp. Phys. Commun.*, 180 (2009) 2115 – 2122.

41. A. Ebaid, A new numerical solution for the MHD peristaltic flow of a bio-fluid with variable viscosity in a circular cylindrical tube via Adomian decomposition method, *Phys. Letters A* 372 (2008) 5321 – 5328.

42. S. Srinivas and M. Kothandapani, The influence of heat and mass transfer on MHD peristaltic flow through a porous space with compliant walls, *Appl. Math. Comput.* 213 (2009) 197 – 208.

43. S. Srinivas and R. Muthuraj, Effects of chemical reaction and space porosity on MHD mixed convective flow in a vertical asymmetric channel with peristalsis, *Math. Comp. Model.* 54 (2011) 1213 – 1227.

44. N. Ali, M. Sajid and T. Hayat, Long wavelength flow analysis in a curved channel, *Z. Naturforsch.* 65*a* (2010) 191 – 196.

45. K. K. Raju and R. Devanathan, Peristaltic motion of a non-Newtonian fluid. *Rheol. Acta* 11 (1972) 170 – 178.

46. K. K. Raju and R. Devanathan, Peristaltic motion of a non-Newtonian fluid II: viscoelastic fluid. *Rheol. Acta* 13 (1974) 944 – 948.

47. G. Bohme, R. Friedrich, Peristaltic Flow of Viscoelastic Liquids, *J. Fluid Mech.* 128 (1983) 109 – 122.

48. R. G. Devi and R. Devanathan, Peristaltic motion of a micropolar fluid. *Proc. Indian Acad. Sci.* 81 (1975) 149 – 163.

49. L. M. Srivastava and V. P. Srivastava, Peristaltic transport of blood; Casson model-II, *J. Biomech.* 17 (1984) 821 – 829.

50. A. M. Siddiqui, A. Provost and W. H. Schwarz, Peristaltic pumping of a second order fluid in a planar channel. *Rheol. Acta* 30 (1991) 249 – 262.

51. A. M. Siddiqui and W. H. Schwarz, Peristaltic flow of a second order fluid in tubes. *J. Non- Newtonian Fluid. Mech.* 53 (1994) 257 – 284.

52. A. M. Siddiqui and W. H. Schwarz, Peristaltic motion of a third order fluid in a planar channel. *Rheol. Acta* 32 (1993) 47 – 56.

53. T. Hayat, Y. Wang, A. M. Siddiqui, K. Hutter and S. Asghar, Peristaltic transport of a third order fluid in a circular cylindrical tube. *Math. Mod. Meth. Appl. Sci.* 12 (2002) 1691 – 1706.

54. T. Hayat, Y. Wang, A. M. Siddiqui and K. Hutter, Peristaltic motion of a Johnson-Segalman fluid in a planar channel. *Math. Probs. Engng.* 1 (2003) 1 – 23.

55. D. Srinivasacharya, M. Mishra and A. R. Rao, Peristaltic pumping of a micropolar fluid in a tube. *Acta Mech.* 161 (2003) 165 – 178.

56. P. Muthu, B. V. R. Kumar and P. Chandra, On the influence of wall properties in the peristaltic motion of micropolar fluid. *ANZIAM J.* 45 (2003) 245 – 260.

57. A. R. Rao and M. Mishra, Peristaltic transport of a power-law fluid in a porous tube, *J. Non-Newtonian Fluid Mech.* 121 (2004) 163 – 174.

58. T. Hayat, Y. Wang, K. Hutter, S. Asghar and A.M. Siddiqui, Peristaltic transport of an Oldroyd-B fluid in a planar channel. *Math. Probs. Engng.* 4 (2004) 347 – 376.

59. M. Elshahed and M. H. Haroun, Peristaltic transport of Johnson-Segalman fluid under effect of a magnetic field, *Math. Prob. Engng.* 6 (2005) 663 – 677.

60. Abd El Hakeem Abd El Naby, A. E. M. El Misery and Ibrahim El Shamy, Hydro magnetic flow of generalized Newtonian fluid through a uniform tube with peristalsis, *Appl. Math. Comput.* 173 (2006) 856 – 871.

61. Y. Wang, Time-dependent Poiseuille flows of visco-elasto-plastic fluids, *Acta Mechanica*, 186 (2006) 187 – 201.

62. T. Hayat and N. Ali, On mechanism of peristaltic flows for power-law fluids, *Physica A* 371 (2006) 188 – 194.

63. M. V. S. Reddy, A. R. Rao and S. Sreenadh, Peristaltic motion of a power-law fluid in an asymmetric channel, *Int. J. Non-linear Mech.* 42 (2007) 1153 – 1161.

64. N. Ali and T. Hayat, Peristaltic motion of a Carreau fluid in an asymmetric channel, *Appl. Math. Comput.* 193 (2007) 535 – 552.

65. T. Hayat, A. Afsar, M. Khan and S. Asghar, Peristaltic transport of a third order fluid under the effect of a magnetic field, *Comp. Math. Appl.* 53 (2007) 1074 – 1087.

66. T. Hayat, M. Khan, A. M. Siddiqui and S. Asghar, Non-linear peristaltic flow of a non-Newtonian fluid under effect of a magnetic field in a planar channel, *Commun. Nonlinear Sci. Numer. Simulat.* 12 (2007) 910 – 919.

67. M. H. Haroun, Effect of Deborah number and phase difference on peristaltic transport of a third-order fluid in an asymmetric channel, *Commun. Nonlinear Sci. Numer. Simulat.* 12 (2007) 1464 – 1480.

68. M. H. Haroun, Non-linear peristaltic flow of a fourth grade fluid in an inclined asymmetric channel, *Comput. Mater. Sci.* 39 (2007) 324 – 333.

69. T. Hayat, M. U. Qureshi and N. Ali, The influence of slip on the peristaltic motion of a third order fluid in an asymmetric channel, *Phys. Letters A* 372 (2008) 2653 – 2664.

70. T. Hayat, N. Ali and S. Asghar, Hall effects on peristaltic flow of a Maxwell fluid in a porous medium, *Phys. Letters A* 363 (2007) 397 – 403.

71. Y. Wang, T. Hayat and K. Hutter, Peristaltic flow of a Johnson-Segalman fluid through a deformable tube, *Theor. Comput. Fluid Dyn.* 21 (2007) 369 – 380.

72. Md. Asif Ikbal, S. Chakravarty and P. K. Mandal, An unsteady peristaltic transport phenomenon of non-Newtonian fluid – A generalized approach, *Appl. Math. Comput.* 201 (2008) 16 – 34.

73. Y. Wang, T. Hayat, N. Ali and M. Oberlack, Magneto hydrodynamic peristaltic motion of a Sisko fluid in a symmetric or asymmetric channel, *Physica A* 387 (2008) 347 – 362.

74. T. Hayat, A. Afsar and N. Ali, Peristaltic transport of a Johnson–Segalman fluid in an asymmetric channel, *Math. Comp. Model.* 47 (2008) 380 – 400.

75. M. Kothandapani and S.Srinivas, Peristaltic transport of a Jeffrey fluid under the effect of magnetic field in an asymmetric channel, *Int. J. Non-Linear Mech.* 43 (2008) 915 – 924.

76. T. Hayat, M. Javed and S. Asghar, MHD peristaltic motion of Johnson-Segalman fluid in a channel with compliant walls, *Physics Letts. A* 372 (2008) 5026 – 5036.

77. T. Hayat, E. Momoniat and F. M. Mahomed, Peristaltic MHD flow of third grade fluid with an endoscope and variable viscosity, *J. Nonlinear Math. Phys.* 1 (2008) 91 – 104.

78. S. Nadeem and S. Akram, Influence of inclined magnetic field on peristaltic flow of a Williamson fluid model in an inclined symmetric or asymmetric channel, *Math. Comp. Model.*, 52 (2010) 107 – 119.

79. T. Hayat, Z. Asghar, S. Asghar and S. Mesloub, Influence of inclined magnetic field on peristaltic transport of fourth grade fluid in an inclined asymmetric channel, *J. Taiwan Inst. Chem. Eng.* 41 (2010) 553 – 563.

80. S. K. Pandey and D. Tripathi, Peristaltic transport of a Casson fluid in a finite channel: Application to flows of concentrated fluids in oesophagus, *Int. J. Biomath.* 03 (2010) 453 *DOI* 10.1142/*S*1793524510001100.

81. D. Tripathi, S. K. Pandey and S. Das, Peristaltic flow of Viscoelastic fluid with fractional Maxwell model through a channel, *Appl. Math. Comp.* 215 (2010) 3645 – 3654.

82. S. K. Pandey, M. K. Chaube and D. Tripathi, Peristaltic transport of multilayered power-law fluids with distinct viscosities: A mathematical model for intestinal flows, *J. Theoret. Bio.* 278 (2011) 11 – 19

83. Y. Abd Elmaboud and Kh.S. Mekheimer, Non-linear peristaltic transport of a second-order fluid through a porous medium, *Appl. Math. Model.* 35 (2011) 2695 – 2710.

84. D. Tripathi, S. K.Pandey and S. Das, Peristaltic transport of a generalized Burgers' fluid: Application to the movement of chyme in small intestine, *Acta Astronautica* 69 (2011) 30 – 38.

85. K. Vajravelu, S. Sreenadh and K. Rajanikanth, C. Lee, Peristaltic transport of a Williamson fluid in asymmetric channels with permeable walls, *Nonlinear Analysis: Real World Application*, 13 (2012) 2804 – 2822.

86. S. K. Pandey and D. Tripathi, Unsteady peristaltic transport of Maxwell fluid through finite length tube: application to oesophageal swallowing, *Appl. Math. Mech. Eng. Ed.* 33 (2012) 15 – 24

87. S. Hina, T. Hayat, S. Asghar and S. Obaidat, Peristaltic flow of Maxwell fluid in an asymmetric channel with wall properties, *Int. J. Phys. Sci.* 7 (2012) 2145 – 2155.

88. H. D. Ceniceros and J. E. Fisher, Peristaltic pumping of a viscoelastic fluid at high occlusion ratios and large Weissenberg numbers, *J. Non-Newtonian Fluid Mechs.* 171−172 (2012) 31 − 41.

89. M. F. El-Sayed, N. T. M. Eldabe, Y. A. Ghaly and M. H. Sayed, Magnetohydrodynamic peristaltic flow of Bingham non-Newtonian fluid in eccentric annuli with slip velocity and temperature jump conditions, *J. Mechs.* 29 (2013) 493 − 506.

90. D. Tripathi and O. A. Beg, Transient magneto-hydro-dynamical study on digestive transport phenomena, *Math. Biosci.* 246 (2013) 72 − 83.

91. N. S. Akbar and S. Nadeem, An analytical and numerical study of peristaltic transport of a Johnson-Segalman fluid in an endoscope, *Chin. Phys. B* 22 (2013) 014703

92. M. Javed, T. Hayat and A. Alsaedi, Peristaltic flow of Burgers' fluid with compliant walls and heat transfer, *Appl. Math. Comput.* 244 (2014) 654 − 671.

93. D. Tripathi and O. A. Beg, Peristaltic propulsion of generalized Burgers' fluids through a non-uniform porous medium: A study of chyme dynamics through the diseased intestine, *Math. Biosci.* 248 (2014) 67 − 77.

94. T. Hayat, S. Shah and N. S. Akbar, Peristaltic Flow of Johnson-Segalman Fluid with Nanoparticles, *J. Aerospace Engng.* 27 (2014) 404 − 413.

95. S. M. Abo-Dahab and A. M. Abd-Alla, Magnetic field and rotation effects on peristaltic transport of a Jeffrey fluid in an asymmetric channel, J. Magnet. Magnet. Mater. 374 (2015) 680 − 689.

96. D. Tripathi, O. Anwar Beg, P. K. Gupta, G. Radhacrishnamacharya and J. Mazumdar, DTM Simulation of Peristaltic Viscoelastic Biofluids flow in asymmetric porous media: A Digestive Transport Model, *J. Bionic Engng.* 12 (2015) 643 − 655.

97. S. Nadeem and N. S. Akbar, Influence of heat transfer on a peristaltic transport of Herschel–Bulkley fluid in a non-uniform inclined tube, *Commun. Nonlinear Sci. Numer. Simulat.* 14 (2009) 4100 − 4113.

98. S. Nadeem and N. S. Akbar, Influence of heat transfer on a peristaltic flow of Johnson Segalman fluid in a non uniform tube, *Int. Commun. Heat Mass Trans.* 36 (2009) 1050 – 1059.

99. T. Hayat, N. Saleem and A. A. Hendi, Slip and heat transfer effects on peristaltic motion of a Carreau fluid in an asymmetric channel", *Z. Naturforschung*, 65*a* (2010) 1121 – 1127.

100. K. Vajravelu, S. Sreenadh and P. Lakshminarayana, The influence of heat transfer on peristaltic transport of a Jeffrey fluid in a vertical porous stratum, *Commun. Nonlinear Sci. Numer. Simulat.* 16 (2011) 3107 – 3125.

101. N. S. Akbar and S. Nadeem, Characteristics of heating scheme and mass transfer on the peristaltic flow for an Eyring-Powell fluid in an endoscope, *Int. J. Heat Mass Trans.* 55 (2012) 375.

102. N. S. Akbar and S. Nadeem, Thermal and velocity slip effects on the peristaltic flow of a six constant Jeffrey's fluid model, *Int. J. Heat Mass Transfer* 55 (2012) 3964 – 3970.

103. O. U. Mehmood, N. Mustapha and S. Shafie, Heat transfer on peristaltic flow of fourth grade fluid in inclined asymmetric channel with partial slip, *Appl. Math. Mech. -Engl. Ed.* 33 (2012) 1313 – 1328.

104. D. Tripathi, S. K. Pandey and O. Anwar Beg, Mathematical modelling of heat transfer effects on swallowing dynamics of viscoelastic food bolus through the human Oesophagus, *Int. J. Thermal Sci.* 70 (2013) 41 – 53.

105. K. Vajravelu, S. Sreenadh and P. Devaki, Peristaltic Transport of a Herschel–Bulkley Fluid in an Elastic Tube, *Heat Trans. Asian Research* 44 (2015) 585 – 598.

106. N. Ali, M. Sajid, Z. Abbas and T. Javed, Non-Newtonian fluid flow induced by peristaltic waves in a curved channel. *Eur. J. Mech. B/Fluids* 29 (2010) 387 – 394.

107. N. Ali, M. Sajid, T. Javed and Z. Abbas, An Analysis of peristaltic flow of a micropolar fluid in a curved channel, *Chin. Phys. Letts.* 28 (2011) 014704.

108. F. M. Abbasi, A. Alsaedi and T. Hayat, Peristaltic transport of Eyring-Powell fluid in a curved channel, *J. Aerospace Engng.* 27 (2014) 04014037.

109. T. Hayat, F. M. Abbasi and B. Ahmed, A. Alsaedi, Peristaltic transport of Carreau-Yasuda fluid in a curved channel with slip effects, *Plos One* 9 (2014) *e*95070.

110. S. Hina, M. Mustafa, T. Hayat and N. D. Alotaibi, On peristaltic motion of pseudoplastic fluid in a curved channel with heat/mass transfer and wall properties, *Appl. Math. Comput.* 263 (2015) 378 – 391.

111. T. Hayat, Quratulain, M. Rafiq, F. Alsaedi and M. Ayub, Soret and Dufour effects on peristaltic transport in curved channel with radial magnetic field and convective conditions, *J. Magnet. Magnet. Mater.* 405 (2016) 358 – 369.

112. T. Hayat, A. Tanveer, F. Alsaedi and G. Mousa, Impact of radial magnetic field on peristalsis in curved channel with convective boundary condition, *J. Magnet. Magnet. Mater.* 403 (2016) 47 – 59.

113. K. Javid, N. Ali, M. Sajid, Simultaneous effects of viscoelasticity and curvature on peristaltic flow through a curved channel, *Meccanica* 51 (2016) 87 – 98.

114. N. Ali, K. Javid, M. Sajid, A. Zaman and T. Hayat, Numerical simulation of Oldroyd 8-constant fluid flow and heat transfer in a curved channel, *Int. J. Heat Mass Trans.* 94 (2016) 500 – 508.

115. T. Hayat, M. Shafique, A. Tanveer and A. Alsaedi, Hall and ion slip effects on peristaltic flow of Jeffrey nanofluid with Joule heating, *J. Magnet. Magnet. Mater.* 407 (2016) 51 – 59.

116. S. E. Ghasemi, M. Vatani, M. Hatami and D. D. Ganji, Analytical and numerical investigation of nanoparticle effect on peristaltic fluid flow in drug delivery systems, *J. Mol. Liq.* 215 (2016) 88 – 97.

117. F. M. Abbasi, T. Hayat and B. Ahmad, Impact of magnetic field on mixed convective peristaltic flow of water based nanofluids with Joule heating, Z. Naturforsch. A: Phys. Sci. 70 (2015) 125 – 132

118. S. A. Shehzad, F. M. Abbasi, T. Hayat and F. Alsaedi, Model and comparative study for peristaltic transport of water based nanofluids, *J. Mol. Liq.*, 209 (2015) 723 – 728.

119. T. Hayat, F. M. Abbasi, M. Al-Yami and S. Monaquel, Slip and Joul heating effects in mixed convection peristaltic transport of nanofluid with Soret and Dufour effects, *J. Mol. Liq.* 194 (2014) 93 – 99.

120. D. Tripathi and O. A. Beg, A study of peristaltic flow of nanofluids: Application in drug delivery systems, *Int. J. Heat Mass Trans.* 70 (2014) 61 – 70

121. N. S. Akbar, S. Nadeem and Z. H. Khan, Numerical simulation of peristaltic flow of a Carreau nanofluid in an asymmetric channel, *Alexand. Engng. J.* 53 (2014) 191 – 197.

122. N. S. Akbar and S. Nadeem, Endoscopic effects on peristaltic flow of a nanofluid, *Commun. Theor. Phys.* 56 (2011) 761 – 768.

123. N. S. Akbar, S. Nadeem, T. Hayat and A. A. Hendi, Peristaltic flow of a nanofluid in a non-uniform tube, *Heat Mass Trans.* 48 (2012) 451 – 459.

124. O. Anwar Beg, M. M. Rashdi, M. Akbari and A. Hosseini, Comparative numerical study of single-phase and two-phase models for bio-nanofluid transport phenomena, *J. Mech. Med. Bio.* 14 (2014) 1450011

125. H. V. Helmholtz, J. Fur die reine und angewandte Mathematik (Crelles Journal) (Wiss. Abh. i. 101) 5 (1958).

126. L. Kelvin (W. Thomson) On vortex motion, *Trans. R. Soc. Edinb.* 25 (1969) 217 – 260

127. K. Oswatitsch, Die ablosebedingungen von Grenzschichten. *In Grenzschicht-forschung (ed. H. Gortler) IUTAM Symposium on Boundary Layer Research ˜Springer-Verlag, Berlin-Heidelberg-New York*, (1958) 357 – 367.

128. A. Davey, Boundary-layer flow at a saddle point of attachment. *J. Fluid Mech.* 10 (1961) 593 – 610.

129. M. J. Lighthill, Attachment and separation in three-dimensional flow. *In Laminar Boundary Layers, (L. Rosenhead Ed.) Clarendon Press, Oxford*, 1963, p. 72.

130. J. C. R. Hunt, C. J. Abell, J. A. Peterka, and H. Woo, "Kinematical studies of the flow around free or surface-mounted obstacles; applying topology to flow visualization," *J. Fluid Mech.* 86 (1978) 179 – 200.

131. M. Brons and J. N. Hartnack, Streamline topologies near simple degenerate critical points in two-dimensional flow away from boundaries, *Phys. of Fluids*, 11 (1999) 314 – 324.

132. F. Gurcan, A. Deliceoglu and P. G. Bakker, Streamline topologies near a non-simple degenerate critical point close to a stationary wall using normal forms, *J. Fluid Mech.* 539 (2005) 299 – 311.

133. J. Jiménez-Lozano and Mihir Sen, Streamline topologies of two-dimensional peristaltic flow and their bifurcations, *Chem. Engng Process.*, 49 (2010) 704 – 715.

134. L. F. Shampine, J. Kierzenka, M. W. Reichelt, Solving boundary value problems for ordinary differential equations in Matlab with bvp4c, *http://ftp.mathworks.com/pub/doc/papers/bvp/.*

135. R. B. Bird, P. J. Dotson and N. L. Johnson, Polymer solution rheology based on a finitely extensible bead-spring chain model, *J. Non-Newtonian Fluid Mech.*, 7 (1980) 213 – 235.

136. M. D. Chilcott and J. M. Rallison, Creeping flow of dilute polymer solutions past cylinders and spheres, *J. Non-Newtonian Fluid Mech.* 29 (1988) 381 – 432.

137. R. R. Huilgol and N. Phan Thien, Fluid mechanics of viscoelasicity, *Amsterdam-Lausanne-New York-Oxford-Shannon-Tokyo*, (1997).

138. A. Peterlin, Hydrodynamics of macromolecules in a velocity field with longitudinal gradient, *J. Polym. Sci., Polym. Letters B*, 4 (1966) 287 – 291.

139. B. Purnode and M. J. Crochet, Polymer-solution characterization with the FENE-P model, *J. Non-Newtonian Fluid Mech.* 77 (1998) 1 – 20.

140. S. Nadeem and N. S. Akbar, Effects of heat transfer on the peristaltic transport of MHD Newtonian fluid with variable viscosity: Application of Adomian decomposition method, *Commun. Nonlinear Sci. Numer. Simulat.* 14 (2009) 3844 – 3855.

141. M. Elshahed and M. H. Haroun, Peristaltic transport of Johnson-Segalman fluid under effect of a magnetic field, *Math. Prob. Engng.* 6 (2005) 663 – 677.

142. T. Hayat and N. Ali, A mathematical description of peristaltic hydromagnetic flow in a tube, *Appl. Math. Comp.* 188 (2007) 1491 – 1502.

143. M. Tobak and D. J. Peake, Topology of three dimensional separated flows, *Ann. Rev. Fluid Mechs.* 14 (1982) 61 – 85.

144. P. G. Bakker, Bifurcations in flow patterns, *Kluwer Academic Publishers, Dordrecht, the Netherland* (1991).

145. R. Seydel, From equilibrium to chaos. Practical bifurcation and stability analysis. Elsevier New York (1988).

146. L. Perko, Differential equations and dynamical systems, *3rd ed. Springer New York* (2000).

147. H. S. Lew, Y. C. Fung and C. B. Lowenstein, Peristaltic carrying and mixing of chyme in small intestine, *J. Biomechs.* 4 (1971) 297 – 315.

148. D. N. Riahi and R. Roy, Mathematical modeling of peristaltic flow of chyme in small intestine, *App. Appl. Math.* 6 (2011) 428 – 444.

149. N. Ali, T. Hayat and Y. Wang, MHD peristaltic flow of a third order fluid in an asymmetric channel, *Int. J. Numer. Methods in Fluids* 64 (2009) 992 – 1013.

150. P. J. Oliveira, An exact solution for tube and slit flow of a FENE-P fluid, *Appl. Math. Comp.* 158 (2002) 157 – 167.